

Dissertation
submitted to the
Combined Faculties for the Natural Sciences and for
Mathematics
of the Ruperto-Carola University of Heidelberg, Germany
for the degree of
Doctor of Natural Sciences

presented by

M. Sc. Pierre Wehler
born in: Hadamar, Germany
oral examination date: April 09, 2019

Engineering optogenetic control of p53

Referees: Prof. Dr. Stefan Wölfel

Prof. Dr. Barbara Di Ventura

Acknowledgements

First and foremost, I want to thank Prof. Barbara Di Ventura for giving me the opportunity to pursue my PhD in her lab. Her wits and enthusiasm were an endless resource for me to learn from. Her curiosity and motivation towards science was contagious, and kept me going to follow our goals, even when I got stuck on a particular problem. Her guidance paved the way throughout this project. I could not have reached the finish line without her patience and trust in myself.

I am also very thankful to Prof. Roland Eils, for accepting me as a PhD student. Not only for the initial funding he provided, but also for welcoming me in the eilslabs family.

I also want to express my special gratitude to Prof. Stefan Wölfl, for taking over the examination of this thesis on short notice without hesitation. Additionally, I am thankful, that I could use the Incucyte[®] system in his lab. At this point, I also need to thank Yannick Theobald, who introduced me to the use of the machine, and shared his knowledge of using the instrument.

Besides Prof. Roland Eils, I want to thank my other TAC members, Prof. Thomas Hofmann and Prof. Friedrich Frischknecht. Their input during my TAC meetings was highly appreciated.

A special thanks to all the Di Ventura lab members I was lucky to work with. Thank you for all your scientific input and ideas, and all the fun we had doing science and other things together. Their continuous support and companionship, also outside of the lab, made lab a second home.

I need to say a big thank you to Albert, Jonas and David, students who helped me in certain aspects of this work. I highly appreciate their passion for my project, and all the discussions we had concerning p53's dynamic life style.

I was extremely lucky, to meet so many great people during my life in Heidelberg, who become close friends. I miss seeing all you guys on a regular basis. I miss my lunch dates with Matthias, my adventures with Nils, my colleagues from my bar keeping days and especially my Schafkopf sit-ins. Friends is what keeps you sane, in moments of despair. Finding guys like you, is like a "Solo-Sie".

Last but not least, I want to thank my parents and my wonderful girlfriend, for the endless love and support through all stages of my life. Their unconditional support was vital for me and kept me going through the ups and downs of my PhD and life in general.

Contributions

If not explicitly stated otherwise, all data were obtained by myself under supervision of **Prof. Barbara Di Ventura**.

Christian Scheeder, a former master student in the Di Ventura Lab, cloned the mammalian expression plasmids Reg4-MIP, Reg5-MIP and Reg5-EA. He also performed the initial characterisation of these constructs in MCF7 cells (Figure 3.1).

All non-tagged LINuS and LEXY constructs were designed and cloned by **Dominik Niopek**. He also provided me with the sequences for the synthetic NES sequences used in (Figure 3.17).

Ben Kachel provided me with the plasmid containing the tetR-Repressor used in generating the stable cell line C29-36 (Figure 3.22).

Jonas Fleck implemented the CLaP protocol and carried out pilot experiments in removing not-activated cells (Figure 3.26C).

During his Master thesis **David Lauer** carried out a lot of experiments supplementing my work. Particularly, the establishment of doxycyclin administration regime, that provides stable p53-LEXY levels over longer time periods (Figure 3.28).

Abstract

Cells respond to external and internal stimuli mostly with changes in transcription of target genes. Gene expression is mediated by transcription factors, central nodes in highly regulated signalling networks. In multiple signalling pathways, different stimuli converge on the same transcription factor, yet induce different cell fates. Recently, the dynamics of transcription factors have been identified to play a key role in converting the received trigger into the appropriate response. It is proposed that the same transcription factor induces different gene expression programs purely depending on its dynamics.

One example of particular interest is the transcription factor p53. Under physiological conditions, p53 levels are kept low by a tightly regulated network. Upon stress, p53 levels increase and show a pulsatile or sustained behaviour, depending on the type and severity of the stress. Interestingly, it was proposed that p53 dynamics dictate which downstream gene expression programs are initiated. However, many questions remain open, such as whether the dynamics are sufficient to drive differential gene expression, or whether stress-induced post-translational modifications of p53 and other interacting factors play a role alongside p53 dynamics. Moreover, it is still unknown, how p53 dynamics are eventually translated into a specific target gene expression programs.

The p53 signalling and regulatory network is both, highly complex and dynamic. Understanding this network requires targeted dissection using specific and precise methods. To address these requirements, I employed optogenetic methods, as light possesses unmatched spatial and temporal resolution. In contrast to chemical perturbation methods, light as a trigger is non-invasive and has a superior specificity. Here, I used optogenetics to reconstitute various p53 dynamics, by controlling the levels and localization of p53, and I investigated the outcome of these manipulations in the absence of upstream stress.

Specifically, I achieved light-mediated control of endogenous p53 levels and its activity. The E3 ubiquitin ligase Mdm2 is known to be the main regulator of p53 levels. I could demonstrate that the p53-Mdm2 inhibitory peptide (PMI) inhibits p53 degradation *in vivo*, and that its effect on p53 levels is localisation-dependent, and only occurs when PMI is present in the nucleus. To control the localization of PMI with light I used a light-inducible nuclear export system (LEXY). LEXY is a versatile protein tag that harbours an engineered AsLOV2 domain exposing a nuclear export sequence (NES) upon blue light illumination, leading to rapid nuclear export of the tagged amino acid sequence, and re-import into the nucleus once the cells are not subjected to blue light anymore. By fusing PMI to LEXY, I could obtain light-mediated control over localisation of PMI-LEXY and thus degradation of p53, resulting in elevated p53 levels. Additionally, expression of the p53 target gene p21 was increased, showing that not only p53 protein levels are increased, but also that p53 is transcriptionally active.

In a second approach, I used LEXY to control the localization of an exogenously expressed p53 with light. I could show that I can repeatedly accumulate p53 tagged with LEXY in and out of the nucleus, effectively generating p53 pulses akin to those obtained under certain stress conditions. I generated a stable cell line expressing p53-LEXY under an inducible promoter, allowing robust expression of p53-LEXY. p53-LEXY is transcriptionally active, and can induce transcription of multiple p53 target genes in the absence of stress. Moreover, p53-LEXY could induce the terminal cell fate senescence. However, prolonged blue light exposure and application of more complex illumination patterns resulted in impaired translocation and cellular stress. Reduction of the light intensity to prevent phototoxicity corresponded to losing the ability to control p53-LEXY with light. Inducing genotoxic stress to stimulate p53 activity increased the expression of some p53 target genes in the stable cell line, yet revealed high variability between biological replicates, questioning the utility of this cell line.

Zusammenfassung

Zellen reagieren auf externe und interne Reize zumeist mit der Anpassung der Transkription von Genen. Genexpression wird von Transkriptionsfaktoren gesteuert, zentralen Knoten in hoch regulierten Signalnetzwerken. In vielen Signalwegen laufen verschiedene Reize in einem Transkriptionsfaktor zusammen, induzieren jedoch unterschiedliche Zellschicksale. Die Dynamiken von Transkriptionsfaktoren scheinen dabei eine Schlüsselrolle dabei zu spielen, wie ein Reiz in die angemessene Reaktion umgewandelt wird. Es wurde postuliert, dass ein und derselbe Transkriptionsfaktor basierend auf der Dynamik seiner Aktivierung unterschiedliche Genexpressionsprogramme induzieren kann.

Ein Beispiel von besonderem Interesse ist der Transkriptionsfaktor p53. Unter physiologischen Bedingungen werden p53 Proteinmengen durch ein eng reguliertes Netzwerk sehr niedrig gehalten. In Reaktion zu Stress erhöhen sich die p53 Proteinmengen und zeigen pulsierende oder ununterbrochene Aktivierung, abhängig von der Art und der Schwere des Stresses. Interessanterweise wurde postuliert, dass p53 Dynamiken die stressinduzierten Genexpressionsprogramme diktieren. Vielen Fragen bleiben jedoch noch ungeklärt, wie zum Beispiel ob die Dynamiken allein ausreichen sind, um differentielle Genexpression herzurufen, oder ob zusätzlich zu den Dynamiken stressinduzierte posttranslationale Modifikation an p53 oder anderen interagierenden Faktoren eine Rolle spielen. Außerdem ist es noch immer unbekannt, wie p53 Dynamiken letztendlich in spezifische Genexpressionsprogramme dekodiert werden.

Das p53 Signal- und Regulationsnetzwerk ist sowohl hochkomplex als auch äußerst dynamisch. Um das Netzwerk verstehen zu können bedarf es gezielter Analyse mittels spezifischer und präziser Methoden. Um diesen Vorgaben gerecht zu werden, habe ich optogenetische Methoden verwendet, da Licht eine unübertroffene räumliche und zeitliche Auflösung innehat. Im Gegensatz zu chemischen Perturbationen ist Licht nicht-invasiv und hat eine überlegene Spezifität. Hier habe ich optogenetische Methoden genutzt, um verschiedene p53 Dynamiken durch die Kontrolle der Proteinmengen und der Lokalisierung von p53 nachzustellen. Außerdem habe ich die Folgen dieser applizierten Dynamiken in der Abwesenheit von Stress untersucht.

Genauer genommen, habe ich licht-basierte Kontrolle über Proteinmengen und Aktivität von endogenem p53 erzielt. Die E3 Ubiquitin Ligase Mdm2 ist der Hauptregulator von p53 Proteinmengen. Ich konnte zeigen, dass das p53-Mdm2 inhibierendes Peptid (PMI) den Abbau von p53 *in vivo* verhindert, und dass die Effekte auf die p53 Proteinmengen abhängig von dem Ort der PMI-Expression ist, und nur auftritt wenn PMI im Zellkern ist. Um die Lokalisierung des PMI Peptids mittels Licht zu kontrollieren nutzte ich das "light-inducible nuclear export system" (LEXY, für lichtinduzierbares Kernexportsystem). LEXY ist ein vielseitig einsetzbares Protein-Tag, welches aus einer optimierten AsLOV2 Domäne besteht, die in Reaktion auf blaues Licht ein Kernexportsignal (NES, für nuclear export sequence) offenlegt, was zu einem schnellen Export des an LEXY angehängten Proteins führt, und zu einem Reimport in den Nukleus, sobald das Licht ausgeschaltet wird. Durch das Anhängen von LEXY an PMI konnte ich licht-basierte Kontrolle über die Lokalisierung von PMI-LEXY und dadurch den Abbau von p53 erreichen, was zu erhöhten p53 Proteinmengen geführt hat. Außerdem wurde die Expression von dem p53 Zielgen p21 erhöht; das demonstriert dass nicht nur p53 Proteinmengen erhöht wurden, sondern dass p53 Transkription induzieren kann.

In einem zweiten Ansatz habe ich die mittels LEXY die Lokalisierung von exogen exprimierten p53 mittels Licht kontrolliert. Ich konnte p53 mit angehängtem LEXY wiederholt im Nukleus und im Cytosol akkumulieren, ein Verhalten das ähnlich dem Pulsieren von p53 als Reaktion auf verschiedene Stressbedingungen ist. Ich habe eine stabile Zelllinie kreiert, welche zuverlässige p53-LEXY Expression mittels eines induzierbaren Promotors ermöglicht. Dabei ist p53-LEXY transkriptionell aktiv und kann die Transkription mehrerer p53 Zielgene in der Abwesenheit von Stress induzieren. Außerdem konnte p53-LEXY das terminale Zellschicksal Seneszenz induzieren. Allerdings hat die lange Belichtungszeit mittels blauem Licht und die Applizierung von komplexeren Licht Mustern in vermindert Translokation und zellulärem Stress resultiert. Die Reduzierung der Lichtintensität zur Vermeidung von Phototoxizität resultierte in dem Verlust der Kontrolle über p53-LEXY mittels Licht. Das Induzieren

von genotoxischem Stress um die Aktivität von p53 zu stimulieren erhöhte die Expression von einigen p53 Zielgenen in der stabilen Zelllinie, hat aber auch die hohe Variabilität zwischen biologischen Replikaten offenbart, die die den Nutzen dieser Zelllinie infrage stellt.

Contents

Acknowledgements	i
Contributions	iii
Abstract	v
Zusammenfassung	vii
1 Introduction	2
1.1 The transcription factor p53 and its regulation	2
1.1.1 The structure of p53	3
1.1.2 Regulation of p53 by Mdm2 and MdmX	4
1.1.3 Stabilisation of p53	5
1.1.4 Transcriptionally independent functions of p53	7
1.2 The dynamic nature of cell signalling	7
1.2.1 Examples of transcription factor dynamics	8
1.2.2 p53 dynamics, causes and consequences	12
1.3 Optogenetics	14
1.3.1 Photoreceptors	15
1.3.2 LOV domains	16
1.3.3 Light-dependent allostery using AsLOV domains in non-neuronal optogenetics	17
1.3.4 LINuS and LEXY, moving proteins in and out of the nucleus	20
1.4 Aim of this study	21
2 Material and Methods	24
2.1 Plasmid generation	24
2.2 Cell culture and cell lines	24
2.2.1 Cell culture and cell lines	24
2.2.2 Transient transfections	24
2.2.3 Generation of the monoclonal stable cell Lines H1299-p53-LEXY	25
2.3 Western blot	25
2.4 Blue light illumination devices	26
2.4.1 Activation within the cell incubator	26
2.4.2 LED-devices for automated microscopy	26
2.5 Microscopy and Imaging	26
2.5.1 Leica SP5	26
2.5.2 Lionheart	26
2.5.3 Image Analysis	27
2.6 Quantitative analysis of mRNA transcript levels by qPCR	27
2.6.1 Primer design and validation	27
2.6.2 cDNA generation	27

2.6.3	qPCR	27
2.6.4	Data analysis	28
2.7	Crystal violet staining	28
2.8	Single cell laser-tag	28
2.8.1	Cell Tagging	28
2.8.2	Fluorescent cell labelling	28
2.8.3	Selective detachment of non-activated cells	28
3	Results	29
3.1	Light-mediated manipulation of endogenous p53 levels	29
3.1.1	Photocaging the MIP peptide in the AsLOV2 domain	29
3.1.2	Characterisation of the MIP peptide in HCT116 cells	31
3.1.3	Employing endogenous p53 sequences to enable light-mediated Mdm2 inhibition	33
3.1.4	Using the PMI peptide to manipulate p53 levels light-dependently	34
3.2	Light-controlled nuclear import using LINuS	43
3.2.1	Characterisation of p53 ^{WT} -LINuS constructs in H1299	43
3.2.2	Impairment of p53's NES allows nuclear accumulation	44
3.2.3	Introduction of compensatory mutations on p53's endogenous NLS	45
3.2.4	Assessment of transcriptional activity of p53 ^{K320AL348AL350A}	47
3.2.5	Acetylation-mimicking mutants do not restore transcriptional activity of p53 ^{K320AL348AL350A}	48
3.2.6	Characterisation of p53 NLS mutants	49
3.2.7	Nucleo-cytoplasmic translocation of p53-LINuS constructs	50
3.2.8	Introduction of a constitutive NES to achieve reversible translocation of p53 ^{R306A} -biLINuS02	51
3.3	Controlling p53 localisation with LEXY	53
3.3.1	Characterisation of transiently transfected p53 ^{WT} -LEXY in H1299 cells	53
3.3.2	Design of a stable cell line expressing p53-LEXY	57
3.3.3	Prolonged light exposure affects p53-LEXY expression	61
3.3.4	Adapting the illumination settings to prevent differential expression of p53-LEXY	63
3.3.5	Tracing translocation of p53-LEXY during ongoing experiments	65
3.3.6	Optimisation of p53-LEXY levels and translocation efficiency	67
3.3.7	Reduction of light intensity still leads to impairment of p53-LEXY translocation	72
3.3.8	Drug treatment reveals high variability in transcriptional response in C29-36 cells	74
3.3.9	Finding the cause of un-reproducibility	78
4	Discussion and Outlook	81
4.1	Controlling endogenous p53 levels by light-dependent inhibition of p53 degradation	81
4.1.1	Light-mediated steric hindrance of peptides or protein domains to control p53 degradation	81
4.1.2	Controlling the localisation of the PMI peptide	82
4.1.3	PMI-induced increase in p53 levels is not reversible	83
4.2	Efficiency of PMI-LINuS and p53-LINuS fusions is low	83
4.3	p53 mutant constructs lack transcriptional activity	84
4.4	Comparing the transcriptional response to pulsatile and sustained p53	85
4.4.1	p53 abundance determines translocation efficiency	85
4.4.2	The effect of doxycycline on p53 transcript levels	85
4.4.3	Prolonged illumination of the cells impairs their import/export capacity and leads to phototoxicity	86

4.4.4	Changing the light application settings to reduce phototoxicity reduced light-dependent transcription of p53 target genes	87
4.5	Un-reproducibility of p53's transcriptional activity in response to drug treatment	88
4.6	Outlook	89
5	Bibliography	91
6	List of Figures	109
7	Appendix	111
7.1	List of Constructs used in this study	111
7.2	List of qPCR Primer	114
7.3	Supplemental Figures	115
7.3.1	Monitoring of translocation kinetics	115
7.3.2	p53 target gene expression upon neocarzinostatin treatment	116
7.3.3	p53 target gene expression upon gefitinib treatment	117
7.3.4	Gefitinib treatment resulted in reproducible puma expression in HCT116 and MCF7-p53-Venus cells	118
7.4	Abbreviations	119

1 Introduction

1.1 The transcription factor p53 and its regulation

Every cell is permanently exposed to a myriad of stress signals, ranging from mild changes in its environment to irreparable DNA damage. Sensing and evaluation of these stress signals is detrimental to maintain cellular homeostasis, and complicated signalling networks have evolved to enable cells to cope with different kind of stresses in the appropriate manner.

A key protein within this network is the transcription factor p53. Also labelled 'guardian of the genome' (Lane, 1992) or 'cellular gatekeeper' (Levine, 1997), p53 integrates various stress signals into the most appropriate cellular response by regulating transcription of specific genes. Due to its significance to uphold genomic integrity, the regulation of p53 itself is carried out by a sophisticated network (Figure 1.1). Discovered in 1979 (Linzer and Levine, 1979), it was first misidentified as an oncogene, until its tumour suppressor function were discovered (Finlay et al., 1989). Not only mutated in most of human cancers (Vogelstein et al., 2000), inactivation of p53 is also associated with a poor patient prognosis (Olivier et al., 2010), highlighting its significance in overseeing cell cycle progression.

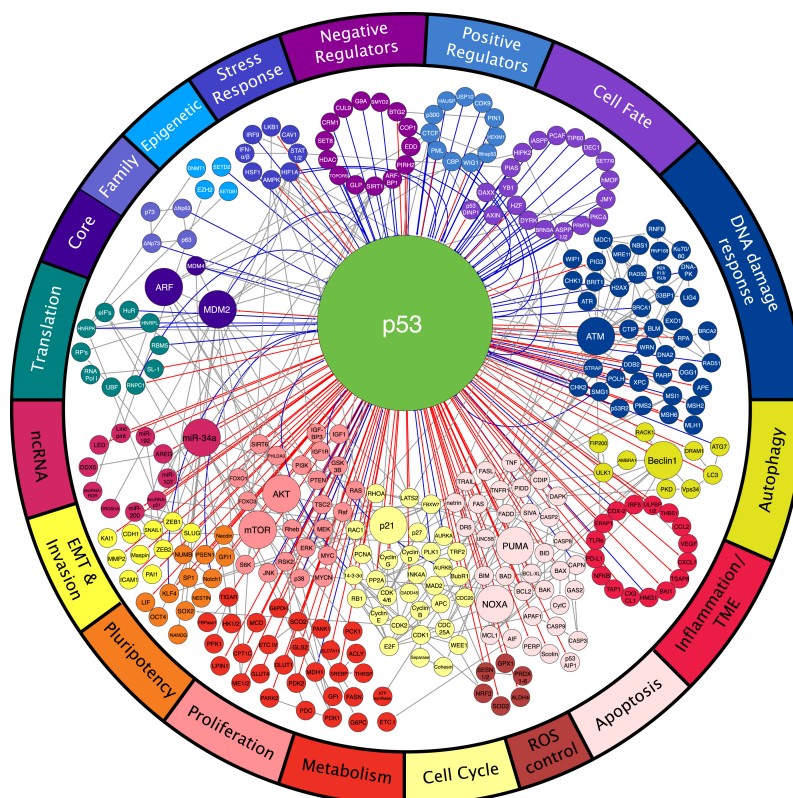


Figure 1.1: The intricacies of p53 regulation

p53 is the central node of a complex, stress sensing network. Blue lines represent stimuli received directly by p53. Red lines indicate transcriptional targets of p53. Grey lines represent the pathway interactions downstream of p53.

Adapted from (Kastenhuber and Lowe, 2017).

As a transcription factor, inherently p53's most vital function is the induction of a specific set of target genes. To this day, more than 3500 target genes in a broad functional spectrum have been discovered to be stimulated in response to various stress situations (Fischer, 2017), showcasing the significant influence p53 has on a cell's transcriptome (Figure 1.1). This is further underlined by the fact that the vast majority of pathogenic mutations of p53 occur within the DNA-binding Domain (DBD). Yet recently there has been a lot of attention on the non-transcriptional functions of p53.

In the following, I will give an overview over the tumour suppressor p53 and its role in orchestrating cell fate in response to internal and external stress signals by inducing transcription of subsets of target genes. I will discuss how cells control p53 levels and highlight some of the recent findings of p53's non-transcriptional functions. I will set a particular focus on p53 dynamics, as these are the main focus of this study.

1.1.1 The structure of p53

The TP53 gene on the short arm of chromosome 17 encodes human p53. The gene spans 20 kb in total, yet canonical p53 consists of 393 amino acids. The gene displays a conservation in vertebrates, yet only minor resemblance to invertebrates (May and May, 1999). p53 contains 6 major functional domains, and distortion of its structural characteristics is a common way to disrupt p53 folding and oligomerization and thus function in human carcinoma (Muller and Vousden, 2013).

At the N-terminus, there are two intrinsically disordered N-terminal transactivation domains (TADs), responsible for controlling transcriptional activity of p53 (Figure 1.2). Initially considered as one domain, the discovery of independent functions of TAD1 (1 - 42) and TAD2 (43 - 63) has led to the appreciation of two distinct functional units. Next, a proline-rich region (PRD) (63 - 97), containing several Src homology 3 (SH3)-domain binding sites, a common motif in cell signalling proteins (Ren et al., 1993).

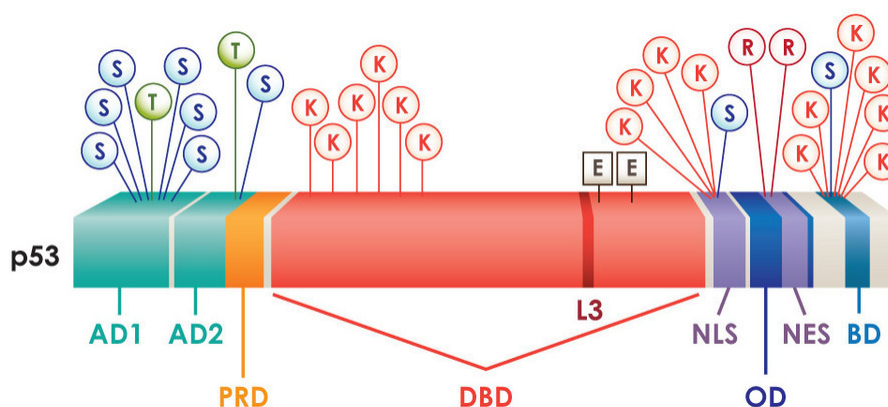


Figure 1.2: Functional domains of p53 and key sites of post-translational modification

p53 consists of 6 major functional subunits and 3 localization sequences. The two N-terminal transactivation domains AD (AD1 and AD2) domains are involved in protein-protein interaction, followed by a proline-rich domain. The core of p53 consists of the DNA-binding domain (DBD). Then, there is bipartite NLS, consisting of two separate stretches. Together with the NES located within the tetramerization domain (here: oligomerization domain) it maintains localization of p53. The C-terminus contains a basic domain (BD). A number of key residues for post translational modifications are shown. Abbreviation: S: Serine; T: Tyrosine; K: Lysine; E: Glutamic Acids. Adapted from Brock (2009).

The central core of p53(100-300) inhabits a structured DNA-binding domain (DBD), which binding motif consists of RRCWVGYYY (R = A, G; W = A,T; Y = C,T) separated by a variable spacer (El-Deiry et al., 1992; Wei et al., 2006). This DBD contains the six most common mutations occurring in cancer (Brosh and Rotter, 2009), and a number of other amino acid residues commonly mutated in tumor cells resulting in deficient DNA interaction properties (Kasthuber and Lowe, 2017). In addition, mutations that handicap the DNA binding properties can

resolve in dominant negative effects even if only one copy is affected, since a single mutated subunit can prevent p53 tetramer complex formation, which is crucial for interaction with the transcription machinery (Muller and Vousden, 2013).

The DBD is followed by a bipartite nuclear localization sequence (NLS) consisting of two basic amino acid groups, Lys-Arg (K305, R306) and Lys-Lys-Lys (K319, K320, K321), separated by a spacer of 12 amino acid residues leading to a nuclear localisation in unstressed conditions (Liang and Clarke, 1999). The tetramerization domain, necessary to form homo-oligomers essential for p53 to become transcriptional active are located upstream of the second NLS stretch (325-356). Located within the tetramerization domain is a nuclear export sequence (NES) (M340, L344, L348, L350), which is blocked once p53 forms a tetramer (Stommel et al., 1999). Finally, a basic, lysine-rich domain at the C-terminus (363-393) comprising an important site for post-translational modifications and regulation of p53 function (Joerger and Fersht, 2008).

The human p53 gene expresses at least 12 different isoforms due to alternative RNA splicing, alternative translation initiation and alternative promoter usage (Khoury and Bourdon, 2011). These isoforms, composed of distinct domain composition, have been demonstrated to have diverse functions, such as interfering with the canonical transcription ability of p53 (Bourdon et al., 2005). p53 isoform expression is commonly misregulated in tumours (Takahashi et al., 2013) and non-carcinogenic pathologies such as premature ageing (Muhlinen et al., 2018).

1.1.2 Regulation of p53 by Mdm2 and MdmX

Given the significance of an appropriate p53 function as a central signalling node involved in the stress response pathway, it is not surprising that the regulation of p53 consists of a complex network to fine-tune the p53 levels and its activation to achieve the appropriate stress response. This is accomplished by a range of protein-interacting partners and an array of post-translational modifications (PTM), on more than 36 amino acids of p53 (Kruse and Gu, 2008).

Under physiological conditions, p53 levels are kept low. The amount of p53 protein is rather determined by the rate of its degradation, than the production rate. In unstressed conditions, protein half-life time is very short, ranging from 5 to 30 minutes, yet dramatically increased in upon stress or in transformed cells (Rogel et al., 1985).

The main regulators of both, p53 activity and protein levels are the oncogene Mdm2 and its homolog MdmX (also known as Mdm4) (Figure 1.3). Amplification or misregulation of either of the two MDM genes is a feature in many tumours, especially in tumours lacking p53 mutation (Momand et al., 1992; Shibagaki et al., 1995; Ito et al., 2010). Both bind a putative helix formed by residues 18-26 of the p53 TAD1 (Kussie et al., 1996) and inhibit p53's ability to regulate the induction of target genes, rendering it transcriptional inactive (Chen et al., 1995; Shvarts et al., 1996). The key difference between Mdm2 and MdmX is the E3 ubiquitin ligase activity towards p53 Mdm2 possesses once it homo-oligomerizes (Haupt et al., 1997; Fang et al., 2000; Cheng et al., 2011).

On binding, Mdm2 either monoubiquitinates p53, which exposes the nuclear export sequence and leads to translocation into the cytoplasm or polyubiquitinates p53, leading to proteasomal degradation of p53 (Figure 1.3) (Tao and Levine, 1999; Lohrum et al., 2001; Li et al., 2003; Carter et al., 2007). The Mdm2-mediated ubiquitination occurs mainly at the six carboxy terminal lysines (K370, K372, K373, K381 and K386) (Rodriguez et al., 2000). Mdm2 can form heterooligomers with MdmX which are proposed to make p53 degradation more efficient by stabilizing Mdm2 (Badciong and Haas, 2002). Mdm2 is an unstable protein, due to autoubiquitination or ubiquitination by other E3 ligases (Fang et al., 2000; Itahana et al., 2007). Eventhough the importance of Mdm2 in degradation can not be overstated, cells of MDM2-deficient mice are able to degrade p53, yet slower compared to Mdm2 expressing cells (Ringshausen et al., 2006).

The relationship between the Mdm homologs and p53 is not unidirectional. While p53-induced transcription of MdmX has only been demonstrated recently, and only occurring under certain conditions (Phillips et al., 2010), the control of Mdm2 expression by p53 is a central feature and has been established already over 25 years ago

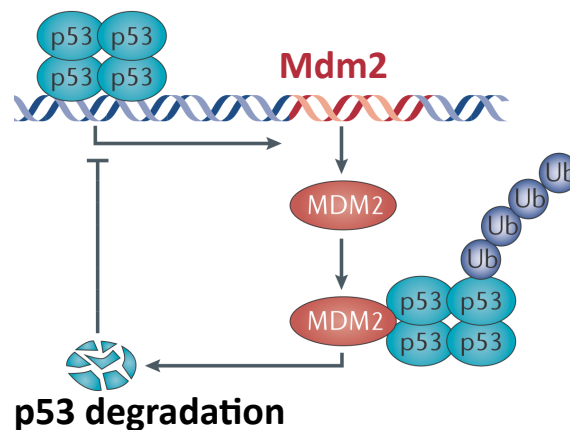


Figure 1.3: MDM2 is the main regulator of p53 protein levels

Levels of p53 are controlled mainly by the ubiquitin E3 ligase, which binds p53's N-terminus and subsequently ubiquitinates p53' C-terminus, rendering it for degradation. MDM2 is also a transcriptional target of p53, creating a negative feedback loop.

Adapted from Williams and Farzaneh (2012).

(Barak and Oren, 1992; Perry et al., 1993). This interplay results in a autoregulatory feedback loop regulating both, the activity of p53 and the expression of Mdm2 under unstressed conditions (Wu et al., 1993).

1.1.3 Stabilisation of p53

The main task of p53 is maintaining genomic integrity of the cell and various stress conditions lead to the interruption of the negative feedback loop that keep p53 levels minimal and thus result in the rapid accumulation of p53 protein levels. For a long time it was hypotised, that only unusual and acute stress results in the rise of p53 levels. Recent studies suggest that also under normal growth and development, p53 activation occurs and plays an essential role beyond its classic trades, for example in regulation of metabolism, antioxidation, development and aging (reviewed in Berkers et al. (2013)). Yet, albeit upstream activators of p53 are manifold and be triggered by distinct stress signals, our understanding of p53's activation and orchestration of cellular fate has been shaped by the investigations on both, single strand and double strand breaks upon genotoxic stress, and these are the processes I want to focus on here.

The classic model of p53 describes a three step process, which is mainly controlled due to PTMs. Under unchallenged conditions, p53 is rapidly turnover. Upon stress, N-terminal phosphorylation leads to stabilization of the short-lived p53, and thus accumulation in the nucleus. Next, p53 forms a homotetrameric complex (Friedman et al., 1993), which is an essential step for binding to DNA and recognizing p53's binding motif (Davison et al., 1998). In this state, p53 transcribes genes like MDM2 or PirH2, which are associated with p53-turnover and cell survival (Leng et al., 2003). Partial acetylation of p53 causes the recruitment of cofactors and expression of genes like p21 and GADD45, genes associated to cell cycle arrest and DNA repair. Finally, p53 is further acetylated, becoming fully active and transcribing genes responsible for irreversible apoptosis like BAX or PUMA (Kruse and Gu, 2009).

While modification and interaction of Mdm2 is a common mechanism, as illustrated for example by the tumour suppressor p14ARF which binds Mdm2, thereby inhibiting Mdm2 functions towards p53 and thus augmenting p53 levels and activity (Kamijo et al., 1998), the majority of mechanisms interrupting the negative feedback loop keeping p53 levels low are aimed at p53 directly. In general, human p53 is a hotspot for post-translational modifications, and while by now, the vast majority of these modifications might be discovered, the arising complexity is still puzzling. The function of these individual adjustments often seem to be interchangeable or mutually exclusive (for example, acetylation and ubiquination both occur on lysine-residues). A number of PTM's have been associated to various outcomes and are often highly context specific and even reversible, as shown by the

deubiquitinating enzyme HAUSP, which prevents both, p53 and MDM2, from degradation by removing already bound ubiquitin (Li et al., 2002, 2004).

Phosphorylation is a key mechanism of regulating p53, and phosphorylation sites are concentrated at the N-terminal transactivation domains. Phosphorylation at the N-terminus is highly redundant, and as a single kinase phosphorylates various sites, a single site is also phosphorylated by various kinases (Kruse and Gu, 2009).

Genetic lesions caused by irradiation or genotoxic chemicals is a threat to DNA, as the inheritance of genetic information is essential and a key process in life, so it is not surprising that the corruption of the genetic code results in activation of the "guardian of the genome".

Persistent single strand breaks (SSB), lead to the rapid activation of ATR (Ataxia telangiectasia and Rad3 related), a serine/threonine-protein kinase, which phosphorylates several sites in p53, most notably S15 (Tibbetts et al., 1999). Similarly, in the presence of double-strand breaks (DSB), the serine/threonine-protein kinase ataxia telangiectasia mutated (ATM) associates with site of genetic lesion, undergoes autophosphorylation and phosphorylates p53 at several sites, including S15 (Canman et al., 1998; Bakkenist and Kastan, 2003).

Phosphorylation of S15 upon genotoxic stress sensed by ATM/ATR is a key step in p53 stabilisation, since it acts as a nucleation event and is precursor for phosphorylation at T18 and S20 (Saito et al., 2002). Phosphorylation at these sites impedes Mdm2/MdmX binding to the N-terminus of p53 and promoting p53's longevity, but it also facilitates the association of the transcriptional coactivator complex p300/CBP (CREB binding protein) (Lambert et al., 1998; Finlan and Hupp, 2004). As described here, for a number of PTMs of p53 it is hard to evaluate whether they result in either the stabilisation of p53 or a potential change in target gene expression, or both. p300/CBP is a histone acetyltransferase (HAT), which acetylates lysine residues within the DBD and the C-terminal domain of p53, thereby preventing the ubiquitination of p53 by Mdm2 and further stabilize p53 (Ogryzko et al., 1996; Ito et al., 2002). Phosphorylation of other N-terminal serine residues further fine tune the affinity between p53's TAD1 and p300/CBP (Teufel et al., 2009). In contrast, S376 and S378 are constitutively phosphorylated, and at least S376 becomes dephosphorylated upon stress creating a binding motif for 14-3-3 proteins and increase DNA-binding affinity (Waterman et al., 1998). In general, the pattern of phosphorylation are not necessarily caused by stress, but are dynamic throughout the cell cycle with specific patterns for each stage (Buschmann et al., 2000).

As mentioned above, acetylation is another key modification p53 undergoes in becoming stable and for the recruitment of cofactors. While phosphorylation is rather associated to increase p53 longevity, acetylation is thought to fine tune the transcriptional response. p53 was the first non-histon protein substrate shown to be regulated by acetylation (Gu and Roeder, 1997). Acetylation by p300/CBP at the very same lysine residues Mdm2 targets for ubiquitination is supposed to prolong p53 protein life (Ito et al., 2002). This implies, the importance of the lysines within C-terminus in regulating p53 turnover, yet studies with cells derived from mice lacking these 6 lysine residues show no impairment in p53 turnover and regulation of cell fate compared to p53^{wt} mice (Krummel et al., 2005). This is a common phenomenon, modifications, which have been demonstrated to occur *in vitro* and regulate p53 function in cell culture experiments have no or only minor implication *in vivo* or in mouse model studies.

Acetyltransferases like p300/CBP, and other cofactors attracted by acetylations like Kat5 and hMof are able to modify histones in the vicinity of p53 target genes and hence making the chromatin more accessible (Goodman and Smolik, 2000). p300/CBP also acetylates K164, a lysine within the DBD. In this case, acetylation is associated with growth arrest, senescence and apoptosis (Tang et al., 2008). Kat5 and hMof also acetylate p53 itself on K120, which one of the few sites of modification conserved throughout all species. The acetylation of this lysine is suggested to be a key switch for transcription of apoptotic genes (Tang et al., 2006; Sykes et al., 2006). As phosphorylations, pattern of acetylations are highly dynamic, histone deacetylase complexes (HDAC) like HDAC1 or Sirt1 can deacetylate lysines in p53 (Luo et al., 2000, 2001; Vaziri et al., 2001).

Even though a number of transcriptional coactivators have been reported to bind p53, there is only evidence of a few proteins which are then recruited to the promoter of p53 target genes (Kruse and Gu, 2009)

1.1.4 Transcriptionally independent functions of p53

p53-controlled transactivation of target genes is an essential feature of the stress response pathway, although some effects of p53 may be independent of transcription. Originally it was thought that export of p53 to the cytosol was only an indirect way to prevent nuclear accumulation and thus transcription. Observation of p53-dependent apoptosis in the absence of p53-induced transcription and the transcriptionally inactive p53 mutant's ability to induce apoptosis in HeLa cells suggested p53's transcriptionally independent role in apoptosis (Caelles et al., 1994; Haupt et al., 1995).

Pioneering studies lay the groundwork of our understanding of the mechanism behind p53's cytosolic function. Once in the cytoplasm, p53 colocalises to the mitochondria and interacts with anti-apoptotic proteins like B-cell lymphoma-extra large (Bcl-xL), and B-cell lymphoma-extra (Bcl 2). This interaction diminishes their anti-apoptotic functions, and causes oligomerization of proapoptotic factors Bcl-2 homologous antagonist killer (Bak) and Bcl-2-associated X protein (Bax), both also transcriptional targets of p53 (Mihara et al., 2003; Chipuk et al., 2004). The oligomerization causes the formation of pores at the mitochondrial outer membrane, a hallmark of mitochondria mediated apoptosis, resulting in the release of cytochrome C and other apoptotic activators into the cytosol (Mihara et al., 2003; Chipuk et al., 2004). Alternatively, by interacting with Mcl1, p53 disrupts the induced myeloid leukemia cell differentiation protein (Mcl1)-Bak complex, causing the release of Bak and rendering it active (Leu et al., 2004).

In some cell types, there is a soluble Bcl-xL fraction within the cytosol. Cytosolic p53 bound to free diffusing Bcl-xL is inactive. In the emergence of stress, nuclear p53 transcribes p53 upregulated modulator of apoptosis (Puma), which subsequently binds the soluble Bcl-xL, releasing p53 to activate Bax and causing disruption of the mitochondrial membrane in the above described fashion (Chipuk et al., 2005).

Next to apoptosis, cytosolic p53 was identified as a contributor to mitochondrial dysfunction in the mouse heart, leading to increased risk of heart failure by inhibiting the autophagy of dysfunctional mitochondria (Hoshino et al., 2013), highlighting once more the broad range of potential, context dependent influence of the tumor suppressor p53.

1.2 The dynamic nature of cell signalling

Many cell signalling pathways are akin in their topology. Multiple upstream signalling nodes converge in a single transcription factor, that triggers expression of different subsets of genes, often linked to a distinct physiological output. Given that a transcription factor can be activated by numerous stimuli and induce a context dependent gene expression, the questions arises how a certain stimuli is encoded into cellular signal, and subsequently decoded in to transcriptional program.

The technical advance in methods on the single cell level have yielded new insights, highlighting the dramatic variations of response of cells treated with the same stimulus (Cohen et al., 2008; Lee et al., 2009). Processes formerly overlooked due to wrongly chosen time points could be observed due to the advent of new fluorescent probes, enabling scientists to visualize temporal highly dynamic cellular processes, showcasing the dynamic nature of cell signalling. Particularly in immune- and stress-related pathways, multiple signalling pathways have been demonstrated to be highly dynamic, particular transcription factors exhibit spatio-temporal patterns of activity.

Currently, there is a lot of focus on trying to reveal how cells encode the extracellular stimulus the signalling web and execute decision making. First approaches considered cell signalling as a boolean network. In contrast to the simplified text book view on any given signalling pathway, the actual *in vivo* composition of a pathway is dependent on cell type and its current state. A intracellular logical gate takes cellular properties like presence of interaction partners or post-translational modification of pathway proteins into account, and triggers a certain output. While this approach yielded some success, it has not led to a comprehensive and more general under-

standing of cell signalling (Saez-Rodriguez et al., 2009).

Similar to analogous signal transmission, the signal-is-information paradigm postulates that the signal itself carries all necessary information to execute the desired outcome. When cells receive stimuli, either intra- or extracellular, the features of the stimulus is encoded into an intracellular signal, usually the activation of a transcription factor. Features of the signal comprise amplitude, frequency, rate of increase, thresholds or the area under the curve, meaning the total accumulated activated signal. These features are then decoded into a specific response (Figure 1.4).

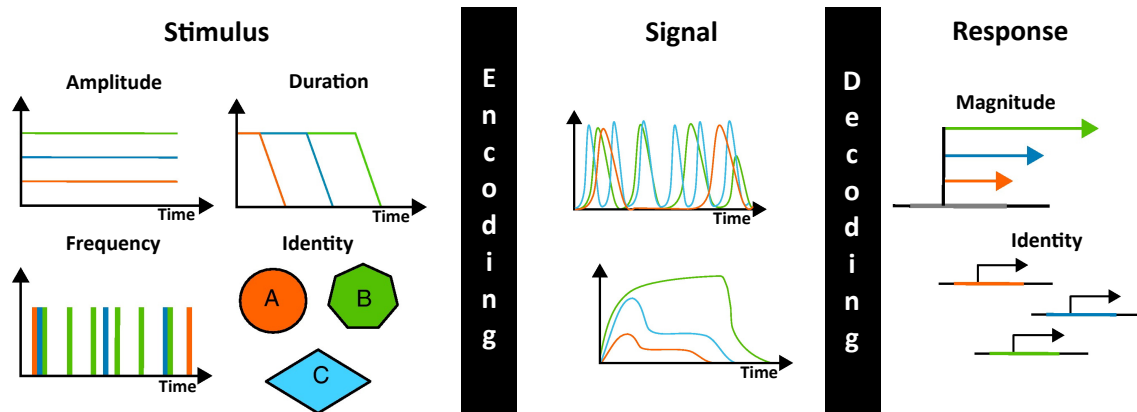


Figure 1.4: Signal as information - A theory of dynamic signal processing

Internal and external stimuli with unique features are encoded into a signal, usually the activity kinetics of a transcription factor. Then, this temporal profile is decoded into the appropriate response.

Adapted from (Behar and Hoffmann, 2010).

Recent studies demonstrated that the intracellular signal is indeed able to convey both identity and quantity of an upstream trigger, and a link between the activation dynamics of a transcription factor and the en- and decoding into a specific response. The formation of these temporal dynamics has been described in several cases (Hoffmann et al., 2002; Batchelor et al., 2008), and specific temporal dynamics have also been linked to distinct cellular outcomes (Marshall, 1995; Purvis et al., 2012; Zambrano et al., 2016; Wilson et al., 2017). While the understanding of how stimuli are encoded into intracellular signals has improved a lot, less evidence is presented for the decoding of the signal.

Here, I want to give a brief overview of the recent discoveries of transcription factor dynamics in eukaryotes. There, I will focus on three well studied cell signalling pathways in mammalian cells, namely the extracellular signal-regulated kinase (Erk) pathway, the NF κ -beta pathway and nuclear factor of activated T cells (Nfat) pathway, followed by a summary of studies about the yeast transcription factor Msn2. Finally, I will focus on the dynamic nature of p53.

1.2.1 Examples of transcription factor dynamics

1.2.1.1 The Erk pathway

The Erk pathway is a mitogen-activated protein kinase (MAPK) family pathway. It is among the first signalling pathways, for which the counter-intuitive behaviour of triggering two opposing outcomes by the same transcription factor has been reported. Treated with nerve growth factor (NGF), rat neuronal precursors start to differentiate, yet applying epidermal growth factor (EGF) causes rapid proliferation (Gotoh et al., 1990; Nguyen et al., 1993; Traverse et al., 1992). In particular, NGF triggers sustained Erk activation, while EGF only results in a short, transient response (Figure 1.5). This observation of distinct activation patterns of Erk by the two different ligands led to the first postulation of dynamics contributing to cellular decision making (Marshall, 1995).

The first clue of the formation of these distinct pulses were reported by Sasagawa and colleagues, who used an

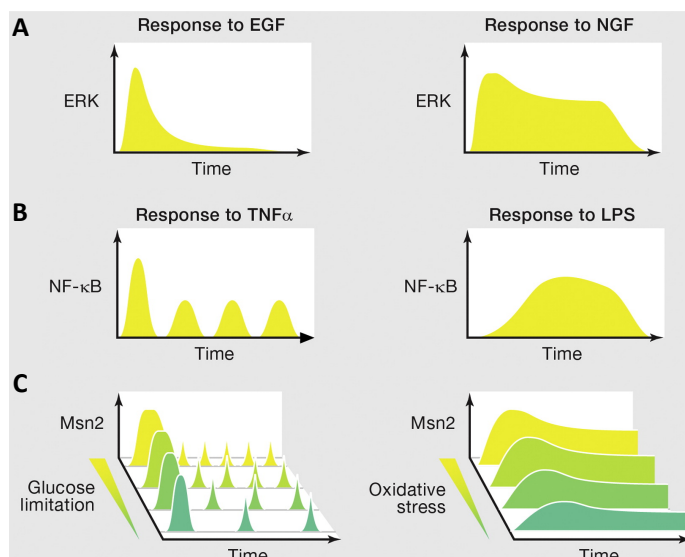


Figure 1.5: Different stimuli trigger distinct temporal behaviours

A | Dynamics of Erk activation in response to either EGF or NGF. EGF treatment causes a transient activation, NGF a sustained activation.

B | Activation of NF κ -beta via TNF α causes an oscillatory response, LPS stimulation triggers sustained activation.

C | Yeast transcription factor Msn2 responds to glucose starvation by a series of bursts, whose length and frequency depend on the severity of starvation. Oxidative stress causes a sustained Msn2 response, the amplitude correlates with its intensity.

Adapted from (Purvis and Lahav, 2013).

elaborate model to predict potential factors shaping Erk dynamics and subsequently verify them *in vivo* (Sasagawa et al., 2005). They provided evidence for a different feedback mechanism, depending on the upstream activator. Activation of the Erk pathway by both NGF and EGF, eventually converge on either Ras or Ras-proximate-1 (Rap1) upstream of Erk, and the temporal properties of Erk activation is partly determined by which of the two small GTPases becomes active. Only NGF treatment causes a full activation of Rap1, blocking the negative feedback on Erk through Son of Sevenless (SOS) and thus generating a sustained Erk activation. Addition of EGF yields only minor activation of Rap1 and consequently only transient activation of Erk. Additionally, only NGF activation is sustained upon receptor activation, further contributing to sustained activation of Erk (Sasagawa et al., 2005). This behaviour here implies that distinct temporal patterns of transcription factor are shaped by distinct topologies of the individual signalling pathway and these topologies are determined by the growth factor context. This is further supported by the discovery of a positive feedback loop for NGF stimulation, yet not in the response to EGF treatment, exemplifying the signal encoding based on the duration of activation (Santos et al., 2007).

Recent observations have demonstrated more elaborate dynamics, like long term oscillations in single cells, stochastic Erk activation pulses linked to proliferation and intercellular propagating waves *in vivo* (Albeck et al., 2013; Aoki et al., 2013; Hiratsuka et al., 2015). The importance of the correct execution of the signal decoding is highlighted by the observation, that well-known oncogenic mutations in the Erk pathway are altering the dynamics properties of the signal transmission (Bugaj et al., 2018).

While the growth factor context shapes Erk activation and triggers distinct cell fates, the elicited profile of immediate-early gene (IEG) mRNA expression, a set of genes which is transcribed within minutes upon a certain stimulus, is surprisingly akin (Murphy et al., 2002). One of these IEGs is c-Fos, upon growth factor stimulation, c-Fos is transcribed rapidly. Due to the rapid production, it occurs independent of the duration of upstream activation. The half life time of newly produced c-fos is between 30 and 45 minutes. Yet, when phosphorylated on C-terminus by prolonged Erk activation, c-fos undergoes a transformational change and exposes the DEF domain. The DEF domain can locally concentrate active Erk and sense small changes in Erk levels (Murphy et al., 2002, 2004). Deletion of the DEF domain disables their sensory functions. Additionally, DEF domains are present in multiple of the IEGs, leading to the hypothesis that this is a general mechanism of Erk signalling, to fine tune nuclear presence of activated Erk and protect it for degradation (Murphy et al., 2002; Murphy and Blenis, 2006). The IEG might act as a first response to a certain stimulus, sense the duration of Erk activation and control the onset of transcription of other genes.

By using an elegant approach combining optogenetics and biochemical activation of Erk, Wilson and colleagues could show that, even though the transcriptional onset of IEGs are similar, their protein synthesis are subject to

another layer of regulation (Wilson et al., 2017). They show a band pass filter like behaviour for IEGs, where repeated pulsatile activation triggers transcription of IEGs more efficiently than sustained activation. Further they present evidence for a different regulation of post-transcription processes for distinct upstream activation (Wilson et al., 2017). They propose a two layer decoding for IEGs, a first layer, which allows slow accumulation of target gene transcript level in the presence of repeated transient Erk activation, and second layer of post transcription control, where timing of translation can be fine tuned in response to distinct combinations of input signals (Wilson et al., 2017).

1.2.1.2 $\text{NF } \kappa\text{-beta}$

Another example is the $\text{NF } \kappa\text{-beta}$ pathway, carrying a key role in regulating the immune response. $\text{NF } \kappa\text{-beta}$ is continuously translocated between the cytosol and the nucleus, yet activation by upstream ligands causes its prolonged retention within the nucleus, enabling gene expression of target genes. Treatment with tumour necrosis factor- α ($\text{TNF}\alpha$) generates an oscillatory behaviour (Hoffmann et al., 2002; Nelson et al., 2004), but adding bacterial polysaccharides triggers a more gradual, sustained period of nuclear $\text{NF } \kappa\text{-beta}$ (Figure 1.5) (Covert et al., 2005; Lee et al., 2009). The shape of the response is mainly determined by the expression and activation of $\text{I}\kappa\text{B}\alpha$, both, a transcriptional target and negative regulator of $\text{NF } \kappa\text{-beta}$. Pulsatile activation results in the expression of inflammatory response genes, prolonged activation triggers comparable expression of these genes, yet additionally induce cytokine secretion and genes related to the adaptive immune response (Werner et al., 2005). The $\text{NF } \kappa\text{-beta}$ pathway can encode up to 8 different TNF concentrations, and even short stimulation for 1 minute can trigger the full apoptotic outcome (Lee et al., 2016; Tudelska et al., 2017).

Using microfluidics, Tay and colleagues could demonstrate a dosage-dependent fraction of cells responding to the stimulus. This response seems to be a digital process, as activated cells induce transcription of IEGs, independent of the signal intensity. However, transcription of late genes require a prolonged nuclear presence of $\text{NF } \kappa\text{-beta}$, which is only triggered at high concentrations of $\text{TNF}\alpha$ stimulation (Tay et al., 2010). Whether the early genes contribute to shaping the late transcriptional response as seen in the Erk pathway remains to be determined. Apparently, the noise itself is able to contribute to robust signalling. Intrinsic and extrinsic noise enables entrainment, a process of two interacting oscillators eventually assuming the same period, allowing amplification of oscillations and thus transcriptional efficiency (Kellogg and Tay, 2015).

Zambrano and colleagues demonstrated different $\text{NF } \kappa\text{-beta}$ target genes can exhibit distinct dynamics in synchronized populations, and different $\text{NF } \kappa\text{-beta}$ dynamics are decoded into expression of distinct, functionally related gene subsets (Zambrano et al., 2016). This finding could be supported in an elegant study combining live microscopy and single-cell RNA sequencing (Lane et al., 2017). By tracing the nuclear abundance of fluorescently-labelled $\text{NF } \kappa\text{-beta}$ in macrophage-like cells treated with bacterial lipopolysaccharide, they identified three sub-population with different temporal dynamics, highlighting again the heterogeneity of the response. The variability in cellular behaviour towards infectious agents might be desired, since heterogeneity is a basis of the immune system. The three different dynamics are correlated to differential gene expression, enabling various response to an infection in a population of immune cells (Lane et al., 2017).

1.2.1.3 NFAT

Calcium levels control a wide range of biological functions, the spatio-temporal patterns of Ca^{2+} are thought to be a key determinant of cellular outcome (Negulescu et al., 1994; Dolmetsch et al., 1997; Berridge et al., 2003). Depending on the frequency and amplitude of Ca^{2+} oscillations, one of three distinct signalling nodes becomes activated, among them NFAT (Dolmetsch et al., 1997). Apparently, calcium oscillations can already partly be decoded at the level of activation of a specific transcriptional regulator.

NFAT is transcription factor that resides phosphorylated in the cytoplasm, once stimulated by an increase in Ca^{2+} NFAT becomes rapidly dephosphorylated by a calcium-dependent phosphatase and can be translocated

into the nucleus (Klee et al., 1998). The translocation of NFAT proceeds slow, likewise the re-phosphorylation in the cytoplasm, once the stimulus is turned off. This rate limiting step is crucial in decoding Calcium oscillations frequency, as only oscillatory stimuli cause an accumulation of dephosphorylated NFAT in the cytosol, and thus in the nucleus. The cytosolic pool of active, not yet translocated NFAT molecules acts as a working memory of calcium activation (Tomida et al., 2003).

The NFAT family consists of five isoforms, named NFAT1 - NFAT5 (Müller and Rao, 2010). Especially NFAT1, NFAT2 and NFAT4 are important regulators in many immune cells (Macian, 2005). Interestingly, Yissacher *et al* could demonstrate, that NFAT1 and NFAT4 have a diverse dynamic response to a static calcium stimulus (Yissacher et al., 2013). While NFAT1 displays a slow, sustained response with the amplitude correlating to the strength of the stimulus, NFAT4 responds in fast, fixed amplitude bursts in stimulus dependent frequency. The authors hypothesize that this duality in response enables fine tuning of expression of genes transcribed by both, yet did not investigate whether a subset of genes is exclusively transcribed by one of the isoforms. Whether isoform contribute to dynamic variability in other pathways has not been elucidated yet. Sub-cellular Ca^{2+} profiles shape the different temporal profiles of NFAT1 and NFAT4 (Kar and Parekh, 2015). NFAT1 reacts solely to cytoplasmic Ca^{2+} while NFAT4 requires both cytoplasmic and nuclear Ca^{2+} to remain nuclear (Kar and Parekh, 2015).

For more than 30 years, it has been postulated that calcium dependent transcription factors decode stimuli based on the frequency of Ca^{2+} oscillations (Berridge and Galione, 1988; Dolmetsch et al., 1997). New technological development enabled Hannanta-anan and Chow to revisit this model. Using an optogenetic approach they could elegantly manipulate both the frequency and duty cycle independently. The duty cycle is the fraction of a single period, in which the signal is active. In contrast to the previous model, they identified the duty cycle of the calcium oscillations to be the key parameter to fine tune NFAT activation (Hannanta-anan and Chow, 2016). These results are consistent with the previously described working memory of calcium signalling, and makes NFAT an integrator of calcium load (Tomida et al., 2003; Hannanta-anan and Chow, 2016).

1.2.1.4 Msn2

Msn2 is a stress sensing transcription factor in yeast, that remains within the cytoplasm and is phosphorylated in its inactive form. Upon stress, Msn2 is rapidly dephosphorylated, which causes the translocation in the nucleus (Görner et al., 1998). It could be demonstrated, that the identity, certain trigger can be encoded in the temporal profile of Msn2 (Figure 1.5). While glucose starvation causes a oscillatory response of Msn2, oxidative stress triggered a sustained activation (Hao and O'shea, 2012). Interestingly, also the intensity of the trigger is conveyed in the signal. The severity of glucose limitation correlates to the length of the first oscillatory burst, and determines the number of following, weaker bursts (Hao and O'shea, 2012). On the other hand, increase in oxidative stress causes a higher amplitude and prolonged activation (Hao and O'shea, 2012) Pioneering work in signal decoding at the cis-promoter level has been done by Hansen and O'Shea. By pharmacological controlling the phosphorylation state of Msn2, thus its localisation, Hansen and O'Shea were able to control the transcriptional activity in a high temporal resolution (Hansen and O'shea, 2013). Combined with the time-lapse microscopy and high-throughput microfluidics, they could demonstrate that multiple gene expression programs can be encoded in the dynamics of a single transcription factor. Dependent on the Msn2 activation kinetics and the resulting gene expression pattern of individual promoters, they could identify two distinct key features of a promoter, namely amplitude thresholds and promoter activation time-scales and could predict gene expression accordingly. Additionally, they report the dependency of promoter activation time-scale on nucleosome remodelling (Hansen and O'shea, 2013). In a second study, they thoroughly analysed the cis -promoter elements of distinct Msn2-target gene threshold and activation kinetics, and could develop a simple model that can predict promoter behaviour on just three parameters, the number of Msn2-binding-sites, the localization of the TATA box, and the nucleosome organization of the promoter (Hansen and O'Shea, 2015).

1.2.2 p53 dynamics, causes and consequences

One reason the dynamics of p53 received a lot attention within the last decade are the clinical potential of a better understanding of p53 signalling could yield, as it is assumed to be mutated in 50 % of all cancers, and mutations in the p53 pathway occur in virtual all cancers (Vogelstein et al., 2000). Mutation causing aberrant dynamics of p53 response can result in undesired cellular outcomes. A single nucleotide morphism (SNP) in the MDM2 promoter has been reported, which leads to elevated protein levels and thus stronger negative feedback on p53 (Bond et al., 2004). Another MDM2 SNP transforms the physiological oscillatory response to γ -radiation into a sustained response (Hu et al., 2007b). However, its studies to evaluate the effect of this SNP have been contradictory (Bond et al., 2006; Petenkaya et al., 2006; Campbell et al., 2006).

Bar-Or and colleagues were the first to describe the dynamic nature of p53-activation in cultured cancer cells in response to DNA-damage caused by γ -radiation as dampened oscillations when assessing p53 levels with Western Blot (Bar-Or et al., 2000). Examination on the single cell level using a fluorescently-tagged p53 later revealed the same height and duration of these pulses, independent of the intensity of the applied γ -radiation (Lahav et al., 2004; Geva-Zatorsky et al., 2006). Varying pulse numbers and lack of synchronization between single cells led to the miss classification as dampened oscillations at the population level.

These oscillations have also been observed *in vivo* in a transgenic mouse line expressing a luciferase driven by a p53-responsive promoter. When irradiated with γ -irradiation, p53 dependent oscillations of luciferase were monitored in the intestinal tissue. The shape of these oscillations was coherent with those seen in cultured cells. Interestingly, the response to DNA damage was tissue specific, hinting to cell-type specific, distinct composition of the p53 network (Hamstra et al., 2006). One possible cause of differential p53 dynamics in response to genotoxic stress among different tissues and cell types despite having comparable p53 abundance, has been identified as the activity of the kinase ATM the cell-specific efficiency in DNA repair (Stewart-Ornstein and Lahav, 2017). By comparing the response of 12 tumour cell lines DNA damage in individual cells, they found that, even though all cell lines respond by activating p53, the dynamics varied strongly. Interestingly, also the type of dynamical response differs among cell lines. In some cell lines, p53 responded dose-independent, in others, the response was rather dose-responsive.

Oscillations depend on recurrent production and degradation, and initially it was assumed that Mdm2 was sufficient to shape a pulsatile p53 response to γ -irradiation. Collecting quantitative data in a high temporal resolution, Batchelor *et al* could demonstrate that the p53-MDM2 feedback loop is not sufficient for creating the observed oscillations (Batchelor et al., 2008). They could identify a second negative feedback loop required for the pulsatile behaviour. By doing quantitative population and single-cell analysis of multiple proteins in the p53 signalling pathway, and using modelling they predicted that rather pulses of upstream proteins that sense DNA-damage and initiate p53 activation shape the dynamic response of p53. The phosphatase Wip1 was identified as the central mediator of this second feedback loop. Wip1 phosphorylates both, ATM and Chk2, both activators of p53 to suppress activation. On the other hand, Wip1 is a transcriptional target of p53. It was hypothesised, that DNA damage is evaluated by ATM, and if not repaired yet, further pulses are triggered.

Originally, p53 pulses have been thought to occur only in stress-conditions. Yet, it could be demonstrated that unstressed cells exhibit transient, spontaneous p53 pulses (Loewer et al., 2010). The correlation of the p53 pulses to cell-cycle stages with increased risk of DNA damage, suggesting that these are caused by spontaneous DNA damage. In contrast to pulses caused by radiation or drugs, the transient activation of p53 in non-stressed cells did not result in expression of p21, or trigger an arrest of the cell cycle. It was further demonstrated, that the p53's acetylation of K373 and K382 differ between non-stressed and stressed conditions, complete acetylation only occurred in stressed conditions, and was almost not present in unstressed conditions.

Batchelor and colleagues were able to show that distinct stresses cause different dynamics of p53 with distinct features (Figure 1.6) (Batchelor et al., 2011). While p53 activation caused by neocarzinostatin (NCS), a DSB causing drug, triggers pulses with a fixed length and amplitude, UV-radiation causes long, sustained activation. In the

latter case, the level of activation is dosage dependent. Continuation of the non-oscillatory, sustained activation of p53 is linked to permanent cell cycle arrest or apoptosis (Chen et al., 2013). The distinct activation patterns between mild DNA damage (NCS treatment or γ -radiation) and more severe stress (UV radiation) correlates to the activation of different subset of target genes in response to the respective stress input (Zhao et al., 2000). Whether the dynamical behaviour of p53 activation actually causes expression of a specific subset of target genes and hence trigger a distinct cellular effect, or whether they are just the byproduct caused by the activation via different upstream pathways remains elusive.

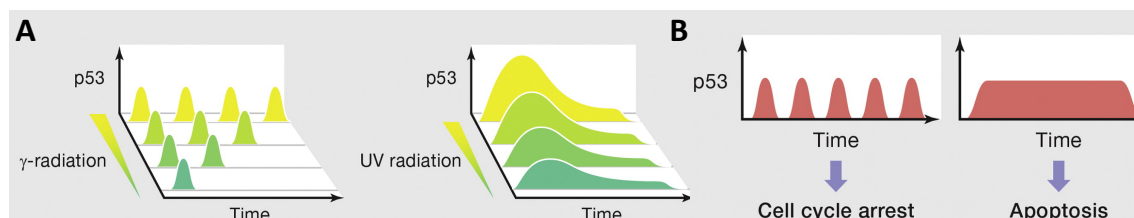


Figure 1.6: Identity and intensity of upstream trigger are decoded in p53 dynamics and determine cellular outcome

A | Activation due to γ -radiation causes an oscillatory response, which frequency is dependent on radiation intensity, while p53 activity is sustained upon UV-radiation. Amplitude is depending on the amount of UV-radiation.

B | Temporal profiles of p53 activity are associated to distinct subsets of target genes, triggering defined phenotypes.

Adapted from (Purvis and Lahav, 2013).

To examine the tie between the p53 activation pattern and the expression of target gene subsets eventually leading to distinct phenotypic outcome, Purvis and colleagues used nutlin3, a small molecule which binds to Mdm2, inhibiting degradation of p53 to shape the p53 response (Purvis et al., 2012). They were able to transform the pulsatile response caused by γ -radiation, into a sustained response by adding nutlin3. By doing so, they could drive cells treated with γ -radiation into senescence, a phenotype caused by UV-radiation. Furthermore, it could be demonstrated that in response to the chemotherapeutic drug cisplatin cell fate is rather determined by the kinetics of p53 accumulation than overall p53 abundance (Paek et al., 2016).

The formation of the different shapes of p53 activation have been investigated thoroughly, and can be described fully by negative feedback loops (Lahav et al., 2004; Batchelor et al., 2008). Since distinct p53 behaviour was linked to different cellular outcomes (Batchelor et al., 2011; Purvis et al., 2012), it seems likely that the dynamical nature of p53 encodes information, most notably the severity of stress, which is then decoded at promoter level, to execute the desired phenotypic outcome.

To answer this question, Hafner *et al* carried out an extensive study, using time-course ChIP-seq measurements and RNA sequencing and correlated nucleosome binding to mRNA expression (Hafner et al., 2017). Several subsets of gene expression patterns had been identified, which had been observed before and are caused by the stability of the single mRNAs (Melanson et al., 2011; Porter et al., 2016). Surprisingly, Hafner and colleagues could not determine differences of p53-binding to the promoter of the distinct gene subsets, rather they observed uniform occupancy of p53-promoters (Hafner et al., 2017).

As fascinating and insightful these studies revealing the impact of p53 dynamic have been, they relied on rather indirect and harsh methods to manipulate p53. Studies relying on γ radiation as a trigger of p53 activation often neglect that such treatment causes a plenty of feedback, yet not limited to p53 response. In absence of p53, γ radiation can still trigger cell cycle arrest or apoptosis (Halacli et al., 2013). Similarly, UV irradiation can induce transcription of p53 target gene p21 independent of p53 (Haapajarvi et al., 1999). In addition, drugs to manipulate p53 levels bear side effects influencing the cellular response. Nutlin 3, used to interfere with MDM2's control of p53 levels, also disturbs MDM2 activity next to p53 regulation, for example regulating DNA repair (Alt et al., 2005; Bouska et al., 2008; Conradt et al., 2013; Carrillo et al., 2015). Additionally, Cisplatin treatment induces a wide range of signalling pathways besides p53 (Dasari and Tchounwou, 2014).

Addressing these experimental limitations require a more specific and direct approach, to enable precise perturbation of the p53 network in the absence of upstream stress signals. Only so, cause and effect can be entangled.

1.3 Optogenetics

The advent of fluorescent probes and high resolution live-cell imaging empowered scientists to observe cellular processes at a unprecedented spatial and temporal resolution (Toettcher et al., 2011). The observation of protein levels and localization demonstrated how dynamic processes are within cells. Yet, as methods for observation dynamic processes led to a new appreciation of molecular processes, the abilities to quantitatively describe their mechanisms lagged behind. Classical genetic perturbation (knockdown, overexpression) enabled thorough interrogation on which proteins contribute to a given phenotype, but are less powerful in explaining underlying mechanisms. Additionally, genetic perturbation are slow and/or irreversible, giving cells enough time to adapt to the perturbed status and thus are more likely to impair rather than adjust the spatio-temporal features of a network.

Chemical perturbation methods like small molecules take effect on a shorter timespan, but lack reversibility unless applied in a more complicated experimental setup. Small molecules lack spatial control, and the number of highly specific small molecules is limited, as these often exhibit undesired off-target effects and thus require extensive engineering (Bishop et al., 2000).

To fully comprehend the dynamic nature of a network in a quantitative manner, perturbation methods are required that grant selective inhibition or activation of targeted nodes within the network. Optogenetics employs light-responsive proteins (photoreceptor) that offer a potential revolutionary new approach to overcome aforementioned limitations. The key features making sensory photoreceptors so versatile encompass the use of light to trigger cellular events, that offers an unmatched spatial and temporal resolution (Ziegler and Möglich, 2015). Light is an inert trigger, penetrating tissue up to a certain wavelength dependent depth (Weissleder and Ntziachristos, 2003). Irradiation with light in the visible spectrum does commonly cause no adverse side effects, unless applied in high intensities or for a prolonged period. Additionally, photoreceptors operate reversibility, enabling repeated and permanent control. As photoreceptors are genetically encoded, they can be combined with a wide range of available and established genetic tools, allowing cell types or tissues specific expression and defined subcellular localization (Ziegler and Möglich, 2015). The combination of these features enabled scientists to actively perturb cellular systems and quantitatively interrogate dynamic processes at a previous unthinkable resolution (Toettcher et al., 2013; Hannanta-anan and Chow, 2016; Wilson et al., 2017).

Nobel laureate Francis H Crick envisioned already in 1999 the possibility to use light to control cellular processes (Crick, 1999), and shortly after, Crick's vision came to life. In 2005, Deisseroth and colleagues were the first to express the microbial, light-gated channelrhodopsin-2 from *Chlamydomonas reinhardtii* in mammalian neurons, and apply blue light pulses to control cell depolarization in a millisecond time scale (Boyden et al., 2005). In the same year, Gottschalk and colleagues demonstrated the exiting *in vivo* possibilities optogenetics offers, when expressing the same channelrhodopsin-2 in *C. elegans* to trigger rapid behavioural changes (Nagel et al., 2005). Shortly after, the term optogenetics was established (Deisseroth et al., 2006). Initially almost exclusively used to control neuron polarisation via light-gated ion channels and light-driven ion pumps, the development of optogenetic tools to control a broad range of non-neuronal, intracellular processes have made optogenetics more accessible and widely used (Möglich et al., 2009a; Levskaia et al., 2009; Mills et al., 2011).

In the following, I want to give a brief overview over photoreceptors, specifically the Light-oxygen-voltage(LOV) domains. A particular focus is on the LOV domain used in this thesis, the AsLOV2 domain. I will review key steps in the history of optogenetic usage of this domain and show examples and strategies of its employment in non-neuronal optogenetics. Lastly, I will present the way the AsLOV2 domain was used to enable light controlled protein translocation.

1.3.1 Photoreceptors

Light is an essential carrier of information, and species of all kingdoms of life employ genetically encoded photoreceptors to integrate light sensing on the molecular level (Briggs and Spudich, 2005). Light-dependent information encompasses a wide range of biological functions, ranging from phototaxis and phototrophism over circadian clock maintenance to visual detection in higher organisms.

As cellular membranes are virtually transparent to light, most photoreceptors are soluble and thus cytoplasmic. Characteristic absorption profiles span the solar spectrum from near UV (350 nm) to far red (750 nm) and matches the light they are usually exposed with. In general, photoreceptors possess two principal functions: First, a photosensory module, which absorbs light, and secondly the effector module that utilizes the energy harvested by photosensory module to exert biological activity. Since neither the polypeptide backbone nor the amino acid side chains absorb light in the visible spectra, photosensors use organic, nonproteinogenic molecules called chromophore within their photosensory module. Thus, the absorption spectra is based on the chromophore. The chromophores are partly unsaturated, and contain a conjugated π electron system allowing electron delocalization upon photon absorption. The size of the conjugated π system determines the extent of electron delocalization and the absorption spectrum. The energy absorbed by the chromophore is then conveyed to the protein causing a transformational change from the so called dark stage to the active lit state and triggering the effector module to exert its function.

Each photoreceptor can revert back from its active state to the inactive, dark state, yet the mechanism of this reversion varies between the different photoreceptor types. Recovery can occur spontaneously with half lives ranging from seconds and minutes (for some LOV domains (Salomon et al., 2000)) up to hours or even days (for UVR8 (ultraviolet-B receptor), (Heijde and Ulm, 2013)). Other photoreceptors like phytochromes, cyanobacteriochromes and many rhodopsins are photochronic, the lit state can be reversed by exposure with light of a defined wavelength (Sharrock and Quail, 1989; Ziegler and Möglich, 2015).

Based on the type and photochemistry of the chromophore, photoreceptors can be classified in several major groups: rhodopsins, LOV domains, BLUF proteins (blue-light sensors utilizing flavin adenine dinucleotide), cryptochromes, phytochromes, and Xanthopsins (Figure 1.7) (Möglich et al., 2010).

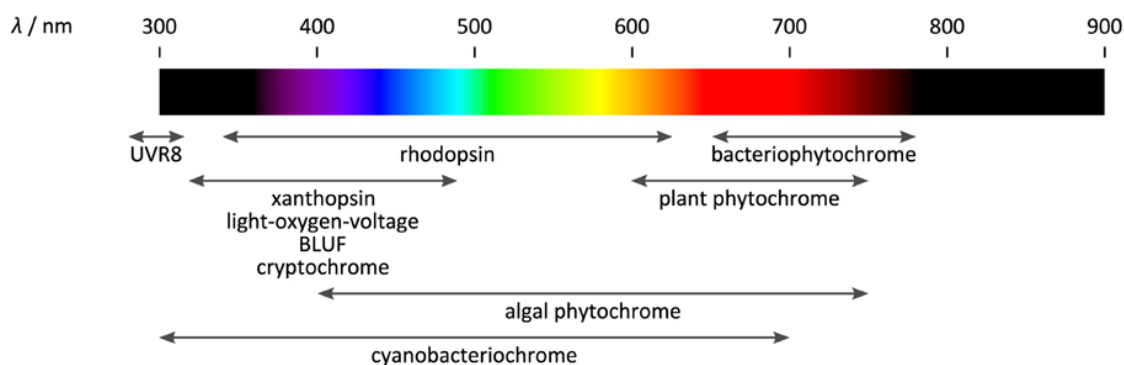


Figure 1.7: Excitation spectra of different photoreceptor families

Adapted from Ziegler and Möglich (2015).

Rhodopsins, further classified in two subgroups, microbial rhodopsins and G protein coupled rhodopsins use a retinal chromophore for photon absorption (Spudich and Bogomolni, 1984). The photoactivity of xanthopsins, also called photoactive yellow proteins (PYP), is based on the chromophore p-coumaric acid (Kort et al., 1996). Phytochromes and cyanobacteriochromes employ bilin-derivatives as chromophores, such as phytochromobilin or phycoviolobilin and phycocyanobilin, respectively (van der Horst and Hellingwerf, 2004). Upon photon absorption, these chromophores undergo cis-trans isomerization, causing the transition into the active lit state (van der Horst and Hellingwerf, 2004). In contrast, cryptochromes, LOV domains and BLUF proteins exhibit a more diverse photochemistry, based on flavin nucleotides (van der Horst and Hellingwerf, 2004). An exception

is the *Arabidopsis thaliana* UVR8 protein, a photoreceptor independent of an externally produced cofactor. UVR8 is dimeric and exhibits pyramid shaped formation. Here, the tryptophan sidechains at the binding interfaces of the dimer-dimer act as a photon absorber and initiates reversible disruption of the dimer-dimer interface and thus the separation of the dimers (Christie et al., 2012; Wu et al., 2012).

1.3.2 LOV domains

The first LOV domain was identified within the *Arabidopsis thaliana* gene non-phototropic hypocotyl (*nph*), being responsible for phototropism and thus subsequently renamed Phototropin 1 (Huala et al., 1997; Salomon et al., 2000). Since the first discovery, they have been shown to exist in algal, fungal, bacterial, protist and plant species, where they mediate the reaction upon blue light absorption (Crosson et al., 2003). In a recent computational analysis across 42 million open reading frames discovered around 6700 LOV domains (Glantz et al., 2016). As a photosensory domain, LOV2 domains can trigger a diverse set of effector domains, for instance, DNA or RNA binding, metabolic function or cell signalling (Crosson et al., 2003). Yet, many of the *in situ* suggested LOV domains, have not been tested in the wet lab, and are associated to effector domains with unknown functions (Glantz et al., 2016). This promises a wide range of new biological activity controllable by blue light, as recently highlighted by the identification of a new LOV domain allowing light controlled membrane association (Glantz et al., 2018).

In general, LOV domains consist of one or more sensor domain(s), responsible for absorbing blue light and exerting action on the effector domain, commonly mediated by a α -helical linker connecting the two parts (Harper et al., 2003). Structurally, LOV domains are part of the Period-ARNT-Single-minded (PAS) domain family, a group of proteins that act as sensors for among others oxygen, redox potential and light (Taylor and Zhulin, 1999). LOV domains associate non-covalently with either a flavin based cofactor, either flavin mononucleotide (FMN) or flavin-adenine dinucleotide (FAD) (Salomon et al., 2000; Möglich et al., 2010).

The core of the LOV domains is constituted by a set of 110 amino acids that form the PAS defining fold of a central, 5-stranded anti-parallel β -sheet and a helical face, that bind the chromophore (Zoltowski and Gardner, 2010). Blue light absorption triggers a covalent thioether bond between the conserved cysteine residues of the PAS core and the cofactor (Salomon et al., 2001; Crosson and Moffat, 2002). The formed covalent adduct conveys a transformation change spreading throughout the LOV domain due to rearrangement of several non-covalent bonds, usually hydrogen bonds (Crosson and Moffat, 2002; Fedorov et al., 2003; Harper et al., 2003). These structural rearrangements are passed on to the effector domain, typically by relaxation of formerly inflexible structures (Harper et al., 2003, 2004).

One of the optogenetic workhorses is the monomeric, LOV domain AsLOV2 domain derived from phototropin 1 of the common oat *Avena sativa* (Harper et al., 2003). In contrast to other members of the LOV domain family, AsLOV2 is a non-associating photoreceptor, meaning formation of the lit signalling state is not accompanied by

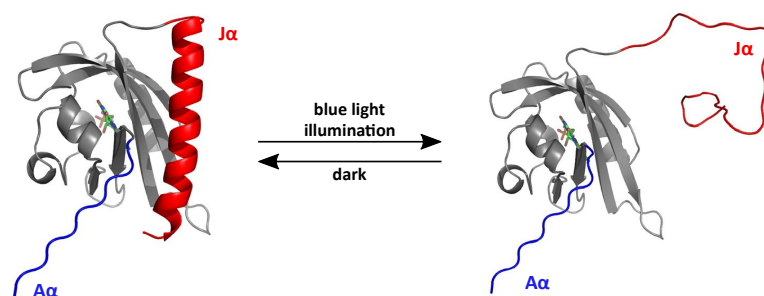


Figure 1.8: Blue light-induced exposure of the C-terminal J α -helix of AsLOV2

Upon blue photon absorption, the Flaviomononucleotide chromophore triggers a structural rearrangement causing a transformational change throughout the AsLOV2 and leads to the exposure of formerly bound J α -helix. Adapted from Zayner et al. (2012).

adjustments of the oligomeric state (Ziegler and Möglich, 2015). The PAS core consists of four α -helices packed to both sides of four antiparallel β -sheets (Möglich et al., 2009b). On the N- and C-terminus there are two additional helices, the $A\alpha$ and the $J\alpha$ (Harper et al., 2003). In the inactive dark state, the C-terminal $J\alpha$ is tightly packed within the PAS core, masking hydrophobic residues of the central β -sheet (Halavaty and Moffat, 2007). Once the chromophore FMN absorb photons (Peak of absorbance at 447 nm), a structural rearrangement occurs and triggers an unfolding of both, the $A\alpha$ and the $J\alpha$ (Halavaty and Moffat, 2007; Zayner et al., 2012) (Figure 1.8). In nature, this conformational change triggers the activation of the kinase domain of phototropin 1 (Harper et al., 2004).

The recovery to the inactive dark state occurs spontaneously and is caused by a base-catalysed mechanism leading an disruption of covalent linkage between the cysteine in the active center of the AsLOV2 domain and its chromophore (Alexandre et al., 2007). With a photocycle lasting around 80 s the AsLOV2 belongs to the group of fast cycling LOV domains (Pudasaini et al., 2015). Yet it is important to note, that LOV domains exhibit rather an equilibrium of caged and an uncaged state rather than a finite defined state (Harper et al., 2003; Halavaty and Moffat, 2007). This equilibrium is shifted towards the caged state in the dark, and vice versa to the active state upon blue photon absorption (Yao et al., 2008). While this dynamic equilibrium is already saturated at moderate light intensities in LOV domains with a slower photocycle, fast cycling LOV domains exhibit a higher sensitivity to light and increased dynamic range in the equilibrium (Pudasaini and Zoltowski, 2013). Over the years, various mutations have been described to shift the equilibrium towards are more desired state, and alter the photocycle kinetics allowing fine tuning activation kinetics to fit a particular need (Strickland et al., 2010; Zayner et al., 2013; Diensthuber et al., 2014).

1.3.3 Light-dependent allostery using AsLOV domains in non-neuronal optogenetics

The majority of optogenetic tools based on LOV domains can be classified in employing two different strategies (Figure 1.9). The first strategy makes use of the key feature of associating LOV domains, the change of the oligomeric state due to the structural change upon blue light illumination. This group can be further subdivided in either blue light responsive homo- or heterodimerization, as well as photoactivatable dissociation of previously associated proteins. The second strategy is based on the light-dependent allostery, meaning a signal activated due to a transformational change of a single LOV domain upon light illumination.

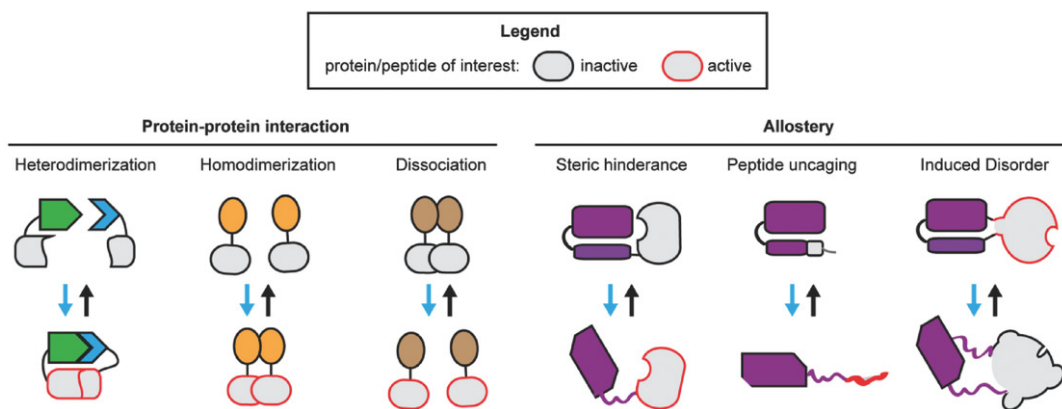


Figure 1.9: Overview of different optogenetic strategies employed using the AsLOV2

Adapted from Hoffmann et al. (2018).

The AsLOV2 domain is a prime example for a photoreceptor utilized in light-dependent allostery. Here, scientist make use of the light induced unwinding and exposure of the initially caged AsLOV2 $J\alpha$ helix. The modular architecture of photoreceptor, with a clear separation between the light absorption module and the signal trans-

mitting module allows for a high degree of customization and the design of a single component tool, with both the AsLOV2 and the effector domain in one construct.

As most cellular processes depend on protein-protein interaction, the possible application are extensive. Yet, the development of such tools is not trivial, as the residual activity in the dark due to the existing equilibrium limits the potential dynamic range of a optogenetic tool. Additionally, it requires substantial engineering to position both parts to guarantee a light controlled activation.

The first successful use of the AsLOV2 was carried out by Strickland et al., by fusing the *E. coli* transcription factor trp repressor (TrpR) to the AsLOV2 creating a light-activatable DNA binding protein called LOV-TAP (Strickland et al., 2008). The characteristic N-terminal helix of TrpP needs to associate with the protein core to trigger DNA binding. Yet, arranging the AsLOV2 domain N-terminal to the TrpR created a chimeric helix composed of the AsLOV2 domain C-terminal J α helix and the N-terminal-helix of TrpR. This chimeric helix is bound to the AsLOV2 domain in the dark, upon photoactivation it disassociates and binds the TrpP core to trigger DNA binding (Strickland et al., 2008). Eventhough the performance of this system was rather weak, it served as proof of concept for further development. Additionally, it could be further improved by the introduction a range of mutations within the chimeric helix to enhance its stability and binding to the core of the AsLOV2 (Strickland et al., 2010).

Shortly after, a strategy to control the function of protein of interest was presented, that aims at introducing the AsLOV2 is introduced in an allosteric surface in proximity to the active center of the protein (Lee et al., 2008). Statistical coupling analysis was used to evaluate sites as potential localization of the AsLOV2 to enable light-dependent control of disruption of the required allosteric surface (Lee et al., 2008). While the chimeric protein designed in this study showed only mild activation, it was a ground breaking approach. This approach was later revised, and several proteins of three different classes were successfully engineered to be controllable by light, due to insertion of the AsLOV2 in computationally determined protein loops close to the active site (Dagliyan et al., 2016). Due to the close proximity of the AsLOV2 N- and C- Terminus, the insertion in protein loops barely causes a loss in function. Upon photoactivation, the distance between the termini increases drastically and causes local disorder close to the active center and thus a loss of function (Dagliyan et al., 2016). This approach established a new subcategory of tools that trigger light induced disorder. Until then, AsLOV2 were widely used for creating a sterical hindrance, which can be turned on and off by light, and by photocaging of small peptides in the J α -helix.

1.3.3.1 Sterical hindrance of accessibility C-terminal attached protein

Steric hindrance is a more simplistic approach introduced by Hahn and coworkers in 2009 (Wu et al., 2009). Rather than creating a complex chimeric fusion protein, they attached the AsLOV2 N-terminally to a protein of interest, namely the Rac1 small GTPase and made use transformational change the AsLOV2 undergoes upon light illumination (Wu et al., 2009). In the dark state, the J α helix is tightly associated to the core of the LOV domain, thus the C-terminally attached protein is located in close proximity to the LOV domain, and hardly accessible to the cellular environment. The fusion protein called photoactivatable Rac1 (PA-Rac1) enabled remote control of motility in fibroblasts expressing PA-Rac1 (Wu et al., 2009). As this perturbation was highly specific, it permitted a better understating of the crosstalk between Rac1 and Rho signalling, both regulators of cell migration (Wu et al., 2009).

Trivial as this strategy may have appeared, difficulties in transferring this approach to control activity of even closely related GTPases surprisingly failed (Winkler et al., 2014). Further structural investigation of the Rac1-LOV2 interface and its light induced transition revealed a serendipitously calcium binding site introduced in the interface, that appears to be essential for the light-dependent function (Winkler et al., 2014).

Nevertheless, this rather straightforward approach of fusing the AsLOV2 N-terminal to a protein of interest was successfully applied to various proteins. Scientist used this approach to engineer a photoactivated caspase 7 to trigger apoptosis (Mills et al., 2011), mediate activity of a Ca²⁺ channel (Pham et al., 2011) or potassium chan-

nel (Cosentino et al., 2015), maintain optical control of mDia, a formin inducing the assembly of nuclear actin network (Baarlink et al., 2013), generate a mean to regulate local peptide ligand concentration by light (Schmidt et al., 2014), ascertain control of light induced post-translational control function by intein-mediated protein splicing (Wong et al., 2015; Jones et al., 2016) or enable the investigation of the unmodified cargo carrier myosin V1 (French et al., 2017).

The apparent limitation of this approach is the dependency of a small spatial proximity of the AsLOV2 and the effector domain to the protein of interest. Efforts in implementing short truncations on either the target proteins N-terminus or the AsLOV2 (Baarlink et al., 2013) and introducing linkers, the room for improvement remains limited. An approach to bypass this limitation is the introduction of the AsLOV2 into inter-domain linkers of the target proteins, as suggest in two studies successfully controlling caspase 3 (Smart et al., 2017) and pyruvate kinase M2 (Gehrig et al., 2017). Yet, this approach affords more complex engineering and optimisation.

1.3.3.2 Photocaging of peptides in the J α helix

An alternative strategy is peptide photocaging. Rather than fusing a effector domain C-terminal to the J α helix and controlling accessibility by due to sterical shielding, a short peptide with a defined biological function attached to the J α helix C-terminus (Figure 1.10). As the crystal structure of the AsLOV2 hints to the possibility to bury small peptides in its core in the dark state, it was proposed that by exchanging parts of the C-terminus of the J α helix by a peptide with a biological function, one can exert this function in response to light, given that the light responsive transformational change is not abolished due to truncation (Halavaty and Moffat, 2007). Introduction of peptide epitope should lead to a limited accessibility in the dark state, due to its size.

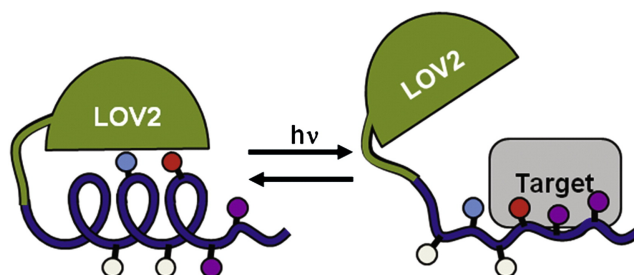


Figure 1.10: Peptide photocaging within the C-terminal J α helix of AsLOV2

Sequence chimera of a peptide and the J α helix can be exposed in a light-dependent fashion. Crucial for photoactivity are both residues crucial for helical folding (blue), residues for peptide function (purple) or both (red). Non-relevant residues can be mutated to fine-tune either peptide activity or photocaging. Adapted from Lungu et al. (2012).

Strickland *et al* created the first optogenetic employing this strategy to enable fine tuned optical control of protein localisation within mammalian cells (Strickland et al., 2012). In an approach labelled tuneable, light-controlled interacting protein tags (TULIPs), the peptide known to bind highly specific to engineered PDC (ePDC) was fused to the C-Terminus of the J α in a serial truncation up to the isoleucine at position 539, as this site is crucial for dark-state recovery (Harper et al., 2004; Strickland et al., 2012). Both the high affinity and specificity of ePDC is dramatically increased due to directed evolution (Huang et al., 2008). EPDZ can be fused to any protein of interest, to enable light controlled association with the AsLOV2. Thus, by defining the localization of the AsLOV2 with localization tags, in this case a membrane binding motif, the protein of interest fused to ePDC can recruited to the membrane in upon blue light photo absorption (Strickland et al., 2012). This system has also been used to modulate kinesin- and dynein dependent transport of organelles (Van Bergeijk et al., 2015), yet its use is limited due to the comparably low dynamic range.

In close analogy, Hahn and colleagues presented two optogenetic tools based on the same principle (Lungu et al., 2012). Yet, instead of choosing peptide candidates due to their exceptional high affinity and specificity,

the screened for peptide sequences, which resemble the endogenous J α helix to limit alteration of its sequence. Using this approach, they could demonstrate light controlled heterodimerisation of AsLOV2-SsrA chimera and any protein of interest fused to the bacterial SspB (Lungu et al., 2012). Eventhough the induction of SsrA-SspBr showed a low dynamic range, it could later be a dramatically improved by a combination of computer aided design and phage display selection, leading to widespread use of the then called improved light-induced dimer (iLID) system (Guntas et al., 2015).

Both, TULIPs and iLID feature peptide-protein interaction originated in bacterial organisms, making them orthogonal tools and limiting unwanted effects on the host system. Yet, manipulation of endogenous proteins is somewhat restricted, unless the protein domains are introduced in the endogenous gene locus, which is laborious and error prone. Thus, to exert function on endogenous proteins, several approaches using short peptides exhibiting a biological function have been used to create chimeric peptide-J α proteins. This approach has been demonstrated successfully in light-dependent recruitment of endogenous vinculin (Lungu et al., 2012), peroxisomal trafficking (Spiltoir et al., 2015), induction of apoptosis (Mart et al., 2016), controlling endogenous kinase activity (Yi et al., 2014) and protein degradation (Renicke et al., 2013; Bongers et al., 2013; Sun et al., 2017).

Important to note, that there is an inherent trade off between truncations too long and compromising the helical structure J α helix and thus the ability to photocage an epitope, and a too short truncations, allowing peptide-protein interaction in both, dark and lit state.

1.3.4 LINuS and LEXY, moving proteins in and out of the nucleus

Many signalling pathways eventually converge in the nucleus to mediate transcription or epigenetic regulation. To enable eucaryotic cells to respond rapidly to internal and external trigger, signalling molecules exerting a nuclear function are often already preproduced, but kept in different compartments, mostly the cytosol. Upon stimulation, localization sequences within the signalling protein become either accessible or blocked, leading to the mediated translocation into the nucleus. Thus, controlling nuclear localization is a common mean to mediate protein activity and grants a more rapid response than starting production upon stimulation (Purvis and Lahav, 2013; Di Ventura and Kuhlman, 2016).

In general, while proteins smaller than 40 kD can passively diffuse into the via nuclear pores, larger proteins dependent on active support of transport receptors when translocating in or out of the nucleus (Mohr et al., 2009). Karyopherins are the most common group of proteins regulating transport of protein cargo, generally by binding to short, linear localization sequences within the cargo protein (Chook and Süel, 2011). Importin- α is the major import receptor and recognizes NLS sequences, while NES sequences are bound by the nuclear export receptor CRM1 (chromosome region maintenance 1, exportin1) (Hutten and Kehlenbach, 2007). Noteworthy, NLS and NES motifs of different affinities exists, which exhibit a wide range of transport efficiencies (Kutay and Güttinger, 2005; Hodel et al., 2006).

As nuclear translocation is at the center of many biological pathways, many tools to take control over localization of proteins have been developed. While several chemical methods to control nuclear translocation have been developed (Klemm et al., 1997; Kudo et al., 1999; Bayle et al., 2006; Kakar et al., 2007; Haruki et al., 2008), they either are irreversible, have slow kinetics and high background or potential side effects, rendering them suboptimal for mimicking a highly dynamic and reversible process. Efforts in combining chemical and light approaches to mediate translocation improved translocation speed and reduced background drastically, yet lacked reversibility (Watai et al., 2001; Engelke et al., 2014).

The first fully reversible tools to control nucleo-cytoplasmic translocation were build using the two-component PyhB/PIF (Pythochon B/Pythochrome interacting factor) system (Yang et al., 2013; Beyer et al., 2015). Illuminated with red light, the two components associate rapidly, and remain in a bound state until irradiated with infrared light (Ni et al., 1999; Zhu et al., 2000). The tools based on the PhyB/PIF system enable fast and reversible translocation (Yang et al., 2013; Beyer et al., 2015), yet demands a more elaborate experimental set up. Due to its

two-component nature, titration of both components is necessary to ensure the right ratio of expression. Additionally, PhyB requires the addition of its chromophore phycocyanobilin (PCB), and illumination with UV light is necessary to reverse nuclear translocation.

To address the limitations of the existing tools, two single-component systems based on the AsLOV2 have been developed (Niopek et al., 2014, 2016). Both are small, versatile protein tags, that expose engineered localization sequence photocaged in the AsLOV2 γ - α helix in response to blue light (Niopek et al., 2014, 2016). LINuS (light-inducible nuclear localization signals) exposes an engineered NLS, triggering rapid photoactivated nuclear translocation of any tagged protein (Niopek et al., 2014), vice versa, LEXY (light-inducible nuclear export system) causes fast cytoplasmic translocation (Niopek et al., 2016) (Figure 1.11). Once deactivated, both systems rapidly recover to the pre-illuminated state (Niopek et al., 2014, 2016).

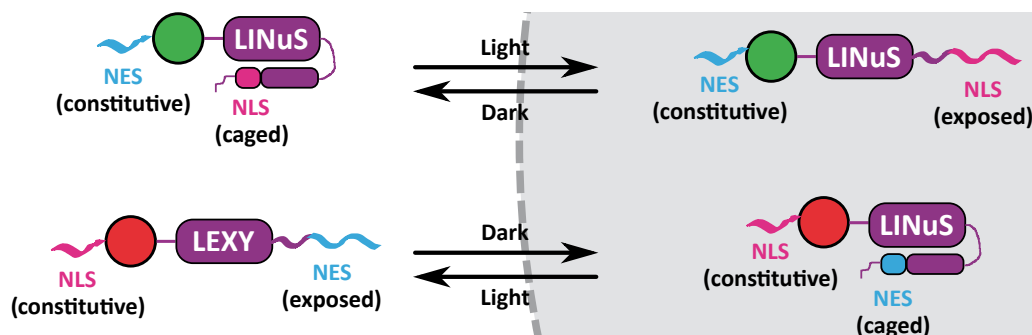


Figure 1.11: LINuS and LEXY - small tags to gain photoactive, reversible control of protein import or export

LINuS or LEXY expose an engineered NLS or NES upon blue light absorption, triggering rapid translocation of fused protein of interest. In the absence of light, both recover to the initial dark state.

Adapted from Hoffmann et al. (2018).

LINuS and LEXY have been demonstrated to robustly translocate a wide range of proteins when fused either to their N- or C-terminus (Niopek et al., 2014, 2016). Several different LINuS and LEXY versions exposing localization sequences exhibiting different translocation efficiencies allowing precise fine-tuning of localization of cargo proteins (Niopek et al., 2014). Moreover, two almost identical systems, LINX and LANS have been developed independently, further highlighting the robustness of this approach in a wide range of protein and cell lines (Yumerefendi et al., 2015, 2016).

1.4 Aim of this study

Many signalling pathways resemble each other in their structure. Multiple inputs converge into a single, central node, commonly a transcription factor. Growing evidence supports the notion that transcription factors integrate information from multiple upstream stimuli and execute the appropriate response by turning on specific gene expression programs.

The tumour suppressor p53 exhibits distinct activation dynamics. p53 dynamics are defined as the shape of the curve characterizing how the levels, activity, modification state or localization of p53 changes over time. The curve encodes information in features such as amplitude or frequency.

p53 dynamics are determined by the stress triggering these dynamics. For instance, in response to γ -radiation p53 levels show pulses of fixed amplitude and period whose number is determined by the intensity of the γ -radiation. Different p53 temporal patterns are linked to different cellular fates. While it has been established which factors determine p53 dynamics, our understanding of the mechanisms at play that decode these dynamics into specific gene expression programs and subsequent cell fates remains limited.

In this study, I aimed at deepening our understanding of the role of p53 dynamics in dictating which genes are expressed using state-of-the-art optogenetic tools to manipulate either p53 levels or localization in mammalian

cells. In this set-up dynamics can be studied in the absence of an upstream stress.

To control protein levels of endogenous p53 I investigated several approaches that ultimately aimed at preventing inactivation and degradation of p53 by the E3 ubiquitin ligase Mdm2. Light-mediated inhibition of degradation would allow fine-tuning of p53 levels, and thus enable application of p53 dynamics.

To control the localisation of exogenously expressed p53 I employed the optogenetic tools LINuS and LEXY. Cytosolic sequestration of transcription factors is a common mechanism to keep these signalling molecules dormant, while active nuclear translocation allows rapid response to external stimuli. Due to the velocity of import and export, active translocation of p53 would allow application of p53 dynamics of high temporal resolution.

Once the methodology to control p53 dynamics is established, I plan to apply distinct p53 dynamics and test if they lead to the expression of different p53 target genes and consequently to different cellular fate. Precise application of p53 dynamics should enable us to understand the regulatory mechanisms involved in decoding these dynamics into specific transcriptional responses.

2 Material and Methods

2.1 Plasmid generation

All plasmids were constructed using traditional restriction enzyme cloning, in some cloning steps also type IIS restriction enzymes were used. Restriction enzymes were obtained from New England Biolabs (NEB). Oligonucleotides were obtained from Sigma-Aldrich. Polymerase chain reaction amplification (PCR) was carried out using Phusion Flash High Fidelity Master Mix (Thermo Fischer Scientific, F548S) according to the manufacturer's protocol. PCR products were visualized in a 1% Agarose gel and subsequently purified with the Qiagen Gel Extraction Kit (Qiagen, 28704). Restriction digests were carried out at 37°C for 1 hour. The PCR purification kit (Qiagen, 28104) was used to purify the digested PCR product. Ligation was carried out with T4 Ligase (NEB, M0202S) according to manufacturer's suggestions. The ligation product was transformed in One Shot™TOP10 Chemically Competent E. coli (Thermo Fischer Scientific C404010). Then, bacterial cells were selected on Lysogeny Broth (LB) agar plates, containing either 100 µg ml⁻¹ ampicillin or 50 µg ml⁻¹ kanamycin. Single Colonies were amplified in liquid LB cultures containing the respective antibiotic. The plasmid DNA extraction was carried out using the Qiagen Plasmid Miniprep Kit (Qiagen, 27104) or the Plasmid Maxi kits (Qiagen, 12162). Isolated DNA was verified by Sanger sequencing, carried out by GATC Biotech. A list of constructs used in this study is provided in the appendix.

2.2 Cell culture and cell lines

2.2.1 Cell culture and cell lines

The human non-small cell lung carcinoma cell line H1299 was kindly provided by Prof. Alexander Loewer, TU Darmstadt. The human colon carcinoma cell line HCT116 p53^{+/+} was kindly provided by Prof. Thomas Hofmann, Uni Mainz. H1299 cells and MCF7 cells were cultured in RPMI 1640 Medium (Thermo Fischer Scientific, A1049101) supplemented with 10% fetal calf serum (FCS, Biochrome, S0115) and 100 U ml⁻¹ penicillin and 100 µg ml⁻¹ streptomycin (PenStrep, Thermo Fischer, 15140-122). HCT116 cells were maintained in Dulbeccos phenol red-free Dulbecco's Modified Eagle Medium (Thermo Fischer, 31053) supplemented with 10% FCS, 2 mM L-glutamine (Thermo Fischer, 25030-024) and 1% PenStrep. All cell lines were cultured at 37°C and 5 % CO₂ in a humidified tissue culture incubator.

2.2.2 Transient transfections

Cells were seeded in 6-well plates (Corning, CLS3335) at densities of 200000 (for H1299), 300000 (HCT116) and 300000 (MCF7-p53-Venus) cell per well for experiments lasting 24 hours post transfection. For longer experiments, cell densities were reduced by 50% per 24 h to prevent overgrowth. The next day, transfection was performed with Lipofectamin 2000 (Invitrogen, 11668019) according to the manufactures protocol. Following DNA and Lipofecatmin amounts were used:

Cell Line	Stuffer DNA	Construct DNA	Lipofectamin
H1299	900 ng	100 ng	2 μ l
HCT116	2250 ng	250 ng	4,8 μ l
MCF7	1750 ng	250 ng	3 μ l
MCF7-p53-Venus	1750 ng	250 ng	3 μ l

In general, pcDNA3.1(+) was used as a stuffer. For microscope experiments 10% of cells, DNA and Lipofectamin used in 6-well plates were used in μ -Slide 8 Well (Ibidi, 80826).

2.2.3 Generation of the monoclonal stable cell Lines H1299-p53-LEXY

To generate a stable cell line expressing p53-LEXY under an inducible promoter, cMyc_tetR-KRAB (kind gift from Ben Kachel, Grimm lab) was cloned in pcDNATM 6\TR yielding pcDNA6_TR-KRAB. Subsequently, the minimal CMV\Tet₂ promoter was amplified from pcDNATM5\FRT\TO and ligated with p53-LEXY and cloned in a pcDNA3.1 (+) Zeo not carrying its CMV promoter yielding FRT_p53_Lexy. Selective antibiotic concentration was determined according to the manufacturer's protocol.

To generate H1299 cells stably expressing tetR_Krab, H1299 cells were transfected with pcDNA6_TR-KRAB. 48 hours after transfection, cells were exposed to media supplemented with 0.03 % Blastcidin. For the next 12 days, media was exchanged every 3 days. Then, the cells were trypsinized and counted. Subsequently, cells were diluted to 0.5 cells per 200 μ l respectively, and seeded in 4 96-well plates each in media containing 0.03 % Blastcidin. 5 days later, all of the 96-well plates were analysed for single colonies. Wells containing single colonies were transferred in to 6-well plates, and subsequently in T25 well flasks. Then, the 65 clones were seeded in 96-well plates in duplicates and transfected with FRT_p53_Lexy. 24h post transfection, cells were supplemented with 100 ng/ml doxycyclin, controls were left untreated. After 24 hours, cells were analysed with the microscope.

The same methodology was carried out generating H1299_TR stably expressing FRT_p53_LEXY. The selection media was supplemented with 0.03 % Blastcidin and 0.05 % Zeocin. To evaluate successful integration, expanded clones were either treated with Doxycyclin or left untreated. The induction was verified with a microscope.

2.3 Western blot

If not mentioned otherwise, cells were seeded into 6 well plates and transfected or induced with the respective constructs or the indicated doxycyclin concentration. In case of an optogenetic experiment, cells were illuminated with the respective illumination device, and the indicated illumination timings. Cells were exposed to light either for 24 or 48 hours. Controls were kept in the dark. Then, cells were collected into ice-cold lysis buffer (20 mM Tris-HCL pH 7.4, 1% Triton X.100, 10% glycerol, 150 mM NaCl, 1% phenylmethylsulfonyl fluoride, 1% Benzonase (Novagen, 70664) and 1 Complete Mini Protease Inhibitor tablet (Roche, 11 836 153 001). Protein concentration was measured by a Bradford assay and adjusted to 1 μ g/ml. 15 μ g were loaded followed by protein separation by SDS-PAGE. Proteins were then transferred onto a polyvinylidene difluoride membrane and the membrane was blocked using 5% BSA in PBS-T. Primary antibodies were diluted in 5% BSA in PBS-T and applied for 1 h to detect p53 (Santa Cruz, sc-126, diluted 1:1000) or p21 (BD Pharmigen, 556430, diluted 1:666) and beta-actin (Abcam, ab8226, diluted 1:1000), followed by incubation with a secondary goat anti-mouse IgG(H+L)-PRPO (Dianova, 115-035-003) for 45 min. Chemiluminescence was detected using the SuperSignal West Pico Chemiluminescent Substrate (Thermo Scientific) and the ChemoCam Imager (Intas). Quantitative analysis of protein expression levels was carried out by measuring the intensity of the respective bands using the ImageJ Gels package. Target gene levels were first normalized to beta-actin levels of the respective sample, then to an indicated control.

2.4 Blue light illumination devices

2.4.1 Activation within the cell incubator

Blue light exposure was carried out using a custom made LED stand positioned within the cell culture incubator. Clear bottom well plates were positioned on a small plexiglass table standing above a LED array consisting of 6 LEDs (LED-TECH, Cree XP-E D5-15, wavelength 458 nm). The distance between LEDs and the table was approximately 20 cm.

Blue light intensity was measured using a Light Meter (LI-COR, LI-250A). Initially, intensity was $\sim 20 \mu\text{mol m}^{-2}\text{s}^{-1}$. In experiments after chapter 2.3.7., light intensity was reduced to $\sim 15 \mu\text{mol m}^{-2}\text{s}^{-1}$.

The LEDs were powered by a power supply (Manson, HCS-3102). A notebook connected to the power supply was used to automatically control light intensity and illumination regimes (Manson software, Version 0.9).

In a first optimisation step, the notebook was exchanged by a Raspberry Pi running a self-written Python script to control the power supplies settings. Using the Raspberry Pi allowed application of more complex illumination patterns, due to lack of maximal number of computer commands.

In a second optimisation step, the LEDs of the incubator array were exchanged by new LEDs having an emission peak at a wavelength of 488 nm (LED-TECH, CREE-XP E2).

2.4.2 LED-devices for automated microscopy

To track localisation during imaging, LEDs were embedded in the lids of well-plates. LEDs were cooled with attached cooling bodies, to prevent overheating. The LEDs were powered by a power supply (Manson, HCS-3102). Activation state and voltage (controls LED intensity) were controlled with a Raspberry Pi running a self-written Python script. Empty wells were filled with PBS, to prevent evaporation of media.

2.5 Microscopy and Imaging

2.5.1 Leica SP5

Confocal laser scanning microscopy was carried out on a Leica Sp5 confocal microscope. Initially, cells were activated with the 458 nm laser at 80 % intensity, then I switched to the 488 nm laser at 80 % intensity to prevent doxycyclin degradation. mCherry was imaged using the 561 nm laser. In general, the 561 nm laser was used to focus cells, to prevent premature translocation processes. The microscope was equipped with a incubation chamber for long term imaging. For experiments with living cells, the chamber was preheated to 37 °C and set to 5 % CO₂. Activation and imaging was done using the 20X objective (NA = 0.7). For translocation experiments, cells were activated for 5 seconds every 30 seconds. mCherry images were taken prior to each blue light illumination. 20000 H1299 or 40000 HCT116 cells were seeded in ibidi μ -slide 8 wells (ibidi, 8226).

2.5.2 Lionheart

Experiments using the self-built LED devices were carried out on the Biotek Lionheart using the proprietary Gen5 software. mCherry was imaged using the texas red filter cube. Images were taken using 20x objective using the laser-based autofocus. LED power was set to 10 and exposure time to 1600 ms. The software package for automated imaging was used for long term imaging. A self written Python script was used to match each time points images and stitch them together to receive one image file.

2.5.3 Image Analysis

Images were taken with the indicated microscopes. Image analysis was performed in Fiji (version 1.51). In general, prior to further analysis, background was subtracted on raw data.

2.5.3.1 Quantification of nuclear/cytoplasmic ratio

For each cell, a region of interest was drawn in the cytosol and the nucleus. Mean intensity was measured, and nuclear fluorescence was normalized to cytosolic fluorescence.

2.5.3.2 Quantification of relative nuclear intensity

A region of interest was drawn in the nucleus of each cell and the mean intensity was measured using Fiji. Next, each cell was tracked in every slide through a given time series, and normalized to the initial intensity. Then, the mean of relative nuclear intensity was calculated for each time point.

2.6 Quantitative analysis of mRNA transcript levels by qPCR

2.6.1 Primer design and validation

qPCR primer were designed by first accessing the DNA sequence of the desired gene sequence and its mRNA transcript on pubmed. Either forward or reverse primer has to span an exon-exon junction to prevent amplification of genomic DNA. The amplicon size and the melting temperature was selected to be as similar as possible throughout all designed primers. Primer3 was used to verify absence of secondary structures of designed Oligos. Each primer pair was validated by serial cDNA dilution. cDNA was diluted in 1:10, 1:100, 1:1000, 1:10000 and 1:100000, while primer concentration was kept constant. In general, primers were designed and validated according to MIQE guidelines (Bustin et al., 2009)

2.6.2 cDNA generation

RNA was isolated using the Qiagen RNeasy Kit (Qiagen, 74104) following the manufacturers protocol. The RT was carried out with the RevertAid First Strand cDNA Syntesis Kit (ThermoFischer, K1621). RT was carried out in PCR tubes, 1 μ l of random primer were added to 1 μ g template RNA diluted in 11 μ l nuclease free H₂O. This mix was then incubated at 65 °C for 5 minutes, followed by 2 minutes of incubation on ice. Then 8 μ l of the master mix containing 4 μ l RT-buffer, 2 μ l dNTP Mix(10 nM), 1 μ l RiboLock and 1 μ l reverse transcriptase was added. Negative controls were carried out lacking the reverse transcriptase. Mixes were incubated at RT for 5 minutes, followed by 1 hour at 42 °C and 70 °C for 5 minutes. cDNA was stored -20 °.

2.6.3 qPCR

qPCR was carried out on either the Applied Biosystems StepOne™ Real-Time PCR System (96-well plates) or the Biorad CFX384™ Touch Real-Time PCR Detection System (384-well plate format) using SYBR™ Green Master Mix (Applied Biosystems, 4309155). Each reaction was done in a 10 μ l volume and consisted of 5 μ l SYBR™ Green Master Mix, 0.2 μ l of both forward and reverse primer (10 μ M) and 0.6 nuclease free H₂O μ l and 4 μ l of cDNA (1:1000). Plates were spun down for 5 minutes at 300 rpm, and the following protocol was applied: Initial 95 °C for 10 minutes followed by 40 cycles of 15 seconds at 95 °C and 30 seconds at 60 °C. After the amplification reaction was finished, a melting curve analysis was carried out. Temperature was ramped up from 60 °C to 90 °C by 0.5 °C per minute to verify proper and consistent dissociation of the primer.

2.6.4 Data analysis

Differential gene expression was calculated by the $2^{-\Delta\Delta CT}$ method (Livak and Schmittgen, 2001). Target levels were first normalized to internal levels of beta actin and Rpl0 then to a indicated control. Data was automatically analysed by a self-written python script.

2.7 Crystal violet staining

After respective treatment, cells were trypsinised and counted. 100 cells per 6 well plate were seeded and placed in the incubator for 10 days. Then, cells were washed two times with cold 1xPBS and subsequently fixed with ice-cold 100% methanol for 10 minutes. After fixation, cells were incubated in 0.5% crystal violet solution (500 mg crystal violet, 25 ml methanol, 75ml dest Water) for 10 minutes. Next, cells washed repeatedly, until no dye is coming off. Then, single colonies were counted by eye using a cell counter, and images on a tabletop microscope were taken.

2.8 Single cell laser-tag

2.8.1 Cell Tagging

One day before the experiment, the cells were seeded on 35 mm glass bottom dishes with a grid (ibidi, 81166) or 8-well plastic bottom chambers with an engraved grid (ibidi, 80826-G500). Cell were incubated in 0.04 mg/ml biotin-4-fluorescein (B4F) (Sigma Aldrich, B9431-5MG) dissolved in medium and subsequently illuminated. The region of interest was imaged using the 473 nm laser at the confocal microscope and the laser intensity set to 100% for 30 seconds. The focal plane was set near the top membrane of the cell. After illumination, the cells were washed 5 times with warm PBS to remove unbound B4F and resupplemented with medium.

2.8.2 Fluorescent cell labelling

The cells were tagged with B4F as described in chapter 4.8.1 and subsequently incubated in 0.05 mg/ml Alexa-488-Streptavidin (Thermo Fisher, S11223) for 15 min at 37 °C and 5% CO₂ to stain tagged cells. The cells were then washed again 5 times with warm PBS before imaging.

2.8.3 Selective detachment of non-activated cells

The region of interest was tagged as described in in 4.8.1. Then cells were rinsed once with warm PBS and treated with 1:1 diluted 0.05% Trypsin-EDTA. Dilution was done in PBS. Cells were incubated in the incubator for 8 minutes. Then, untagged cells were detached by gently shaking the dish in a circular motion. The remaining cells were washed twice very gently with medium before imaging.

3 Results

Due to complexity of the network regulating p53 and its high sensitivity towards stress, experimentally investigating p53 can be challenging. To overcome limitations of indirect or harsh experimental set ups, we set out to use optogenetic approaches to allow precise perturbation of p53 in the absence of upstream stress or unspecific activation. Both approaches aim at deciphering how p53 transcription dynamics are decoded into a specific gene transcription program, and thus the intended phenotype. In section 2.1, I describe optogenetic approaches to control endogenous levels of p53 by aiming at blocking Mdm2 binding to p53, thus impeding p53 degradation. In section 2.2 and 2.3 I explain how I use optogenetic tools to control nucleocytoplasmic translocation as a means of controlling p53 transcriptional activity. To this end, I employed two different strategies, first I used LINuS to control import of p53 (section 2.2), then LEXY, to manipulate export of p53 (section 2.3). For data obtained by others, their names are indicated in the respective figure legends and in corresponding paragraphs.

3.1 Light-mediated manipulation of endogenous p53 levels

3.1.1 Photocaging the MIP peptide in the AsLOV2 domain

3.1.1.1 Preliminary work by others

Prior to the start of this work, several students working in our lab tried to achieve light-mediated control of p53 degradation as a means to control its levels, using different strategies. While p53's activity is mainly controlled by Mdm2 and MdmX, p53 protein levels are regulated only by Mdm2, which binds to a motif present in p53's N-terminal TAD and subsequently ubiquitinates lysine residues on the p53's C-terminus, ultimately causing the degradation of p53 (Wu et al., 1993; Haupt et al., 1997). Controlled interruption of this feedback, should allow adjustable fine-tuning of p53 levels.

As overexpression of Mdm2, a phenomenon commonly observed in cancerous cells, abolishes p53's ability to induce cell cycle arrest or apoptosis in cells (Chen et al., 1996), reducing Mdm2 activity towards p53 is a potential therapeutic target in oncology. Several small-molecule inhibitors disrupting this interaction have been developed or are in current clinical trials (Wang et al., 2017). Some promising candidates are proteinogenic peptides.

Initially, former Bachelor student Jan Marcel Smykalla, fused the p53 N-terminal TAD1 to the AsLOV2 domain C-terminus, generating wtLOV-TAD. By doing so, he hypothesized the tight interaction between the J α -Helix and the AsLOV2 domain core in the non-active dark state would sterically hinder accessibility of the TAD attached to its C-terminus. Blue light illumination allows controlled, reversible exposure of the C-terminal TAD and thus permit Mdm2 binding. Yet, initially results obtained in yeast were contradictory.

A second strategy was applied by Bachelor student Jan Marcel Smykalla and Master student Christian Scheeder, who employed the TULIP approach (Strickland et al., 2012). Rather than fusing p53's whole functional domain to the AsLOV2 domain, a small bioactive peptide was fused to two C-terminal AsLOV2 truncations. Due to the reduced size of the C-terminally attached sequence, the photocaging should be facilitated. Additionally, bioactive peptides usually possess a higher affinity towards the it was designed to bind to than the endogenous interaction partner.

Initially, they selected the pDI peptide (peptide Dual Inhibitor, sequence: LTFEHYWAQLTS), a peptide that blocks interaction with both Mdm2 and MdmX (Hu et al., 2007a). Yet, initial results in yeast could not demon-

strate any diminished interaction of p53 and Mdm2. Next, they selected the Mdm2 inhibitory peptide (MIP, Sequence: PRFWYWLRLME), which has proved to be very efficient in disrupting Mdm2's binding to p53 (Shiheido et al., 2011). The peptide was fused to two different truncations of the As LOV2 domain, register 4 (Reg4) and register 5 (Reg5), truncated at I539 and D540 respectively (Figure 3.1A).

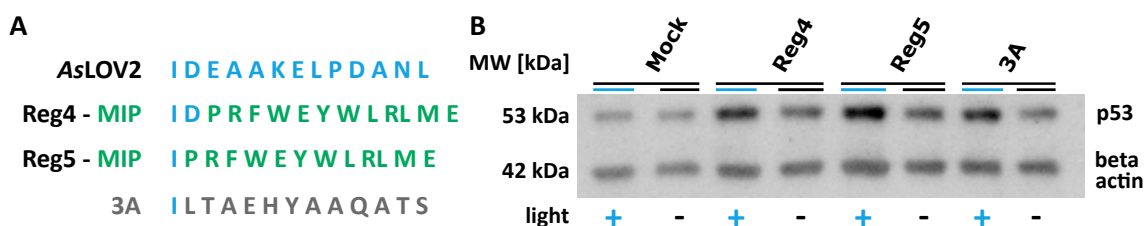


Figure 3.1: Evaluation of effect of photocaged MIP peptide on p53 levels in MCF7

A | Depiction of design strategy of MIP constructs. Mdm2 inhibitory peptide (MIP) was fused to either I539 yielding construct Reg5-MIP or D540 generating Reg4-MIP. The 3A peptide is a control peptide supposedly not binding Mdm2.

B | Western Blot of p53 levels. MCF7 cells were transfected with the indicated constructs. 24 hours post transfection, cells were illuminated for 24 hours with blue light for 5 seconds every 20 seconds. Controls were kept in the dark. Subsequently, cells were lysed, blotted and stained with the indicated antibodies. Experiment carried out by Christian Scheeder.

Initial experiments in yeast carried out by Jan Marcel Smykalla and Christian Scheeder showed promising results. In yeast, transformed Mdm2 and p53 exhibit co-localisation, unless the interaction is inhibited (Di Ventura et al., 2008). Both constructs, Reg4-MIP and Reg5-MIP showed a light-controlled disassociation of Mdm2 and p53 (data not shown).

To verify these results in mammalian cells, Christian Scheeder cloned both Reg4-MIP and Reg5-MIP in mammalian expression vectors and expressed the constructs in MCF7 cells. On the next day, cells were either subjected to blue light, or kept in the dark. To limit phototoxicity, light was applied for 5 seconds every 20 seconds. Endogenous p53 levels were determined by Western Blot (Figure 3.1B).

Both samples expressing the MIP peptide fused to different truncations of the AsLOV2 domain exhibited elevated p53 levels upon blue light stimulation (Figure 3.1B). Curiously, the supposedly non-functional Reg5-3A also affected p53 levels to a similar extent than Reg4-MIP. Yet, as mock transfected cells did not differ in their p53 levels, the elevation of p53 throughout the other samples was likely not due to blue light exposure. When Christian Scheeder repeated the experiment, the observed increase in p53 levels was even stronger (data not shown) compared to samples expressing Reg5-3A, yet a mock-transfected control was missing. These results suggest that the MIP peptide can be used to control p53-levels in a light-mediated manner, yet the observed effect has been variable.

3.1.1.2 Characterisation of the MIP peptide in MCF7 cells

I began working on this project by independently reproducing the results obtained by Christian Scheeder. To this end, I repeated the experiment in the exact fashion as carried out by Christian Scheeder. Contradictory to his results, I could not observe an increase of endogenous p53 levels as observed by Christian (Figure 3.2AB). Throughout the experiments, p53 levels seemed to be constant, implying that the constructs do not impact p53 levels.

Throughout all replicates, the transfection efficiency was the same and similar to those indicated by Christian. I also resequenced the plasmids, to exclude unlikely mutations due to repeated freeze-thaw cycles of the DNA. In general, if constructs carried a fluorescent marker, usually mCherry, the transfection efficiency was verified prior to cell lysis using a fluorescence table top microscope. If the fluorescent signal or the number of fluorescent cells was lower than the levels usual achieved with transfection, or cells seemed to be too stressed after transfection, the experiment was aborted.

Even though the inhibition of Mdm2 binding to p53 should have an integrative behaviour, meaning the longer the binding is inhibited, the more p53 should accumulate, I reasoned to measure p53 at different time points. In stressed cells, p53 and Mdm2 protein levels display a negative feedback loop behaviour. They are oscillating with a certain offset, as p53 induces Mdm2 expression, which subsequently promotes p53 degradation. Thus, I decided to take time points at 3, 6, 12 and 24 hours, and evaluate p53 levels.

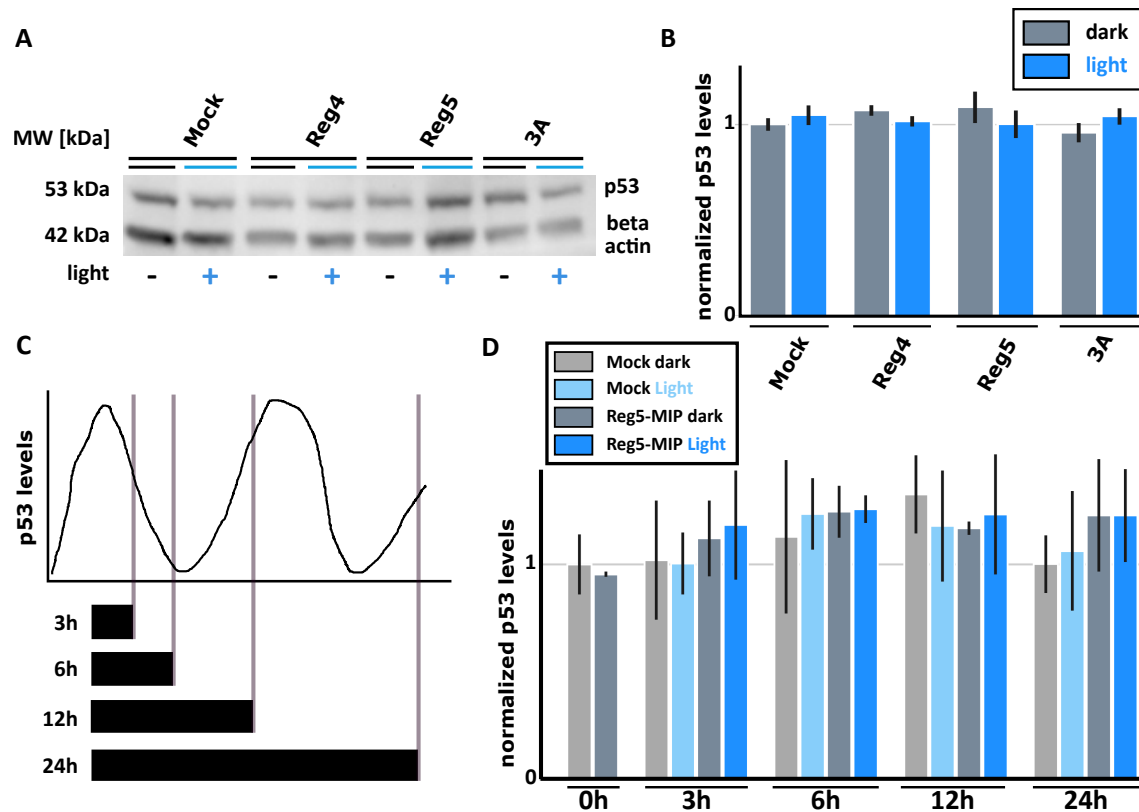


Figure 3.2: Re-evaluating the light-dependent effect of the photocaged MIP peptide on endogenous p53 levels

A | Exemplary Western Blot of p53 levels. MCF7 cells were transfected with the indicated constructs. 24 hours post transfection, cells were illuminated for 24 hours with blue light for 5 seconds every 15 seconds. Controls were kept in the dark. Subsequently, cells were lysed, blotted and stained with the indicated antibodies.

B | Quantification of relative p53 expression levels of **A**. p53 levels were first normalized to beta actin, then to the mock-transfected, non-illuminated sample (mean \pm SD, $n=3$).

C | Exemplary behaviour of oscillatory p53 expression in stressed cells and indication of selected time points.

D | Quantification of relative p53 levels corresponding to **C**. MCF7 cells were transfected with the indicated constructs. 6 hours post transfection, cells were illuminated for the indicated timings with blue light for 5 seconds every 15 seconds. Controls were kept in the dark. Subsequently, cells were lysed, blotted and stained with beta actin and p53 antibodies. p53 levels were first normalized to beta actin, then to the mock-transfected, non-illuminated sample at time point 0 h (mean \pm SD, $n=3$).

To this end, I transfected MCF7 cells with either a stuffer DNA or Reg5-MIP, the construct which showed the highest elevation of p53 levels in the results presented by Christian Scheeder. Similar to the previous experiment, the p53 levels were comparable throughout the samples and individual replicates. As p53 levels did not increase upon blue illumination, it appears that the peptide itself is either caged, and thus not accessible for Mdm2, or, the p53-Mdm2 axis in MCF7 cells is less susceptible for interruption.

3.1.2 Characterisation of the MIP peptide in HCT116 cells

The MIP peptide has been identified in a two-stage mRNA display and has been demonstrated to successfully inhibit p53-Mdm2 interaction in the human colon cancer cell line HCT116, a cell line widely used in p53 research

(Shiheido et al., 2011).

To investigate the peptide's functionality in HCT116, I expressed Reg4-MIP and Reg5-MIP in HCT116 cells and exposed the transfected cells to blue light to analyse changes in p53 levels. To assess p53 levels upon stimulation, control samples were treated with Nutlin-3. Nutlin-3 is a small molecule inhibitor binding to Mdm2 and thereby abolishing its control over p53 levels (Vassilev et al., 2004). Our peptide approach resembles nutlin-3 treatment, as both inhibit p53 degradation by competing with p53 for Mdm2 binding.

Similarly as in MCF7 cells, I could not observe a light-induced increase in p53 levels upon blue light illumination (Figure 3.3AB). p53 levels in samples transfected with MIP constructs were constant in both, dark and illuminated conditions, as well as mock-transfected samples, arguing that MIP is not able to bind to Mdm2. On the other hand, samples treated with Nutlin-3 exhibited an approximately 9-fold increase in endogenous p53 levels, independent of blue light illumination. Thus, HCT116 cells are sensitive to inhibition of the p53-Mdm2 interaction, yet the photocaged MIP constructs can not exert this inhibition.

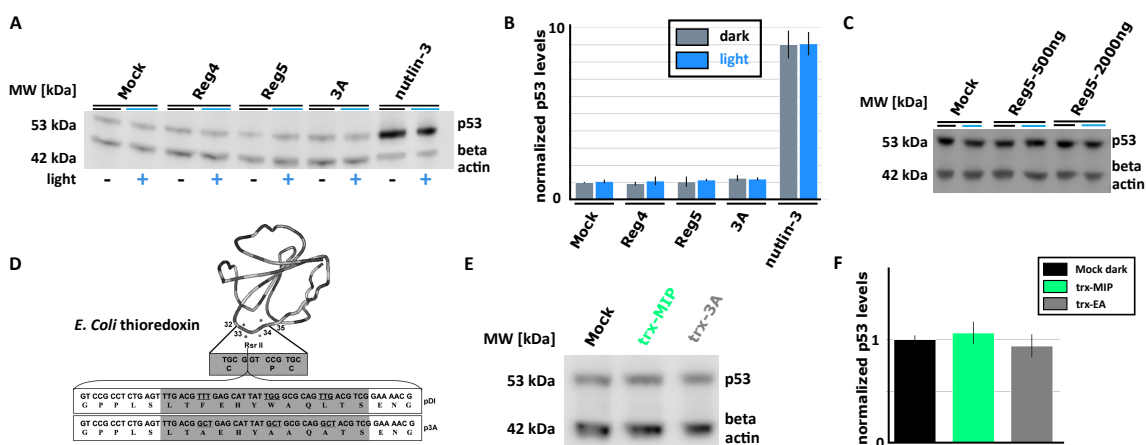


Figure 3.3: Characterisation of the MIP peptide in HCT116 cells

A | Exemplary Western Blot of p53 levels in HCT116 cells. HCT116 cells were transfected with the indicated constructs. 24 hours post transfection, indicated samples were treated with $8\mu\text{M}$ Nutlin-3. Then, cells were illuminated for 24 hours with blue light for 5 seconds every 20 seconds. Controls were kept in the dark. Subsequently, cells were lysed, blotted and stained with the indicated antibodies.

B | Quantification of relative p53 expression levels of **A**. p53 levels were first normalized to beta actin, then to the mock-transfected, non-illuminated sample (mean \pm SD, $n=3$).

C | Western Blot of p53 levels. HCT116 cells were transfected with the indicated constructs. 24 hours post transfection, cells were illuminated for 24 hours with blue light for 5 seconds every 15 seconds. Controls were kept in the dark. Subsequently, cells were lysed, blotted and stained with the indicated antibodies.

D | Design strategy to facilitate peptide administration into cells. Peptides were introduced in *E. Coli* thioredoxin scaffold in between G33 and P35 (Hu et al., 2007a).

E | Exemplary Western Blot of p53 levels. HCT116 cells were transfected with the indicated constructs. 36 hours post transfection, cells were lysed, blotted and stained with the indicated antibodies.

F | Quantification of relative p53 levels of **E**. p53 levels were first normalized to beta actin, then to the mock-transfected sample (mean \pm SD, $n=3$).

As there is the possibility that the MIP is binding to Mdm2, yet the number of correctly folded MIP molecules is not sufficient to pass a potential threshold causing observable alterations in p53 levels, I transfected either twice (500 ng) or eight times (2000 ng) the amount of Reg5-MIP in HCT116 cells, and exposed the cells to blue light for 24 hours (Figure 3.3C). Even though expression of the mCherry transfection marker was clearly stronger than in previous experiments, the p53 levels remained unchanged. Apparently, also excessive amounts of MIP-Reg5 do not impact Mdm2's control over p53. Mock-transfected cells exhibit the same level of p53 than those transfected with Reg5-MIP, so either the MIP peptide is not properly folded or sterically inaccessible. Otherwise, this would suggest that, contrary to the reported results, MIP does not have an impact on p53 levels *in vivo* (Shiheido et al., 2011).

Next, I wanted to exclude missfolding or sterical hindrance as a cause of the apparent lack of Mdm2 inhibition. Thus, I reconstructed the plasmids used by Shiheido *et al.* to demonstrate the functionality in HCT116 cells (Shiheido *et al.*, 2011). As peptides can not be easily added to the cell culture media, the MIP peptide was cloned in a freely accessible loop of *E. coli* thioredoxin, in between G33 and P35 and a N-terminal mCherry, yielding the construct trx-MIP (Figure 3.3D). Due to its small size and high stability, thioredoxin is a perfect scaffold, providing a platform that can present bioactive peptides within a cellular environment (Böttger *et al.*, 1997).

Shihedo and colleagues used a viral transduction system, in contrast to the chemical transfection method used here, to introduce the constructs into HCT116 cells, so it is hard to compare the actual amount of construct expressed within cells. Thus, I transfected 2000 ng of trx-MIP, and incubated cells for 48 hours to ensure sufficient amount and time for perturbation of the p53-Mdm2 axis. Yet, in contrast to the published results, I could not observe any changes in p53 levels 24 hours after transfecting trx-MIP (Figure 3.3EF).

Taken these results together, it appears that I can not reproduce the proposed bioactive function of the MIP peptide, therefore I stopped working with this peptide.

3.1.3 Employing endogenous p53 sequences to enable light-mediated Mdm2 inhibition

3.1.3.1 Photocaging the p53-Mdm2 binding interface

Since the MIP peptide did not show any functionality in any experiments done by myself, I decided to use p53's endogenous sequences, which are bound by Mdm2 to block p53 activity and subsequently induce its degradation. Here, I use the AsLOV2 domain to expose the endogenous binding interface in a light-dependent manner. This endogenous binding interface (sequence: TFSDLWKLL) is located at amino acid position 16-28 of p53's TAD1 (Figure 3.4A) (Kussie *et al.*, 1996). It has been shown in *in vitro* studies, that this isolated peptide itself is sufficient to bind Mdm2, even when it is out of its natural structural context within the p53 TAD (Shiheido *et al.*, 2011). As residues next to the binding interface can contribute to binding conformation, I fused the endogenous binding interface in 4 different versions, differing in neighbouring amino acid residues added, to the AsLOV domains I539, generating the constructs Reg5-enBI 1-4 (Figure 3.4A).

Blue light exposure did not result in any observable elevation in p53 protein levels. As samples transfected with Reg5-enBI1-4 are comparable to the mock-transfected cells, either the sequence is caged too tightly, also in the lit-state, or the sequence itself is not in the correct conformation to allow binding to Mdm2. As the three dimensional structure is often determined by the surrounding residues and their secondary and tertiary structure, it is not surprising, that solely the endogenous binding interface is not sufficient in resembling the correct structural arrangement, and an interaction *in vitro* can not fully recapitulate *in vivo* kinetics. However, as a control of the effect of the peptide itself is missing, it remains unclear whether the lack of effect on p53 levels is due to the peptide itself, or too tight caging even in the lit-state.

3.1.3.2 Photocaging p53's transactivation Domain

To acknowledge the structural impact of the neighbouring amino acids and allow the formation of the correct three dimensional structure and thus allow binding to Mdm2, I fused the whole TAD of p53 to the AsLOV2 domains C-terminal J α -helix. Fusing the whole domain, I wanted to achieve light-mediated sterical hindrance of access to the binding-interface, and so control Mdm2 binding based on illumination conditions. As described in chapter 1.3.3.1, this common optogenetic approach employs structural rearrangement that the AsLOV2 domain undergoes upon blue photon absorption. This response is obtained by fusing the protein of interest C-terminally to the AsLOV2 domain. In the dark state, the fused protein domain is supposedly tightly caged to the AsLOV2 domains core, while blue light activation results in exposure of the fused protein and its accessibility for interacting partners (Wu *et al.*, 2009).

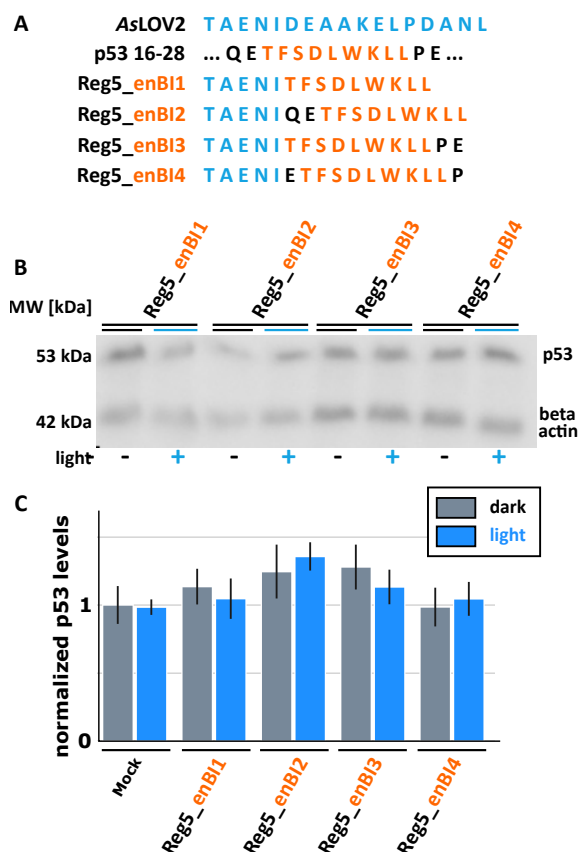


Figure 3.4: Photocaging the endogenous Mdm2-binding site of p53

A | Design strategy of constructs. The endogenous Mdm2-binding site (enBI) of p53 was fused to I539 of AsLOV. Different combinations of adding the amino acids next to the endogenous binding site were tested.

B | Exemplary Western blot of p21 levels upon transfection of constructs depicted in **A**. HCT116 cells were transfected with the indicated constructs. 24 hours post transfection, cells were illuminated for 24 hours with blue light for 5 seconds every 15 seconds. Controls were kept in the dark. Subsequently, cells were lysed, blotted and stained with the indicated antibodies.

C | Quantification of relative p21 levels of **B**. p21 levels were first normalized to beta actin, then to the untransfected, non-illuminated sample at time point 0h (mean \pm SD, n=3).

In this case, the exposed p53's TAD acts as a bait for endogenous Mdm2 and thereby disrupting proper degradation of p53. As I539 of the AsLOV2 is crucial for the recovery from lit to the dark state, truncating this amino acid residue results in a virtual permanent lit state (Harper et al., 2004), thus serving as a positive control.

To verify whether this approach is suitable for controlling p53 levels, I fused the p53-TAD (AA 1 - 63) to different truncations of the wt AsLOV2 domain, starting at N538 until P547, generating 539-TAD, with numbers indicating the site of TAD attachment (Figure 3.5A). Next, these constructs were transfected into HCT116 cells, and one day after transfection, cells were exposed for 24 hours to blue light. I selected p21 levels as a readout, as they should reflect the impact on p53 better. Both Mdm2 and MdmX interact with p53's TAD and preventing transcriptional activity of p53, yet only Mdm2 binding leads ultimately to degradation of p53. Thus, rather than p53 levels, p53 activity might be effected more and act as better read out for the light-mediated effects of the TAD constructs.

In the initial experiments, three constructs with AsLOV2 truncations at 539, 541 and 545 showed slight elevation in p21 levels upon blue light exposure, yet this effect could not be replicated (Figure 3.5BC). Throughout all transfected samples, p21 expression is quiet homogeneous (Figure 3.5C). No light-induced changes could be observed, posing the question whether this approach is worthwhile pursuing. It has been highlighted, that photocageable domains are rather found serendipitously, than by rational design (Winkler et al., 2014), but here it appears rather that exposure of the TAD has not the desired effect, as also the putative positive control 538-TAD does not exhibit any detectable changes in p21 levels compared to mock transfected cells.

3.1.4 Using the PMI peptide to manipulate p53 levels light-dependently

3.1.4.1 Characterisation of the PMI peptide in a trx scaffold

Both strategies employing endogenous sequences to promote light-mediated Mdm2 binding failed. As the positive control 538-TAD failed to induce changes in p21 levels, it appears that it is not sufficient to overload cells with p53-TAD. Thus, a sequence with a stronger affinity towards Mdm2 is required.

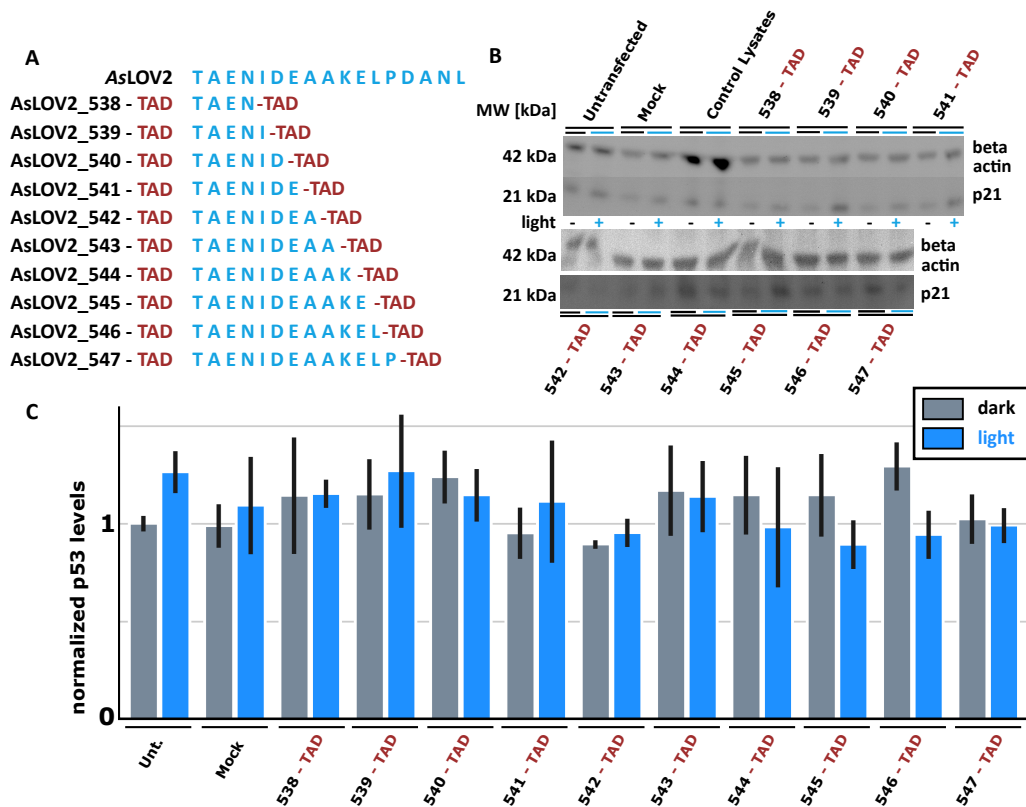


Figure 3.5: Photocaging p53's endogenous transactivation domain.

A | Design strategy of TAD-constructs. p53's TAD was fused to the C-terminus of the J α -helix at different truncations, starting at N538.

B | Exemplary Western blot of p21 levels upon transfection of constructs depicted in **A**. HCT116 cells were transfected with the indicated constructs. 24 hours post transfection, cells were illuminated for 24 hours with blue light for 5 seconds every 15 seconds. Controls were kept in the dark. Subsequently, cells were lysed, blotted and stained with the indicated antibodies.

C | Quantification of relative p21 levels of **B**. p21 levels were first normalized to beta actin, then to the untransfected, non-illuminated sample at time point 0h (mean \pm SD, n=3).

Searching the literature, I discovered several peptides supposedly inhibiting p53-Mdm2 interaction in a superior manner. Yet, the majority of these consisted partly of non-proteinogenic amino acids (for example: Chang et al. (2013)) and thus not useful here. The peptide PMI (p53-MDM2/MDMX inhibitor; sequence: TSFAEYWNLLSP), appeared to be a promising candidate (Pazgier et al., 2009). PMI supposedly has a higher affinity towards Mdm2 than both p53's endogenous binding site and the MIP peptide used in the beginning of my work (Figure 3.6). PMI was identified in a phage display, using the p53-binding domains of Mdm2 and Mdm4. Pazgier and colleagues only present *in vitro* data, so first I wanted to verify whether the peptide exerts an impact on p53 levels *in vivo* (Pazgier et al., 2009).

To this end, I cloned the PMI peptide into a thioredoxin scaffold in between G33 and P35 (as described in Chapter 2.1.2), generating the construct trx-PMI. This construct was expressed in HCT116, together with the trx-3A and trx-MIP constructs. Cells transfected with trx-PMI exhibited a clear increase in p53 levels 36 hours after transfection, implying that degradation of p53 is inhibited (Figure 3.6B). As seen in previous experiments, expression of trx-3A and trx-MIP does not result in an p53 increase. Taken this promising first result, I wanted to verify whether I could obtain light-dependent control over peptide accessibility.

To this end, I fused the PMI peptide to truncation of the AsLOV2 domain's C-terminus, ranging from I539 to 543A, generating the constructs 539-PMI to 543-PMI (Figure 3.6C). These constructs were expressed in HCT116 cells. One day after transfection, cells were exposed to light for 24 hours and subsequently harvested for analysing p53 levels. Unlike expression of trx-PMI, none of the putative light-responsive constructs caused an elevation of

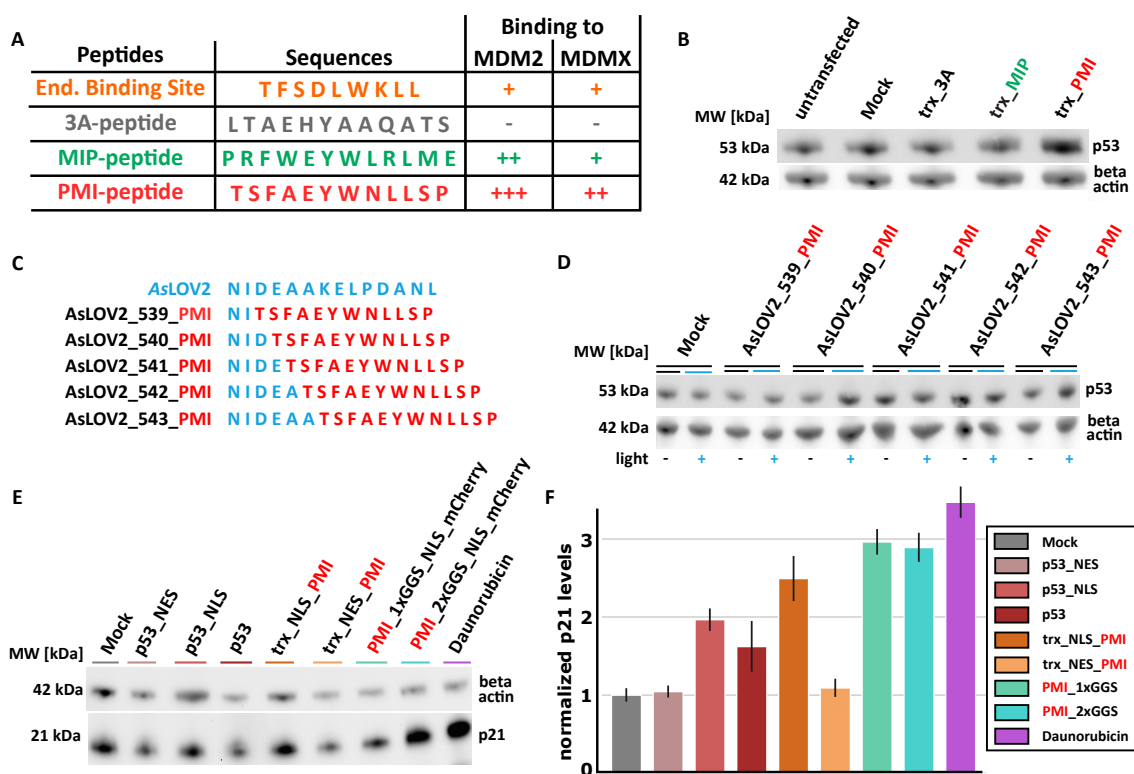


Figure 3.6: Characterisation of the PMI peptide in HCT116 cells

- A** | Comparison of amino acid sequences and bioactivity of employed Mdm2-p53 inhibitory peptides and a control. One plus sign equals approximately one order of magnitude.
- B** | Western Blot of effect of PMI peptides on p53 levels. HCT116 cells were transfected with the indicated constructs. 36 hours post transfection, cells were lysed, blotted and stained with the indicated antibodies.
- C** | Design strategy of constructs to photocage the PMI-peptide. PMI was fused to the C-Terminus to various sites on the C-terminus of the AsLOV domain starting at I539.
- D** | Western Blot of effect of constructs shown in **C** on p53 levels. HCT116 cells were transfected with the indicated constructs. 24 hours post transfection, cells were illuminated for 24 hours with blue light for 5 seconds every 15 seconds. Controls were kept in the dark. Subsequently, cells were lysed, blotted and stained with the indicated antibodies.
- E** | Exemplary Western Blot of effect of PMI peptides on p53 levels. HCT116 cells were transfected with the indicated constructs. 0.5 μ M Daunorubicin was applied 8 hours after transfection. 32 hours post transfection, cells were lysed, blotted and stained with the indicated antibodies.
- F** | Quantification of relative p53 expression levels of **E**. p53 levels were first normalized to beta actin, then to the mock-transfected sample (mean \pm SD, n=3).

p53 levels upon illumination (Figure 3.6D). As p53 levels remain constant throughout all samples, it appears that Mdm2 can not bind the peptide, neither in the dark nor the lit state due to too tight caging and thus sterical hindrance.

Next, I wanted to investigate the *in vivo* function PMI further. First, I sought to compare the effect of PMI on p53 target gene p21 to overexpression of p53 itself and addition of the DSB-inducing drug Daunorubicin. Additionally, I examined whether the effect of PMI is dependent on its localisation within the cell, so I added either a NLS or a NES to the trx-PMI construct, yielding trx-NLS-PMI and trx-NES-PMI. Moreover, I explored whether the trx-scaffold is necessary as a scaffold, or if it is possible to just fuse PMI N-terminally to mCherry, separated by either one or two GGS-linker and a NLS to ensure nuclear localisation, yielding constructs 1xGGG-PMI and 2xGGG-PMI. Transfected HCT116 cells were incubated for 36 hours, an untransfected sample was treated with 0.5 μ M Daunorubicin for 24 hours before cells were lysed to measure p21 levels.

Overexpression of wild type p53 led to a two-fold increase in p21 levels (Figure 3.6EF), a similar elevation is observed in samples overexpressing p53-NLS. In the absence of any localization tag, p53 remains nuclear, explaining

the similarity of the response. In contrast, p53-NES is largely cytoplasmic, and thus does not exhibit any elevation in p21 levels. Interestingly, not only was the effect of exposure of PMI on p21 was stronger than solely overexpression of p53, it is apparently also dependent on a nuclear localisation. This supports the hypothesis that Mdm2 binds p53 in the nucleus and guides its nuclear export eventually leading to the degradation of p53 (Freedman and Levine, 1998).

p21 levels exhibited a three-fold change in cells transfected with PMI-mCherry, showing that the trx-scaffold is not necessary to present peptides to a cellular environment. In general, it appears that inhibition of p53 degradation is more effective way in increasing p21 expression than plainly overexpressing p53. This might be due to the negative feedback loop, overexpression of p53 causes also an increased production of Mdm2 and MdmX, thus compensate for the elevated p53 levels. Treatment with 0.5 μ M Daunorubicin causes an approximately 3.3 fold increase, which goes in line with previously reported results (Seoane et al., 2002).

PMI exerting almost the same level of p21 activation as Daunorubicin treatment, with being highly specific to the p53-Mdm2 axis and putatively causing less side effect than drug treatment, is a very promising result. Next, I wanted to control the localisation of PMI light-dependent to switch degradation on and off.

3.1.4.2 Light-mediated import of PMI-LINuS

As the function of PMI is dependent on its localisation, I decided to use LINuS to control its nuclear import in a light-dependent fashion. LINuS is a small versatile tag to reversibly control nuclear import for any kind of protein (Niopek et al., 2014). LINuS consists of the AsLOV2 domain with a C-terminally attached synthetic NLS (Figure 3.7A). Visualisation and tracking of the localisation is achieved by an mCherry fused to the AsLOV2 domain. An additional Pk1t NES supports a more cytosolic localisation prior to illumination. LINuS is a modular tag, and a wide range of NESs and NLSs with differing strengths can be chosen to optimize the localisation of the protein of interest.

I selected three LINuS versions, differing in their initial localisation and the nuclear accumulation after illumination in Hek293 cells (Figure 3.7B). PMI was fused N-terminally to biLINuS 02, 09 and 22, creating the respective constructs (Figure 3.7A). HCT116 cells were transfected with the PMI-LINuS constructs, and then either exposed to blue light for 24 hours or kept in the dark to determine p21 levels after activation. In parallel, initial localisation and light-induced translocation was examined on the confocal microscope.

A general nuclear accumulation of PMI-LINuS constructs could not be observed in HCT116 cells (Figure 3.7C). Some single cells responded to blue light by showing an elevated level of nuclear signal, while the majority of cells did not exhibit any change in localisation of the fluorescent signal. Interestingly, initially cellular distribution of PMI-LINuS constructs in HCT116 cells differed to those observed in Hek293 cells expressing LINuS variants lacking PMI. For example, biLINuS02 had a evenly distributed signal in Hek293 cells, yet PMI-LINuS02 was more cytosolic in HCT116 cells. Additionally, biLINuS02 had the strongest nuclear signal of all tested LINuS versions in Hek293 cells, but PMI-LINuS exhibited the weakest in HCT116 cells. Whether this is due to the attachment of the PMI peptide, or due to cell-type specific variation remains to be seen. The lack of nuclear accumulation of PMI-02 and PMI-22 could also be observed when analysing p21 expression upon blue light illumination (Figure 3.7D).

While PMI-02 and PMI-22 transfected cells exhibited a mild increase in p21 levels compared to the mock-transfected sample, samples expressing PMI-09 showed a stronger increase in p21. Yet, nuclear levels of PMI-09 after activation appeared to be only mildly elevated, compared to the other constructs. This suggests that a certain threshold of nuclear abundance has to be passed, that PMI-LINuS can exert a biological function. Apparently, LINuS accumulation is either impaired by PMI, or HCT116 cells in general have a low potential dynamic range using LINuS, thus making the system not useful in our case.

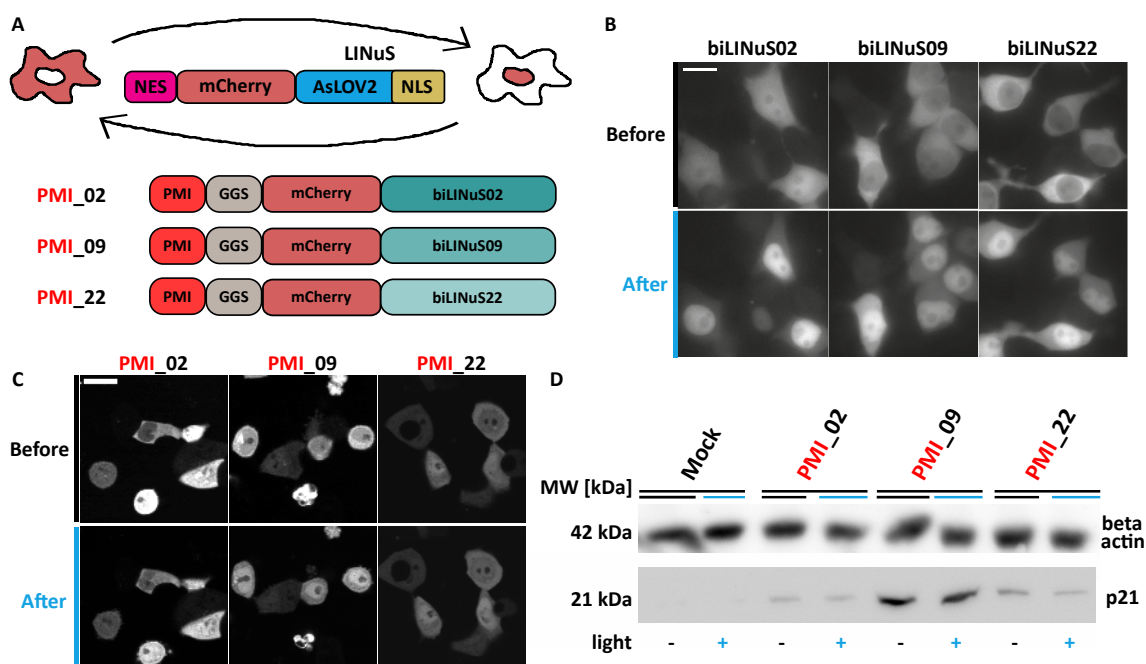


Figure 3.7: Using LINuS to control PMI localization by blue light

A | LINuS is a small tag consisting of an NES, mCherry and a AsLOV2 domain photocaging an engineered NLS of varying strength. Three LINuS versions differing in their initial cytoplasmic nuclear localization and strength of nuclear accumulation upon blue light activation were selected for generating PMI_LINuS constructs.

B | Representative images of the three selected LINuS candidates lacking PMI in HEK293T cells before and after 15 minutes of activation. 24 hours post transfection, cells expressing the indicated constructs were illuminated for 1 second every 30 seconds. Adapted from Niopek et al. (2014). Scale Bar=15 μ m.

C | Representative fluorescence images of HCT116 cells expressing the indicated constructs from **A** before and after activation. 24 hours post-transfection, cells expressing the indicated constructs were illuminated for 5 seconds every 30 seconds. Scale Bar=20 μ m.

D | Western Blot of effects of PMI-LINuS constructs on p21 levels. HCT116 cells were transfected with the indicated constructs. 24 hours post transfection, cells were illuminated for the indicated time with blue light for 5 seconds every 15 seconds. Controls were kept in the dark. Subsequently, cells were lysed, blotted and stained with the indicated antibodies.

3.1.4.3 Optogenetic control of PMI-LEXY

In contrast to LINuS, LEXY is a optogenetic tool to mediate light-dependent nuclear export (Niopek et al., 2016). Instead of a NLS, it exposes a NES in response to light (Figure 3.8A). LEXY has been shown to work right away with a wide range of proteins. However, the initial nuclear localisation can be problematic, if the peptide/protein fused to LEXY exerts its function in the nucleus. This can be addressed by blue light administration after transfection, yet it increases the overall illumination times and thus increases phototoxicity. Nonetheless, I fused PMI and two linker sequences differing in their length to the N-terminus of LEXY, thereby creating PMI-1xGGS-LEXY and PMI-2xGGS-LEXY. Then, I expressed PMI-2xGGS-LEXY in HCT116 cells to observe initial localisation and evaluate its response to blue light.

The initial florescent signal was visible throughout the cells, yet strongest in the nucleus (Figure 3.8B). To observe the potential reaction to blue light, I exposed cells expressing PMI-2xGGS-LEXY to blue light for 40 minutes. After the activation, nuclear intensity was strongly reduced in the majority of cells, with a low number of cells exhibiting only minor changes in nuclear intensity or no reaction at all.

To verify the recovery potential of PMI-2xGGS-LEXY, I subjected cells to two activation/recovery cycles (40 minutes either in the dark or illuminated, total cycle time: 80 minutes) (Figure 3.8BC). HCT116 cells could repeatedly translocate PMI-2xGGS-LEXY into the cytosol and back upon blue light activation or inactivation, respectively. The relative nuclear intensity dropped to 36 %, and reverts back to the initial values.

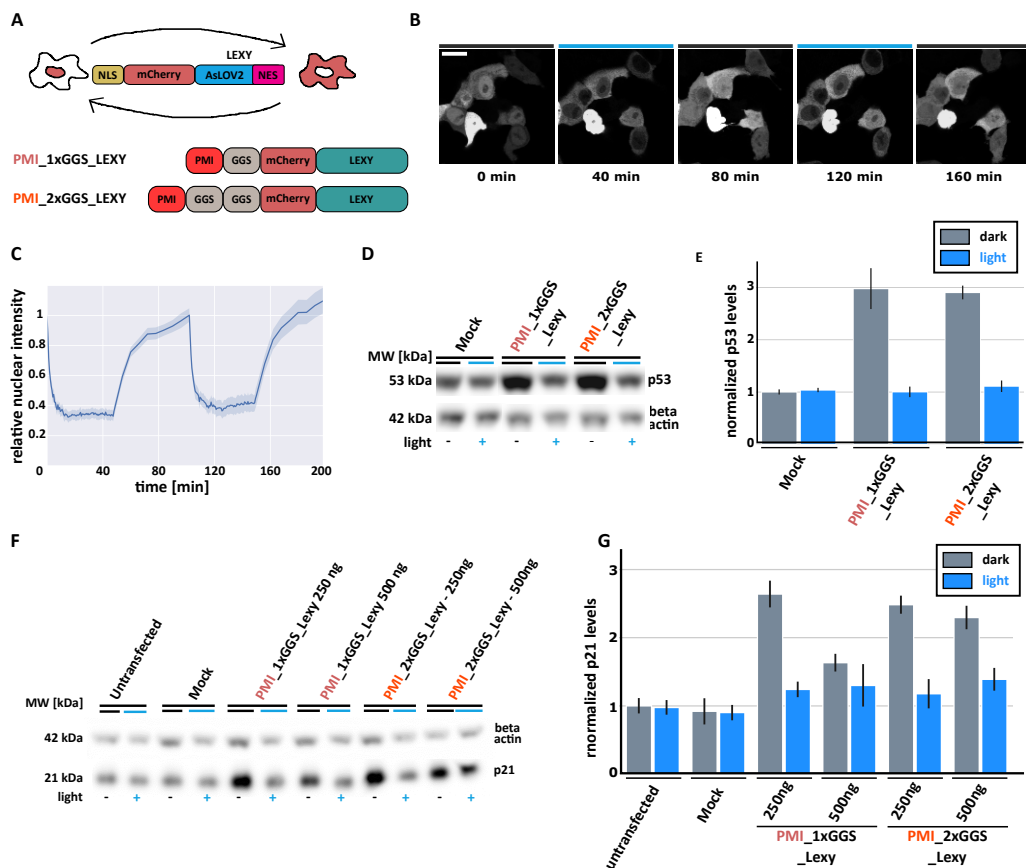


Figure 3.8: Using LEXY to control PMI translocation by light

A | LEXY is a small tag consisting of an NLS, mCherry and a AsLOV2 domain photocaging an engineered NES of varying strength. PMI was fused to LEXY yielding PMI-LEXY constructs differing in the length of their linker.

B | Representative images of HCT116 cells expressing PMI_1xGGGS_LEXY repeatedly activated for 40 minutes. 24 hours post transfection, cells were illuminated for 5 seconds every 30 seconds. In between activation periods, cells were not exposed to blue light. The mCherry channel was imaged every 30 seconds during activation cycles, and every 5 minutes during recovery. Scale Bar=20 μ m.

C | Quantification of relative nuclear intensity of **B**. Nuclear intensity over time was normalized to initial nuclear intensity (mean \pm SD, n=23).

D | Exemplary Western Blot of effect of PMI-LEXY on p53 levels. HCT116 cells were transfected with the indicated constructs and immediately exposed to blue light. 24 hours post transfection, cells were either illuminated for 24 hours, or not. Then cells were lysed, blotted and stained with the indicated antibodies.

E | Quantification of relative p53 expression levels of **D**. p53 levels were first normalized to beta actin, then to the illuminated mock-transfected sample (mean \pm SD, n=3).

F | Exemplary Western Blot of effect of PMI-LEXY on p53 levels. HCT116 cells were transfected with the indicated amount of the respective constructs and immediately exposed to blue light. 24 hours post transfection, cells were either illuminated for 24 hours, or not. Then cells were lysed, blotted and stained with the indicated antibodies.

G | Quantification of relative p21 expression levels of **F**. p53 levels were first normalized to beta actin, then to the illuminated mock-transfected sample (mean \pm SD, n=3).

As seen in other experiments, nuclear export appeared to be more rapid than the import. Half-life of nuclear export, meaning the time it takes for half of the final translocation to occur, was $93 \text{ s} \pm 18 \text{ s}$. In contrast, nuclear import took more than 4 times as long, namely $397.7 \text{ s} \pm 21 \text{ s}$.

Noteworthy, the achieved reduction of the relative nuclear intensity in the second activation period is slightly lower compared to the first activation period. As the intensity was also stronger after the second recovery period, this is likely due to continued expression of PMI-2xGGGS-LEXY during imaging. This suggests, that a fixed fraction of construct can be exported.

Next, I wanted to see, whether cells expressing PMI-LEXY exhibit light-dependent differential expression of

p53 target gene p21. To this end, I transfected HCT116 cells with either PMI-1xGGS-LEXY or PMI-2xGGS-LEXY and incubated them over night. Then, I exposed cells to blue light for 24 hours and measured p53 and p21 expression. Even though the translocation into the cytoplasm had appeared to be strong, this did not result in differential levels of p53 and expression of p21 (data not shown). Expression of p21 levels were equal in cells exposed to light or not, yet higher than in the mock-transfected control. I reasoned that overnight incubation in the dark, and thus nuclear PMI-LEXY was sufficient to increase p53 levels and induce p21 expression.

I repeated the experiment, but blue light was already applied immediately after transfection. Cells were incubated over night and exposed to blue light. On the next day, the dark control was removed from light and placed in a dark metal box shielded from light. 24 hours later, cells were lysed and p53 and p21 levels were determined.

Indeed, the application of light during transfection prevented premature function of PMI-LEXY in the nucleus. Cells expressing PMI-LEXY exposed to blue light exhibited the same p53 levels as mock-transfected samples (Figure 3.8DE). Yet, samples expressing one of the PMI-LEXY constructs which were removed from the initial blue light illumination had a three-fold increase in p53 levels. The increase in p53 levels was equal between both PMI constructs.

As seen in p53 levels, a clear light-mediated change in p21 levels was observable (Figure 3.8FG). While both mock- and untransfected cells were constant in the p21 levels independent off the illumination condition, both PMI-LEXY exhibited an approximately 2.6 fold increase in p21 levels when not exposed to blue light. Additionally, I verified effects on increased amount of transfected construct. When I transfected twice the amount of construct

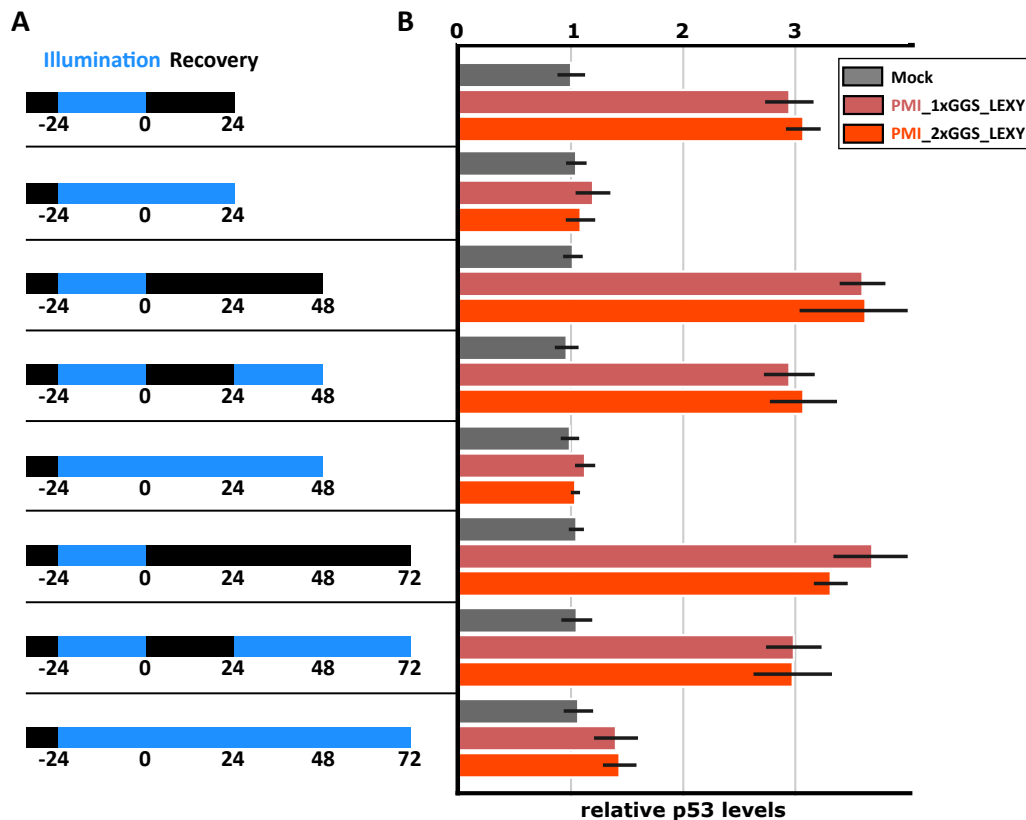


Figure 3.9: Evaluation of recovery potential of PMI_LEXY

A | Illumination and recovery pattern for different samples. All samples were transfected (-24 h) with PMI-1xGGS-LEXY or PMI-2xGGS-LEXY and immediately exposed to 24 hours of pulsatile blue light (5 seconds, 15 seconds). At time point 0 h, they received different illumination schemes to evaluate the recovery of p53 levels.

B | Quantification of relative p53 expression levels. HCT116 cells were transfected with the indicated constructs and immediately exposed to blue light. 24 hours post transfection, cells were exposed to illumination schemes displayed in A. Then cells were lysed, blotted and stained with the p53 and beta actin antibodies. p53 levels were first normalized to beta actin, then to the illuminated mock-transfected sample (mean \pm SD, n=3).

DNA, effects on p21 level seem to be reduced. Especially PMI-1xGGS-LEXY had a severely reduced impact on p21 levels when construct DNA was doubled.

This correlation between abundance of proteins to shuttle and their translocation efficiency has been observed in a wide range of experiments using either LINuS or LEXY and is probably caused by an overload of the cellular import-export machinery. Yet, the reason why p21 expression is weaker in cells transfected with PMI-1xGGS-LEXY than cells expressing PMI-2xGGS-LEXY remains elusive. Potentially, the length of the linker influences the translocation efficiency.

One of the main advantages of optogenetic tools based on the AsLOV2 is recovery after blue light activation into the dark state. As the localisation of PMI-LEXY is reversible (Figure 3.8B), I wanted to verify whether also p53 can revert back to normal physiological levels once blue light exposure is terminated. To this end, I transfected HCT116 cells with either PMI-1xGGS-LEXY or PMI-2xGGS-LEXY and exposed them to multiple light regimes differing in recovery timings (Figure 3.9A). Subsequently, cells were lysed and p53 levels were analysed.

As previously observed, p53 levels were three-fold elevated when cells were shielded from the light for 24 hours. In general, both constructs exhibited the same behaviour, thus I will refer now only to PMI-LEXY. Samples protected from light for prolonged periods continued to have high p53 levels (Figure 3.9B).

Cells exposed to light permanently for up to 72 hours did not show any increase in p53 levels, same as mock-transfected cells. Only cells exposed to blue light for 96 hours have slightly elevated levels of p53. This could be due to improper retention of PMI-LEXY in the cytosol, caused by increasing levels of PMI-LEXY and problems for the import-export machinery coping with the workload, or stress caused due to prolonged blue light exposure.

However, it appears that it is not possible to reverse the effect on p53 levels. Samples expressing PMI-LEXY shielded from the blue light after the initial exposure for 24 hours, had high levels of p53 independent of time period they were re-exposed to blue light. Neither 24 hours nor 48 hours of recovery is sufficient to lower p53 levels in a visible extent. This in contrast to the previous findings, that PMI-LEXY could be repeatedly and reversibly translocated between nucleus and cytosol, yet only in shorter time periods.

Taken together, while it is possible to increase endogenous p53 levels in a light-mediated fashion by using LEXY to control localization of the PMI-peptide, it seems as if p53 levels remain at the high level they exhibit once PMI-LEXY was nuclear for a certain period of time. Thus, reversibly control of endogenous levels could not be achieved.

3.2 Light-controlled nuclear import using LINuS

Translocation of proteins from one cellular compartment to another enables cells to react rapidly to changes in the environment. Especially transcription factors involved in stress signal pathways are commonly kept dormant in the cytoplasm, only to get actively translocated into the nucleus upon the necessary signal (Di Ventura and Kuhlman, 2016).

Here we wanted to mimic this general feature, even though p53's activity is usually regulated by keeping it at low levels in unstressed conditions. p53 activation dynamics, defined as the shape of the curve its transcriptionally activity changes over time, have been linked to specific upstream stress signals, as well as to distinct cell fates (Lahav et al., 2004; Batchelor et al., 2008; Purvis et al., 2012). While it has been established, which factors shape p53 activation dynamics, it remains unknown how specific activation dynamics are decoded into the appropriate gene expression. Here, we use optogenetic tools to control localisation of p53 by light, making use of its unmatched spatial and temporal resolution. By assuming that p53 is transcriptionally active once it is in the nucleus, light-mediated control over translocation would allow fine-tuning of nuclear abundance and the application of temporal dynamics, thus the amplitude and frequency of p53 signalling in the absence of stress.

3.2.1 Characterisation of p53^{wt}-LINuS constructs in H1299

To achieve optogenetic control over p53's localisation, I decided to employ LINuS. LINuS is a small versatile tag consisting of the AsLOV2 domain and a synthetic NLS incorporated in its J α -helix (Figure 3.10A) (Niopek et al., 2014). Variants of LINuS differing in their C-terminal NLS exhibit contrasting nuclear accumulation. As initial localisation and accumulation of LINuS is dependent on several factors, including the cell type, the expression levels, and both, presence of localisation sequences and size of the tagged protein, usage potentially requires fine-tuning of LINuS and the tagged protein itself.

I selected H1299 cells as a model to apply p53 dynamics, since this human non-small lung cancer cell line lacks expression of p53 protein due to a homozygous partial deletion of the p53 protein. The absence of endogenous p53 renders this cell line a good model system, and the cell line has been used in a wide range of studies in the p53 area.

I selected two LINuS variants, biLINuS02 and biLINuS22, and fused these to p53^{wt} (Figure 3.10A). Both variants differ in their localisation prior to blue light illumination, and the degree of nuclear accumulation upon activation (see also Figure 3.7B). p53^{wt} itself tagged with mCherry is localised exclusively in the nucleus (data not shown). Thus I decided to add a constitutive PKit NES to the p53^{wt}-LINuS constructs, to prevent nuclear localisation prior to activation. I expressed these constructs in H1299 cells and imaged the cells at the confocal microscope.

Prior to activation, both constructs localised exclusively within the cytosol (Figure 3.10B). After 40 minutes of blue light exposure, a minor increase in nuclear intensity could be observed within single cells, yet the majority of transfected cells did not react to blue light. In general, if not specifically mentioned otherwise, light was applied in light pulses. Periodic light pulses are sufficient to activate AsLOV2, as these pulses are shorter than the LOV-domains reversion time. Additionally, light pulses reduce light applied to cells, reducing any potential toxic effect. Pulses of 5 seconds every 30 seconds are considered as constant illumination.

Localisation of proteins appears to be a steady state, yet it is rather an equilibrium of ongoing import and export. The net localisation of a protein is determined by the presence and strength of NLS and/or NES sequences, which eventually result in a localisation balance. Here, localisation of the constructs is strongly cytosolic, thus I decided to remove the constitutive PKit NES on the one hand, and also try the weaker I κ B α NES. I expressed both constructs in H1299 cells and observed localisation in the absence of blue light. Constructs lacking a constitutive NES were exclusively nuclear (Figure 3.10), making blue light activation futile. Adding a weaker NES had the same effect on localisation of p53^{wt}-biLINuS22, fluorescence was only visible in the nucleus (data not shown).

On the contrary, p53^{wt}-biLINuS02 localised mostly within the nucleus, yet a cytosolic signal was also observ-

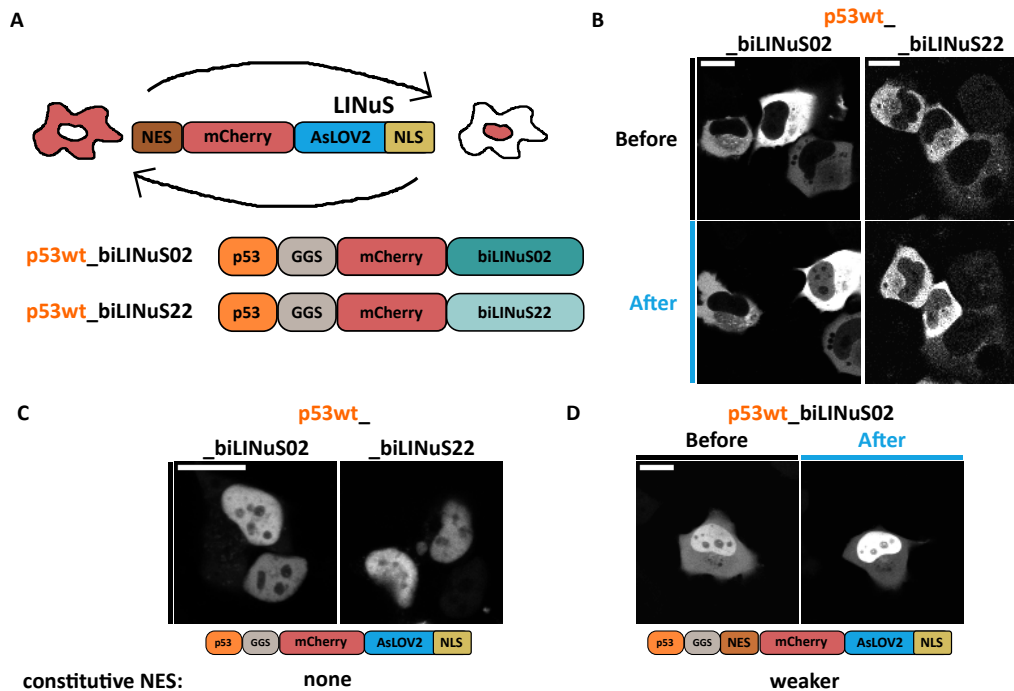


Figure 3.10: Characterisation of p53wt-LINuS in H1299 cells

A | LINuS is a small tag consisting of the AsLOV2 domain photocaging an engineered NLS of varying strength. p53^{wt} was fused N-terminally to a constitutive NES, mCherry and one of two LINuS versions differing in their initial cytoplasmic-nuclear localization and strength of nuclear accumulation upon blue light activation, yielding the constructs p53^{wt}-biLINuS02 and p53^{wt}-biLINuS22.

B | Representative images of the indicated p53^{wt}-LINuS shown in **A** expressed in H1299 cells before and after 40 minutes activation. 24 hours post transfection cells were illuminated for 5 seconds every 30 seconds using a blue laser. Scale Bar=20 μ m.

C | Representative images of the indicated p53^{wt}-LINuS constructs lacking the constitutive NES of LINuS expressed in H1299 cells. 24 hours post transfection cells were analysed on the microscope. Due to initial nuclear accumulation cells were not exposed to blue light. Scale Bar=40 μ M.

D | Representative images of p53^{wt}-biLINuS harbouring the weaker constitutive I κ B α NES expressed in H1299 cells before and after 40 minutes activation. 24 hours post transfection cells were illuminated for 5 seconds every 30 seconds using a blue laser. Scale Bar=20 μ m.

able. Even though this initial localisation is unfavoured in my case, due to putative transcriptional activity prior to activation, I wanted to verify whether p53^{wt}-biLINuS02 translocated in response to blue light. Thus, I activated the sample 40 minutes using the blue laser of the confocal microscope. Indeed, after exposure a clear nuclear accumulation was visible in most of the observed cells. This suggests that LINuS can be used to translocate p53^{wt} in the nucleus, yet further optimisation on the localisation state prior illumination is necessary.

3.2.2 Impairment of p53's NES allows nuclear accumulation

So far, the two investigated p53^{wt}-LINuS constructs did not show the desired characteristics of being exclusively cytosolic before activation, and displaying a nuclear localisation sufficient to induce transcriptional activity. Manipulation of the constitutive NES had an apparent bivalent behaviour: either the constructs were initially cytosolic and remained cytosolic after activation, or exhibited a strong nuclear localisation already prior to activation. Thus, I decided to manipulate rather p53's endogenous NES than the NES fused in between p53 and LINuS.

p53's localisation is determined by a bipartite NLS sequence, and a C-terminal NES sequence (Figure 3.11A) (O'Keefe et al., 2003). While p53 possesses functions within the cytosol, its main task is transcription and thus requires nuclear localisation. The NES consists of 4 amino acid residues, namely M340, L344, L348 and L350. M340 and L344 are associated to the hereditary disease Li-Fraumeni, which pre-disposes patients to cancer develop-

ment (Malkin et al., 1990; Kawaguchi et al., 2005). Thus, I mutated the two leucines at residue 348 and 350 to alanines and fused p53^{L348AL350A} to biLINuS02 or biLINuS22. Additionally, I added a constitutive NES. Both constructs were transfected and subsequently visualised at the confocal microscope.

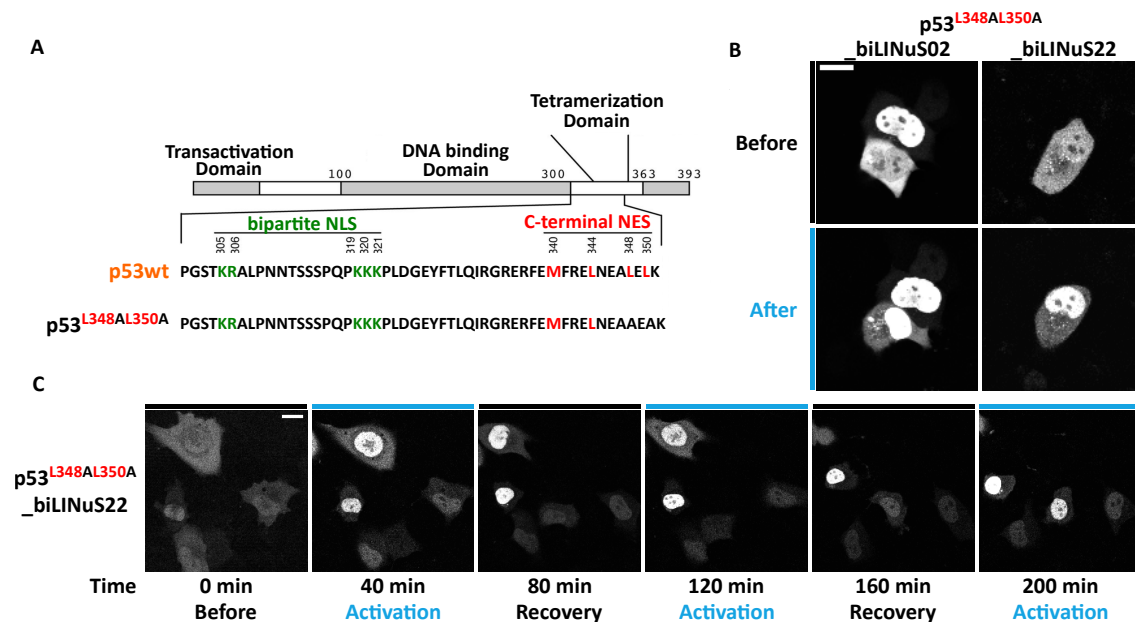


Figure 3.11: Manipulation of p53's endogenous NES sequence

A | Schematics of p53 and its localization sequences. NLS sequences are highlighted in green, NES sequences in red. Adapted from O'Keefe et al. (2003).

B | Representative images of the indicated p53^{L348AL350A}-LINuS expressed in H1299 cells before and after 40 minutes activation. 24 hours post transfection cells were illuminated for 5 seconds every 30 seconds using a blue laser. Scale Bar=20 μm .

C | Representative images of the p53^{L348AL350A}-biLINuS22 throughout several activation-recovery cycles. 24 hours post transfection, the same cells were repeatedly subjected to blue light for 5 seconds every 30 seconds for 40 minutes, then left in the dark to recover. Scale Bar=20 μm .

p53^{L348AL350A}-biLINuS02 displayed a strong nuclear signal prior to activation (Figure 3.11B). In the majority of cells expressing the construct, the fluorescent signal was exclusively nuclear. Few cells had evenly distributed signal. Within these cells, a clear accumulation in the nucleus after 40 minutes of blue light exposure could be observed.

Most cells expressing p53^{L348AL350A}-biLINuS22 displayed a evenly distributed signal prior to activation (Figure 3.11B). Once activated by blue light for 40 minutes, a clear accumulation was observable.

To verify whether this accumulation was reversible, I repeatedly activated the same field of view for 40 minutes with blue light, followed by 40 minutes recovery intervals during which cells were not subjected to blue light (from now on referred to as 40 minute activation/recovery intervals). As seen before, p53^{L348AL350A}-biLINuS22 translocates into the nucleus upon activation, yet the nuclear signal remains strong during the recovery periods. Rather, with every activation period, some cells accumulate the construct even further, or start accumulating it within the nucleus. Interestingly, some cells only displayed nuclear accumulation in the second or third activation period, not before. As reversibility is crucial to apply pulsatile p53 dynamics, p53^{L348AL350A}-biLINuS22 had to be further optimised.

3.2.3 Introduction of compensatory mutations on p53's endogenous NLS

I reasoned that both, initial nuclear localisation and nuclear retention after blue light exposure might be reduced by manipulating p53's endogenous NLS sequence. p53 harbours a bipartite NLS, the first stretch consists of a lysine at position 305 and an arginine at position 306. The second part of the p53's NLS consists of three lysines at

positions 319, 320 and 321 (Figure 3.12A) (O’Keefe et al., 2003). While these mutants have been studied already in the combination with mutations to p53’s NES (Figure 3.11, I wanted to analyse their contribution to localisation of p53 individually, independent of the NES mutation. To this end, I mutated every individual lysine into an alanine. Additionally, in one construct, I mutated both K305 and R306. These mutants were created in the p53^{L348AL350A}-biLINuS22 background. I expressed each construct in H1299 cells, and examined the localisation of the constructs.

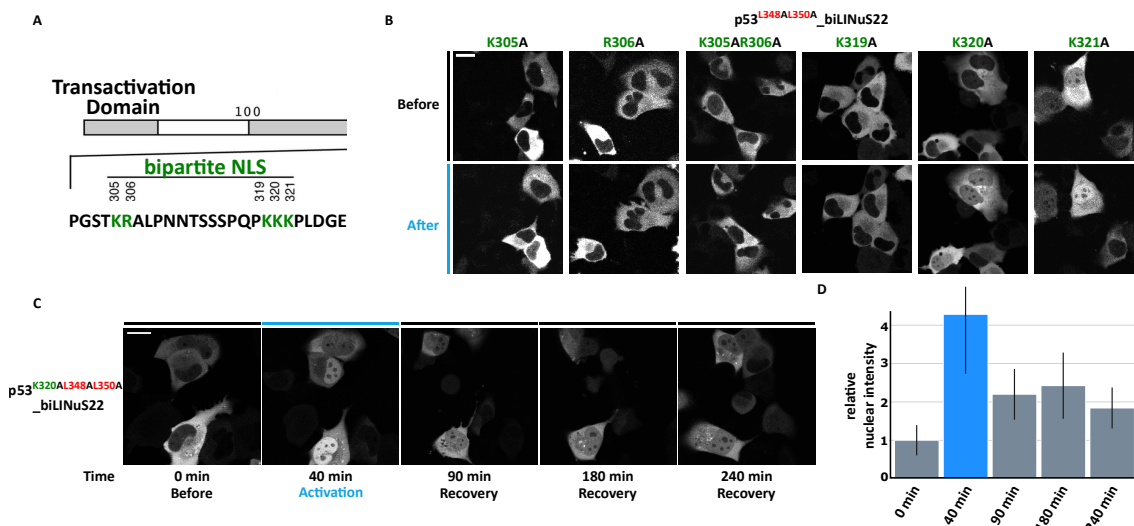


Figure 3.12: Mutation of p53’s NLS sequence to improve translocation properties

- A** | p53 possesses two separated NLS sequences, here highlighted in green. Adapted from O’Keefe et al. (2003).
- B** | Representative images of mutated NLS residues in the p53^{L348AL350A}-biLINuS22 background. H1299 cells expressing indicated constructs before and after 40 minutes activation. 24 hours post transfection cells were illuminated for 5 seconds every 30 seconds using a blue laser. Scale Bar=20 μ M.
- C** | Representative images of p53^{K320AL348AL350A}-biLINuS22 construct expressed in H1299 cells. 24 hours post transfection, cells were exposed to blue light for 40 minutes, then continuously imaged for 200 minutes in the absence of blue light. Scale Bar=20 μ M.
- D** | Quantification of relative nuclear intensity of cells before activation and during recovery. Nuclear intensity was normalized to initial values (mean \pm SD, n=28).

Single and double mutants of K305 and R306 exhibited the same behaviour (Figure 3.12B). Prior to activation, the signal was almost exclusively within the cytosol, yet after 40 minutes of activation, only a minority of cells had detectable nuclear fluorescence.

Like the K305 and R306 mutants, p53^{K319AL348AL350A}-biLINuS22 exhibited an exclusively cytoplasmic signal, which remained at its initial localisation even after activation (Figure 3.12B). p53^{K320L348AL350A}-biLINuS22 was faintly visible within the nucleus of the majority of cells prior to blue light exposure. Upon activation, a clear translocation was observable, leading to an increased nuclear fluorescence. Yet, a cytoplasmic signal remained, and tended to have a similar intensity as the nuclear signal.

p53^{K321AL348AL350A}-biLINuS22 exhibited a stronger nuclear intensity before activation (Figure 3.12B). The majority of cells responded to blue light by accumulating it further in the nucleus. Cells responding to blue light displayed a higher nuclear-cytoplasmic intensity ratio as cells transfected with p53^{K320L348AL350A}-biLINuS22. These findings suggest that the first basic stretch of p53’s bipartite NLS contributes more to the nuclear localisation of p53 than the second stretch, as the nuclear translocation appears to be dependent on the integrity of K305 and R306.

I selected p53^{K320AL348AL350A}-biLINuS22 for further analysis, due to its favourable initial equilibrium, and the high fraction of cells responding to blue light activation. To verify the reversibility of nuclear accumulation, I exposed cells expressing the construct to blue light for 40 minutes and subsequently tracked the sample in the absence of blue light. As previously seen, a nuclear accumulation was observable after activation (Figure 3.12CD).

The nuclear intensity increased approximately four-fold (Figure 3.12D). Once blue light is deactivated, the nuclear intensity decreased, yet remained more than two-fold higher compared to the initial state prior to activation for 40 minutes. This suggests that p53^{K319AL348AL350A}-biLINuS22 can translocate back into the cytosol once p53-LINuS is activated, but only to a certain extent. The initial cytosolic state could not be fully reverted.

3.2.4 Assessment of transcriptional activity of p53^{K320AL348AL350A}

p53^{K320AL348AL350A}-biLINuS22 is the first p53-LINuS candidate that fulfilled the two main criteria required to achieve light-regulated transcriptional activity of p53. First, p53^{K320AL348AL350A}-biLINuS22 was located primarily in the cytoplasm prior to activation. Second, the construct could be accumulated in the nucleus.

I wanted to verify the transcriptional activity of p53^{K320AL348AL350A}-biLINuS22 and observe, whether the p53 target gene p21 was differentially expressed in cells subjected to blue light. To this end, I expressed p53^{K320AL348AL350A}-biLINuS22 in H1299 cells and subjected cells either to 24 hours of blue light, or incubated them in a light-shielded environment.

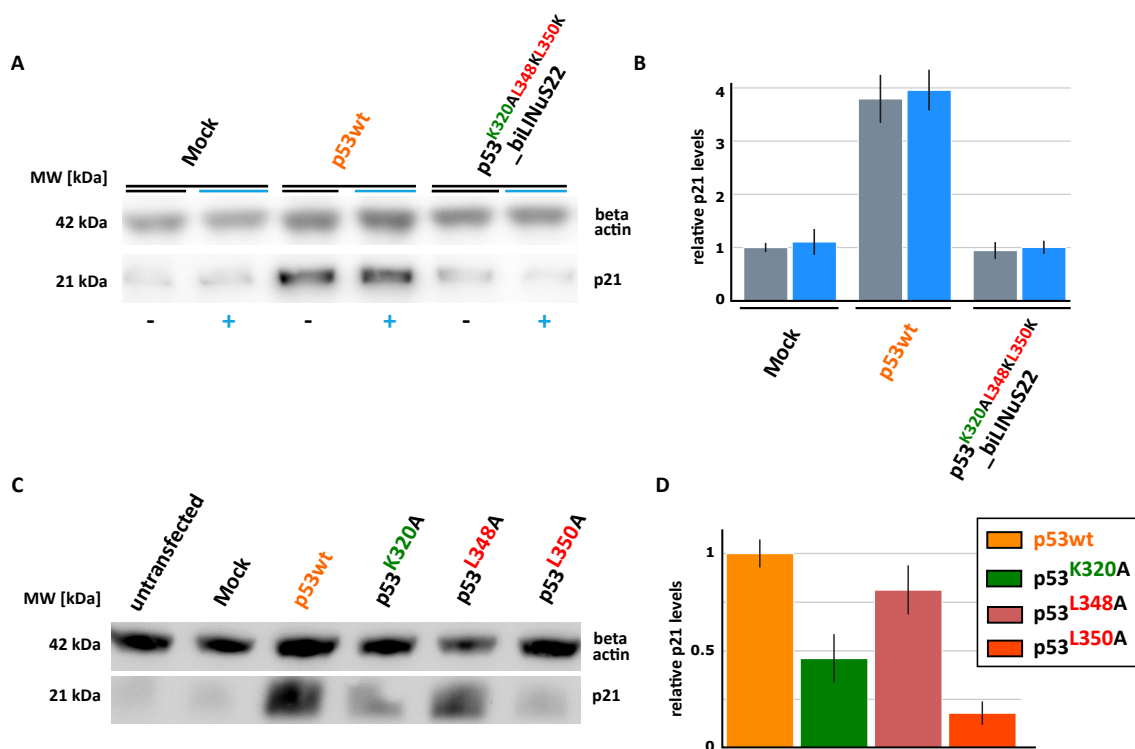


Figure 3.13: Evaluation of impact on transcriptional activity of introduced p53 mutations

A | Exemplary Western blot of p21 levels upon transfection with indicated constructs. 24 hours post transfection, H1299 cells were illuminated for 24 hours in the presence of blue light (5 seconds/15 seconds). Controls were kept in the dark. Subsequently, cells were lysed, blotted and stained with the indicated antibodies.

B | Quantification of relative p21 levels of **A**. p21 levels were first normalized to beta actin, then to the mock-transfected, non-illuminated sample (mean \pm SD, n=3).

C | Exemplary Western blot of p21 levels upon transfection with indicated constructs. 36 hours post transfection, H1299 cells were lysed, blotted and stained with the indicated antibodies.

D | Quantification of relative p21 levels of **C**. p21 levels were first normalized to beta actin, then to the p53^{wt} transfected sample (mean \pm SD, n=3).

Expression of p53^{wt} resulted in a four-fold increase of p21 expression, independent of blue light exposure (Figure 3.13A, B). On the other hand, p53^{K320AL348AL350A}-biLINuS22 exhibited approximately the same level of p21 expression as the mock-transfected sample. I reasoned that the lack of transcription can be either caused by an insufficient amount of nuclear p53, or that the introduced mutations might impair the transcriptional activity of

p53^{K320AL348AL350A}. I decided to first investigate the latter possibility, since the transcriptional activity is essential for the continuation with this construct.

I introduced the three individual mutations K320A, L348A and L350A in the p53^{wt} background and fused them to mCherry. To ensure nuclear localisation, I added a constitutive NLS. Then, I expressed the constructs in H1299 cells to verify transcriptional activity of each single mutant. All introduced mutations decreased p53's transcriptional activity (Figure 3.13C, D). The L350A mutation had the strongest negative effect on p53 transcriptional activity, as it caused a five-fold reduction of p21 levels compared to p53^{wt}. Mutating K320A resulted in a 50% decrease in p21 levels. Mutation of L348A reduced p21 levels by 20%.

Compared to p53^{wt}, the transcriptional activity of the triple mutant p53^{K320AL348AL350A} was only slightly more reduced as the transcriptional activity of p53^{L350A}.

3.2.5 Acetylation-mimicking mutants do not restore transcriptional activity of p53^{K320AL348AL350A}

Due to the essential functions of transcription factors, their regulation has developed into a highly complex process. While regulation at the level of transcription or translation takes rather long (minutes to hours), other regulatory steps occur in seconds. Particularly post-translational modifications such as phosphorylation and acetylation have been demonstrated to regulate transcription factors, allowing a fine-tuned and rapid reaction to stimuli (Planey et al., 2013).

p53 itself undergoes a wide range of post-translational modifications. While phosphorylation is rather linked to stabilisation of p53, acetylation is implicated in regulating p53's affinity to a subset of target genes, including p21 (Meek, 2004; Kruse and Gu, 2008; Tang et al., 2008). This hypothesis is based on *in vitro* and cell culture studies; the role of acetylation on the transcriptional activity of p53 has not been established in animal studies. I thought to stimulate the transcriptional activity of p53^{K320AL348AL350A} by introducing acetylation-mimicking mutations at the key residues K120, K164 and K165 (see Chapter 1.1.3). K120 is located within the DNA-binding domain of p53, and its acetylation is supposedly required for transcriptional activity and induction of apoptosis (Berns et al., 2004; Sykes et al., 2006; Tang et al., 2006). K164 and K165 have been particularly linked to p21 expression (Tang et al., 2008).

Introduction of a glutamine at these individual sites mimics acetylation, thus should stimulate p21 expression. To verify this idea, I introduced acetylation-mimicking mutations in the p53^{K320AL348AL350A}-biLINuS22 background and expressed the constructs in H1299 cells to verify p21 expression.

Introduction of the acetylation-mimicking mutations did not result in an increase in p21 levels (Figure 3.14A, B). The mutants were not transcriptionally active, as demonstrated by the fact that p21 levels were as high as

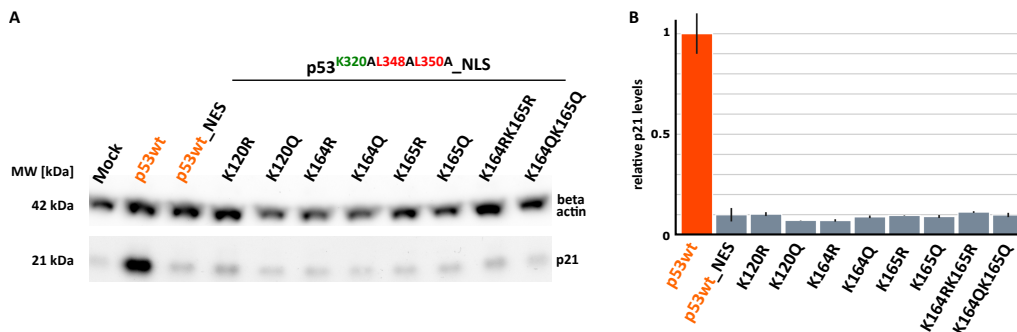


Figure 3.14: Introduction of acetylation mimicking mutants to recover transcriptional activity

A | Exemplary Western blot of p21 levels upon transfection with indicated constructs. 36 hours post transfection, H1299 cells were lysed, blotted and stained with the indicated antibodies.

B | Quantification of relative p21 levels of **A**. p21 levels were first normalized to beta actin, then to cells expressing p53^{wt} (mean \pm SD, n=3).

those obtained with the negative control (cytoplasmic p53). Notably, according to the literature, loss of acetylation on one residue can be compensated by acetylation of another site, thus one acetylated site should be sufficient to drive transcription (Tang et al., 2008). As transcriptional activity is mandatory for studying how p53 dynamics regulate the selection of target genes, I stopped working with this construct.

3.2.6 Characterisation of p53 NLS mutants

The initial p53^{wt}-LINuS constructs lacking a constitutive NES had been exclusively nuclear, while the constructs harbouring a constitutive NES were localised in the cytosol (Figure 3.10). Due to previous observations, I decided against mutating p53's endogenous NES to prevent impairment of tetramer formation. I reasoned that the net localisation of p53^{wt}-LINuS constructs lacking a constitutive NES could be shifted towards a more cytosolic localisation by manipulating p53's endogenous NLS sequence. Yet, prior to investigating potential translocation efficiencies of individual p53 NLS mutant-LINuS constructs, I wanted to assess the initial localisation of p53 NLS mutants to estimate the contribution of individual residues to overall localisation. Additionally, I needed to verify the transcriptional activity of individual mutants. To do so, I fused each p53 NLS mutant to mCherry to observe its localisation. Additionally, I fused the p53 NLS mutants to a NLS-tagged mCherry to evaluate p21 expression (Figure 3.15A).

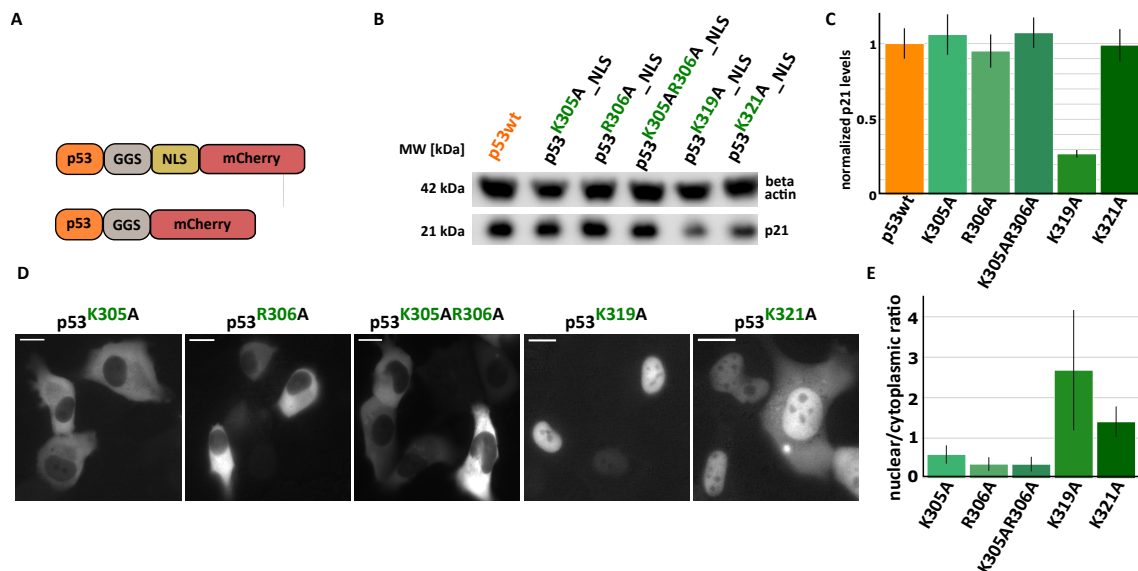


Figure 3.15: Characterisation of p53 NLS mutants

- A** | Schematic overview over p53-NLS mutant constructs cloned. p53 mutants were fused to NLS-mCherry to assess transcriptional activity. Localization of NLS mutants was visualized with fused mCherry.
- B** | Exemplary Western blot of p21 levels upon transfection with indicated NLS-mutant. 36 hours post transfection, H1299 cells were lysed, blotted and stained with the indicated antibodies.
- C** | Quantification of relative p21 levels of **A**. p21 levels were first normalized to beta actin, then to cells expressing p53^{wt} (mean \pm SD, n=3).
- D** | Representative images of the p53 NLS-mutants expressed in H1299 cells. Scale Bar=20 μ M.
- E** | Quantification of nuclear/cytoplasmic intensity of indicated NLS-mutants (mean \pm SD, n=30).

p53^{K305A}, p53^{K306A} and p53^{K321A} were not affected in their transcriptional activity (Figure 3.15B, C). Mutation of K319 led to a dramatic reduction of p21 expression. This leads to the conclusion, that only the NLS residues K319 and the previously analysed K320 are necessary for p21 expression.

Next, I expressed the p53-NLS mutants fused to mCherry in H1299 cells, and examined their localisation. Mutations in the first basic stretch of p53's bipartite NLS had severe effects on the localisation of the construct, as they led to a cytosolic localisation (Figure 3.15D, E). Mutation of the K319A exhibited a nuclear localisation, as observed in cells expressing p53^{wt}. Mutation of K321A led to a clear nuclear signal. Some cells also exhibited

cytosolic fluorescence, yet the nucleus had the most prominent fluorescent signal in all cells. As the contribution of the first stretch of p53's bipartite NLS sequence to nuclear localisation appears to be stronger, as well as mutating K305 and R306 did not affect transcriptional activity, I selected the single mutants K305A and R306A and the double mutant K305AR306A to further investigate their potential translocation ability when fused to LINuS variants.

3.2.7 Nucleo-cytoplasmic translocation of p53-LINuS constructs

LINuS variants differ in the strength of their photocaged NLS. I selected variants with a strong NLS caged in the AsLOV2, since the selected p53-NLS mutants displayed a strong cytosolic localisation. I fused either biLINuS02, biLINuS09 or biLINuS11 to each of the three selected p53 NLS mutants p53^{K305A}, p53^{R306A} and p53^{K305AR306A}, and expressed the constructs in H1299 cells, to observe their initial localisation. Noteworthy, all constructs lack a constitutive NES.

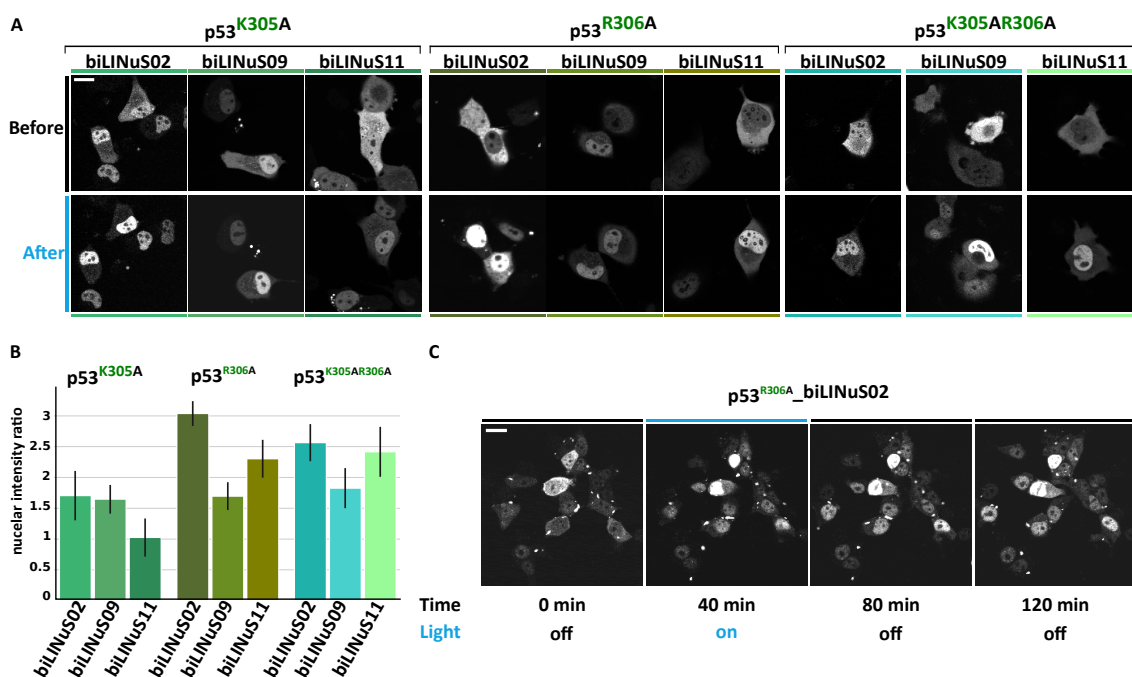


Figure 3.16: Screening of p53 NLS mutant-LINuS variants to investigate their translocation efficiency

A | Representative images of the indicated p53-NLS mutant to the respective LINuS-variant before and after 40 minutes activation. 24 hours post transfection cells were illuminated for 5 seconds every 30 seconds using a blue laser. Scale Bar=20 μ M.

B | Quantification of nuclear intensity ratio before and after blue light activation of **B** (mean \pm SD, n=22).

C | Representative images of p53^{R306A}-biLINuS02 expressed in H1299 cells. 24 hours post transfection, cells were exposed to blue light for 40 minutes, then continuously imaged for 80 minutes in the absence of blue light. Scale Bar=20 μ M.

In general, all p53 NLS mutant-LINuS constructs displayed nuclear accumulation after blue light exposure (Figure 3.16A). p53^{K305A}-LINuS constructs exhibited already a strong nuclear fluorescent signal prior to illumination. Activation with blue light led to a stronger nuclear accumulation for p53^{K305A}-biLINuS02 and p53^{K305A}-biLINuS09, with an increase in nuclear accumulation up to 60 % (Figure 3.16B).

p53-LINuS variants harbouring the R306A mutation tended to have a more cytosolic localisation compared to p53^{K305A}-LINuS constructs before cells were activated. Particularly p53^{R306A}-biLINuS02 exhibited a rather cytosolic signal prior to activation, and a three-fold increase in nuclear intensity upon blue light illumination. Also p53^{R306A}-biLINuS11 exhibited a similar behaviour, nuclear intensity was 2.3-fold elevated after blue light activation.

Constructs harbouring the double mutant K305AR306A were initially rather evenly distributed between the nucleus and the cytosol, and exhibited a two to 2.5-fold increase in nuclear intensity upon blue light exposure.

I selected p53^{R306A}-biLINuS02 for further investigation, as it was located primarily in the cytosol prior to activation, and showed the highest fold-change in nuclear intensity after blue light stimulation. Additionally, the response was homogeneous, the majority of cells reacted to blue light by increasing nuclear abundance of the construct.

Next, I wanted to assess the reversibility of the nuclear accumulation of p53^{R306A}-biLINuS02. Thus, I activated cells expressing p53^{R306A}-biLINuS02 for 40 minutes, and then continued imaging for 80 minutes in the absence of blue light. While a clear nuclear accumulation appeared upon blue light exposure, no reduction in nuclear intensity could be observed during the recovery phase in the absence of light, suggesting that re-translocation into the cytosol impaired.

3.2.8 Introduction of a constitutive NES to achieve reversible translocation of p53^{R306A}-biLINuS02

The lack of reversibility of nuclear accumulation prohibits application of pulsatile p53 dynamics. So far, the only p53 mutant that showed at least partial re-translocation into the cytosol once blue light was turned off was p53^{K320AL348AL350A}, yet the introduced mutations rendered it transcriptionally inactive. Presumably, this mutant was impaired in forming tetramers, due to the mutations within p53's NES sequence. This suggests that the formation of tetramers might cause the impairment of re-translocation into the cytosol once illumination is turned off. Under physiological conditions, p53 can be exported in the cytosol. However, p53 is more likely to form tetramers at high nuclear levels. p53 tetramer dissociation half-times have been estimated to be around 40 minutes in unstressed conditions (Natan et al., 2009), thus might lead to the translocation impairment of p53^{R306A}-biLINuS02 (Figure 3.16).

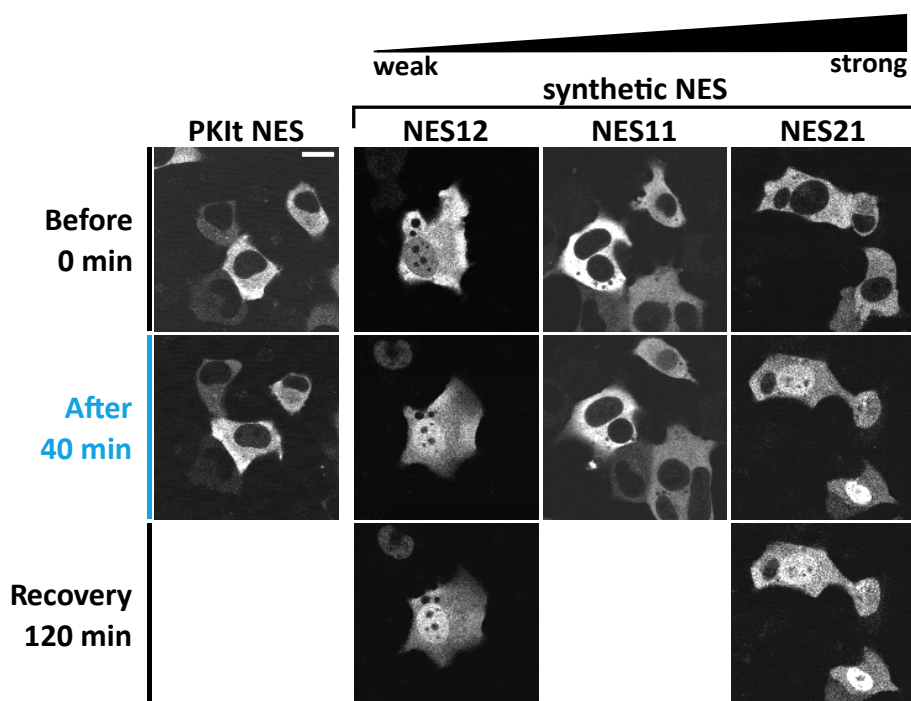


Figure 3.17: Assessment of effect of introducing NES's on translocation of p53^{R306A}-biLINuS02
Representative images of indicated NESs possessing varying strength cloned in between p53^{R306A} and biLINuS02. H1299 cells expressing the indicated constructs were subjected to blue light for 40 minutes. If a visible nuclear accumulation could be detected, cells were incubated for 40 minutes at the absence of light. Scale Bar=20 μ M.

But the sheer size might not be the cause of the nuclear retention. The net localisation is an equilibrium of p53^{R306A}'s localisation sequences and those of LINUS. During blue light stimulation, the increase in nuclear abundance putatively leads to the formation of tetramers. As p53's tetramerisation domain and its NES sequence partly overlaps, the NES sequence is shielded after tetramer formation (Stommel et al., 1999). Once the NES is not accessible any more, the localisation equilibrium could be shifted to a more nuclear position, which is not reversible until the tetramers dissociate.

I reasoned that adding a constitutive NES might lead to a more cytosolic signal prior to activation, and would potentially enable reversibility once p53 becomes nuclear and forms tetramers. To this end, I added either a PKit NES, or three synthetic NESs from a NES library created by Dominik Niopek, ranging from weak to strong. I inserted the NES in between p53^{R306A} and LINUS and expressed the respective construct in H1299 cells to observe the cells at the microscope.

The strength of the PKit NES is average and supposedly similar to the synthetic NES11. Introducing these two NESs to p53^{R306A}-LINUS02 resulted in a cytoplasmic localisation of the construct (Figure 3.17). Upon light stimulation, only a minority of cells seemed to respond by a slight increase in nuclear intensity. Due to these unfavourable translocation conditions, the experiments were not continued.

Introduction of the synthetic NES12, the supposedly weakest of the tested NESs, did not result in any change of initial localisation, compared to the construct lacking a constitutive NES (Figure 3.16). The most prominent signal was visible in the cytosol, yet also nuclear fluorescence could be seen. Upon blue light exposure, a clear increase in nuclear intensity was observable, which was not shuttling back into the cytosol once blue light was turned off.

As suspected, introduction of the synthetic NES21 caused a clear cytosolic signal, with no nuclear signal visible. Surprisingly, blue light exposure led to nuclear translocation, even though the NES is supposedly the strongest selected NES. The nuclear accumulation was not reversible.

However, using LINUS to control localisation of p53 by light was not successful. Manipulation of p53's endogenous localisation sequences was necessary to enable light-mediated translocation into the nucleus. Only the transcriptionally inactive p53^{K320AL348AL350A} exhibited partial re-translocation into the cytosol, once illumination was turned off. At this point, I stopped working with LINUS, and began trying to control localisation of p53 by LEXY.

3.3 Controlling p53 localisation with LEXY

3.3.1 Characterisation of transiently transfected p53^{wt}-LEXY in H1299 cells

Similarly to LINuS, LEXY is an optogenetic tool to control localisation of tagged proteins (Niopek et al., 2016). Instead of exposing a NLS sequence upon blue light illumination, a NES is unmasked. Therefore, a protein initially located in the nucleus can be translocated into the cytoplasm. LEXY consists of the AsLOV2 domain harbouring a NES within its J α helix (Figure 3.18A). LEXY is usually fused to mCherry, to track localisation, and a constitutive NLS, to provide a nuclear localisation of the tagged protein prior to activation. Yet the necessity of the constitutive NLS depends solely on the cargo protein and its localisation sequences.

3.3.1.1 Light-mediated translocation of p53^{wt}

Due to the irreversibility of nuclear translocation observed in p53-LINuS constructs, I wanted to verify whether p53^{wt} can be translocated using LEXY as straightforward as other proteins, or whether further optimisation was necessary. One disadvantage when using LEXY to control localisation of transcription factors like p53 is the nuclear localisation prior to blue light exposure, potentially inducing transcription prior to the start of an experiment. Yet, p53-LINuS constructs were either transcriptionally inactive, or could not be fully re-translocated into the cytoplasm once the construct was nuclear, thus can not be used to apply p53 dynamics. Therefore, I decided that it was worth nonetheless trying to control p53 dynamics with LEXY, even if that meant shining light from the beginning on to prevent p53 transcriptional activity before the start of the experiment.

I started out by fusing p53^{wt} to LEXY, and added either the constitutive cMyc NLS, or the weaker cMyc^{P1A} NLS (Figure 3.18A). Additionally, I inserted mCherry, to monitor localisation of the p53^{wt}-LEXY constructs. I expressed both constructs in H1299 cells. Both constructs showed a clear, nuclear localisation prior to blue light exposure (Figure 3.18B).

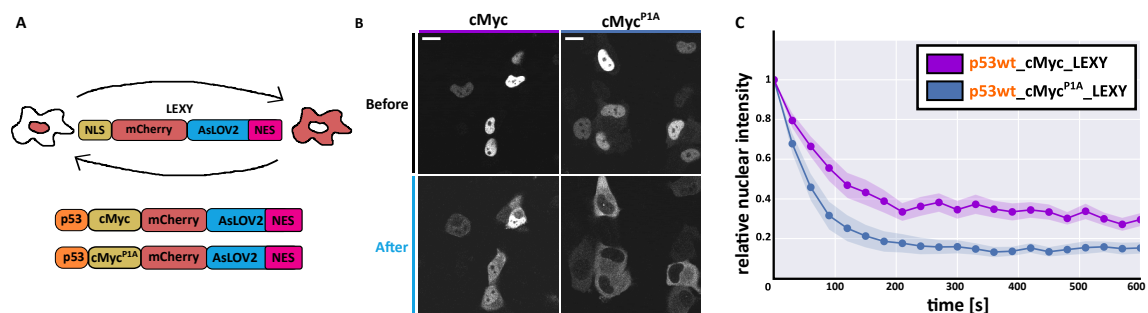


Figure 3.18: Characterisation of p53^{wt}-LEXY

A | LEXY is a small tag consisting of an AsLOV2 domain photocaging an engineered NES. p53^{wt} was fused N-terminally to mCherry, one of two constitutive NLS sequences of differing strength, and LEXY.

B | Representative images of the indicated p53^{wt}-LEXY constructs shown in **A** expressed in H1299 cells before and after 40 minutes of activation. 24 hours post transfection cells were illuminated for 5 seconds every 30 seconds using a blue laser (458 nm). Scale Bar=20 μ m.

C | Quantification of the relative nuclear intensity of the indicated constructs shown in **B**. Nuclear intensity over time was normalized to the initial nuclear intensity of the respective construct. Dots represent images taken (mean \pm SD, n=30).

The nuclear signal was stronger in cells expressing the construct harbouring the stronger cMyc NLS. The cMyc^{P1A}-construct was also predominantly nuclear before activation. 40 minutes of activation with the blue laser resulted in a visible translocation of both constructs into the cytosol, yet more effective for p53^{wt}-LEXY harbouring the weaker cMyc^{P1A}.

In contrast, once activated with blue light, the cMyc^{P1A} construct was almost exclusively in the cytosol, with only barely visible nuclear fluorescence in a minority of cells. In general, translocation was observed in the majority

of cells expressing the constructs, yet translocation efficiency was depending on the abundance of the respective construct. The higher the protein levels, the less efficient the translocation appeared to be.

Cytoplasmic translocation occurred faster and more efficiently for the cMyc^{P1A}-construct, a reduction of nuclear intensity to approximately 20% was observed (Figure 3.18C). The p53^{wt}-LEXY construct possessing the stronger cMyc NES exhibited a reduction of nuclear intensity to around 30% upon activation. The high nuclear intensity prior to activation led to a still prominent nuclear signal, even though more than two thirds of the expressed construct was translocated.

Based on its translocation kinetics, I selected p53^{wt}-LEXY harbouring the cMyc^{P1A} NLS, from now on referred to as p53-LEXY, for further analysis. Next, I wanted to observe whether p53-LEXY could be reversibly translocated between the cytoplasm and the nucleus, thus I expressed p53-LEXY in H1299 cells and repeatedly activated cells for 40 minutes with blue light, followed by 40 minute recovery phases. In contrast to any of the p53-LINuS constructs, p53-LEXY could be repeatedly shuttled between the nucleus and the cytosol without any manipulation on p53's localisation sequences (Figure 3.19A). Half-time of nuclear export was $83s \pm 27.5s$, half-life time of import was about $462s \pm 39.4s$ (Figure 3.19B). As seen before, for both LINuS and LEXY constructs, nuclear export occurred more rapid than nuclear import.

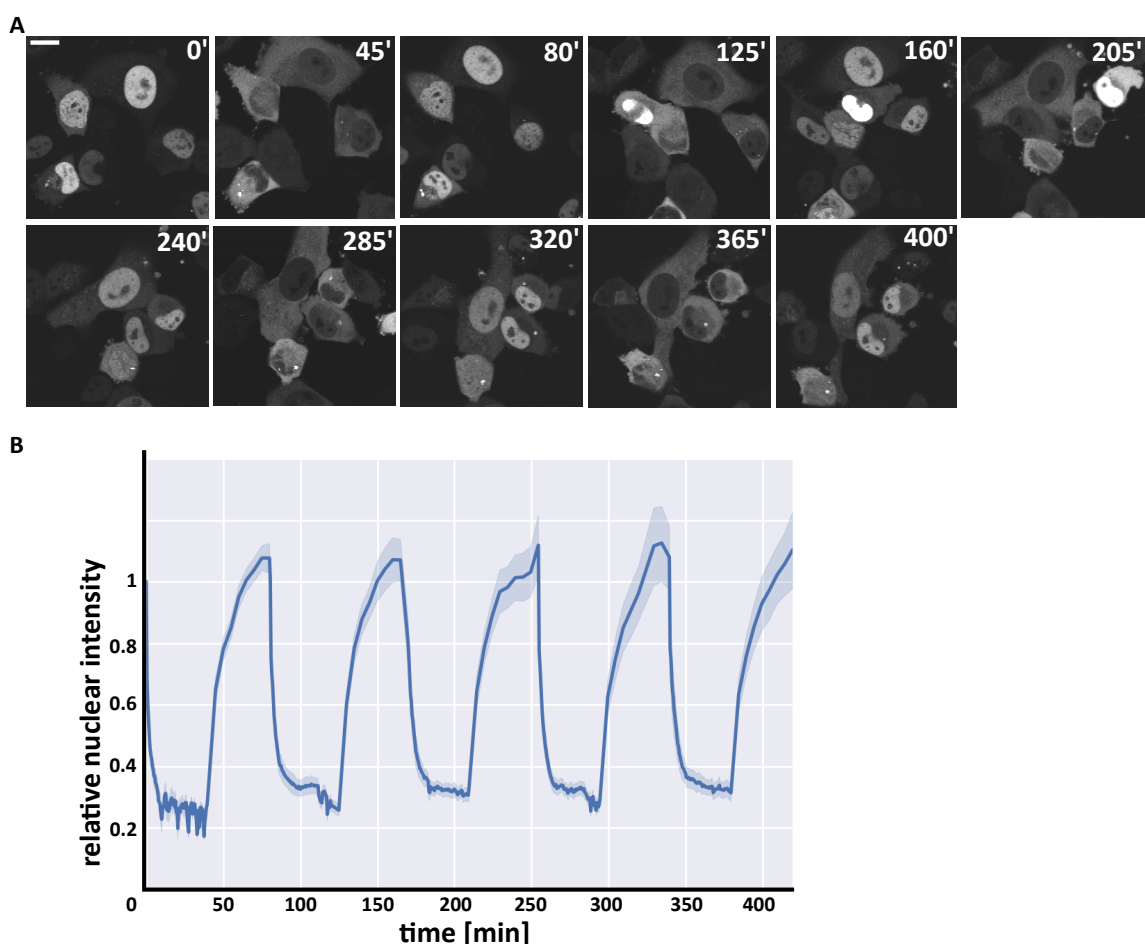


Figure 3.19: p53^{wt}-LEXY can be repeatedly translocated into the cytosol

A | Representative images of p53^{wt}-LEXY repeatedly activated for 40 minutes. 24 hours post transfection cells were subjected to 40 minute activation and recovery intervals. Scale Bar=20 μ m.

B | Quantification of the relative nuclear intensity of p53^{wt}-LEXY. Nuclear intensity over time was normalized to the initial nuclear intensity (mean \pm SD, n=29).

Within the first seconds of each activation phase, relative nuclear intensity reached almost its minimum, with only a slight further reduction during the remaining activation period. Re-import into the nucleus during the

recovery period was slower. In the course of the experiment, there was a slight increase in nuclear fluorescence, probably due to continued expression of p53-LEXY.

These data suggest that p53^{wt} can be reversibly translocated, in contrast to data obtained with p53-LINuS constructs. LEXY was shown to efficiently translocate a range of tagged proteins, with, if at all, only minor adjustments necessary. Yet, as both optogenetic tools make use of the endogenous translocation machinery, it remains puzzling that LEXY shuttling appears to be reversible, yet LINuS-induced translocation is not.

3.3.1.2 Light-mediated control over transcriptional activity of p53

p53-LEXY's ability to be reversibly accumulated in and out of the nucleus is a first step towards the application of p53 dynamics. Next, I needed to verify whether p53-LEXY remains transcriptionally active. To this end, I expressed p53-LEXY in H1299 cells. 24 hours post transfection, cells were either exposed to light or not. Expression levels of p21 were high in both, illuminated and non-illuminated samples (data not shown). Probably, the initial incubation in the absence of light leads to nuclear p53 levels high enough to trigger a full transcriptional response that cannot further be increased/decreased. Thus, I repeated the experiment, and exposed cells immediately after transfection to blue light to prevent premature expression of p53 target genes. 24 hours later, illumination was either continued or stopped.

The adapted protocol led to differential p21 expression in cells expressing p53-LEXY, dependent on blue light exposure (Figure 3.20A). Cells not receiving light had p21 expression levels similar to samples expressing p53^{wt}, while light-exposed p53-LEXY samples exhibited a three-fold reduction in p21 expression (Figure 3.20B). Light-exposed p53-LEXY expressing cells possessed slightly higher p21 levels than mock-transfected or p53^{wt}-NES-expressing cells. Presumably, the prolonged activation did not result in complete cytosolic translocation.

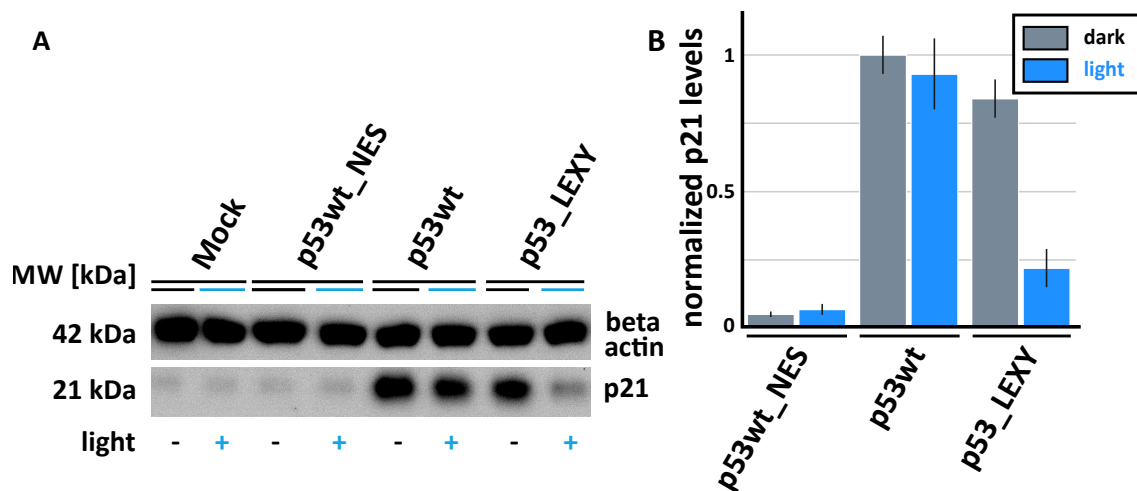


Figure 3.20: Light-mediated expression of p21 by p53^{wt}-LEXY

A | Exemplary Western Blot of light-dependent effect of p53^{wt}-LEXY on p21 levels. H1299 cells were transfected with the indicated constructs and immediately exposed to blue light. 24 hours post transfection, cells were either illuminated for 24 hours, or not. Then cells were lysed, blotted and stained with the indicated antibodies.

B | Quantification of relative p21 expression levels of **A**. p53 levels were first normalized to beta actin, then to the illuminated p53^{wt}-transfected control (mean ± SD, n=3).

Taken together, p53-LEXY could be reversibly translocated between cytosol and nucleus, while remaining transcriptionally active. Additionally, the transcriptional activity could be controlled by blue light exposure. Thus, p53-LEXY possesses all necessary features to apply p53 dynamics in the absence of upstream stress.

3.3.1.3 High and heterogeneous p53-LEXY expression impairs its translocation

Since p53-LEXY is transcriptionally active and can be reversibly translocated, I decided to apply pulses resembling the physiological p53 dynamics observed upon γ -irradiation. The number of these pulses induced by DNA damage correlate to the severity of DNA damage, while the period of the pulses is apparently fixed at about 4 hours (Batchelor et al., 2011). Prolonged pulsatile activation has been linked to cell cycle arrest, whereas continuous activation of p53 induced by UV-radiation triggers apoptosis (Purvis et al., 2012). Applying the different patterns lacking the upstream stress and thus any side-effects of the induced stress could help elucidate the precise role of p53 dynamics.

So far, I only applied simple illumination schemes, meaning either light is turned on or off. These experiments have been carried out in the incubator. Cells have been either shielded from the light, or were illuminated by 6 LEDs located within the cell incubator driven by an external power box. The power box was connected to a notebook running the manufacturer's software to manipulate the two settings of the power box, the voltage, and thus the intensity of the LEDs, and the activation state, meaning the on/off state of the LEDs. The software lacked functionality to generate more complex illumination routines, mostly due to a limited amount of commands that could be entered and sent to the power box. Additionally, the software did not have a logging-system, so no record of executed commands could be retrieved after an experiment. To address these issues with the manufacturer's program, I decided to use a Raspberry Pi, a small single-board computer, to control the power box.

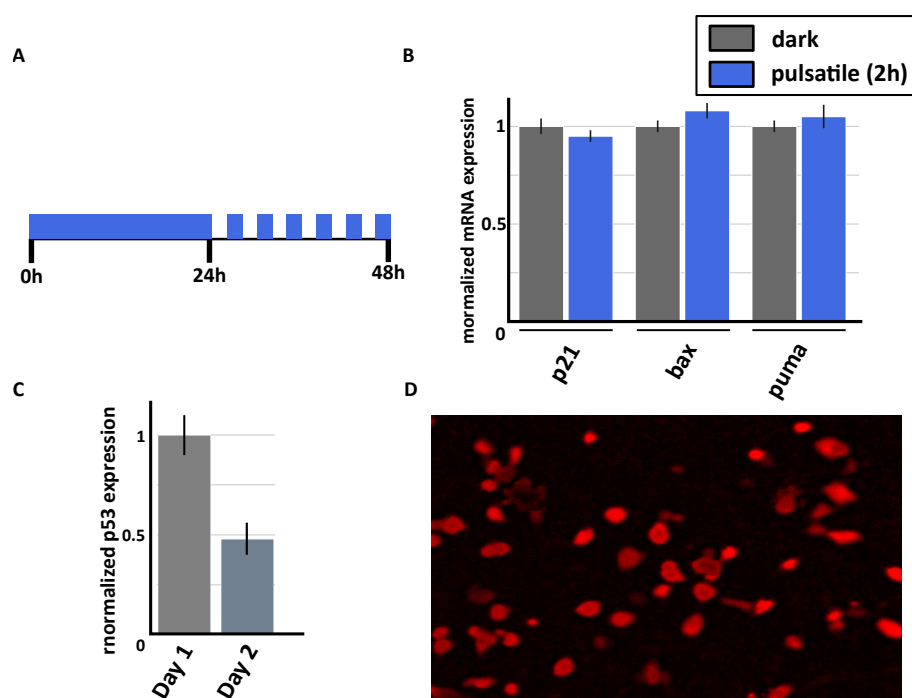


Figure 3.21: High p53-LEXY expression levels impair translocation

A | Schematics of the illumination pattern applied in **B**. Immediately after transfection, H1299 cells were exposed to blue light. 24 hours later, cells received 6 periods of 2 hours remaining in the dark and 2 hours of light exposure.

B | Normalized mRNA expression of indicated p53 target genes after application of illumination pattern described in **A**. Control cells were shielded from light after initial 24 hours of blue light exposure. Then, cells were lysed and RNA was extracted. Expression levels were first normalized to beta actin and Rpl0, then to the expression values of the sample remaining in the dark for 24 hours (mean \pm SD, technical replicates $n=3$).

C | Normalized mRNA expression of p53 of identical treated replicates on different days. After 24 hours of exposure to blue light, H1299 cells expressing p53-LEXY were lysed and RNA was extracted. Expression levels were normalized to beta actin and Rpl0 (mean \pm SD, technical replicates $n=3$).

D | Representative image of fixed H1299 cells expressing p53-LEXY after being subjected to the pulsatile light scheme shown in **A**. Picture taken with a table top microscope. Scale Bar=20 μ m.

The Raspberry Pi runs a python script written by me to control activation and intensity of the LEDs, which can be customized to any possible light illumination regime.

I expressed p53-LEXY in H1299 cells, and exposed cells to blue light immediately after transfection. Then I applied either repeatedly 2 hour activation-recovery intervals, or kept cells in the dark (Figure 3.21A), resembling either pulsatile activation by γ -irradiation or continuous activation triggered by UV-radiation. p53 target genes involved in cycle arrest (p21) and apoptosis (bax and puma) were not differentially expressed after application of the two different illumination regimes (Figure 3.21B).

The fact that there was no difference between the two conditions could be due to a technical or a biological reason. Technical reasons comprise heterogeneous p53 levels. If p53 levels are very different among cells and if the difference between p53 dynamics were apparent only at a specific concentration of p53, a population-based readout, like the RT-PCR I am using, won't be able to capture the response of individual cells. Additionally, cells with too high levels of p53-LEXY may not be able to export it efficiently, thus naturally responding as if p53 levels were always high, masking the difference between the pulses and the constant activation.

When I set out to repeat the experiment, I immediately realised that the fluorescent signal was weaker than the intensity observed during the first experiment. Thus I compared expression of p53 in biological replicates after the initial illumination period, to verify if p53 levels were similar. I expressed p53-LEXY in cells for 24 hours during light exposure on two different days and compared p53 expression levels. In two different days, p53 levels were highly variable, exhibiting a two-fold difference in expression (3.21C). Presumably, the difference is caused by different transfection efficiencies between experiments.

The difference in p53 levels was worrying, as it was technically not possible at this time to observe the translocation in cells during an optogenetic experiment carried out in the incubator. To compensate for this, I decided to fix cells during the experiment to visualize the efficiency of translocation. I decided to first verify localisation at the end of the pulsatile illumination scheme. I expressed p53-LEXY in H1299 cells, and illuminated cells for 24 hours. Then, I applied pulsatile illumination for 24 hours and fixed cells right before the end of the last activation phase. The cells displayed widely heterogeneous expression of p53-LEXY within a single sample (Figure 3.21D). Most cells expressed so much p53-LEXY that it was not possible to distinguish between the cytosol and the nucleus. As seen in previous experiments, high expression of LINuS or LEXY constructs impaired translocation. This suggests that expression levels are too high for the import-export-machinery to cope with the ongoing translocation between nucleus and cytosol, and the lack of differential gene expression observed here is due to lack of p53-LEXY translocation.

3.3.2 Design of a stable cell line expressing p53-LEXY

Transfection of p53-LEXY resulted in a highly heterogeneous expression within and between samples. Additionally, expression over prolonged time was too high, and not constant, which is a requirement for ensuring long-term application of p53 dynamics. Lowering the transfected amount of DNA resulted in an overall reduction of p53-LEXY expression, yet increased the heterogeneity between cells (data not shown). Thus, I decided to generate a stable cell line expressing p53-LEXY, as stable integration enables a homogeneous expression of a protein of interest.

3.3.2.1 Integration of TetR and p53-LEXY in H1299 cells

Cells respond to stress by stabilisation and activation of p53, and continuous activity of p53 eventually triggers irreversible cell fates, such as apoptosis or senescence (Purvis et al., 2012). Thus, an inducible gene expression system for regulation of p53-LEXY expression is required to prevent constitutive p53-LEXY expression. Inducible gene expression systems enable triggering the expression of the gene of interest at a specific time point via the addition of an activator, for instance a small molecule.

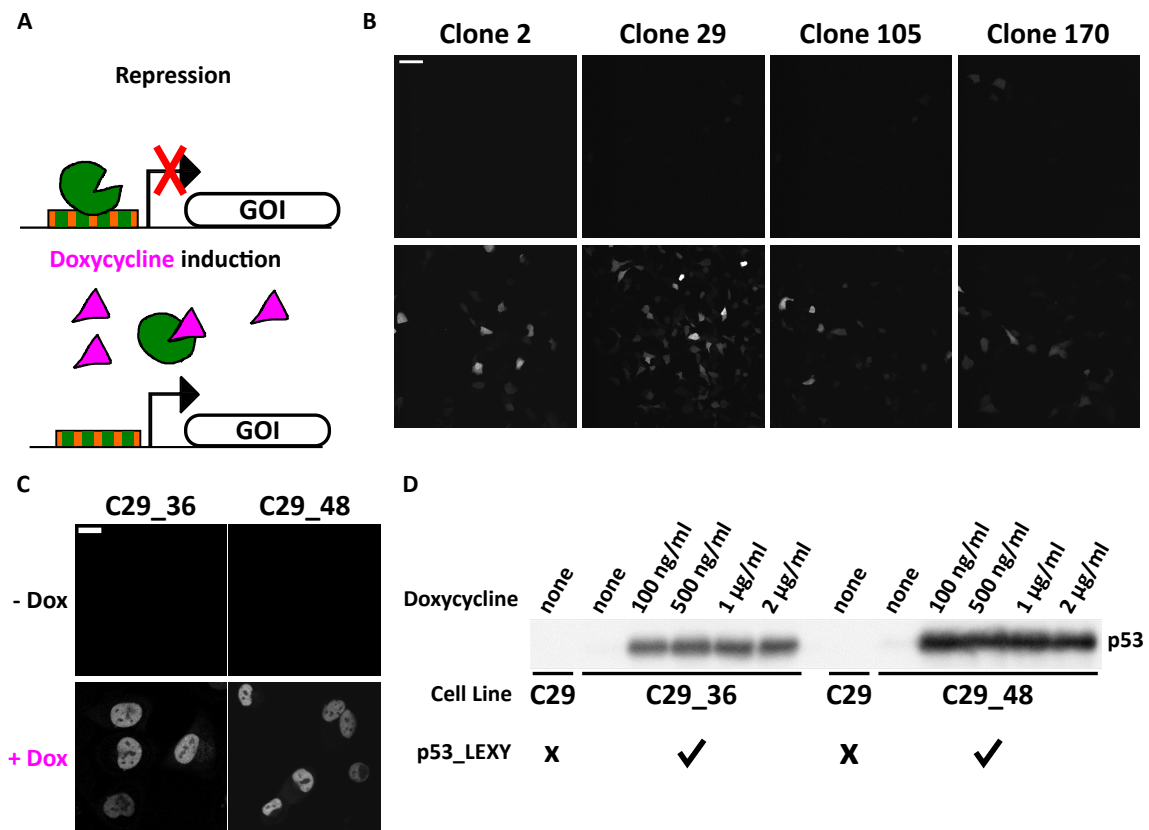


Figure 3.22: Generation of a stable cell line expressing p53-LEXY

A | Schematic representation of the T-REx™ system. In the absence of doxycyclin, TetR is tightly bound to the tetO binding sites within the minimal cmv promoter. Upon doxycyclin treatment, doxycyclin binds TetR and sequesters it from the tetO sites, thus stimulating expressing the gene of interest. GOI=Gene of interest.

B | Representative images of 4 clones after integration of constitutively expressed TetR transfected with a plasmid harbouring a tet-responsive promoter driving mCherry. Cells were transfected with the plasmid and incubated for 24 hours. Then, cells were treated with 1000 ng/ml doxycyclin for 24 hours. Then, clones were screened for differentially expressed mCherry. Scale Bar=40 µM.

C | Representative images of two clones expressing integrated p53-LEXY upon doxycyclin stimulation. Clones were either treated with 1000 ng/ml or not, and screened for differentially expressed p53-LEXY. Scale Bar=20 µM.

D | Western Blot of doxycyclin-dependent p53-LEXY expression. Indicated clones were incubated with the respective doxycyclin conditions for 24 hours. Then cells were lysed, blotted and stained with a p53 antibody.

I decided to use the T-REx™ system to enable inducible gene expression of p53-LEXY in response to doxycyclin (Yao et al., 1998). It consists of two plasmids, the first harbouring a constitutively expressed tet repressor protein (TetR) and a blasticidin resistance and the second plasmid containing a minimal CMV promoter with two integrated tetracycline operator sequences (tetO) sites, regulating expression of a gene of interest and a constitutively expressed Zeocin™ resistance gene. In the inactivated state, the constitutively expressed TetR forms homodimers and binds the tetO sequences in the minimal CMV promoter, and thus prohibits expression of the target gene (Figure 3.22A) (Hillen and Berens, 1994). Doxycyclin binds the TetR repressor, which subsequently can not bind the tetO sequences any more. Thus addition of doxycyclin corresponds to the release of the transcriptional repression, allowing expression of the gene of interest.

First, I generated a stable cell line constitutively expressing TetR. After incubation of cells transfected with the plasmid carrying the TetR and the blasticidin resistance in media supplemented with the experimentally determined minimal selective concentration of blasticidin (0.03%), samples were seeded out in 96-well plates at a concentration of 0.5 cells per well. Two weeks later, 96 well-plates were screened for individual colonies. Wells lacking cells or having more than one single colony were neglected. Monoclonal colonies were further expanded

and then transfected with a plasmid harbouring a TetR-responsive promoter driving mCherry. From 243 clones, 4 displayed the desired behaviour upon doxycycline treatment. mCherry fluorescence prior to doxycycline was not visible or weak, while fluorescence was high after induction (Figure 3.22B).

I selected the clones 2 and 29 for integrating p53-LEXY, since they had either no, or a very weak mCherry expression in the absence of doxycycline, while displaying strong homogeneous expression after induction. I decided not to focus on a single clone, as integration into the genome is a stochastic process and the site of integration contributes to the expression of the integrated gene of interest. Here, I needed to have sufficient levels of TetR high enough to repress p53-LEXY in the absence of doxycycline but low enough to be able to allow expression in the presence of the molecule. I reasoned that this balance of repression and activation can rather be achieved when assessing p53-LEXY integration in multiple clones.

Then, I cloned p53-LEXY into the plasmid carrying the TetR-responsive promoter and transfected the plasmid into both clones cultured in the presence of 0.03% blasticidin and 0.05% Zeocin™. After applying the previously described work flow, two clones out of 378 displayed no expression in the absence of induction, and a clear nuclear signal after 24 hours of doxycycline treatment (Figure 3.22C). Interestingly, both clones derived from the same parental clone C29.

Surprisingly, while clone C29-48 expressed higher levels of p53 than clone C29-36, the concentration of doxycycline did not affect expression levels (Figure 3.22D). Presumably, doxycycline concentrations did affect p53-LEXY levels to some degree, yet the Western Blot was not sensitive enough to detect subtle changes in expression. Notably, in the absence of doxycycline there was no detectable p53-LEXY expression, like in the parental C29 cell line.

This suggests, that regulation of p53-LEXY expression was tight enough in the absence of doxycycline. Upon doxycycline addition, repression is relieved, and thus expression of p53-LEXY is initiated.

As mentioned above, both the TetR repressor and p53-LEXY are randomly inserted into the genome. Random integration brings the risk that integration occurred in important genetic regions. Even though I could not detect changes in cellular appearance or cell proliferation, the chance remained that integration occurred in a general regulatory region or even on a node within p53's regulatory network, which displays no phenotype in the absence of stress, yet is crucial in regulating p53's transcriptional response.

To investigate the localisation of the random integration of the two transfected plasmids, I repeatedly tried inverse PCR with several protocols and various primers, but could not identify the site of integration (data not shown).

3.3.2.2 Characterisation of the stable cell line

Next, I wanted to verify whether p53-LEXY expression was more homogeneous in the stable cell lines C29-36 and C29-48 than in transiently transfected H1299 cells. Homogeneous expression is a requirement for population-based experiments.

I expressed p53-LEXY, either by transient transfection or doxycycline induction, and compared their normalized intensity of p53-LEXY expression (Figure 3.23A). It is important to note that clones stably expressing p53-LEXY upon induction were imaged with identical microscopy settings, while the transiently transfected sample was imaged using less laser intensity due to the higher expression levels. The heterogeneity of expression within the transiently transfected sample, represented by the error bar, is high, while the expression of p53-LEXY was more heterogeneous in the created stable cell lines.

Doxycycline induced expression was about 2.5-fold higher in C29-48. Relative to the overall intensity, the heterogeneity of expression was almost identical between the two clones. While C29-36 cells displayed comparable p53 levels in independent experiments, C29-48 reduced both intensity of individual cells and the number of fluorescent cells over the course of two weeks (data not shown). Even though I initially considered working with both cell lines, I continued focussing on C29-36.

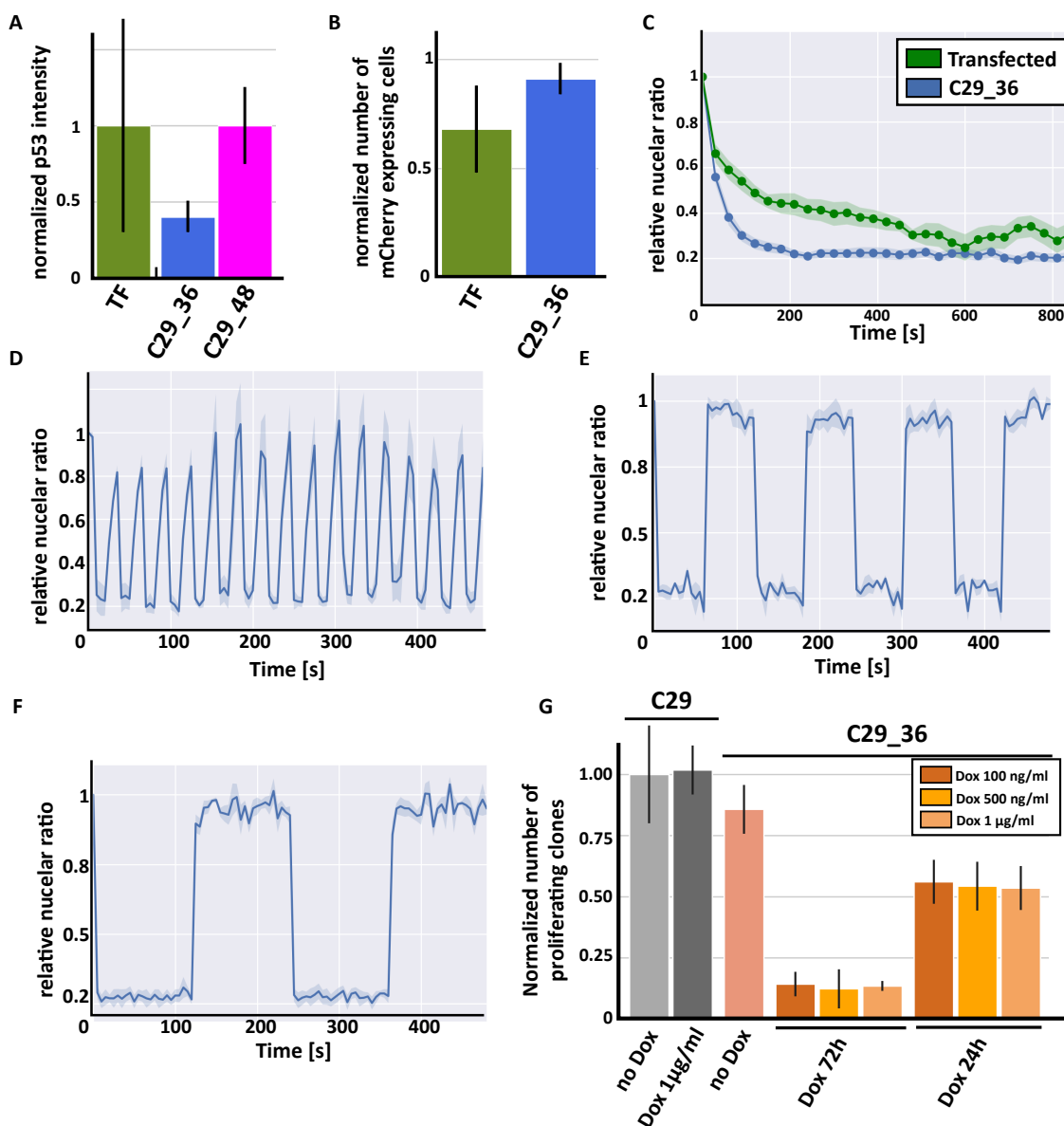


Figure 3.23: Characterisation of the monoclonal C29-36 cell line

A | Quantification of the relative fluorescent intensity of transfected and induced C29-36 cells after 24 hours of p53-LEXY expression. Different microscope settings were used for transiently transfected cells and stable cell lines (mean \pm SD, n=37).

B | Quantification of percentage of either H1299 or C29-36 cells expressing p53-LEXY after transient transfection or induction with 100 ng/ml for 24 hours (mean \pm SD, samples=3, cells per sample n=27).

C | Quantification of relative nuclear intensity of indicated constructs expressed for 24 hours. Then, cells were illuminated for 40 minutes with blue light. Nuclear intensity over time was normalized to initial nuclear intensity of the respective construct. Dots represent imaged time points (mean \pm SD, n=23).

DEF | Quantification of the relative nuclear intensity of C29-36 expressing p53-LEXY for 24 hours exposed to 15 minute pulses (**C**), 1 h pulses (**D**) or 2 hour pulses (**E**) of blue light. Nuclear intensity over time was normalized to the initial nuclear intensity of the respective construct (mean \pm SD, n=32).

G | Quantification of the number of formed colonies after p53-LEXY expression. C29-36 cells and the parental cell line were either incubated for 24 hours or 72 hours in the presence of indicated doxycycline concentrations. Then, cells were trypsinized, counted, and 100 cells were seeded in a new well. Cells were incubated for 10 days, then cells were fixed and subsequently stained with Crystal Violet. Numbers of colonies were normalized to non-induced C29 cells (mean \pm SD, n=3).

The amount of C29-36 cells expressing p53-LEXY after doxycycline induction was higher than 90%, while only

about 65% of the transiently transfected H1299 cells expressed p53-LEXY (Figure 3.23B). This means, that a third of the cells did not express the construct at all. Additionally, heterogeneity in transfection or induction efficiency across three independent experiments was higher in transfected cells. This shows that the stable cell line C29-36 ensures a more robust expression of p53-LEXY than transiently transfected H1299 cells.

Next, I sought to compare the translocation kinetics in the transiently transfected H1299 cells and the stable cell line C29-36. Translocation occurred faster, and more efficiently in the C29-36 cells (Figure 3.23C). It has to be mentioned, that the transiently transfected p53-LEXY did translocate slower and remained more nuclear than in previous experiments during blue light exposure, highlighting once more that the heterogeneity in transiently transfected samples can impact population-based read-outs.

p53-LEXY expressed in C29-36 cells could be repeatedly translocated in a pulsatile fashion, with periods of 30 minutes (15 minutes activation/recovery intervals), 2 hour (1 hour activation/recovery intervals) and 4 hours (2 hour activation/recovery intervals) (Figure 3.23D, E, F), thus covering a wide range of periods, even faster than physiological p53 pulses, which show periods of about 4 hours upon activation (Batchelor et al., 2011).

Constitutive p53 expression has been linked to senescence (Batchelor et al., 2011). I wanted to evaluate whether prolonged nuclear presence of p53-LEXY can trigger the physiological effect. I could show that transiently transfected p53-LEXY remained transcriptionally active, and that p21 levels increased due to nuclear abundance of p53-LEXY. Yet, an increase of p21 protein levels do not necessarily result in senescence as perturbation of a complex network does not necessarily result in a change of outcome, due to the high regulation of individual nodes.

Especially for senescence, it is suggested that a single marker is not sufficient to correctly define its onset (Hernandez-Segura et al., 2018). To facilitate the readout, and avoid complex marker combinations, I selected a more straight-forward approach. I induced C29-36 and the parental C29 cell line with different doxycycline concentrations. As p53-LEXY levels seemed to be similar for different doxycycline concentrations after 24 hours, I incubated C29-36 cells either 24 or 72 hours in the presence of doxycycline. I reasoned that longer incubation period could result in higher p53-LEXY levels. C29 cells were incubated only at the highest doxycycline concentration for 72 hours. Then, 100 cells of each sample were seeded in a new well to evaluate their colony-forming potential. After 10 days of incubation, single colonies were visualized by Crystal Violet Staining.

The number of newly formed colonies of C29-36 was clearly dependent on p53-LEXY levels (Figure 3.23G). Doxycycline induction for 24 hours led to 33% reduction in the number of colonies, independent of the doxycycline concentration. Longer doxycycline incubation periods caused a more severe phenotype, as the colony number was 8-fold reduced. Prolonged doxycycline exposure did not affect colony number in the parental C29 cell line. Thus, the reduction of colonies is due to p53-LEXY levels.

Notably, no stress has been applied, the induction of senescence is solely triggered by p53-LEXY expression. Either post-translational modifications of p53 only play a minor role in causing senescence, or prolonged nuclear abundance caused the required modifications.

Non-induced C29-36 cells exhibited about 80% of the colony number of the parental C29 cell line. Presumably, basal p53-LEXY expression occurred even in the repressed state, and contributed to the reduction in colony formation. This is in contrast to the p53-LEXY levels determined by Western Blot, as there was no p53 signal visible in non-induced C29-36 cells (Figure 3.22D).

In conclusion, p53-LEXY stably integrated in H1299 cells exhibits homogeneous expression, can be reversibly translocated in pulses of different frequencies and can induce senescence in the absence of stress. This makes the C29-36 cell line a suitable model system to analyse differential gene expression triggered by p53 dynamics.

3.3.3 Prolonged light exposure affects p53-LEXY expression

The stable cell line C29-36 exhibits reliable and homogeneous expression of p53-LEXY, which can be reversibly translocated. I reasoned that the optimised expression system should address the problems that occurred during the first application of pulsatile activation (Figure 3.21), namely heterogeneity of expression and too high expres-

sion levels. Thus, I repeated the pulsatile p53 activation, to compare the transcriptional response between cells subjected to pulses and cells subjected to sustained p53 levels.

I choose to apply the illumination scheme resembling physiological p53 pulses (Figure 3.24A). I selected 4 target genes, associated with either cell cycle arrest (p21), senescence (pml) or apoptosis (bax and puma). Pulsatile p53 translocation caused differential expression of pml, which exhibited an almost two-fold increase (Figure 3.24B). Apoptosis-related target genes were transcribed at the same level in both conditions, independent of the subjected illumination scheme. Puzzling, the strongest effect was observed in p53 transcript levels, exhibiting an almost 2.5 fold increase in cells subjected to the pulsatile illumination regime.

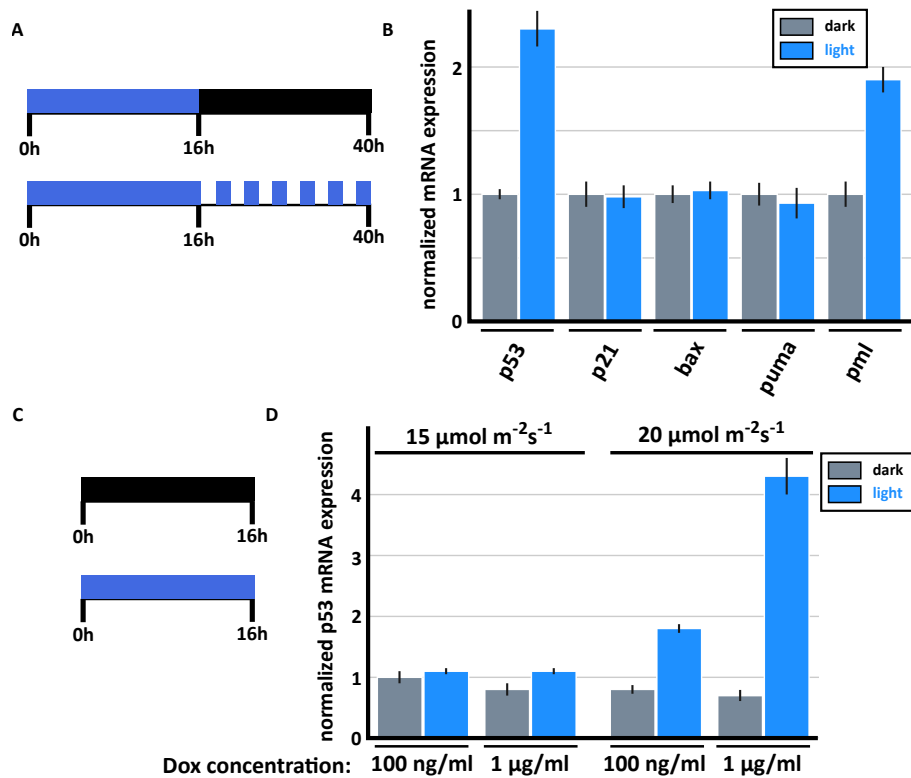


Figure 3.24: p53-LEXY transcription correlates with blue light intensity and doxycycline concentration

A | Schematics of the illumination pattern applied in **B**. Immediately after induction with 100 ng/ml, C29-36 cells were exposed to blue light. 24 hours later, cell received 6 periods of 2 hours remaining in the dark and 2 hours of light exposure.

B | Normalized mRNA expression of p53 and indicated p53 target genes after application of illumination pattern described in **A**. Control cells were shielded from light after the initial 24 hours of blue light exposure. Then, cells were lysed and RNA was extracted. Expression levels were first normalized to beta actin and Rpl0, then to the expression values of the sample remaining in the dark for 24 hours (mean \pm SD, technical replicates n=3).

C | Schematics of the illumination pattern applied in **D**. Immediately after induction with 100 ng/ml, C29-36 cells were exposed to blue light for 16 hours.

D | Normalized mRNA expression of p53 after application of illumination pattern described in **C**. Blue light was applied either with $\sim 20 \mu\text{mol m}^{-2}\text{s}^{-1}$ (normal intensity) or $\sim 15 \mu\text{mol m}^{-2}\text{s}^{-1}$ (reduced intensity). Control cells were shielded from the light. After 16 hours, cells were lysed and RNA was extracted. Expression levels were first normalized to beta actin and Rpl0, then to the expression values of the dark sample induced with 100 ng/ml doxycycline (mean \pm SD, technical replicates n=3).

p53-LEXY expression is supposedly only dependent on doxycycline. The difference in transcript levels can only be caused by a stabilization effect that pulsatile activation may have on p53-LEXY mRNA, as samples shielded from the light and samples subjected to pulsatile light were induced with the same doxycycline concentration. While mechanisms of mRNA regulation have been described for p53, these occur only in the 5' or 3' UTR regions (Yin et al., 2002; Vilborg et al., 2009).

The only difference in the treatment of samples shielded from light and subjected to pulsatile activation is the illumination scheme, and thus the total amount of light cells were exposed to. While both received the initial 16 hours of light to prevent premature nuclear localisation of p53-LEXY, the sample exposed to the pulsatile light regime received additional 12 hours of light. Doxycycline has been reported to be photosensitive, and a reduction of photostability is observed under UV-light (Kogawa et al., 2014). Moreover, these data suggest that expression of p53-LEXY is stimulated by blue light, rather than reduced. Thus, light-induced doxycycline degradation can not explain the increased p53 mRNA levels.

As p53-LEXY expression is controlled by an orthogonal system driven by a TetR-responsive CMV promoter, regulation of expression by other cellular processes as a response to blue light can be ruled out.

To further investigate the effect of blue light intensity on p53-LEXY mRNA levels, I induced cells with either 100 ng/ml or 1000 ng/ml doxycycline and exposed them to blue light or not for 16 hours (Figure 3.24C). Blue light was either applied with the commonly used intensity ($\sim 20 \mu\text{mol m}^{-2}\text{s}^{-1}$), or a reduced intensity ($\sim 15 \mu\text{mol m}^{-2}\text{s}^{-1}$).

The p53 transcript levels correlated with light intensity and doxycycline concentration (Figure 3.24D). Samples exposed to blue light with reduced intensity had approximately the same p53 transcript levels. Samples subjected to the usually applied intensity showed differential p53 expression, dependent on the doxycycline concentration.

This clearly indicates that blue light triggers the differential expression levels of p53-LEXY. Yet, the reason for different expression levels remains elusive. Regulation on the expression levels of both, p53-LEXY and TetR can be excluded, due to orthogonal promoters driving the expression of both proteins. Potentially, the p53-LEXY mRNA levels are stabilized upon blue light exposure due to an unknown mechanism.

3.3.4 Adapting the illumination settings to prevent differential expression of p53-LEXY

Since the energy of an electromagnetic wave is directly proportional to its intensity and inversely proportional to its wavelength, I thought of adjusting these parameters to reduce the impact of light on doxycycline. First, I decided to evaluate the effect of reducing the intensity. I induced p53-LEXY expression and analysed translocation on the confocal microscope. In previous experiments, I set the laser intensity to 80%, leading to the cytoplasmic translocation of about 80% of p53-LEXY molecules (Figure 3.23C). The reduction of intensity led to reduced translocation efficiency of p53-LEXY (Figure 3.25A). Lowering the laser intensity to 70% resulted in a translocation of 70% of p53-LEXY molecules. Thus, reduction of intensity was not possible without compromising performance of LEXY.

When looking at the absorption spectrum of the AsLOV2, the main peak is located around 445 nm (Figure 3.25B). The laser line on the confocal and the LEDs used for activation emit light at a wavelength of 458 nm. The absorption at 458 nm is only slightly higher than that in correspondence to the second peak around 490 nm. The difference of 30 nm corresponds roughly to a reduction of 6% light energy. To verify the effects of an increased activation wavelength, I activated cells expressing p53-LEXY with different laser lines and quantified translocation (Figure 3.25C). Activation with 488 nm triggered the same p53-LEXY translocation efficiency as the initially used 458 nm laser. Yet, going even further towards the yellow spectrum is not possible, as light exposure using the 499 nm laser caused reduced translocation.

As there was no detectable differences between using the 458 nm and the 488 nm lasers, I decided to switch to using the 488 nm light to activate cells. I updated the current setup to illuminate cells within the incubator by exchanging the old LEDs (458 nm) with LEDs emitting blue light with a 488 nm wavelength. Then, I assessed the effect of prolonged light exposure with 488 nm LEDs on p53 transcript levels (Figure 3.25D).

Activation with higher wavelengths did not cause differential expression between illuminated and light-shielded samples after the initial 16 hours period (Figure 3.25E). Even prolonged blue light exposure up to 40 hours in the presence of doxycycline did not result in the differential expression of p53. Apparently, using higher wavelengths

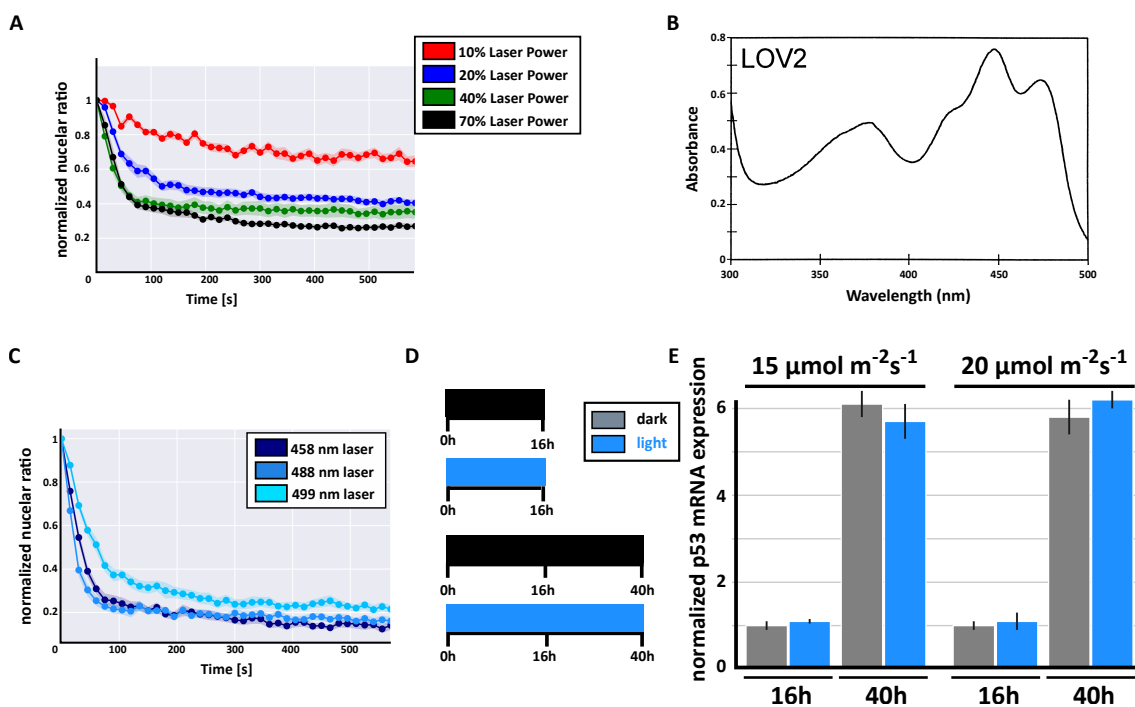


Figure 3.25: Evaluation of translocation efficiency upon activation with reduced light energy

A | Quantification of relative nuclear intensity of C29-36 expressing p53-LEXY activated with the indicated laser intensities. Cells were induced with 100 ng/ml doxycycline and incubated for 24 hours. Then, cells were illuminated for 40 minutes with blue light with indicated intensities. Nuclear intensity over time was normalized to initial nuclear intensity at time point 0 h. Dots represent imaged time points (mean \pm SD, $n=26$).

B | Photoabsorption spectrum of the AsLOV2 domain. Adapted from Salomon et al. (2000).

C | Quantification of relative nuclear intensity of C29-36 expressing p53-LEXY activated with indicated laser wavelengths. Cells were induced with 100 ng/ml doxycycline and incubated for 24 hours. Then, cells were illuminated for 40 minutes with blue light with indicated wavelength. Nuclear intensity over time was normalized to initial nuclear intensity at time point 0 h. Dots represent imaged time points (mean \pm SD, $n=22$).

D | Schematics of the illumination pattern applied in **E**. C29-36 cells were induced for 16 hours with 100 ng/ml doxycycline. Cells were exposed to blue light (488 nm) throughout the induction period or not. Cells incubated for 40 hours in the presence of light or in the dark received new, doxycycline-free media after 16 hours. Light was applied at indicated intensities.

E | Normalized mRNA expression of p53 after application of illumination pattern described in **D**. Then, cells were lysed and RNA was extracted. Expression levels were first normalized to beta actin and Rpl0, then to the p53 expression values of the sample remaining in the dark for 16 hours exposed to low intensity of blue light (mean \pm SD, technical replicates $n=3$).

was sufficient to have consistent p53 transcript levels during different illumination patterns.

No differential expression in samples due to their illumination state is a sign of the absence of a light-induced effect on p53 transcription. Also general transcription seemed not to be influenced by light, as transcription levels of reference genes Rpl0 and beta actin remained constant throughout all samples. Yet, the six-fold increase of p53-LEXY expression after 40 hours compared to the 16 hours time point was problematic. The transcription of p53-LEXY after cells are supplemented with new media lacking doxycycline is presumably caused by residual doxycycline in the cells. Having constant p53-LEXY levels during an experiment is vital for the experimental validity and the comparison between individual time points. Additionally, p53-LEXY translocation efficiency is dependent on its expression levels, as increased levels can cause impairment of translocation.

Thus, I needed to adapt the doxycycline protocol, to provide stable p53-LEXY levels over the course of the experiment, and to achieve reliable translocation.

3.3.5 Tracing translocation of p53-LEXY during ongoing experiments

Even though I could solve the problem of the light-dependent increase in p53 transcript levels, p53-LEXY levels were still not constant throughout an experiment. Moreover, I lacked the possibility to trace translocation during experiments in the incubator to verify cellular behaviour according to the applied illumination pattern. Yet, the microscope I used for the initial characterisation of p53-LEXY constructs could only activate a subset of cells, since the same field of view has to be activated every 30 seconds. The vast majority of cells remain inactivated, distorting the results taken on a population level. In contrast, whole cell populations can be activated using the LED set up in the incubator, yet can not be monitored. To address these limitations, I could either apply blue light to a limited number of field of views at the confocal microscope and remove non-activated cells, or investigate how to track cells in the incubator during illumination regimes.

3.3.5.1 Single Cell Laser Tag

Binan and colleagues presented a method to selectively stick cells to an adherent surface, called cell labelling via photobleaching (CLaP) (Figure 3.26A) (Binan et al., 2016). Culture media was supplemented with biotin-4-fluorescein, a compound forming crosslinks with the cellular membrane upon photoactivation with a GFP laser. The crosslinked biotin can then be labelled with fluorescently-labelled streptavidin. Alternatively, the GFP laser activation induces biotin-crosslinks with the surface of the culture dish cells are grown in, and thus increases adherence strength. After activation, non-activated cells can be selectively detached by trypsinization.

In a first experiment, I tested the feasibility with our setup. I grew C29-36 cells in the presence of biotin-4-fluorescein and either activated half of the field of view with a GFP laser, or not. Then, I stained cells with Alexa-488-streptavidin. After the staining process, GFP fluorescence was visible in the GFP laser-exposed half of the field of view, while non-activated cells were not stained (Figure 3.26B). Importantly, GFP fluorescence is not visible in samples not supplemented with biotin-4-fluorescein.

The sharp border separating the activated and non-activated parts highlights the spatial resolution of labelling CLaP can achieve. Interestingly, activated cells on the border of the activated side distributed the fluorescent signal evenly in the membrane within seconds.

Together with master student Jonas Fleck, we developed a protocol allowing application of an illumination scheme, subsequent addition of biotin-4-fluorescein and selective labelling of blue light-exposed cells. Cells were seeded in wells with an engraved grid on the bottom, to allow us to find back the activated cells after the staining and washing procedures. Using the protocol, we could selectively remove cells, which had not been illuminated, exemplified here with H1299 cells transiently transfected with mCherry (Figure 3.26C). Only a small number of cells outside the activated area remained adherent.

As I was now able to discard all cells not receiving the applied light illumination scheme, I needed to extract RNA from the remaining cells. Initially, I tried using the standard RNA extraction kit, yet no RNA could be detected after RNA isolation. In the 4 fields of view that can be activated on the confocal microscope within 30 seconds there were roughly 100 cells, which is not sufficient to yield enough RNA via standard methods. Next, I used SmartSeq2, a method to generate cDNA libraries from single cells (Picelli et al., 2013), yet eventually failed to yield detectable RNA levels. Presumably, RNA could not be amplified due to a too large reaction volume. Also a commercially available kit based on SmartSeq2 and SmartSeq4 failed to yield detectable amounts of RNA. Eventually, I discontinued optimising the RNA isolation, as I found a way to observe translocation during ongoing experiments in the meantime.

3.3.5.2 Self-built LED devices enable concomitant tracking and activation of cells

The inability to monitor cells activated in the incubator during an optogenetic experiment leaves the suspicion that a certain outcome may be due to failed translocation of p53-LEXY at some point during the experiment.

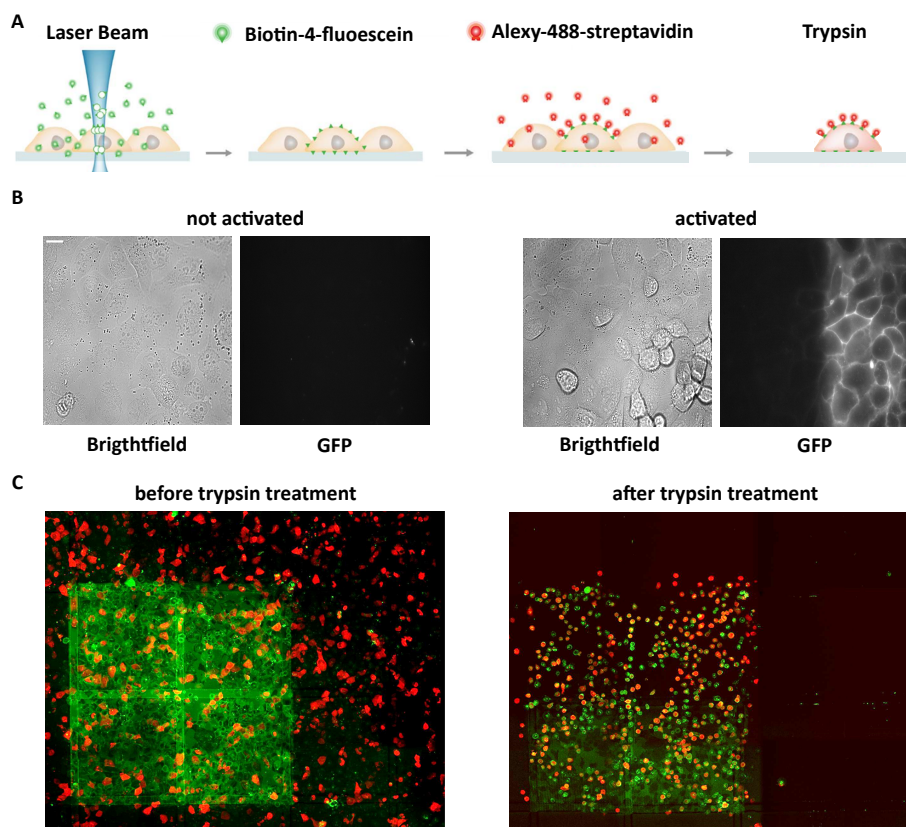


Figure 3.26: Induction of selective fluorescence and increased adherence of individual cells using single-cell laser tag.

A | Schematic workflow of single-cell laser tag. In the presence of biotin-4-fluorescein, individual cells are activated with the GFP laser, causing crosslinking of biotin-4-fluorescein and the activated cells. Crosslinked cells can then be labeled with a streptavidin tagged fluorophore. Crosslinking leads to an increased adherence strength, making cells less resistant to trypsin. Adapted from Binan et al. (2016).

B | Representative images of C29-36 cells either grown in the presence of biotin-4-fluorescein or not. Either half of the field of view was illuminated with the GFP laser (activated) or not (not activated). Then, cells were washed with PBS and incubated with 488-streptavidin and imaged. Scale Bar=20 μm .

C | Representative images of H1299 cells transfected with mCherry grown in the presence of biotin-4-fluorescein before and after trypsin treatment. 4 fields of view were activated with the GFP laser. Then, cells were labeled with 488-streptavidin and subsequently treated with trypsin. Experiment carried out by Jonas Fleck. Scale Bar=20 μm .

Ideally, I would need to monitor the translocation in all cells at all time points to be able to link the effect on target gene expression to p53 dynamics. As common microscopes are not able to image and/or activate a whole cell population given the constraint imposed by the photocycle of the AsLOV2 domain whereby light has to be applied every 30 seconds if I wish to keep the construct in the activated state. I could not use the microscope for blue light activation given that my read-out is not in individual cells but is population-based. Additionally, I wanted to establish a versatile method to apply light, without being restricted to a single microscopical setup or a single experimental workflow.

Together with people from the electrical workshop, I designed new LED illumination devices, in which blue light LEDs were embedded in the lids of well plates, enabling highly reproducible illumination of a given well (Figure 3.27A). As most fluorescence microscopes are inverted light microscopes, I decided to place the LEDs on top of the well plates. LEDs were attached to cooling bodies to prevent overheating. Possible spatial limitations were addressed by selecting small cooling bodies with an enlarged surface.

Initially, I decided to use 24-well plates, as these plates seemed to offer a good compromise between the surface area to illuminate and the total number of cells that grow in a single well. I selected LEDs with a high beam

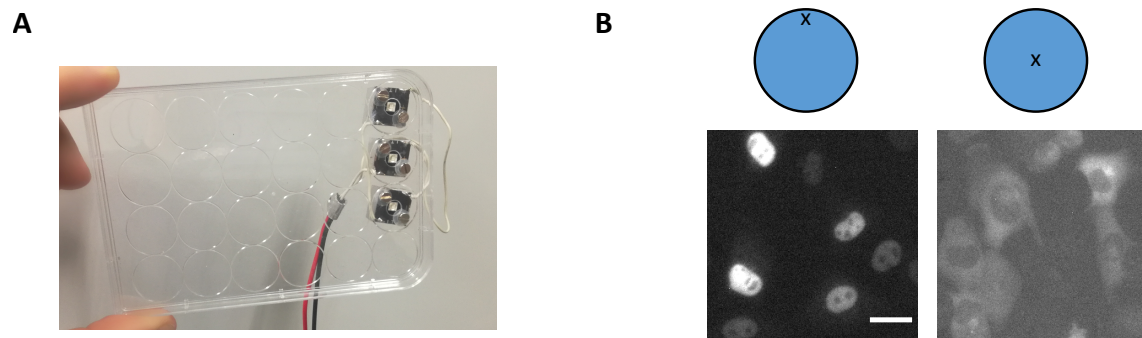


Figure 3.27: Design of self-made LED chambers to track translocation during an experiment

A | Picture of a self-made 24-LED chamber. Blue light LEDs were integrated in the lid of a 24-well plate, and glued to cooling bodies. The LEDs were powered by a power box connected to a Raspberry Pi running a self-written python script to control illumination patterns.

B | Representative images of C29-36 cells grown in 24-well plates covered with the LED-lid shown in **A**. Cells were induced with 100 ng/ml doxycycline. Cells were subjected to blue light, and different areas of the well plate were imaged. Scale Bar=20 μm .

angle, essentially the width of light emitted from the LEDs, to provide a homogeneous illumination on the whole well. A single 24-well plate yields sufficient biological material for downstream analysis, avoiding more elaborate, and thus time consuming and error prone sample collection procedures.

Yet, initial experiments using the self-built 24-well plates to apply blue light during imaging were not successful. Live tracking of cells was possible, yet an inhomogeneous translocation behaviour was revealed (Figure 3.27B). While cells in the center of a well translocated p53-LEXY in the cytosol, cells located at the outer rim of the same well exhibited a nuclear signal. Increasing the intensity to an extent that cells residing close to the outer perimeter exhibited translocation of p53-LEXY resulted in cell death of cells growing in the center, presumably due to phototoxicity (data not shown). Thus, the area to be illuminated needed to be reduced.

I continued embedding LEDs in 96-well plates. I reasoned that the reduced surface would allow for a more homogeneous illumination. Yet, the drawback in using 96-well plates is the limited biological material to be yielded, thus I needed to pool several wells for downstream analysis of target gene expression. Application of blue light in 96-well plates covered with the LED lid resulted in a homogeneous translocation in the whole well (data not shown). Therefore, monitoring of cells during an ongoing optogenetic experiment was possible using the new LED lids.

3.3.6 Optimisation of p53-LEXY levels and translocation efficiency

3.3.6.1 Adjustment of doxycycline treatment leads to constant p53-LEXY levels

During the time I was exploring approaches to monitor cells during an ongoing experiment, David Lauer, a master student in our lab, established an updated doxycycline administration protocol, that ensured stable p53-LEXY protein levels over at least 40 hours. He reduced the initial doxycycline treatment to 8 hours, followed by incubation of cells with blue light for 16 hours (Figure 3.28A). Additionally, he found that reducing the light activation pulses applied during illumination from 5 seconds every 20 seconds to 2.5 seconds every 30 seconds resulted in the same translocation kinetics of p53-LEXY, although light exposure is reduced more than three-fold.

When I tested the updated doxycycline administration protocol in C29-36 using the illumination chambers placed in the incubator, p53 target genes were differentially expressed in samples exposed to constant, meaning 2.5 seconds blue light every 30 seconds or kept in the dark (Figure 3.28B). Cells shielded from light after the initial illumination exhibited a strong increase in p21 transcript levels, and a more than two-fold increase in mdm2 expression. Xpc, a marker for DNA damage, was only mildly increased.

However, when I repeated the experiment in the Lionheart, an automated table top microscope, to monitor

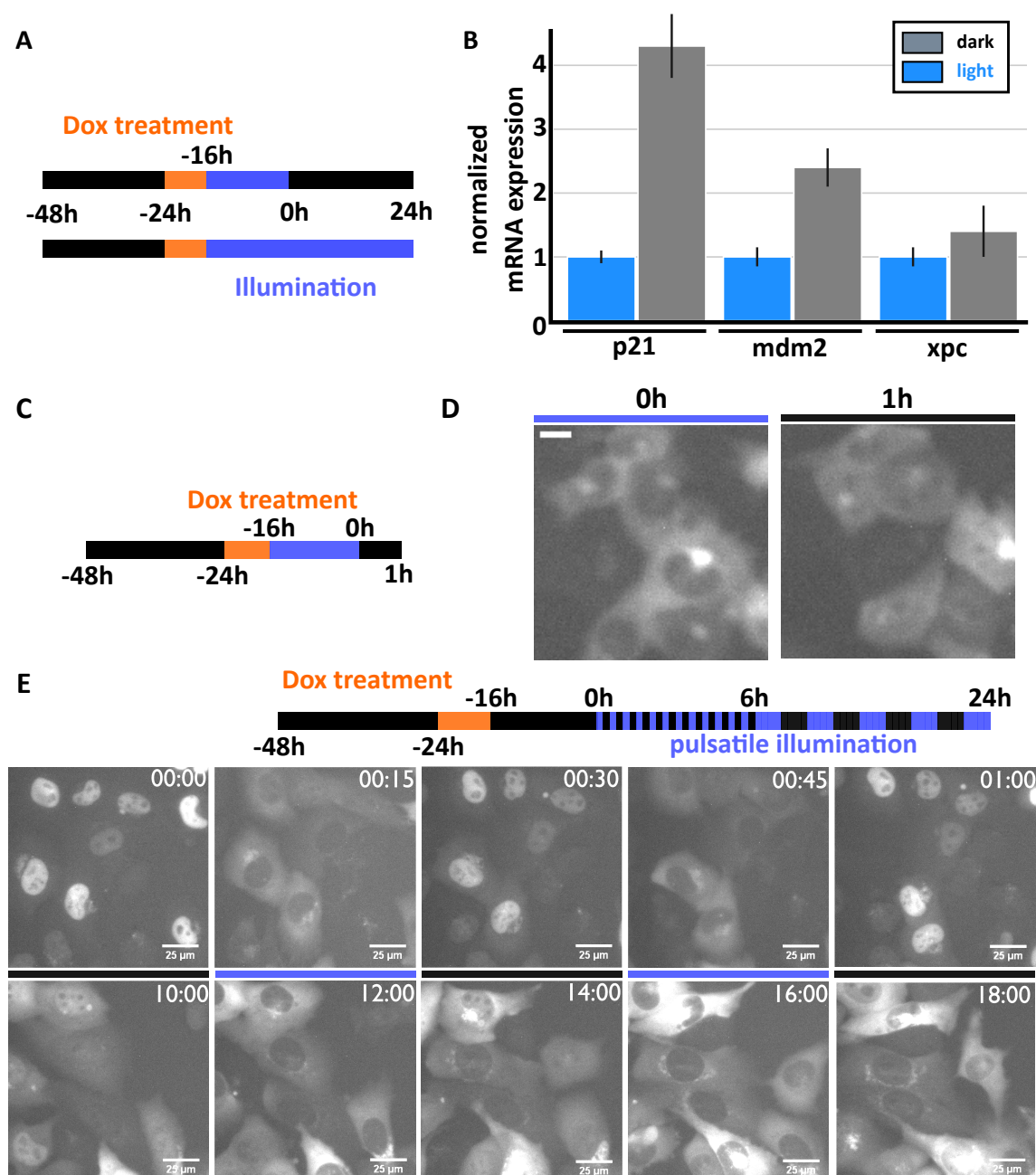


Figure 3.28: Live cell monitoring visualizes impaired translocation of p53-LEXY

A | Schematics of the newly established protocol by Master student David Lauer. 24 hours post seeding, C29-36 cells were induced with 100 ng/ml doxycycline for 8 hours. Then, cells were washed and exposed to blue light for 16 hours. Subsequently, cells were either kept in the dark, or exposed to blue light for 24 hours.

B | Normalized mRNA expression of p53 target genes after application of illumination pattern described in **A**. Then, cells were lysed and RNA was extracted. Expression levels were first normalized to beta actin and Rpl0, then to the p53 expression values of the sample exposed to blue light (mean \pm SD, technical replicates $n=3$).

C | Schematic protocol of doxycycline and illumination administration. Cells were induced with 100 ng/ml doxycycline for 8 hours, followed by 16 hours incubation in the light. Then, cells were left in the dark for 1 hour.

D | Representative images of C29-36 treated according to the protocol shown in **C**. Scale Bar= $20\ \mu\text{M}$.

E | Representative images of C29-36 expressing p53-LEXY treated according to above protocol. Cells were induced with 100 ng/ml doxycycline for 8 hours, followed by 16 hours incubation in the dark. Then, cells were subjected to six 15 min activation/recovery intervals. Next, cells received eight 2 hour activation/recovery intervals.

translocation during the experiment, I observed impaired translocation when using the same protocol (Figure 3.28C, D). As expected, cells exhibited a cytosolic signal at the end of the 16 hour illumination period (Figure

3.28C). Yet, when light was deactivated to trigger nuclear re-import of p53-LEXY, the fluorescent signal remained mainly cytosolic (Figure 3.28D). A limited number of cells eventually had an even distribution between the cytoplasm and the nucleus, while the majority of cells exhibited either a weak or no nuclear signal. The same translocation impairment has been observed in experiments carried out in a second Lionheart or in an Incucyte, a live-cell analysis system to monitor cells within an incubator (data not shown). Thus, I would exclude the possibility of technical malfunctions during the incubation causing the observed impairment.

Previously, I could demonstrate that p53-LEXY can induce transcription of p53 target genes and increase p21 protein levels, despite having illuminated cells with blue light for 16 or 24 hours (Figure 3.20 and Figure 3.28). Presumably, the limited amount of nuclear p53 observed here is sufficient to drive this increase in expression.

As I had observed ongoing translocation induced by 15 minute activation pulses in cells that had not been exposed to blue light during or shortly after doxycycline induction, I reasoned that the initial 16 hours of light exposure might impair translocation. To investigate the impact of the initial blue light exposure, I expressed p53-LEXY using the newly established doxycycline regime, but did not expose cells to blue light immediately after induction (Figure 3.28E (top)). 24 hours later, I subjected cells to twelve 15 minute activation/recovery intervals, and then switched to 2 hour activation/recovery intervals.

In the absence of the initial blue light exposure, the 15 minute activation/recovery intervals led to the respective export and import of p53-LEXY (Figure 3.28E (bottom)). Only after 10 hours of repeated shuttling, translocation appeared to be impaired. The cytoplasmic signal remained present during non-illumination phases, while only a fraction of p53-LEXY molecules became nuclear (time point 10:00 h). From this time point on, during each recovery interval less p53-LEXY was re-imported into the nucleus. Similarly, application of different illumination regimes of prolonged periods of light exposure led to the cytoplasmic localisation of p53-LEXY (data not shown).

These data suggest that prolonged light exposure causes impairment of translocation efficiency. It is unclear, whether these findings are due the light illumination or prolonged cytosolic localisation of p53.

3.3.6.2 Translocation impairment of p53-LEXY is not caused by p53

I could show that prolonged blue light exposure impairs p53-LEXY translocation efficiency. This has not been observed for other LEXY constructs, yet nobody has applied dynamics after an initial period of constant light illumination like the illumination regime used here. The reason for the observed impairment of translocation and the resulting cytosolic localisation is unknown. I thought it to be crucial to find the causes for the observed behaviour.

One possible reason is the forced and prolonged cytoplasmic localisation of p53 during illumination. High levels of p53 are only observed in case of severe damage, when p53 co-localises with mitochondrial membrane proteins to facilitate apoptosis (Chipuk et al., 2004, 2005). Cytosolic retention of p53 has been observed in the presence of Parc, a cytoplasmic anchor for p53 (Nikolaev et al., 2003). To investigate the effect of reduced Parc levels on p53-LEXY translocation efficiency, I co-expressed two shRNA directed against Parc in p53-LEXY-expressing C29-36 cells and applied blue light for 16 hours. Yet, p53-LEXY translocation remained impaired (data not shown). As the experiment lacked a proper control of Parc levels, the informative value of the experiment is weak.

Thus, I decided to investigate the translocation kinetics of mCherry-LEXY lacking p53 after prolonged blue light exposure. Additionally, I tested whether the impairment of translocation also occurred in H1299 cells transiently transfected with p53-LEXY. To this end, I transfected either p53-LEXY or mCherry-LEXY in H1299 cells. I reduced the time cells were supplemented with the transfection mix from 24 hours to 8 hours, to reduce the overall abundance of the respective construct, as expression levels affected translocation efficiency. Immediately after transfection or induction, cells were exposed to blue light for 16 hours (Figure 3.29A).

Translocation was impaired in all samples (Figure 3.29B, C, D). Neither transfected p53-LEXY nor mCherry-LEXY could be translocated into the nucleus after prolonged blue light exposure. This suggests, that the impairment of translocation of p53-LEXY is not caused by p53.

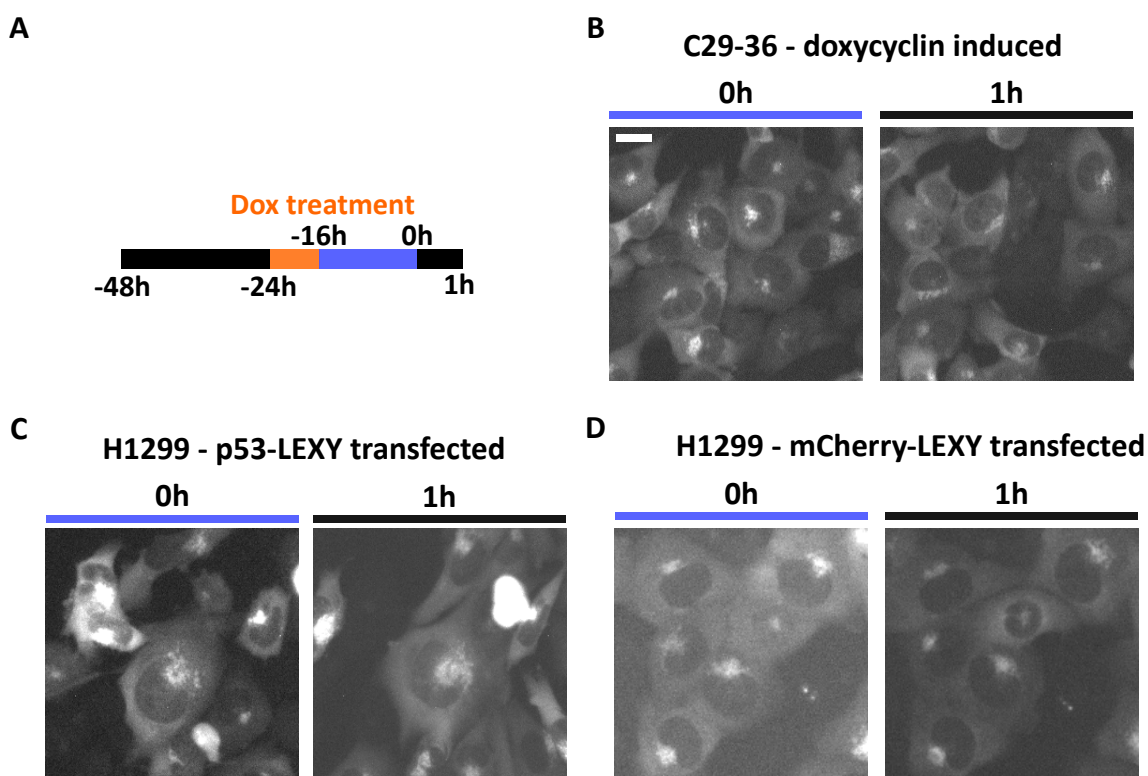


Figure 3.29: Cytosolic localisation of p53-LEXY after prolonged activation is independent of p53

A | Schematics of the applied protocol. 24 hours post seeding, C29-36 cells were induced with 100 ng/ml doxycycline and H1299 cells were transfected with the indicated construct for 8 hours. Then, cells were washed and exposed to blue light for 16 hours. Subsequently, cells were kept in the dark and imaged.

B | Representative images of C29-36 treated according to the protocol shown in **A**. Scale Bar=20 μ M.

C | Representative images of H1299 cells transfected with p53-LEXY treated according to the protocol shown in **A**. Scale Bar=20 μ M.

D | Representative images of H1299 cells transfected with mCherry-LEXY treated according to the protocol shown in **A**. Scale Bar=20 μ M.

During his PhD in our lab, Dominik Niopek has illuminated cells with blue light for 24 hours and subsequently assessed phototoxicity by carrying out a MTT cell proliferation and viability assay and could not detect any light-induced effects on the physiology of cells. Similarly, prior to starting this work I have done multiple γ H2AX immunostainings after blue light exposure. γ H2AX is a histone variant, that associates with double strand breaks and subsequently forms aggregates at the site of genetic lesion, and thus acts as marker for DNA damage (Kuo and Yang, 2008). Yet staining of light-exposed cells did not reveal any γ H2AX aggregates (data not shown).

However, while cells undergo neither morphological changes, nor changes in proliferation, they can apparently not cope with the stress induced either by blue light or continuous nucleocytoplasmic protein transport.

3.3.6.3 Reduction of the initial illumination period

As the period of blue light exposure clearly contributed to cytosolic retention of LEXY constructs and induced stress, I decided to shorten the blue light exposure period cells are subjected to prior to the start of an experiment. I reasoned that blue light exposure is only necessary when doxycycline-induced cells start expressing p53-LEXY. To estimate when the translation of p53-LEXY occurs, I induced p53-LEXY expression in C29-36 cells and imaged them immediately. Within the first 8 hours, no fluorescence was observable (data not shown). I supplemented cells with media lacking doxycycline and continued imaging. Slowly, mCherry fluorescence became visible, and the number of fluorescent cells rose linearly, similarly to the total number of cells per field of view (Figure 3.30A). Both, number and intensity of fluorescent cells increased over time. At the end of the incubation period, approx-

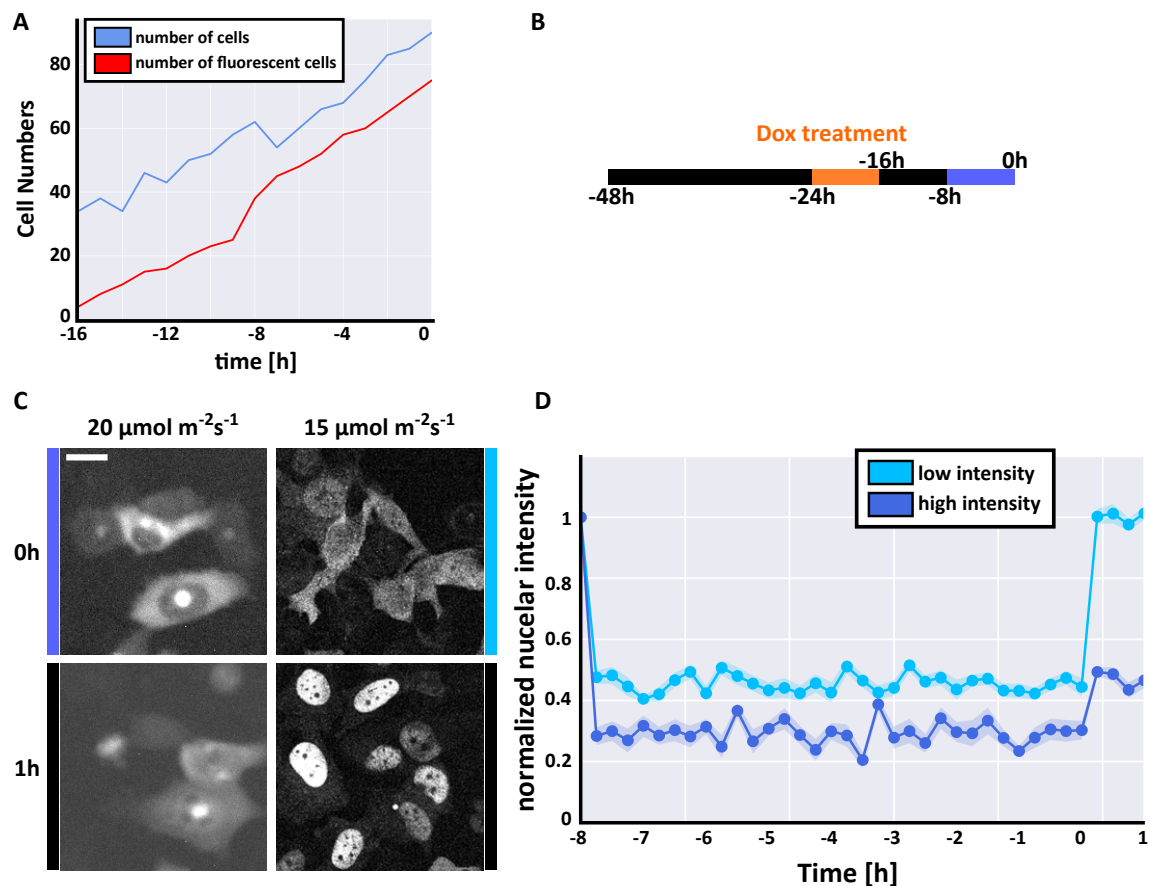


Figure 3.30: Adjustment of the initial illumination period increased translocation efficiency

A | Quantitative time course of proliferation and p53-LEXY expression upon induction with 100 ng/ml. Cells were induced in the microscope and imaged every 30 minutes. Number of total (blue) and number of fluorescent cells (red) were counted.

B | Schematic protocol of doxycycline and illumination administration. Cells were induced with 100 ng/ml doxycycline for 8 hours, followed by 8 hours incubation in the dark. Then, cells were subjected to 8 hour light activation.

C | Representative images of C29-36 cells induced with 100 ng/ml treated like depicted in (B). Cells were exposed with to indicated blue light intensities and imaged after the 8 hour light treatment (time point 0 h) and 1 hour after recovery in the dark (1h). Scale Bar=20 μM .

D | Quantification of relative nuclear intensity of C29-36 cells activated with the indicated blue light intensities. Nuclear intensity over time was normalized to initial nuclear intensity of the respective sample. Dots represent images taken (mean \pm SD, n=30).

imately 90% of the cells exhibited fluorescence.

Notably, while fluorescence was heterogeneous in the beginning, it was homogeneous throughout all cells 16 hours post induction. In a compromise between shortening the light exposure, and preventing premature nuclear accumulation, I decided to change the protocol by exposing cells to light for 8 hours prior to the start of an experiment (Figure 3.30B). Even though about 40% of the cells had a visible p53-LEXY expression 8 hours after doxycycline was washed away (time point -8 h), the intensity was rather low in the majority of the fluorescent cells.

Application of the adapted illumination scheme led to an exclusively cytosolic p53-LEXY at the end of the 8 hour illumination period (Figure 3.30C). Yet, translocation was not fully reversible once blue light was turned off. The majority of p53-LEXY remained localised in the cytosol, while only a fraction translocated into the nucleus (Figure 3.30D). Apparently, the reduced light application time still impacted translocation efficiency. I reduced the light intensity by one quarter from 20 $\mu\text{mol m}^{-2}\text{s}^{-1}$ to 15 $\mu\text{mol m}^{-2}\text{s}^{-1}$, and repeated the experiment. Cells re-

ceiving 8 hours of reduced blue light intensity displayed a rather even distribution of fluorescent signal between the nucleus and the cytosol, however, once the illumination was stopped, p53-LEXY became nuclear, and reached the same nuclear intensity as prior to the illumination phase. This suggests, that the reduced light intensity lowers the stress applied on cells, since translocation was fully reversible.

Despite being insufficient to completely deprive the nucleus of p53-LEXY, the lower blue light intensity resulted in a better dynamic range. While residual nuclear p53-LEXY could induce target genes independent of the applied illumination pattern, the impaired translocation kinetics seen in samples illuminated with $20 \mu\text{mol m}^{-2}\text{s}^{-1}$ blue light intensity renders these illumination settings not useful. I did not want to further reduce initial illumination time, as p53-LEXY protein levels increased 8 hours prior of the experimental begin (Figure 3.28). Thus, I decided to illuminate cells 8 hours after doxycycline induction with the reduced light intensity.

3.3.7 Reduction of light intensity still leads to impairment of p53-LEXY translocation

With the revised doxycycline administration protocol and the reduced light intensity during blue light activation, p53 levels remained constant over the experimental run time, and translocation was apparently more reliable. Additionally, the LED devices now enabled monitoring translocation during an experiment. With the updated experimental setup, I set out to investigate differential gene expression in samples subjected to either pulsatile or constitutive activation of p53-LEXY.

Like in previous experiments, I decided to use 2 hour pulses of activation, as these resemble the pulsatile response of p53 observed when cells are exposed to γ -radiation (Batchelor et al., 2008). Due to the previously observed effect of prolonged light illumination on translocation, I decided to limit experimental run time to 8 hours, to ensure reliable translocation throughout the experiment and to reduce the applied stress on cells caused by blue light.

After the initial 8 hours of illumination, I subjected C29-36 cells expressing p53-LEXY either to permanent blue light exposure, to 2 h activation pulses or placed them in the dark (Figure 3.31A). I collected time points every 2 hours. Cells were monitored during the experiment, and translocation kinetics for each sample were determined (Supplementary Figure 7.1)

Overall, there was no consistent differential gene expression detectable between the different illumination conditions (Figure 3.31B). A maximum of 1.5-fold increase in transcription levels of the investigated genes was observed. Changes in expression appeared to be rather arbitrary and not dependent on p53. Apart from puma and pml, gene expression of p53 target genes in samples not exposed to light exhibited a trend of slightly increasing expression during the time course, reaching the highest level at 8 hours.

Samples subjected to pulsatile activation exhibited only mild changes in expression. Except for puma, whose expression peaked after 4 hours, but decreased at later time points.

For some p53 target genes, the light-exposed sample exhibited the highest fold change in gene expression, for example the cell cycle arrest marker p21 after 2 hours, or the apoptosis marker puma after 4 hours, yet as these are individual time points, and the respective levels are reduced or back to base levels in later time points, the expression is presumably not indicating stress.

In general, it appears that p53-LEXY expression of illuminated and non-illuminated samples exhibited only minor differences. As the tracked translocation kinetics followed the applied illumination patterns (Supplementary Figure 7.1), the lack of differentially gene expression between constantly illuminated and non-illuminated samples can not be explained by impaired translocation. Only cells receiving pulsatile activation exhibited a reduced translocation efficiency during later time points. Cells shielded from light exhibited a roughly two-fold increase in nuclear p53-LEXY intensity, compared to cells exposed to light. Yet, this increase apparently does not cause differential gene expression.

As described in Chapter 3.3.6.1, already a small increase in nuclear intensity can apparently induce gene expression. Reduction of blue light intensity resulted in higher nuclear levels of p53-LEXY during blue light expo-

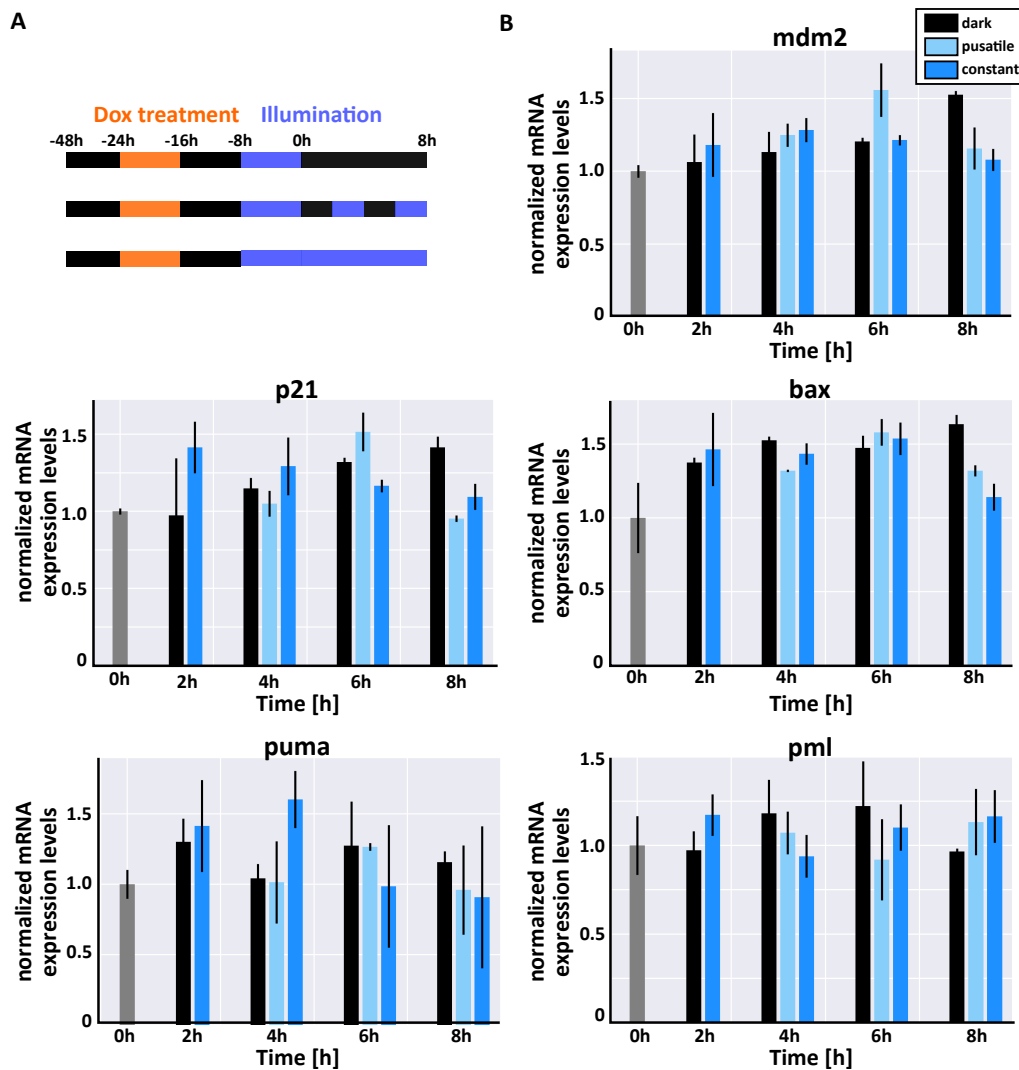


Figure 3.31: Expression of p53 target genes upon exposure with different illumination regimes

A | Schematic protocol of the experimental work flow. Cells were induced with 100 ng/ml doxycycline for 8 hours, followed by 8 hours of incubation in the dark. Then, cells were exposed to blue light for 8 hours. Next, cells were either left in the dark, exposed to constant light or subjected to 2 hour intervals of light activation and recovery in the dark. Time points were taken every 2 hours.

B | Normalized mRNA expression of indicated p53 target genes after application of illumination patterns described in **A**. Then, cells were lysed and RNA was extracted. Expression levels were first normalized to beta actin and Rpl0, then to the expression values of the control sample at time point 0 h (mean \pm SD, technical replicates $n=3$).

sure, and is presumably sufficient to trigger p53 target gene expression. However, it is puzzling, that the two-fold increase of nuclear intensity in cells shielded from the dark is not sufficient to further stimulate transcription.

Additionally, the observed impairment of translocation in samples exposed to pulsatile illumination suggests that the reduced illumination regime still imposes stress on the cells. Potentially, the stress induced by light is highest in the sample exposed to blue light permanently, thus the transcriptional readout might not be trusted. Yet, transcription of house keeping genes was constant in all conditions.

This highlights how difficult it is to balance the parameters in optogenetic experiments. High blue light intensity caused translocation impairment and cellular stress, while reduced intensity led to higher abundance of nuclear p53-LEXY, and thus presumably to higher background expression of p53 target genes, while still causing stress to cells.

3.3.8 Drug treatment reveals high variability in transcriptional response in C29-36 cells

Cytosolic and nuclear p53-LEXY localisation did not result in a consistent differential expression of p53 target genes. The transcriptional response at individual time points did not exhibit any visible trend, and fluctuated independently of the illumination scheme. Presumably, increasing the experimental run time to potentially achieve higher transcript levels would increase phototoxicity and have a detrimental effect on translocation efficiency, as translocation was already impaired in shorter experiments.

In physiological conditions, p53 becomes rapidly active once the cell encounters a stress situation. Subsequently, p53 induces transcriptional programs to cope with the encountered situation, and eventually triggers cell fate according to the severity of the stress. Here, I wanted to investigate effects of p53 dynamics in the absence of stress. Yet, I could not find settings which allowed reversible translocation without causing phototoxic stress and still yield differential expression of p53 target genes.

Thus, I decided not to expose cells to light prior to the start of the experiment, but rather manipulate localisation of p53-LEXY during the application of stress to cells. I selected two drugs to induce stress, neocarzinostatin (NCS) and gefitinib.

3.3.8.1 Neocarzinostatin treatment reveals un-reproducibility of observed transcriptional response in C29-36 cells

NCS is an antibiotic used as a chemotherapeutic drug in cancer treatment (Ishida et al., 1965). NCS triggers sequence-specific DNA damage, and subsequently causes activation of the DNA-damage repair pathway leading to p53 activation by the ATM kinase (D'Andrea and Haseltine, 1978; Banin et al., 1998). I reasoned that the DNA damage should activate p53 to its full extent, and thus induce p53 target genes. I applied the same doxycycline-induction scheme as before, yet I omitted the initial blue light period, due to the apparent stress it caused to the cells (Figure 3.32A). The absence of blue light will lead to a nuclear p53-LEXY pool prior to NCS administration. p53-LEXY will then either reside in the nucleus, or be translocated to the cytosol due to blue light exposure, leading to either nuclear or cytosolic p53-LEXY during NCS treatment.

Additionally, I selected further p53 target genes to investigate, based on a study elucidating p53 target gene mRNA expression kinetics (Porter et al., 2016). Porter and colleagues grouped mRNAs according to their expression profiles in strongly or weakly pulsing, or rising in expression. I picked the strongest responding genes from the group of strongly pulsing genes, namely eGadd45, btg2 and wip1, and the strongest from the group of weakly pulsing genes, namely fas, and took time points at 2 hours and 6 hours, according to the described peaks of the respective pulses (Porter et al., 2016).

Of the eight selected target genes, eGadd45, fas, pml and bax exhibited only minor fluctuations in expression (Supplementary Figure 7.2). p21 and wip1 had higher fold changes in transcript levels, and both peaked at the 2 hour time point. Notably, drug-treated samples appeared to have higher expression levels of p53 target genes after 2 hours. After 6 hours, expression of p21 and wip1 in cells expressing p53-LEXY was more similar, independent of the illumination condition and drug treatment.

After 2 hours, btg2 expression was approximately two times higher in the dark than in the corresponding light-exposed control (Figure 3.32B (left)). Even in non-induced cells, an almost two-fold increase was observable, presumably due to residual p53 expression. C29-36 cells expressing p53-LEXY had a four-fold increase in btg2 levels, cells additionally treated with NCS exhibited a six-fold increase in btg2 levels. This suggests that p53-LEXY can induce btg2 expression, yet the expression can further be stimulated by NCS treatment.

Also cells exposed to blue light and thus supposedly having cytosolic p53-LEXY showed an increase in btg2 transcript levels upon NCS treatment. As p53 levels are stable throughout the experiment, the cells supposedly had the same amount of residual nuclear p53-LEXY, yet the NCS treatment caused a higher transcriptional activity of p53-LEXY. In general, fold changes were reduced after 6 hours.

The btg2 fold changes in samples treated with NCS resembled the results reported by Porter and colleagues

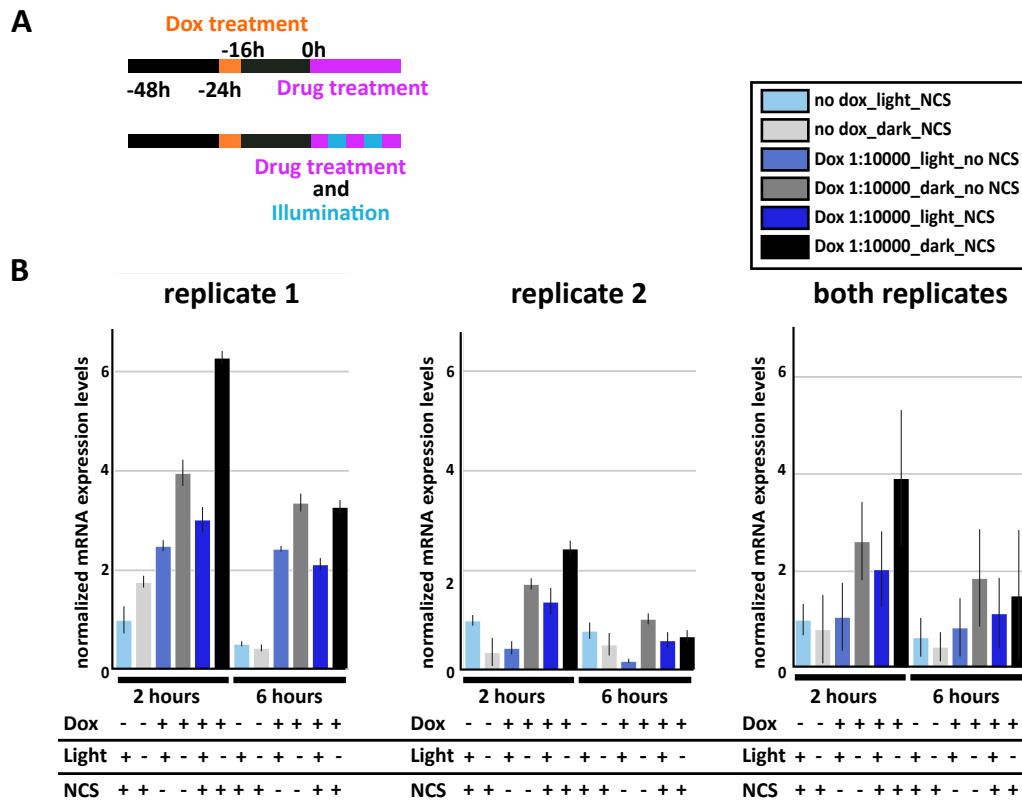


Figure 3.32: Evaluation of *btg2* expression upon NCS treatment

A | Schematic protocol of the experimental work flow. Cells were induced with 100 ng/ml doxycycline for 8 hours, followed by 16 hour incubation in the dark. Then, cells were treated with 500 ng/ml NCS for 2 or 6 hours and either exposed to blue light or not.

B | Normalized mRNA expression of *btg2* after application of illumination patterns described in **A**. Then, cells were lysed and RNA was extracted. Expression levels were first normalized to beta actin and Rpl0, then to the expression values of the non-induced, light exposed and NCS treated sample at time point 2 h. (left) mean \pm SD, technical replicate 1, $n=3$ (middle) mean \pm SD, technical replicate 2, $n=3$ (right) \pm SD, biological replicate $n=2$, technical replicates $n=2 \times 3$)

(Porter et al., 2016), who, having a higher temporal resolution in their read-out, claimed a pulsatile activation of *btg2* upon treatment with NCS. Cells treated with NCS for 6 hours showed the same fold changes as untreated cells.

These results were promising, as clear fold changes dependent on p53 localisation were observed, and previously published results demonstrated the same effect on *btg2* levels as described here (Porter et al., 2016). *btg2* and *puma* showed the highest differential expression (Figure 3.32 and Figure 3.33), thus I selected these two genes for further investigation.

When the experiment was repeated, *btg2* transcript levels were not reproducible (Figure 3.32B (middle)). In general, fold changes were drastically reduced. Only cells expressing nuclear p53-LEXY treated with NCS exhibited higher than two-fold change in expression. Similarly to the first replicate, expression of *btg2* was higher at the first time point than at the second time point. Statistical analysis of both replicates revealed the high error, demonstrating the heterogeneous response in cells (Figure 3.32B(right)).

Similarly to *btg2*, *puma* exhibited a drastic difference of the fold changes between individual replicates (Figure 3.33 (left) and (middle)). While the first replicate exhibited a similar expression profile as *btg2*, the second replicate exhibited only minor fluctuations in target gene expression. C29-36 cells expressing p53-LEXY exhibited similar expression levels of *puma* in the first replicate, independent of illumination and NCS treatment. Solely the sample additionally treated with NCS and shielded from the light displayed a six-fold change. It appears, that nuclear levels of p53 are not the main determinant of *puma* transcription, as non-illuminated and light-exposed

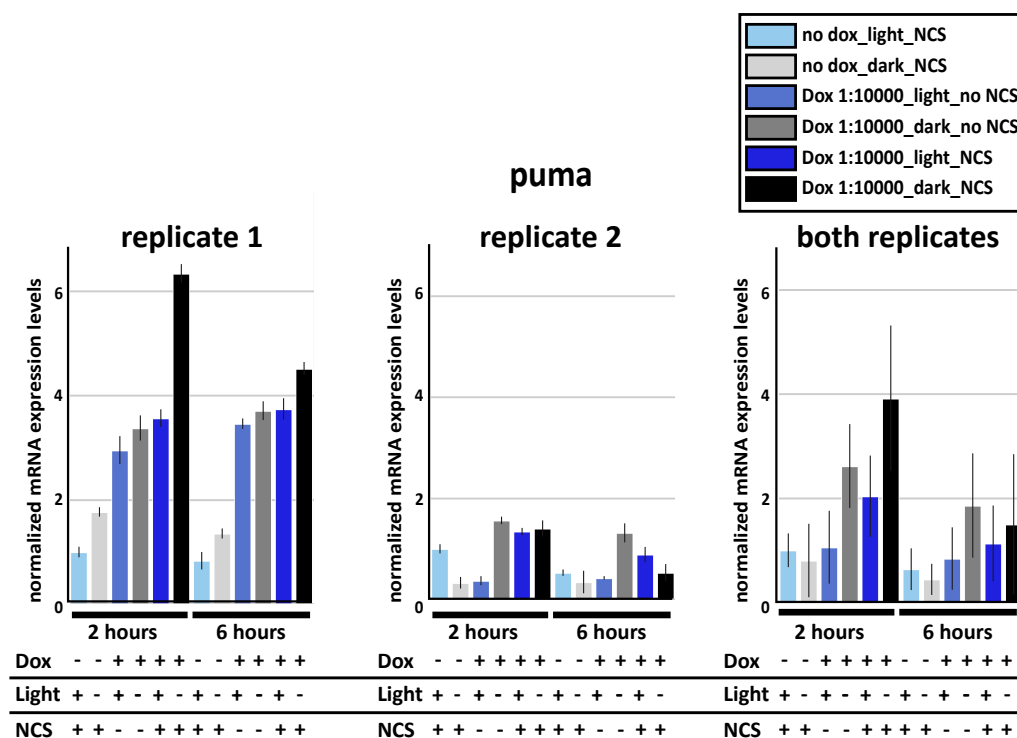


Figure 3.33: Evaluation of puma expression upon NCS treatment

Normalized mRNA expression of puma after application of illumination patterns described in Figure 3.32 A. Then, cells were lysed and RNA was extracted. Expression levels were first normalized to beta actin and Rpl0, then to the expression values of the non-induced, light exposed and NCS treated sample at time point 2 h. (left) mean \pm SD, technical replicate 1, n=3) (middle) mean \pm SD, technical replicate 2, n=3) (right) \pm SD, biological replicate n=2, technical replicates n= 2x3)

samples exhibited almost the same puma expression levels. The nuclear levels of p53-LEXY only contributed to puma in the presence of NCS. In non-induced samples, puma levels are only slightly elevated in samples kept in the dark compared to samples exposed to blue light.

Yet, in replicate 2, illuminated, non-induced samples are more elevated as in light-shielded samples. NCS treatment did not have a stimulating effect on puma levels as seen in the first replicate. While non-NCS-treated C29-36 cells showed stronger light-induced transcription, NCS-treated cells expressing p53-LEXY appeared to be not responsive to light.

Technical errors in preparation of the RNA and cDNA can be excluded, as both, isolation of RNA and reverse transcription, were carried out in parallel. Also the identical qPCR master mix was used, and both replicates were run on the same plate. Additionally, cells appeared normal in both replicates when checked at the microscope, and the Ct values of the reference genes were constant in all RNA samples. Thus, the heterogeneity was probably not caused by technical issues.

Due to the heterogeneity observed here, no definitive conclusion can be drawn from this data set.

3.3.8.2 Gefitinib treatment confirms un-reproducibility of transcription of p53 target genes in C29-36 cells

Gefitinib is a tyrosine kinase inhibitor used as a chemotherapeutic agent (commercial name: Iressa). Gefitinib specifically targets the EGFR receptor and triggers apoptosis (Rho et al., 2007). Additionally, gefitinib administration causes rapid activation of p53 (Chang et al., 2008). Here, I wanted to assess p53 localisation-dependent target gene expression upon gefitinib treatment. Expression of p53-LEXY was induced applying the updated doxycycline administration protocol and cells were then treated for either 2 or 6 hours with 1 μ M gefitinib. During the drug administration, cells were illuminated with blue light, or shielded from light (Figure 3.32A).

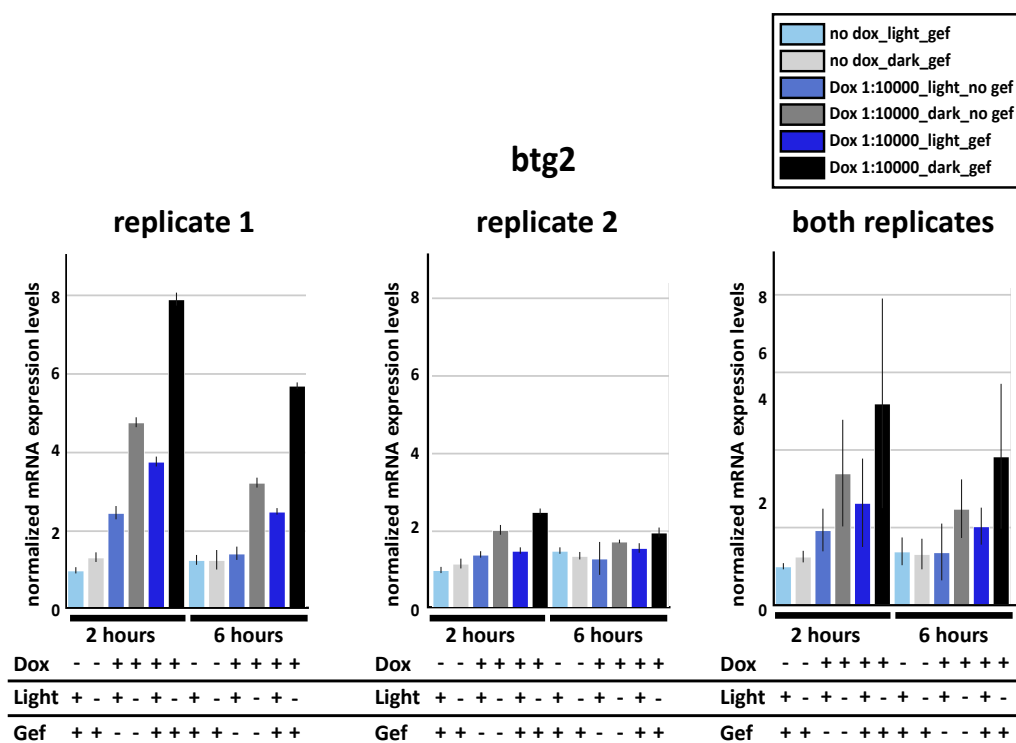


Figure 3.34: Evaluation of btg2 expression upon gefitinib treatment

A | Normalized mRNA expression of btg2. Cells induced with 100 ng/ml doxycycline for 8 hours, followed by 16 hour incubation in the dark. Then, cells were treated with 1 μ M gefitinib for 2 or 6 hours and exposed to blue light, or not. Next, cells were lysed and RNA was extracted. Expression levels were first normalized to beta actin and Rp10, then to the expression values of the non-induced, light exposed and 1 μ M gefitinib treated sample at time point 2 h (mean \pm SD, technical replicates n=3). **B** | Normalized mRNA expression of btg2. Cells were induced with 100 ng/ml doxycycline for 8 hours, followed by 16 hour incubation in the dark. Then, cells were induced with doxycycline and treated with gefitinib for 2 or 6 hours. Next, cells were lysed and RNA was extracted. Expression levels were first normalized to beta actin and Rp10, then to the expression values of the non-induced, light exposed and gefitinib treated sample at time point 2 h. (left) mean \pm SD, technical replicate 1, n=3) (middle) mean \pm SD, technical replicate 2, n=3) (right) \pm SD, biological replicate n=2, technical replicates n= 2x3)

Similar to NCS treatment, the highest fold change upon gefitinib treatment could be observed in btg2 and puma levels. eGadd45 and pml showed only mild increase of transcript expression throughout all conditions (Supplementary Figure 7.3). Wip1 and fas exhibited a light-dependent increase in transcription, yet overall elevation in transcription was weak (1.5 fold induction). Bax and p21 expression was three-fold increased in gefitinib-treated cells shielded from light. Depended on the illumination, both genes were differentially expressed after 2 hours, yet after 6 hours expression exhibited similar levels in all conditions. Gefitinib treated samples shielded from dark had strongly elevated p21 transcript levels.

In the first replicate, btg2 levels resembled a pulsatile response, with transcript levels higher after 2 hours than after 6 hours (Figure 3.34 (left)). As seen before, the highest fold change was observed in the non-illuminated sample expressing p53-LEXY upon gefitinib treatment for 2 hours. btg2 levels were generally two-fold increased when p53-LEXY was nuclear.

A second independent experiment, however, had very different results (Figure 3.34 (middle), (right)). Fold changes were drastically reduced, the maximal increase in transcription levels decreased from eight- to two-fold. The effect of gefitinib treatment was neglectable. Expression was slightly higher after 2 hours, yet overall changes were marginal. Apparently, un-reproducibility is persistent, and not caused by NCS.

The same unreproducible results were obtained for puma (Figure 3.35). As seen before, fold changes were reduced in the replicate. Taken together, drug treatment resulted in a highly variable response. Initial promising results were not reproducible. As reproducibility is key for any experiment and usually points to an underlying

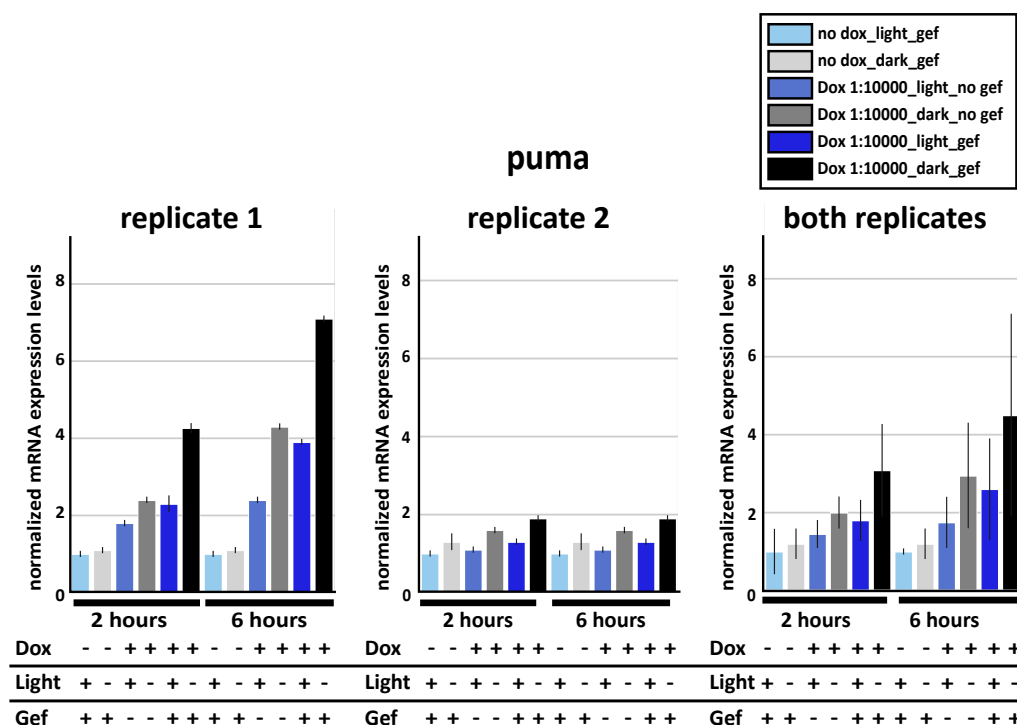


Figure 3.35: Evaluation of puma expression upon gefitinib treatment

A | Normalized mRNA expression of puma. Cells were induced with 100 ng/ml doxycycline for 8 hours, followed by 16 hour incubation in the dark. Then, cells were treated with 1 μ M gefitinib for 2 or 6 hours and either exposed to blue light or not. Next, cells were lysed and RNA was extracted. Expression levels were first normalized to beta actin and Rpl0, then to the expression values of the non-induced, light exposed and NCS treated sample at time point 2 h (mean \pm SD, technical replicates n=3).

B | Normalized mRNA expression of puma. Cells were induced with 100 ng/ml doxycycline for 8 hours, followed by 16 hour incubation in the dark. Then, cells were induced with doxycycline and treated with gefitinib for 2 or 6 hours. Next, cells were lysed and RNA was extracted. Expression levels were first normalized to beta actin and Rpl0, then to the expression values of the non-induced, light exposed and NCS treated sample at time point 2 h. (left) mean \pm SD, technical replicate 1, n=3) (middle) mean \pm SD, technical replicate 2, n=3) (right) \pm SD, biological replicate n=2, technical replicates n= 2x3)

problem in the experimental setup, I needed to find the origin of the heterogeneous response.

3.3.9 Finding the cause of un-reproducibility

So far, experiments resulted only in mild changes of transcript levels, or obtained results were un-reproducible. The cause of the previously observed variation could not be identified. There was no apparent correlation between the variation and any of the treatments cells were subjected to, as un-reproducibility was observed throughout all samples. Prior to trying to further optimise the experimental setup, I decided to look for the possible cause of this strong unreliability.

I decided to investigate whether a similar variation in transcriptional response could be observed in other cell lines. To this end, I selected the colon carcinoma cell line HCT116, a cell line commonly used in p53 research. Additionally, I used MCF7 cells with an integrated p53-Venus, a stable cell line created by Batchelor and colleagues (Batchelor et al., 2008). This cell line has been used intensively for investigating p53 dynamics, and harbours a constitutively expressed p53 tagged with Venus (Batchelor et al., 2008, 2011; Purvis et al., 2012; Stewart-Ornstein and Lahav, 2017). I treated HCT116 and MCF7-p53-Venus cells with gefitinib for 2 or 6 hours and investigated btg2 and puma mRNA levels (Figure 3.36A).

In contrast to the previous experiments, these experiments were nicely reproducible. Gefitinib treatment triggered an increase in transcript levels of btg2 in both cell lines (Figure 3.36B, C). HCT116 exhibited an almost two-

fold change in transcription of *btg2*, at both investigated time points. *btg2* expression in MCF7-p53-Venus resembled a pulsatile transcription profile, reaching a three-fold increase after 2 hours, then decreasing to a two-fold

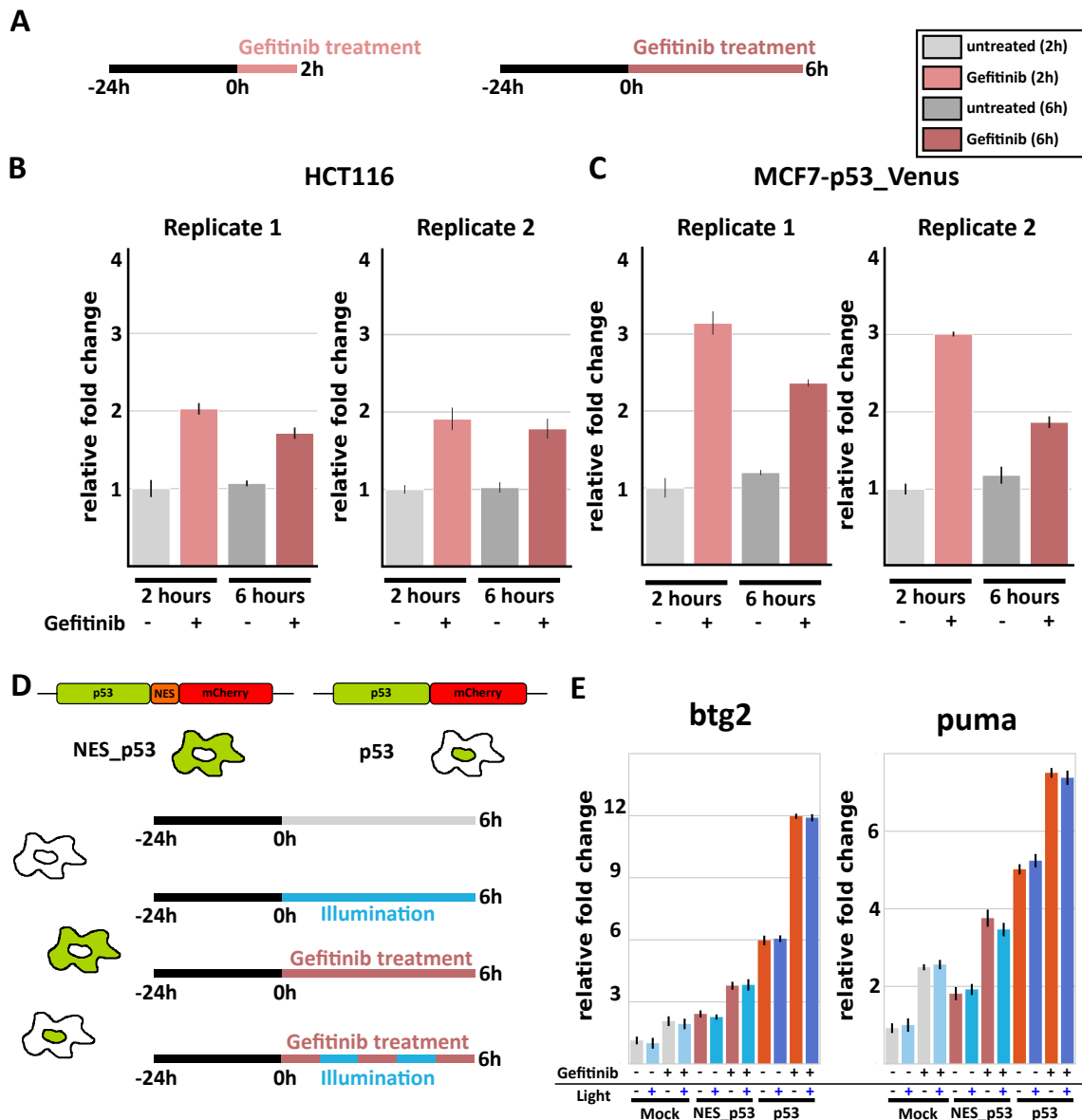


Figure 3.36: Evaluation of the contribution to un-reproducibility of the individual treatments

A | Schematic protocol of the experimental workflow. Cells were treated with $1 \mu\text{M}$ gefitinib for 2 h or 6 h.

B | Normalized mRNA expression levels of *btg2* in HCT116 cells treated according to protocol shown in **A**. Then, cells were lysed and RNA was extracted. Expression levels were first normalized to beta actin and Rpl0, then to the expression values of the non-treated sample at time point 2 h. (left) replicate 1 (mean \pm SD, $n=3$), (right) replicate 2 (mean \pm SD, $n=3$).

C | Normalized mRNA expression of *btg2* in MCF7-p53-Venus cells treated according to protocol shown in **A**. Then, cells were lysed and RNA was extracted. Expression levels were first normalized to beta actin and Rpl0, then to the expression values of the non-treated sample at time point 2 h. (left) replicate 1 (mean \pm SD, $n=3$), (right) replicate 2 (mean \pm SD, $n=3$).

D | Schematic protocol of the experimental workflow. Cells were transfected with p53-mCherry or p53-NES-mCherry and treated with Gefitinib and/or blue light for 6 h.

E | Normalized mRNA expression of indicated p53 target genes in HCT116 transfected with indicated constructs. Cells were treated according to protocol shown in **C**. Then, cells were lysed and RNA was extracted. Expression levels were first normalized to beta actin and Rpl0, then to the expression values of the non-treated sample at time point 6 h. (mean \pm SD, biological replicates 2, technical replicates 2x $n=3$).

change after 6 hours. Non-treated samples had constant *btg2* transcript levels.

Puma expression was likewise reproducible (Supplementary Figure 7.4B, C). Drug treatment resulted in a continuous increase of puma levels in HCT116 cells, exhibiting a minor increase after 2 hours, and higher than a 2.5 fold increase after 6 hours. In MCF7-p53-Venus cells, there was a 1.5-fold increase of puma levels upon stimulation, which was slightly reduced after 6 hours.

These results suggest that gefitinib is not the cause of the previously observed un-reproducibility, as *btg2* and puma expression was reproducible in both, HCT116 and MCF7-p53-Venus cells. Another possible cause of un-reproducibility could be the high abundance of cytosolic p53 during illumination periods. In physiological conditions, high cytosolic p53 levels are observed in case of severe stress to induce apoptosis (Chipuk et al., 2004, 2005). Thus, I reasoned this unnatural localisation might contribute to un-reproducibility, especially when cells are additionally exposed to blue light.

To test this hypothesis I expressed either nuclear or cytosolic p53 in HCT116 cells, and subjected cells to blue light for 6 hours (Figure 3.36D). Controls were shielded from blue light. In general, cells reacted similarly to the stimulation, and expressed similar levels of *btg2* and puma in both replicates. *Btg2* expression levels were independent of light, and increased upon gefitinib treatment (Figure 3.36E). Transfection of cytosolic p53 stimulated expression of both, *btg2* and puma in respect to the mock-transfected control, presumably due to residual nuclear p53.

These results suggest that p53 localisation and expression levels do not contribute to differences between replicates. Between replicates, the transcription level of *btg2* and puma were similar. Lastly, also the blue light did not cause un-reproducibility.

Thus, the only remaining factor is the stable cell line C29-36. Apparently, the transcription is highly variable in this cell line, as even unstressed cells exhibit huge variations. As the project depends on reliable p53-LEXY expression and a consistent response to the p53-LEXY translocation, this cell line turned out not to be appropriate for the aim of this project.

4 Discussion and Outlook

Cellular signalling is a truly dynamic process. At the centre of many signalling networks is a transcription factor (TF), which senses various internal and external stimuli and translates these inputs in the appropriate response. The term "dynamics" indicates the shape of the curve describing the temporal profile of a certain feature of the transcription factor, such as its concentration, localisation or activity (Purvis and Lahav, 2013). It is suggested that TF dynamics determine the transcriptional outcome.

p53 is a transcription factor vital for the cell; it mediates the cellular response to multiple internal and external stress signals. Different p53 dynamics have been linked to distinct transcription profiles and thus cellular fates (Batchelor et al., 2011; Purvis et al., 2012). Typically, investigation of p53 dynamics are based on experiments using chemical perturbation or radiation to induce them. Both treatments trigger cellular stress, thus potentially lead to undesired side effects influencing the transcriptional response.

While it is well understood how different stress signals induce different p53 dynamics, the mechanism used by the cells to "interpret" these dynamics to selectively activate target gene expression remains unknown.

Moreover, it is unclear whether the dynamics alone are sufficient to induce specific gene expression, or whether further factors are involved in shaping p53's appropriate transcriptional response. In this work, I used optogenetic methods to artificially create different p53 dynamics, and analyse the transcriptional output derived from them in the absence of upstream stress. In the following, I will discuss the results I obtained.

4.1 Controlling endogenous p53 levels by light-dependent inhibition of p53 degradation

4.1.1 Light-mediated steric hindrance of peptides or protein domains to control p53 degradation

p53 levels are mainly regulated by the E3 ubiquitin ligase Mdm2, which binds p53 N-terminal TAD eventually leading to p53 degradation. MdmX, a homologue of Mdm2, binds to same binding interface as Mdm2, but is not able to induce p53 degradation. Yet, MdmX binding inhibits p53 transcriptional activity. Here, I applied optogenetic methods to inhibit p53 degradation light-dependently using two proteinogenic peptide candidates designed to have a higher affinity towards Mdm2 and MdmX than the endogenous TAD of p53.

Initially, I applied the Tulip approach to enable light-controlled inhibition of p53 degradation. The approach employs the natural property of the AsLOV2 domain to expose its $J\alpha$ helix upon blue light illumination (Salomon et al., 2001; Crosson and Moffat, 2002; Strickland et al., 2012). This structural change is harnessed to enable light-controlled exposure of a peptide which is incorporated within or appended to the $J\alpha$ helix (Strickland et al., 2012).

Preliminary work of Christian Scheeder in our group suggested that fusing the MIP peptide (Shiheido et al., 2011) to two truncations of the AsLOV2 domain enabled light-mediated control of p53 levels (Figure 3.1). However, when I tried to replicate his findings, I could not observe any effect on p53 levels (Figure 3.2 and Figure 3.3). Un-reproducibility in experiments is often caused by changes in experimental set up and work flow. However, Christian and I used the same protocol, constructs, lab instruments and reagents. Thus it remains unclear why he could observe an effect and I could not.

My own data indicate that the MIP peptide has no effect on p53 levels (Figure 3.3). This is in contrast also to

published findings (Shiheido et al., 2011). Shiheido and colleagues reported increased p53, Mdm2 and p21 protein levels in HCT116 cells expressing the MIP peptide within the thioredoxin scaffold. The higher levels of Mdm2 and p21 depend on endogenous p53 levels, as the increase is absent in HCT-p53^{-/-} cells. In their work, a viral transduction system was used, in contrast to the chemical transfection method used here, thus expression levels are not comparable. Yet, not even increasing 8-fold the amount of transfected DNA resulted in higher p53 protein levels. Moreover, I could not find further literature supporting the *in vivo* effects of the MIP peptide. Structural data suggest that the MIP peptide binds Mdm2 with higher affinity than endogenous p53 (Nagata et al., 2014). Yet, in my own experiments high levels of the MIP peptide within the thioredoxin scaffold were not sufficient to impact p53 levels, suggesting that the affinity determined *in vitro* is either too low, or different *in vivo*.

The second peptide candidate was the PMI peptide, which supposedly has a superior affinity to Mdm2 and MdmX than the MIP peptide (Pazgier et al., 2009). I could show that the PMI peptide is a potent inhibitor of p53 degradation and deactivation (Figures 2.6 and 2.8). As Pazgier and colleagues have only presented *in vitro* data, this is to my knowledge the first *in vivo* validation of the potency of this peptide (Pazgier et al., 2009).

As with the MIP peptide, I was not able to find AsLOV2-PMI fusion proteins, which elevated p53 levels, even though multiple C-terminal AsLOV2 domain truncations were investigated (Figure 3.6). Additionally, hybrids of AsLOV2 domain and p53 TAD did not result in increase of p53 levels in mammalian cells, independent of the illumination conditions I used (Figure 3.5). The fact that p53 levels do not increase after exposing cells to blue light suggests that the fusion constructs are unable to undergo the light-induced conformational change that would result in the uncaging of the peptide. Whether this is caused by an impaired structural rearrangement due to altered biochemical properties of the fusion proteins, or whether Mdm2/MdmX are sterically hindered to bind the exposed sequences due to the presence of the AsLOV2 domain is unknown. Interestingly, N-terminal fusions of PMI to mCherry connected via a linker could inhibit p53 degradation (Figure 3.6).

During their investigation of how to best photocage peptides within the J α helix of AsLOV2, Strickland and colleagues tested numerous C-terminal truncations of the AsLOV2, and only a minority resulted in the desired light-dependent behaviour (Strickland et al., 2012). In general, most optogenetic tools based on fusing peptides or functional domains to truncations of the AsLOV2 domain have undergone screening processes, and only a limited number of tested constructs exhibited the desired light-dependent function (Wu et al., 2009; Renicke et al., 2013; Bongers et al., 2013). Standardisation of this process has revealed to be ineffective. Design criteria cannot be transferred, even for closely related proteins (Winkler et al., 2014). Thus, further screening of AsLOV2-PMI fusions might be necessary to identify candidates exhibiting favourable behaviour.

A more rational design process was developed in our laboratory by my colleague Dominik Niopek (Niopek et al., 2016). In an iterative process called J α helix topping, instead of simply fusing a peptide to the J α helix, the native helix is progressively mutated in order to match key conserved residues that are necessary for the activity of the peptide to be caged. Since several residues are kept unmutated, the J α helix is more likely to maintain its photo-responsiveness. Obviously, this approach requires a certain similarity between the J α helix and the amino acid sequence of the peptide to be caged, but it was shown to be very effective in the design of LEXY.

However, Albert Fàbregas Flavià, a Bachelor student in our lab, tried to use this method (J α helix topping) to embed into the J α helix the PMI peptide, but failed to find a promising candidate.

4.1.2 Controlling the localisation of the PMI peptide

I could demonstrate that the effect of the PMI peptide is dependent on its cellular localisation (Figure 3.6). This suggests that Mdm2 binds p53 predominantly in the nucleus, as inhibition of the Mdm2-p53 complex in the cytoplasm did not alter p53 levels.

Several models have been proposed of how p53 activation can lead to selective transcriptional responses. One of these models states that acetylation of key residues of p53 alters its binding affinity towards specific promoters (Kruse and Gu, 2009). This model hypothesises that the number of acetylated residues of p53 correlates to the

severity of the encountered stress.

p21 is a marker for cell cycle arrest and a prominent target gene of p53 (Gartel et al., 1996). According to this model, expression of p21 is dependent on acetylation of p53 (Kruse and Gu, 2009). Expression of PMI-mCherry led to p21 levels close to levels observed in cells treated with the genotoxic drug Daunorubicin. This suggests that PMI administration is sufficient to drive p21 levels in the absence of stress. Whether the acetylation of p53 still occurs upon PMI transfection, or whether acetylation of p53 is not essential for it to transcribe p21 needs to be clarified.

4.1.3 PMI-induced increase in p53 levels is not reversible

Using LEXY, I could control the localisation of PMI with blue light. PMI-LEXY could repeatedly be exported out of the nucleus when activation periods were short (40 minutes) (Figure 3.8). The fact that p53 levels decreased only marginally in samples where light was re-applied after 24 h of darkness (Figure 3.9) could be interpreted in two ways: a) cells are unable to efficiently export PMI-LEXY and therefore enough peptide remains nuclear and continues to block Mdm2. This could be due to the fact that PMI binds Mdm2 in the nucleus and the Mdm2/PMI-LEXY complex might be too big for LEXY to efficiently drive its export. Moreover, Mdm2 itself possesses a NLS and a NES (Roth et al., 1998), which might play a role in the localisation of the complex.

PMI-LEXY is exported in complex with Mdm2, which is therefore still unable to exert its function towards p53. Once dissociated from the complex, Mdm2 might bind to residual cytosolic PMI-LEXY due to the increased binding affinity towards the PMI peptide, thus remaining sequestered in the cytosol away from nuclear p53, which would remain at high concentrations.

In either case, it is unclear how a limited pool of peptide (indeed, after some hours transcription from the plasmid can only decrease) can so efficiently inhibit Mdm2, whose levels are bound to increase with time due to new transcription of the gene by the stabilized p53.

To discern between these two scenarios, localisation of PMI-LEXY should be traced during an ongoing experiment, to investigate whether PMI-LEXY remains in the nucleus once cells are subjected to blue light after 24 h of darkness, which would argue for an impediment of nuclear export. Moreover, immunostaining of Mdm2 in cells exposed to light regimes including a prolonged recovery time should reveal its localisation, and thus whether it is bound to PMI in the cytosol.

4.2 Efficiency of PMI-LINuS and p53-LINuS fusions is low

Cellular localisation of any protein is an equilibrium of its localisation sequences, namely its NES and NLS sequences. Protein localisation is not a finite state, as import and export are dynamic processes. The net localisation of a protein is determined by the relative strength of its NLS and NES. Thus, achieving control over nucleocytoplasmic transport requires balancing of NLS and NES sequences.

I initially tried to achieve optogenetic control of PMI localisation by using LINuS. Yet, PMI fused to selected LINuS variants did not behave as expected in HCT116 cells (Figure 3.7). LINuS has been shown to work in a variety of cell lines (Niopek et al., 2014), however it had not been used so far in HCT116 cells. As the size of the cells seems to contribute to translocation efficiencies, the fact that HCT116 cells are small compared to most common cell lines may be the reason of this inefficiency.

In previous work for collaboration partners, I could observe similar effects. N- or C-terminal peptide fusion to LINuS or LEXY could alter the initial localisation drastically, even though the peptides were not localisation sequences. While it is obvious, that tagged proteins that contain localisation sequences can alter the initial state, it remains elusive why peptides can have such a high impact on the localisation of peptide LINuS or LEXY fusions.

As LINuS has been shown to work in several cell lines, it is unlikely that LINuS cannot be used in HCT116 cells as the import-export machinery LINuS employs is highly conserved in eukaryotes (Cautain et al., 2015). Yet, mam-

malian cell lines deviate in total and relative abundance of transport receptors and nuclear pores, thus some cell lines might require optimisation of LINuS constructs for them to be able to robustly translocate upon exposure to light citepmaul1977quantitative, van2014elevated. Moreover, AsLOV2-based optogenetic tools, such as LEXY and LINuS, require the co-factor FMN. The number of freely available FMN molecules could thus affect translocation of LINuS constructs. It has been shown that FMN concentrations can vary significantly between different cell types; unfortunately, numbers for HCT116 cells are lacking (Hühner et al., 2015).

Putatively, import and export receptor isoforms possess different binding and dissociation affinities towards specific localisation sequences. This could explain why NLS and NES sequences have different relative strengths in different cell lines, as seen in the evaluation of various constitutive synthetic NESs in p53^{K306A}-biLINuS02 constructs (Figure 3.17) compared to their strength in Hek293T cells.

In contrast to PMI-LINuS, PMI-LEXY constructs were able to reversibly translocate, and induce light-dependent changes in p53, and consequently, p21 levels (Figure 3.8). Similarly, p53-LEXY could reversibly translocate in and out of the nucleus, while various LINuS candidates were not able to do so (Figure 3.10 and Figure 3.18).

During the course of optimisation of p53-LINuS constructs, I mutated both endogenous NLS and NES sequences, yet ultimately failed to generate a p53-LINuS variant which could be reversibly accumulated in the nucleus while remaining transcriptionally active. Manipulation of endogenous localisation sequences has been successfully demonstrated to optimize translocation of Cyclin B1 (Niopek et al., 2014), yet did not yield the favoured results here.

Impaired translocation is obviously not dependent on p53, since p53-LEXY exhibited the desired translocation kinetics without any optimisation. It remains unclear why p53-LINuS accumulation was never fully reversible. Initial assumptions, that it could not exit the nucleus due to the formation of tetramers, can be excluded, given that p53-LEXY could reversibly translocate in and out of the nucleus and, being transcriptionally active, is likely able to tetramerize. A potential reason might be that, while export of NES-harboring proteins is dependent on only one receptor (Crm1), import may depend on several receptors (importin alpha and beta), depending on the type of NLS (Marfori et al., 2011). For the nuclear localisation sequences photocaged in certain LINuS variants it is not known whether importin alpha is required for their import, making it hard to compare p53-LINuS and p53-LEXY constructs. Apparently, LINuS requires more optimisation and fine-tuning of NLS/NES balancing. In both, LINuS and LEXY, nuclear export requires more time than the import (This work, (Niopek et al., 2014, 2016).

4.3 p53 mutant constructs lack transcriptional activity

p53^{K320AL348AL350A}-biLINuS22 was the only p53-LINuS variant that exhibited good nuclear accumulation upon blue light stimulation, while still being partly re-accumulating into the cytoplasm once blue light was switched off (Figure 3.12). Unfortunately, the introduced mutations rendered it transcriptionally inactive (Figure 3.13). I was so focused on finding a way to control the localization of p53 that I did not realize right away that touching the NES would have an influence on tetramerisation. L348 and L350 are located in the tetramerisation domain and are implicated in the formation of tetramers. Tetramerisation are essential for p53 to become fully transcriptionally active (Stommel et al., 1999). p53^{L348AL350A} double mutant can indeed form tetramers only at very high concentrations (Itahana et al., 2007). In my experiments, tetramerisation seemed to have a stronger impact than acetylation as introduction of acetylation-mimicking mutations did not stimulate p53 target expression (Figure 3.14).

Also the impact on transcriptional activity of K320 has been investigated. The histone acetyl transferase PCAF specifically acetylates p53 on lysine 320 (K320) upon DNA damage (Liu et al., 1999). This acetylation increases p53-DNA binding *in vitro*, yet *in vivo* changes in transcription were minor (Love et al., 2012). It is suggested that K320 is one of the residues crucial to be acetylated, and required for p53 to bind to other co-factors, which are essential for p21 transcription (Barlev et al., 2001). Yet, Barlev and colleagues only present data for a p53 mutant

having four lysines (K320/373/381/382R) mutated.

Since the only p53 mutant whose localisation I could control with LINuS lacked transcriptional activity, I moved on and tested another optogenetic tool, LEXY.

4.4 Comparing the transcriptional response to pulsatile and sustained p53

4.4.1 p53 abundance determines translocation efficiency

I could show that LEXY can be used to control p53 translocation and thus its transcriptional activity with light (Figure 3.18). Moreover, diverse p53 dynamics akin to physiological ones could be applied (Figure 3.23).

Initial comparison between constant and pulsatile p53 resembling stress-induced p53 dynamics did not reveal differential expression of selected target genes (Figure 3.21). Yet, these results were tainted by the inhomogeneous expression levels of p53-LEXY in the cells. We have observed in multiple LINuS and LEXY applications that the translocation efficiency correlates with the protein abundance. Presumably, too high concentrations of the p53-LEXY construct result in the saturation of the export machinery, leading to less efficient export after illumination. Unfortunately, reducing the amount of transfected DNA resulted in a reduced number of transfected cells, and therefore in more heterogeneity, rather than in a decrease of transfected protein levels. For this reason, I decided to generate a stable cell line, to ensure homogeneous expression and stable p53-LEXY levels during the course of an experiment.

4.4.2 The effect of doxycycline on p53 transcript levels

After the elaborate process of generating a stable cell line with an inducible expression system regulating p53-LEXY, protein abundance was reduced and could be tightly controlled. Using this stable cell line, I repeated the experiment to compare constant to pulsatile p53 activation (Figure 3.24). Even though expression levels were reduced, pulsatile activation resulted only in the differential expression of the senescence marker PML. Yet, the highest elevation in transcript levels was observed for p53 itself.

p53-LEXY is regulated by the T-REx™ system, which enables expression of a target gene by doxycycline. The parental cell line H1299 is p53^{-/-} and expresses only partial p53 mRNA due to a homozygous partial deletion of the TP53 gene. Therefore, the introduced p53-LEXY is the sole source of expressed, full-length p53 transcripts in the cell. The integrated p53-LEXY is driven by a CMV_{min} promoter containing two tetO₂ sequences, which are bound tightly by the continuously expressed TetR, thus preventing transcription of p53-LEXY. Upon doxycycline induction, TetR is removed from the promoter, and therefore transcription is activated. Consequently, p53 levels should not be under any regulation other than doxycycline. Light should not affect p53 levels; it is expected to have only an effect on its target genes, due to the regulation of p53 localization and not abundance.

Heterogeneity in p53-LEXY expression was observed in H1299 cells transiently transfected with p53-LEXY. Yet in this experiment, the stable line C29-36 was used, and doxycycline induction triggered similar expression levels across cells and resulted in a rather homogeneous expression of p53-LEXY protein.

It is suggested that doxycycline possesses a low photostability when exposed to UV light (Kogawa et al., 2014); nevertheless, existing inducible induction systems based on chemically-caged doxycycline use UV light as a trigger for expression and do not report any side-effects (Cambridge et al., 2009). Anyway, if prolonged light illumination was indeed inducing doxycycline degradation, then this should lead to decreased p53-LEXY mRNA levels in the samples exposed to light; however, I observed the opposite trend, with higher p53-LEXY mRNA levels in cells exposed to light of higher intensity.

Interestingly, the observed effect on p53-LEXY mRNA levels could not be observed when cells were activated with blue light of longer wavelength (488nm) (Figure 3.25). As translocation efficiency is not affected by the change of light wavelength, the observed increase in p53-LEXY mRNA levels under pulsatile illumination must

have been triggered by the illumination regime. The overall reduction in the energy the cells are subjected to when being exposed to light of longer wavelength is, however, only minimal. If any manipulation of doxycycline occurs at 458 nm, it supposedly also happens at 488 nm, potentially on a smaller scale. Light-induced chemical degradation of doxycycline can be excluded, as expression levels, and thus doxycycline levels, were higher in the presence of light.

A general increase in mRNA levels could not be observed, as levels of reference and p53 target genes beside PML remained unaffected. One possible explanation for the increase of p53-LEXY mRNA levels is an increase in mRNA stability due to prolonged light exposure. Several mechanisms for the regulation of p53 mRNA have been reported (Yin et al., 2002; Vilborg et al., 2009), and it has been demonstrated that transcript variants exhibit different stability (Zydowicz-Machtel et al., 2018). Yet, all reported regulation steps are mediated on either the 5' or the 3' UTR regions of p53 mRNA, which are lacking in my construct. Alternatively, the observed increase in mRNA levels could also be independent of p53, but rather due to mCherry or LEXY. To investigate this further, one could transfect either only untagged p53, mCherry or LEXY, and measure the respective mRNA levels after blue light exposure.

4.4.3 Prolonged illumination of the cells impairs their import/export capacity and leads to phototoxicity

In multiple experiments I have observed that, after a prolonged illumination period, cells were unable to re-import LEXY-tagged proteins into the nucleus once put back in the dark. This was true regardless of the specific protein fused to LEXY, suggesting that the problem is the toxicity of the light to the cells.

Particularly in my initial experiments with p53-LEXY, I could observe that prolonged blue light exposure caused sequestration of the construct in the cytosol (Figure 3.28, Figure 3.29 and Figure 3.30). This has not been observed before.

Also in shorter experiments, an increase in p53-LEXY molecules that remain cytosolic during the dark recovery phase is visible after some hours of blue light exposure (Figure 3.19). Given that I could observe efficient repeated nuclear/cytosolic translocation events of p53-LEXY for more than 30 hours when the illumination regime was made of shorter light phases (15 min), I would conclude that prolonged illumination causes phototoxicity to the cells, rendering them progressively unable to efficiently import/export proteins. While the selected light settings did not affect phenotype or proliferation of cells, recent studies suggest that prolonged blue light illumination can indeed alter expression profiles and differentiation potential in primary cells (Cheng et al., 2016; Stockley et al., 2017). Moreover, blue light exposure causes oxidative stress, which has been linked to nuclear accumulation of import receptors, and thus import blockage (Kodiha et al., 2004; Godley et al., 2005).

In support of this conclusion, I could exclude that the cytoplasmic retention was p53-specific. Even though p53 is known to interact with Bcl-family proteins in the cytosol and on the mitochondrial membrane (Li et al., 1999; Chipuk et al., 2004), as well to bind to the cytosolic anchor Parc (Nikolaev et al., 2003), mCherry-LEXY exhibited the same impaired translocation as p53-LEXY (Figure 3.29). Additionally, it can be excluded that stable integration of TetR or p53-LEXY has occurred at genetic locations that corrupt the import/export machinery, since also the transiently transfected LEXY construct exhibited the same behaviour.

As this effect has only been observed in H1299 cells, it might be cell type specific. As mentioned before, cell lines differ in their expression levels of particular components of the import/export machinery (Maul and Deaven, 1977; Van der Watt et al., 2009, 2014). Yet, whether potential differences contribute to the observed phenotype is unknown.

In general, nuclear import seems to be a rate-limiting step in H1299 cells. Cells with cytoplasmically-sequestered LEXY molecules exhibit bright speckles close to the nucleus. Presumably, these are p53-LEXY aggregates, which cannot be re-imported in the nucleus. As the speckles are located close to each other and do not move, they are apparently not freely diffusing in the cell, which suggests they are either within or associated to a cellular

compartment. Since their number and intensity increase over time, correlating to higher inefficiency of nuclear import, it is likely that these speckles are associated to the failed import of p53-LEXY.

To verify whether this phenotype is indeed caused by phototoxicity or by too many translocation events, one could reduce p53-LEXY expression levels. Alternatively, it is possible to reduce the dark recovery kinetics of the AsLOV2 domain. The AsLOV2 domain has been extensively studied, and several mutations are known, which affect dark recovery kinetics (Alexandre et al., 2007; Zoltowski et al., 2009; Raffelberg et al., 2011). Increasing the dark recovery time would reduce the stress on the import-export machinery, since the AsLOV2 would remain in its excited state for longer times and therefore the NES would be exposed for longer, all in all leading to a longer cytoplasmic localisation without the need for shining light every 30-40 seconds.

4.4.4 Changing the light application settings to reduce phototoxicity reduced light-dependent transcription of p53 target genes

Once the doxycycline administration regime was optimised to permit stable p53-LEXY protein levels during the experimental window, I re-applied p53 pulsatile and sustained dynamics to analyse their effects on p53 target genes (Figure 3.31). Optimisation of the illumination conditions and shortening of the duration of the experiment resulted in reliable translocation in samples exposed to constant (always intended as short repeated light pulses with 30 sec interval) blue light, (Supplemental Figure 7.1). On the other hand, pulsatile translocation resulted in a reduction of translocation efficiency with every new illumination phase. Presumably, the reduction is due to an overload in the nuclear-cytosolic translocation system.

Exposure to either no light, pulsatile light or "constant" light resulted only in marginal changes in gene expression (Figure 3.31). In general, the transcriptional response to nuclear presence of p53 was minor, as the greatest observed change in expression was 1.5 fold. Purvis and colleagues report higher fold-changes for p53 targets under different p53 dynamics. For example, after 8 hours, p21 mRNA levels increased for them 16-fold when p53 was sustained compared to when it was pulsatile (Purvis et al., 2012).

In previous experiments, I could observe a light-dependent induction of >2-fold of the p53 target genes Mdm2 and p21 (Figure 3.28); yet after changing the illumination set up, the differential expression was marginal. This is presumably caused by the reduced light intensity used in this experiment, to reduce phototoxicity and allow translocation to occur (Figure 3.30). While the reduction of light intensity indeed resulted in an efficient translocation (Supplemental Figure 7.1), a two times larger fraction of p53-LEXY molecules remained in the nucleus during the illumination phase (Figure 3.30). Potentially this increase in nuclear p53-LEXY in cells subjected to light is sufficient to drive p21 expression to the same extent than cells which remain in the dark. This, however, would suggest that a two-fold increase in nuclear levels of p53 observed in samples shielded from the dark after the initial illumination period do not increase expression further, which seems unlikely. Alternatively, it can be that even the reduced light settings cause phototoxic effects and influence the transcriptional activity of the cells, which renders these results unreliable.

Taken together, p53-LEXY could be reliably and reversibly translocated between the cytosol and nucleus. Cells exposed to activation/recovery intervals of 15 minutes or 2 hours could translocate p53-LEXY for more than 15 hours, yet longer constant illumination periods caused an decrease in translocation efficiency. If possible I would advise to use LINuS instead of LEXY when investigating transcription factors, as LINuS is located in the cytosol when cells are shielded from the light, thus rendering the initial illumination period unnecessary. exposure would become no longer necessary.

4.5 Un-reproducibility of p53's transcriptional activity in response to drug treatment

As exposing cells to blue light for several hours to keep p53-LEXY inactive until the beginning of the experiment led to phototoxicity and impaired LEXY functioning, I decided to change entirely my experimental set up. I reckoned that I should leave the cells in the dark in the initial phase, after induction with doxycycline. Clearly this would lead to nuclear p53-LEXY, and therefore to activation of gene expression, before the start of the experiment. However, my idea was to rather test the response of the cells to a drug treatment depending on p53 dynamics. Cells would have a certain amount of p53-LEXY to begin with at the time at which the stress-inducing agent is applied, but this would be similar across conditions. Then I would apply different light regimes and see if cells responded differently if p53-LEXY was left always nuclear to when it was brought in and out of the nucleus in pulses. Unfortunately, while performing the first control experiments to check if there was a difference between always nuclear and always cytoplasmic p53-LEXY after addition of the drug, I discovered that the stable cell line I generated is unreliable (Figure 3.32, Figure 3.33, Figure 3.32 and Figure 3.33). The data were highly variable between biological replicates and this was true for all samples, independent of a single factor. p53 response to stress is known to be highly variable (personal communication with Jared Toettcher); however, here the response seemed binary: in replicate 1, the fold-change in transcription of *btg2* and *puma* was similar to previously published results (Porter et al., 2016), while replicate 2 exhibited hardly an increase in transcription.

First, I want to exclude several technical causes of lack of reproducibility:

Preparation of cDNA, and subsequent reverse transcription were run in parallel for both replicates. Yielded RNA concentrations were similar, and the A260/A280 ratio, a value for RNA purity, was > 2.0 in both cases (indicating that the RNA was pure). The same master mix was used for cDNA preparation and qPCR. Samples were distributed over several qPCR plates, to avoid a plate bias. Melting curves of primers were validated. Additionally, the absolute Ct values of the reference genes *beta-actin* and *Rpl0* were constant. I would also exclude experimental work-flow-related factors. The same aliquot of the respective drugs was used. Additionally, the cells used for both experiments were at the same passage number and stemmed from the same batch. Cells were seeded at the same density, and p53-LEXY fluorescence was verified on the Lionheart, showing similar levels. Effects caused by different cell cycle stages should be minor, since the whole population of cells was collected. Taken together, I would exclude technical reasons for lack of reproducibility, suggesting that this is due to some biological property of either the p53-LEXY construct or the cell line.

To understand if the problem was the cell line, I decided to analyse in the same way two different cell lines. In contrast to the results observed in C29-36 cells, MCF7-p53-Venus and HCT116 cells responded consistently to the applied stress (Figure 3.36). I also tested whether the problem could be high levels of cytosolic p53 (a rather unphysiological condition), by transiently transfecting a NES-p53-mCheryR construct. The results, however, clearly indicate that neither drug administration, nor light exposure nor cytosolic p53 are the reason behind the lack of reproducibility. I am left with the conclusion that the cell line C29-36 is the problem. The parental cell line H1299 previously exhibited reliable results with transiently transfected p53-LEXY (Figure 3.18), thus integration of TetR and p53-LEXY is the likely cause.

Stable cell lines tend to silence transgenes by methylation, particularly expression driven from the CMV promoter has been shown to be down-regulated over time (Brooks et al., 2004). While this could explain why the second successfully generated stable cell line C29-48 lost expression over time, it is not the reason for lack of reproducibility in C29-36 cells, where p53-LEXY levels are stable.

This suggests that the random integration of TetR, p53-LEXY or both occurred presumably in a genomic location that contributes to the variance in response. However, it is hard to come up with potential mechanisms, as biological noise is observed in single cells, yet is unlikely to exert differences in a population-based read-out. Since reference genes are stably expressed, and cells exhibit no observable morphological changes, effects on

general transcription are unlikely. Likely integration occurred on genomic loci associated to the p53 regulatory network.

4.6 Outlook

Here, I presented two approaches to take control over p53 dynamics. First, I tried to achieve optogenetic control over the inhibition of p53 degradation, aiming at fine-tuning levels of endogenous p53 levels. In a second approach, I tried to control nucleocytoplasmic translocation of p53, assuming that only nuclear p53 would be transcriptionally active.

In the current state, both approaches could not be used for the intended purpose, that is, applying defined p53 dynamics and linking them to the respective downstream transcriptional response.

While PMI-LEXY was successfully used to inhibit degradation of p53, the lack of reversibility renders application of p53 dynamics impossible. The cause for the irreversibility could not be identified, yet further investigation could improve re-translocation into the cytosol, particular examining shorter periods of the individual activation or recovery intervals, which would also reflect better the physiological response to stress.

Alternatively, re-examining LINuS variants in HCT116 cells, or selecting a cell line where LINuS has been established, might improve translocation of PMI-LINuS. Translocation efficiency of potential PMI-LINuS variants could be further improved by using LOVTRAP, an optogenetic system used to trigger light-induced dissociation of the AsLOV2 domain and Zdk, a protein that selectively binds the AsLOV2 domain in the dark state (Wang et al., 2016). This would allow, for instance, tethering the AsLOV2 domain of PMI-LINuS to the cellular membrane during non-illuminated periods, while not impairing translocation during blue light exposure, thereby reducing occurring translocation during non-illuminated phases.

Working with LEXY to control p53 localisation, it became apparent that prolonged blue light exposure harms cells. In several steps, the light energy applied to cells was lowered, but the reduction was not sufficient to ensure p53 translocation over the whole experimental run time. Thus, it is vital to further reduce blue light exposure. This could be achieved by reducing the AsLOV2's reversion half-life, meaning the time it takes for the AsLOV2 to spontaneously rearrange to the dark state. The illumination timings used during illumination are dependent on the photocycle of the AsLOV2 domain, thus increasing the time of one photocycle would allow for further reduction of illumination, while still allowing the application of p53 dynamics observed in physiological stress situations.

The experiments using LEXY have demonstrated that p53 can be repeatedly translocated. Thus, it might be reasonable to screen various combinations of constitutive NESs and LINuS variants, to achieve light-mediated nuclear import of previously cytosolic p53-LINuS. Using LINuS, the initial blue light exposure would become no longer necessary.

Additionally, the stable cell line C29-36 has turned out to be compromised, given the lack of reproducibility I obtained when analysing its response to any kind of treatment. Yet, turning back to transfection is not advisable, due to the heterogeneous expression of the transfected target gene. Rather, commercial systems with specific genome integration sites or lentiviral transduction should be used, to guarantee homogeneous and reliable expression.

Next to the optimisation of the control of p53 dynamics, further development should be done to find the best downstream read-out. Single cell studies have revealed that observations on the population-based level can be misleading, particularly when investigating noisy processes as cell signalling. Thus, a read-out at single cell resolution should be used in further experiments. Staining procedures like single molecule FISH would allow for application of p53 dynamics followed by direct quantification of gene expression in the same cells, thus a direct link between the frequency and amplitude of nuclear p53 and the number of target mRNAs at specific time points would be possible. Moreover, more sophisticated fluorescent labelling approaches have been developed that allow quantification of transcription and translation of target genes, using modern gene editing tools like

CRISPR/Cas9 to introduce the fluorescent tags in the endogenous loci of the respective target genes.

Overall, I believe that optogenetic approaches can contribute to investigating p53 regulatory network and cell signalling pathways in general, as the unmatched spatial and temporal resolution of light enables investigation and perturbation of individual nodes in these highly dynamic cellular systems.

5 Bibliography

- Albeck, J. G., Mills, G. B., and Brugge, J. S. (2013). Frequency-modulated pulses of erk activity transmit quantitative proliferation signals. *Molecular cell*, 49(2):249–261.
- Alexandre, M. T., Arents, J. C., van Grondelle, R., Hellingwerf, K. J., and Kennis, J. T. (2007). A base-catalyzed mechanism for dark state recovery in the *avena sativa* phototropin-1 lov2 domain. *Biochemistry*, 46(11):3129–3137.
- Alt, J. R., Bouska, A., Fernandez, M. R., Cerny, R. L., Xiao, H., and Eischen, C. M. (2005). Mdm2 binds to nbs1 at sites of dna damage and regulates double-strand break repair. *Journal of Biological Chemistry*.
- Aoki, K., Kumagai, Y., Sakurai, A., Komatsu, N., Fujita, Y., Shionyu, C., and Matsuda, M. (2013). Stochastic erk activation induced by noise and cell-to-cell propagation regulates cell density-dependent proliferation. *Molecular cell*, 52(4):529–540.
- Baarlink, C., Wang, H., and Grosse, R. (2013). Nuclear actin network assembly by formins regulates the srf coactivator mal. *Science*, 340(6134):864–867.
- Badciong, J. C. and Haas, A. L. (2002). Mdmx is a ring finger ubiquitin ligase capable of synergistically enhancing mdm2 ubiquitination. *Journal of Biological Chemistry*, 277(51):49668–49675.
- Bakkenist, C. J. and Kastan, M. B. (2003). Dna damage activates atm through intermolecular autophosphorylation and dimer dissociation. *Nature*, 421(6922):499.
- Banin, S., Moyal, L., Shieh, S.-Y., Taya, Y., Anderson, C., Chessa, L., Smorodinsky, N., Prives, C., Reiss, Y., Shiloh, Y., et al. (1998). Enhanced phosphorylation of p53 by atm in response to dna damage. *Science*, 281(5383):1674–1677.
- Bar-Or, R. L., Maya, R., Segel, L. A., Alon, U., Levine, A. J., and Oren, M. (2000). Generation of oscillations by the p53-mdm2 feedback loop: a theoretical and experimental study. *Proceedings of the National Academy of Sciences*, 97(21):11250–11255.
- Barak, Y. and Oren, M. (1992). Enhanced binding of a 95 kda protein to p53 in cells undergoing p53-mediated growth arrest. *The EMBO journal*, 11(6):2115–2121.
- Barlev, N. A., Liu, L., Chehab, N. H., Mansfield, K., Harris, K. G., Halazonetis, T. D., and Berger, S. L. (2001). Acetylation of p53 activates transcription through recruitment of coactivators/histone acetyltransferases. *Molecular cell*, 8(6):1243–1254.
- Batchelor, E., Loewer, A., Mock, C., and Lahav, G. (2011). Stimulus-dependent dynamics of p53 in single cells. *Molecular systems biology*, 7(1):488.
- Batchelor, E., Mock, C. S., Bhan, I., Loewer, A., and Lahav, G. (2008). Recurrent initiation: a mechanism for triggering p53 pulses in response to dna damage. *Molecular cell*, 30(3):277–289.
- Bayle, J. H., Grimley, J. S., Stankunas, K., Gestwicki, J. E., Wandless, T. J., and Crabtree, G. R. (2006). Rapamycin analogs with differential binding specificity permit orthogonal control of protein activity. *Chemistry & biology*, 13(1):99–107.

- Behar, M. and Hoffmann, A. (2010). Understanding the temporal codes of intra-cellular signals. *Current opinion in genetics & development*, 20(6):684–693.
- Berkers, C. R., Maddocks, O. D., Cheung, E. C., Mor, I., and Vousden, K. H. (2013). Metabolic regulation by p53 family members. *Cell metabolism*, 18(5):617–633.
- Berns, K., Hijmans, E. M., Mullenders, J., Brummelkamp, T. R., Velds, A., Heimerikx, M., Kerkhoven, R. M., Madiredjo, M., Nijkamp, W., Weigelt, B., et al. (2004). A large-scale rna screen in human cells identifies new components of the p53 pathway. *Nature*, 428(6981):431.
- Berridge, M. J., Bootman, M. D., and Roderick, H. L. (2003). Calcium: calcium signalling: dynamics, homeostasis and remodelling. *Nature reviews Molecular cell biology*, 4(7):517.
- Berridge, M. J. and Galione, A. (1988). Cytosolic calcium oscillators. *The FASEB Journal*, 2(15):3074–3082.
- Beyer, H. M., Juillot, S., Herbst, K., Samodelov, S. L., Müller, K., Schamel, W. W., Römer, W., Schäfer, E., Nagy, F., Strähle, U., et al. (2015). Red light-regulated reversible nuclear localization of proteins in mammalian cells and zebrafish. *ACS synthetic biology*, 4(9):951–958.
- Binan, L., Mazzaferri, J., Choquet, K., Lorenzo, L.-E., Wang, Y. C., Affar, E. B., De Koninck, Y., Ragoussis, J., Kleinman, C. L., and Costantino, S. (2016). Live single-cell laser tag. *Nature communications*, 7:11636.
- Bishop, A. C., Ubersax, J. A., Petsch, D. T., Matheos, D. P., Gray, N. S., Blethrow, J., Shimizu, E., Tsien, J. Z., Schultz, P. G., Rose, M. D., et al. (2000). A chemical switch for inhibitor-sensitive alleles of any protein kinase. *nature*, 407(6802):395.
- Bond, G. L., Hirshfield, K. M., Kirchhoff, T., Alexe, G., Bond, E. E., Robins, H., Bartel, F., Taubert, H., Wuerl, P., Hait, W., et al. (2006). Mdm2 snp309 accelerates tumor formation in a gender-specific and hormone-dependent manner. *Cancer research*, 66(10):5104–5110.
- Bond, G. L., Hu, W., Bond, E. E., Robins, H., Lutzker, S. G., Arva, N. C., Bargonetti, J., Bartel, F., Taubert, H., Wuerl, P., et al. (2004). A single nucleotide polymorphism in the mdm2 promoter attenuates the p53 tumor suppressor pathway and accelerates tumor formation in humans. *Cell*, 119(5):591–602.
- Bonger, K. M., Rakhit, R., Payumo, A. Y., Chen, J. K., and Wandless, T. J. (2013). General method for regulating protein stability with light. *ACS chemical biology*, 9(1):111–115.
- Böttger, A., Böttger, V., Sparks, A., Liu, W.-L., Howard, S. F., and Lane, D. P. (1997). Design of a synthetic mdm2-binding mini protein that activates the p53 response in vivo. *Current Biology*, 7(11):860–869.
- Bourdon, J.-C., Fernandes, K., Murray-Zmijewski, F., Liu, G., Diot, A., Xirodimas, D. P., Saville, M. K., and Lane, D. P. (2005). p53 isoforms can regulate p53 transcriptional activity. *Genes & development*, 19(18):2122–2137.
- Bouska, A., Lushnikova, T., Plaza, S., and Eischen, C. M. (2008). Mdm2 promotes genetic instability and transformation independent of p53. *Molecular and cellular biology*, 28(15):4862–4874.
- Boyden, E. S., Zhang, F., Bamberg, E., Nagel, G., and Deisseroth, K. (2005). Millisecond-timescale, genetically targeted optical control of neural activity. *Nature neuroscience*, 8(9):1263.
- Briggs, W. R. and Spudich, J. L. (2005). *Handbook of photosensory receptors*. John Wiley & Sons.
- Brock, T. (2009). Big time protein in a big time field. *Caymanchem*.
- Brooks, A. R., Harkins, R. N., Wang, P., Qian, H. S., Liu, P., and Rubanyi, G. M. (2004). Transcriptional silencing is associated with extensive methylation of the CMV promoter following adenoviral gene delivery to muscle. *J. Gene Med.*, 6(4):395–404.

- Brosh, R. and Rotter, V. (2009). When mutants gain new powers: news from the mutant p53 field. *Nature Reviews Cancer*, 9(10):701.
- Bugaj, L., Sabnis, A., Mitchell, A., Garbarino, J., Toettcher, J., Bivona, T., and Lim, W. (2018). Cancer mutations and targeted drugs can disrupt dynamic signal encoding by the ras-erk pathway. *Science*, 361(6405):eaao3048.
- Buschmann, T., Adler, V., Matusevich, E., Fuchs, S. Y., and Ronai, Z. (2000). p53 phosphorylation and association with murine double minute 2, c-jun nh2-terminal kinase, p14arf, and p300/cbp during the cell cycle and after exposure to ultraviolet irradiation. *Cancer Research*, 60(4):896–900.
- Bustin, S. A., Benes, V., Garson, J. A., Hellems, J., Huggett, J., Kubista, M., Mueller, R., Nolan, T., Pfaffl, M. W., Shipley, G. L., Vandesompele, J., and Wittwer, C. T. (2009). The MIQE guidelines: minimum information for publication of quantitative real-time PCR experiments. *Clin. Chem.*, 55(4):611–622.
- Caelles, C., Helmberg, A., and Karin, M. (1994). p53-dependent apoptosis in the absence of transcriptional activation of p53-target genes. *Nature*, 370(6486):220.
- Cambridge, S. B., Geissler, D., Calegari, F., Anastassiadis, K., Hasan, M. T., Stewart, A. F., Huttner, W. B., Hagen, V., and Bonhoeffer, T. (2009). Doxycycline-dependent photoactivated gene expression in eukaryotic systems. *Nat. Methods*, 6(7):527.
- Campbell, I. G., Eccles, D. M., and Choong, D. Y. (2006). No association of the mdm2 snp309 polymorphism with risk of breast or ovarian cancer. *Cancer letters*, 240(2):195–197.
- Canman, C. E., Lim, D.-S., Cimprich, K. A., Taya, Y., Tamai, K., Sakaguchi, K., Appella, E., Kastan, M. B., and Slicano, J. D. (1998). Activation of the atm kinase by ionizing radiation and phosphorylation of p53. *Science*, 281(5383):1677–1679.
- Carrillo, A. M., Hicks, M., Khabele, D., and Eischen, C. M. (2015). Pharmacologically increasing mdm2 inhibits dna repair and cooperates with genotoxic agents to kill p53-inactivated ovarian cancer cells. *Molecular Cancer Research*.
- Carter, S., Bischof, O., Dejean, A., and Vousden, K. H. (2007). C-terminal modifications regulate mdm2 dissociation and nuclear export of p53. *Nature cell biology*, 9(4):428.
- Cautain, B., Hill, R., de Pedro, N., and Link, W. (2015). Components and regulation of nuclear transport processes. *The FEBS journal*, 282(3):445–462.
- Chang, G.-C., Yu, C.-T. R., Tsai, C.-H., Tsai, J.-R., Chen, J.-C., Wu, C.-C., Wu, W.-J., and Hsu, S.-L. (2008). An epidermal growth factor inhibitor, gefitinib, induces apoptosis through a p53-dependent upregulation of pro-apoptotic molecules and downregulation of anti-apoptotic molecules in human lung adenocarcinoma a549 cells. *European journal of pharmacology*, 600(1-3):37–44.
- Chang, Y. S., Graves, B., Guerlavais, V., Tovar, C., Packman, K., To, K.-H., Olson, K. A., Kesavan, K., Gangurde, P., Mukherjee, A., et al. (2013). Stapled α -helical peptide drug development: A potent dual inhibitor of mdm2 and mdmx for p53-dependent cancer therapy. *Proceedings of the National Academy of Sciences*, 110(36):E3445–E3454.
- Chen, J., Lin, J., and Levine, A. J. (1995). Regulation of transcription functions of the p53 tumor suppressor by the mdm-2 oncogene. *Molecular medicine*, 1(2):142.
- Chen, J., Wu, X., Lin, J., and Levine, A. J. (1996). mdm-2 inhibits the g1 arrest and apoptosis functions of the p53 tumor suppressor protein. *Molecular and cellular biology*, 16(5):2445–2452.

- Chen, X., Chen, J., Gan, S., Guan, H., Zhou, Y., Ouyang, Q., and Shi, J. (2013). Dna damage strength modulates a bimodal switch of p53 dynamics for cell-fate control. *BMC biology*, 11(1):73.
- Cheng, K. P., Kiernan, E. A., Eliceiri, K. W., Williams, J. C., and Watters, J. J. (2016). Blue Light Modulates Murine Microglial Gene Expression in the Absence of Optogenetic Protein Expression. *Sci. Rep.*, 6:21172.
- Cheng, Q., Cross, B., Li, B., Chen, L., Li, Z., and Chen, J. (2011). Regulation of mdm2 e3 ligase activity by phosphorylation after dna damage. *Molecular and cellular biology*, 31(24):4951–4963.
- Chipuk, J. E., Bouchier-Hayes, L., Kuwana, T., Newmeyer, D. D., and Green, D. R. (2005). Puma couples the nuclear and cytoplasmic proapoptotic function of p53. *Science*, 309(5741):1732–1735.
- Chipuk, J. E., Kuwana, T., Bouchier-Hayes, L., Droin, N. M., Newmeyer, D. D., Schuler, M., and Green, D. R. (2004). Direct activation of bax by p53 mediates mitochondrial membrane permeabilization and apoptosis. *Science*, 303(5660):1010–1014.
- Chook, Y. M. and Süel, K. E. (2011). Nuclear import by karyopherin- β s: recognition and inhibition. *Biochimica et Biophysica Acta (BBA)-Molecular Cell Research*, 1813(9):1593–1606.
- Christie, J. M., Arvai, A. S., Baxter, K. J., Heilmann, M., Pratt, A. J., O'Hara, A., Kelly, S. M., Hothorn, M., Smith, B. O., Hitomi, K., et al. (2012). Plant uvr8 photoreceptor senses uv-b by tryptophan-mediated disruption of cross-dimer salt bridges. *Science*, 335(6075):1492–1496.
- Cohen, A. A., Geva-Zatorsky, N., Eden, E., Frenkel-Morgenstern, M., Issaeva, I., Sigal, A., Milo, R., Cohen-Saidon, C., Liron, Y., Kam, Z., et al. (2008). Dynamic proteomics of individual cancer cells in response to a drug. *science*, 322(5907):1511–1516.
- Conradt, L., Henrich, A., Wirth, M., Reichert, M., Lesina, M., Algül, H., Schmid, R. M., Krämer, O. H., Saur, D., and Schneider, G. (2013). Mdm2 inhibitors synergize with topoisomerase ii inhibitors to induce p53-independent pancreatic cancer cell death. *International journal of cancer*, 132(10):2248–2257.
- Cosentino, C., Alberio, L., Gazzarrini, S., Aquila, M., Romano, E., Cermenati, S., Zuccolini, P., Petersen, J., Beltrame, M., Van Etten, J. L., et al. (2015). Engineering of a light-gated potassium channel. *Science*, 348(6235):707–710.
- Covert, M. W., Leung, T. H., Gaston, J. E., and Baltimore, D. (2005). Achieving stability of lipopolysaccharide-induced nf- κ b activation. *Science*, 309(5742):1854–1857.
- Crick, F. (1999). The impact of molecular biology on neuroscience. *Philosophical Transactions of the Royal Society of London B: Biological Sciences*, 354(1392):2021–2025.
- Crosson, S. and Moffat, K. (2002). Photoexcited structure of a plant photoreceptor domain reveals a light-driven molecular switch. *The plant cell*, 14(5):1067–1075.
- Crosson, S., Rajagopal, S., and Moffat, K. (2003). The lov domain family: photoresponsive signaling modules coupled to diverse output domains. *Biochemistry*, 42(1):2–10.
- Dagliyan, O., Tarnawski, M., Chu, P.-H., Shirvanyants, D., Schlichting, I., Dokholyan, N. V., and Hahn, K. M. (2016). Engineering extrinsic disorder to control protein activity in living cells. *Science*, 354(6318):1441–1444.
- D'Andrea, A. D. and Haseltine, W. A. (1978). Sequence specific cleavage of dna by the antitumor antibiotics neocarzinostatin and bleomycin. *Proceedings of the National Academy of Sciences*, 75(8):3608–3612.
- Dasari, S. and Tchounwou, P. B. (2014). Cisplatin in cancer therapy: molecular mechanisms of action. *European journal of pharmacology*, 740:364–378.

- Davison, T. S., Yin, P., Nie, E., Kay, C., and Arrowsmith, C. H. (1998). Characterization of the oligomerization defects of two p53 mutants found in families with li–fraumeni and li–fraumeni-like syndrome. *Oncogene*, 17(5):651.
- Deisseroth, K., Feng, G., Majewska, A. K., Miesenböck, G., Ting, A., and Schnitzer, M. J. (2006). Next-generation optical technologies for illuminating genetically targeted brain circuits.
- Di Ventura, B., Funaya, C., Antony, C., Knop, M., and Serrano, L. (2008). Reconstitution of mdm2-dependent post-translational modifications of p53 in yeast. *PLoS One*, 3(1):e1507.
- Di Ventura, B. and Kuhlman, B. (2016). Go in! go out! inducible control of nuclear localization. *Current opinion in chemical biology*, 34:62–71.
- Diensthuber, R. P., Engelhard, C., Lemke, N., Gleichmann, T., Ohlendorf, R., Bittl, R., and Möglich, A. (2014). Biophysical, mutational, and functional investigation of the chromophore-binding pocket of light-oxygen-voltage photoreceptors. *ACS synthetic biology*, 3(11):811–819.
- Dolmetsch, R. E., Lewis, R. S., Goodnow, C. C., and Healy, J. I. (1997). Differential activation of transcription factors induced by ca²⁺ response amplitude and duration. *Nature*, 386(6627):855.
- El-Deiry, W. S., Kern, S. E., Pietenpol, J. A., Kinzler, K. W., and Vogelstein, B. (1992). Definition of a consensus binding site for p53. *Nature genetics*, 1(1):45.
- Engelke, H., Chou, C., Uprety, R., Jess, P., and Deiters, A. (2014). Control of protein function through optochemical translocation. *ACS synthetic biology*, 3(10):731–736.
- Fang, S., Jensen, J. P., Ludwig, R. L., Vousden, K. H., and Weissman, A. M. (2000). Mdm2 is a ring finger-dependent ubiquitin protein ligase for itself and p53. *Journal of Biological Chemistry*, 275(12):8945–8951.
- Fedorov, R., Schlichting, I., Hartmann, E., Domratcheva, T., Fuhrmann, M., and Hegemann, P. (2003). Crystal structures and molecular mechanism of a light-induced signaling switch: the phot-lov1 domain from *Chlamydomonas reinhardtii*. *Biophysical Journal*, 84(4):2474–2482.
- Finlan, L. and Hupp, T. R. (2004). The n-terminal interferon-binding domain (ibid) homology domain of p300 binds to peptides with homology to the p53 transactivation domain. *Journal of Biological Chemistry*, 279(47):49395–49405.
- Finlay, C. A., Hinds, P. W., and Levine, A. J. (1989). The p53 proto-oncogene can act as a suppressor of transformation. *Cell*, 57(7):1083–1093.
- Fischer, M. (2017). Census and evaluation of p53 target genes. *Oncogene*, 36(28):3943.
- Freedman, D. A. and Levine, A. J. (1998). Nuclear export is required for degradation of endogenous p53 by mdm2 and human papillomavirus e6. *Molecular and cellular biology*, 18(12):7288–7293.
- French, A. R., Sosnick, T. R., and Rock, R. S. (2017). Investigations of human myosin vi targeting using optogenetically controlled cargo loading. *Proceedings of the National Academy of Sciences*, page 201614716.
- Friedman, P. N., Chen, X., Bargonetti, J., and Prives, C. (1993). The p53 protein is an unusually shaped tetramer that binds directly to dna. *Proceedings of the National Academy of Sciences*, 90(8):3319–3323.
- Gartel, A. L., Serfas, M. S., and Tyner, A. L. (1996). p21—negative regulator of the cell cycle. *Proceedings of the Society for Experimental Biology and Medicine*, 213(2):138–149.
- Gehrig, S., Macpherson, J. A., Driscoll, P. C., Symon, A., Martin, S. R., MacRae, J. I., Kleinjung, J., Fraternali, F., and Anastasiou, D. (2017). An engineered photoswitchable mammalian pyruvate kinase. *The FEBS journal*, 284(18):2955–2980.

- Geva-Zatorsky, N., Rosenfeld, N., Itzkovitz, S., Milo, R., Sigal, A., Dekel, E., Yarnitzky, T., Liron, Y., Polak, P., Lahav, G., et al. (2006). Oscillations and variability in the p53 system. *Molecular systems biology*, 2(1).
- Glantz, S. T., Berlew, E. E., Jaber, Z., Schuster, B. S., Gardner, K. H., and Chow, B. Y. (2018). Directly light-regulated binding of rgs-lov photoreceptors to anionic membrane phospholipids. *Proceedings of the National Academy of Sciences*, 115(33):E7720–E7727.
- Glantz, S. T., Carpenter, E. J., Melkonian, M., Gardner, K. H., Boyden, E. S., Wong, G. K.-S., and Chow, B. Y. (2016). Functional and topological diversity of lov domain photoreceptors. *Proceedings of the National Academy of Sciences*, 113(11):E1442–E1451.
- Godley, B. F., Shamsi, F. A., Liang, F.-Q., Jarrett, S. G., Davies, S., and Boulton, M. (2005). Blue Light Induces Mitochondrial DNA Damage and Free Radical Production in Epithelial Cells. *J. Biol. Chem.*, 280(22):21061–21066.
- Goodman, R. H. and Smolik, S. (2000). Cbp/p300 in cell growth, transformation, and development. *Genes & development*, 14(13):1553–1577.
- Görner, W., Durchschlag, E., Martinez-Pastor, M., Estruch, F., Ammerer, G., Hamilton, B., Ruis, H., and Schüller, C. (1998). Nuclear localization of the c2h2 zinc finger protein msn2p is regulated by stress and protein kinase a activity. *Gene Dev*, 12:586–597.
- Gotoh, Y., Nishida, E., Yamashita, T., Hoshi, M., Kawakami, M., and Sakai, H. (1990). Microtubule-associated-protein (map) kinase activated by nerve growth factor and epidermal growth factor in pc12 cells: Identity with the mitogen-activated map kinase of fibroblastic cells. *European journal of biochemistry*, 193(3):661–669.
- Gu, W. and Roeder, R. G. (1997). Activation of p53 sequence-specific dna binding by acetylation of the p53 c-terminal domain. *Cell*, 90(4):595–606.
- Guntas, G., Hallett, R. A., Zimmerman, S. P., Williams, T., Yumerefendi, H., Bear, J. E., and Kuhlman, B. (2015). Engineering an improved light-induced dimer (ilid) for controlling the localization and activity of signaling proteins. *Proceedings of the National Academy of Sciences*, 112(1):112–117.
- Haapajärvi, T., Kivinen, L., Heiskanen, A., Des Bordes, C., Datto, M. B., Wang, X.-F., and Laiho, M. (1999). Uv radiation is a transcriptional inducer of p21 cip1/waf1 cyclin-kinase inhibitor in a p53-independent manner. *Experimental cell research*, 248(1):272–279.
- Hafner, A., Stewart-Ornstein, J., Purvis, J. E., Forrester, W. C., Bulyk, M. L., and Lahav, G. (2017). p53 pulses lead to distinct patterns of gene expression albeit similar dna-binding dynamics. *Nature Structural and Molecular Biology*, 24(10):840.
- Halacli, S. O., Canpinar, H., Cimen, E., and Sunguroglu, A. (2013). Effects of gamma irradiation on cell cycle, apoptosis and telomerase activity in p53 wild-type and deficient hct116 colon cancer cell lines. *Oncology letters*, 6(3):807–810.
- Halavaty, A. S. and Moffat, K. (2007). N-and c-terminal flanking regions modulate light-induced signal transduction in the lov2 domain of the blue light sensor phototropin 1 from *avena sativa*. *Biochemistry*, 46(49):14001–14009.
- Hamstra, D. A., Bhojani, M. S., Griffin, L. B., Laxman, B., Ross, B. D., and Rehemtulla, A. (2006). Real-time evaluation of p53 oscillatory behavior in vivo using bioluminescent imaging. *Cancer research*, 66(15):7482–7489.
- Hannanta-anan, P. and Chow, B. Y. (2016). Optogenetic control of calcium oscillation waveform defines nfat as an integrator of calcium load. *Cell systems*, 2(4):283–288.

- Hansen, A. S. and O'shea, E. K. (2013). Promoter decoding of transcription factor dynamics involves a trade-off between noise and control of gene expression. *Molecular systems biology*, 9(1):704.
- Hansen, A. S. and O'Shea, E. K. (2015). cis determinants of promoter threshold and activation timescale. *Cell reports*, 12(8):1226–1233.
- Hao, N. and O'shea, E. K. (2012). Signal-dependent dynamics of transcription factor translocation controls gene expression. *Nature structural & molecular biology*, 19(1):31.
- Harper, S. M., Christie, J. M., and Gardner, K. H. (2004). Disruption of the lov- $j\alpha$ helix interaction activates phototropin kinase activity. *Biochemistry*, 43(51):16184–16192.
- Harper, S. M., Neil, L. C., and Gardner, K. H. (2003). Structural basis of a phototropin light switch. *Science*, 301(5639):1541–1544.
- Haruki, H., Nishikawa, J., and Laemmli, U. K. (2008). The anchor-away technique: rapid, conditional establishment of yeast mutant phenotypes. *Molecular cell*, 31(6):925–932.
- Haupt, Y., Maya, R., Kazaz, A., and Oren, M. (1997). Mdm2 promotes the rapid degradation of p53. *nature*, 387(6630):296.
- Haupt, Y., Rowan, S., Shaulian, E., Vousden, K., and Oren, M. (1995). Induction of apoptosis in hela cells by trans-activation-deficient p53. *Genes & development*, 9(17):2170–2183.
- Heijde, M. and Ulm, R. (2013). Reversion of the arabidopsis uv-b photoreceptor uvr8 to the homodimeric ground state. *Proceedings of the National Academy of Sciences*, 110(3):1113–1118.
- Hernandez-Segura, A., Nehme, J., and Demaria, M. (2018). Hallmarks of cellular senescence. *Trends in cell biology*.
- Hillen, W. and Berens, C. (1994). Mechanisms underlying expression of tn 10 encoded tetracycline resistance. *Annual review of microbiology*, 48(1):345–369.
- Hiratsuka, T., Fujita, Y., Naoki, H., Aoki, K., Kamioka, Y., and Matsuda, M. (2015). Intercellular propagation of extracellular signal-regulated kinase activation revealed by in vivo imaging of mouse skin. *Elife*, 4:e05178.
- Hodel, A. E., Harreman, M. T., Pulliam, K. F., Harben, M. E., Holmes, J. S., Hodel, M. R., Berland, K. M., and Corbett, A. H. (2006). Nuclear localization signal-receptor affinity correlates with in vivo localization in *s. cerevisiae*. *Journal of Biological Chemistry*.
- Hoffmann, A., Levchenko, A., Scott, M. L., and Baltimore, D. (2002). The $i\kappa b$ - $nf-\kappa b$ signaling module: temporal control and selective gene activation. *Science*, 298(5596):1241–1245.
- Hoffmann, M. D., Bubeck, F., Eils, R., and Niopek, D. (2018). Controlling cells with light and lov. *Advanced Biosystems*, 2(9):1800098.
- Hoshino, A., Mita, Y., Okawa, Y., Ariyoshi, M., Iwai-Kanai, E., Ueyama, T., Ikeda, K., Ogata, T., and Matoba, S. (2013). Cytosolic p53 inhibits parkin-mediated mitophagy and promotes mitochondrial dysfunction in the mouse heart. *Nature communications*, 4:2308.
- Hu, B., Gilkes, D. M., and Chen, J. (2007a). Efficient p53 activation and apoptosis by simultaneous disruption of binding to mdm2 and mdmx. *Cancer Research*, 67(18):8810–8817.
- Hu, W., Feng, Z., Ma, L., Wagner, J., Rice, J. J., Stolovitzky, G., and Levine, A. J. (2007b). A single nucleotide polymorphism in the mdm2 gene disrupts the oscillation of p53 and mdm2 levels in cells. *Cancer research*, 67(6):2757–2765.

- Huala, E., Oeller, P. W., Liscum, E., Han, I.-S., Larsen, E., and Briggs, W. R. (1997). Arabidopsis nph1: a protein kinase with a putative redox-sensing domain. *Science*, 278(5346):2120–2123.
- Huang, J., Koide, A., Makabe, K., and Koide, S. (2008). Design of protein function leaps by directed domain interface evolution. *Proceedings of the National Academy of Sciences*, 105(18):6578–6583.
- Hühner, J., Ingles-Prieto, Á., Neusüß, C., Lämmerhofer, M., and Janovjak, H. (2015). Quantification of riboflavin, flavin mononucleotide, and flavin adenine dinucleotide in mammalian model cells by ce with led-induced fluorescence detection. *Electrophoresis*, 36(4):518–525.
- Hutten, S. and Kehlenbach, R. H. (2007). Crm1-mediated nuclear export: to the pore and beyond. *Trends in cell biology*, 17(4):193–201.
- Ishida, N., Miyazaki, K., Kumagai, K., and Rikimaru, M. (1965). Neocarzinostatin, an antitumor antibiotic of high molecular weight. *The Journal of antibiotics*, 18:68.
- Itahana, K., Mao, H., Jin, A., Itahana, Y., Clegg, H. V., Lindström, M. S., Bhat, K. P., Godfrey, V. L., Evan, G. I., and Zhang, Y. (2007). Targeted inactivation of mdm2 ring finger e3 ubiquitin ligase activity in the mouse reveals mechanistic insights into p53 regulation. *Cancer Cell*, 12(4):355–366.
- Ito, A., Kawaguchi, Y., Lai, C.-H., Kovacs, J. J., Higashimoto, Y., Appella, E., and Yao, T.-P. (2002). Mdm2–hdac1-mediated deacetylation of p53 is required for its degradation. *The EMBO journal*, 21(22):6236–6245.
- Ito, M., Barys, L., O'Reilly, T., Young, S., Gorbacheva, B., Monahan, J. E., Zumstein-Mecker, S., Choong, P. F., Dickinson, I., Crowe, P., et al. (2010). Comprehensive mapping of p53 pathway alterations reveals an apparent role for both snp309 and mdm2 amplification in sarcomagenesis. *Clinical Cancer Research*, pages clincanres–2050.
- Joerger, A. C. and Fersht, A. R. (2008). Structural biology of the tumor suppressor p53. *Annu. Rev. Biochem.*, 77:557–582.
- Jones, D., Mistry, I., and Tavassoli, A. (2016). Post-translational control of protein function with light using a lov-intein fusion protein. *Molecular BioSystems*, 12(4):1388–1393.
- Kakar, M., Davis, J. R., Kern, S. E., and Lim, C. S. (2007). Optimizing the protein switch: altering nuclear import and export signals, and ligand binding domain. *Journal of controlled release*, 120(3):220–232.
- Kamijo, T., Weber, J. D., Zambetti, G., Zindy, F., Roussel, M. F., and Sherr, C. J. (1998). Functional and physical interactions of the arf tumor suppressor with p53 and mdm2. *Proceedings of the National Academy of Sciences*, 95(14):8292–8297.
- Kar, P. and Parekh, A. B. (2015). Distinct spatial ca²⁺ signatures selectively activate different nfat transcription factor isoforms. *Molecular cell*, 58(2):232–243.
- Kastenhuber, E. R. and Lowe, S. W. (2017). Putting p53 in context. *Cell*, 170(6):1062–1078.
- Kawaguchi, T., Kato, S., Otsuka, K., Watanabe, G., Kumabe, T., Tominaga, T., Yoshimoto, T., and Ishioka, C. (2005). The relationship among p53 oligomer formation, structure and transcriptional activity using a comprehensive missense mutation library. *Oncogene*, 24(46):6976.
- Kellogg, R. A. and Tay, S. (2015). Noise facilitates transcriptional control under dynamic inputs. *Cell*, 160(3):381–392.
- Khoury, M. P. and Bourdon, J.-C. (2011). p53 isoforms: an intracellular microprocessor? *Genes & cancer*, 2(4):453–465.

- Klee, C. B., Ren, H., and Wang, X. (1998). Regulation of the calmodulin-stimulated protein phosphatase, calcineurin. *Journal of Biological Chemistry*, 273(22):13367–13370.
- Klemm, J. D., Beals, C. R., and Crabtree, G. R. (1997). Rapid targeting of nuclear proteins to the cytoplasm. *Current Biology*, 7(9):638–644.
- Kodiha, M., Chu, A., Matusiewicz, N., and Stochaj, U. (2004). Multiple mechanisms promote the inhibition of classical nuclear import upon exposure to severe oxidative stress. *Cell death and differentiation*, 11(8):862.
- Kogawa, A. C., Zoppi, A., Quevedo, M. A., Salgado, H. R. N., and Longhi, M. R. (2014). Increasing doxycycline hyclate photostability by complexation with β -cyclodextrin. *Aaps Pharmscitech*, 15(5):1209–1217.
- Kort, R., Hoff, W., Van West, M., Kroon, A., Hoffer, S., Vlieg, K., Crielaand, W., Van Beeumen, J., and Hellingwerf, K. J. (1996). The xanthopsins: a new family of eubacterial blue-light photoreceptors. *The EMBO journal*, 15(13):3209–3218.
- Krummel, K. A., Lee, C. J., Toledo, F., and Wahl, G. M. (2005). The c-terminal lysines fine-tune p53 stress responses in a mouse model but are not required for stability control or transactivation. *Proceedings of the National Academy of Sciences*, 102(29):10188–10193.
- Kruse, J.-P. and Gu, W. (2008). Snapshot: p53 posttranslational modifications. *Cell*, 133(5):930–930.e1.
- Kruse, J.-P. and Gu, W. (2009). Modes of p53 regulation. *Cell*, 137(4):609–622.
- Kudo, N., Matsumori, N., Taoka, H., Fujiwara, D., Schreiner, E. P., Wolff, B., Yoshida, M., and Horinouchi, S. (1999). Leptomycin b inactivates crm1/exportin 1 by covalent modification at a cysteine residue in the central conserved region. *Proceedings of the National Academy of Sciences*, 96(16):9112–9117.
- Kuo, L. J. and Yang, L.-X. (2008). γ -h2ax-a novel biomarker for dna double-strand breaks. *In vivo*, 22(3):305–309.
- Kussie, P. H., Gorina, S., Marechal, V., Elenbaas, B., Moreau, J., Levine, A. J., and Pavletich, N. P. (1996). Structure of the mdm2 oncoprotein bound to the p53 tumor suppressor transactivation domain. *Science*, 274(5289):948–953.
- Kutay, U. and Gütinger, S. (2005). Leucine-rich nuclear-export signals: born to be weak. *Trends in cell biology*, 15(3):121–124.
- Lahav, G., Rosenfeld, N., Sigal, A., Geva-Zatorsky, N., Levine, A. J., Elowitz, M. B., and Alon, U. (2004). Dynamics of the p53-mdm2 feedback loop in individual cells. *Nature genetics*, 36(2):147.
- Lambert, P. F., Kashanchi, F., Radonovich, M. F., Shiekhattar, R., and Brady, J. N. (1998). Phosphorylation of p53 serine 15 increases interaction with cbp. *Journal of Biological Chemistry*, 273(49):33048–33053.
- Lane, D. P. (1992). Cancer. p53, guardian of the genome. *Nature*, 358:15–16.
- Lane, K., Van Valen, D., DeFelice, M. M., Macklin, D. N., Kudo, T., Jaimovich, A., Carr, A., Meyer, T., Pe'er, D., Boutet, S. C., et al. (2017). Measuring signaling and rna-seq in the same cell links gene expression to dynamic patterns of nf- κ b activation. *Cell systems*, 4(4):458–469.
- Lee, J., Natarajan, M., Nashine, V. C., Socolich, M., Vo, T., Russ, W. P., Benkovic, S. J., and Ranganathan, R. (2008). Surface sites for engineering allosteric control in proteins. *Science*, 322(5900):438–442.
- Lee, R. E., Qasaimeh, M. A., Xia, X., Juncker, D., and Gaudet, S. (2016). Nf- κ b signalling and cell fate decisions in response to a short pulse of tumour necrosis factor. *Scientific reports*, 6:39519.

- Lee, T. K., Denny, E. M., Sanghvi, J. C., Gaston, J. E., Maynard, N. D., Hughey, J. J., and Covert, M. W. (2009). A noisy paracrine signal determines the cellular $\text{nf-}\kappa\text{b}$ response to lipopolysaccharide. *Sci. Signal.*, 2(93):ra65–ra65.
- Leng, R. P., Lin, Y., Ma, W., Wu, H., Lemmers, B., Chung, S., Parant, J. M., Lozano, G., Hakem, R., and Benchimol, S. (2003). Pirh2, a p53-induced ubiquitin-protein ligase, promotes p53 degradation. *Cell*, 112(6):779–791.
- Leu, J.-J., Dumont, P., Hafey, M., Murphy, M. E., and George, D. L. (2004). Mitochondrial p53 activates bak and causes disruption of a bak–mcl1 complex. *Nature cell biology*, 6(5):443.
- Levine, A. J. (1997). p53, the cellular gatekeeper for growth and division. *cell*, 88(3):323–331.
- Levskaia, A., Weiner, O. D., Lim, W. A., and Voigt, C. A. (2009). Spatiotemporal control of cell signalling using a light-switchable protein interaction. *Nature*, 461(7266):997.
- Li, M., Brooks, C. L., Kon, N., and Gu, W. (2004). A dynamic role of hausp in the p53-mdm2 pathway. *Molecular cell*, 13(6):879–886.
- Li, M., Brooks, C. L., Wu-Baer, F., Chen, D., Baer, R., and Gu, W. (2003). Mono-versus polyubiquitination: differential control of p53 fate by mdm2. *Science*, 302(5652):1972–1975.
- Li, M., Chen, D., Shiloh, A., Luo, J., Nikolaev, A. Y., Qin, J., and Gu, W. (2002). Deubiquitination of p53 by hausp is an important pathway for p53 stabilization. *Nature*, 416(6881):648.
- Li, P.-F., Dietz, R., and Von Harsdorf, R. (1999). p53 regulates mitochondrial membrane potential through reactive oxygen species and induces cytochrome c-independent apoptosis blocked by bcl-2. *The EMBO journal*, 18(21):6027–6036.
- Liang, S.-H. and Clarke, M. F. (1999). A bipartite nuclear localization signal is required for p53 nuclear import regulated by a carboxyl-terminal domain. *Journal of Biological Chemistry*, 274(46):32699–32703.
- Linzer, D. I. and Levine, A. J. (1979). Characterization of a 54k dalton cellular sv40 tumor antigen present in sv40-transformed cells and uninfected embryonal carcinoma cells. *Cell*, 17(1):43–52.
- Liu, L., Scolnick, D. M., Trievel, R. C., Zhang, H. B., Marmorstein, R., Halazonetis, T. D., and Berger, S. L. (1999). p53 sites acetylated in vitro by pcaf and p300 are acetylated in vivo in response to dna damage. *Molecular and cellular biology*, 19(2):1202–1209.
- Livak, K. J. and Schmittgen, T. D. (2001). Analysis of relative gene expression data using real-time quantitative pcr and the $2^{-\Delta\Delta\text{ct}}$ method. *methods*, 25(4):402–408.
- Loewer, A., Batchelor, E., Gaglia, G., and Lahav, G. (2010). Basal dynamics of p53 reveal transcriptionally attenuated pulses in cycling cells. *Cell*, 142(1):89–100.
- Lohrum, M. A., Woods, D. B., Ludwig, R. L., Bálint, É., and Vousden, K. H. (2001). C-terminal ubiquitination of p53 contributes to nuclear export. *Molecular and cellular biology*, 21(24):8521–8532.
- Love, I. M., Sekaric, P., Shi, D., Grossman, S. R., and Androphy, E. J. (2012). The histone acetyltransferase pcaf regulates p21 transcription through stress-induced acetylation of histone h3. *Cell Cycle*, 11(13):2458–2466.
- Lungu, O. I., Hallett, R. A., Choi, E. J., Aiken, M. J., Hahn, K. M., and Kuhlman, B. (2012). Designing photoswitchable peptides using the aslov2 domain. *Chemistry & biology*, 19(4):507–517.
- Luo, J., Nikolaev, A. Y., Imai, S.-i., Chen, D., Su, F., Shiloh, A., Guarente, L., and Gu, W. (2001). Negative control of p53 by sir2 α promotes cell survival under stress. *Cell*, 107(2):137–148.

- Luo, J., Su, F., Chen, D., Shiloh, A., and Gu, W. (2000). Deacetylation of p53 modulates its effect on cell growth and apoptosis. *Nature*, 408(6810):377.
- Macian, F. (2005). Nfat proteins: key regulators of t-cell development and function. *Nature Reviews Immunology*, 5(6):472.
- Malkin, D., Li, F. P., Strong, L. C., Fraumeni, J. F., Nelson, C. E., Kim, D. H., Kassel, J., Gryka, M. A., Bischoff, F. Z., Tainsky, M. A., et al. (1990). Germ line p53 mutations in a familial syndrome of breast cancer, sarcomas, and other neoplasms. *Science*, 250(4985):1233–1238.
- Marfori, M., Mynott, A., Ellis, J. J., Mehdi, A. M., Saunders, N. F., Curmi, P. M., Forwood, J. K., Bodén, M., and Kobe, B. (2011). Molecular basis for specificity of nuclear import and prediction of nuclear localization. *BBA*, 1813(9):1562–1577.
- Marshall, C. (1995). Specificity of receptor tyrosine kinase signaling: transient versus sustained extracellular signal-regulated kinase activation. *Cell*, 80(2):179–185.
- Mart, R. J., Meah, D., and Allemann, R. K. (2016). Photocontrolled exposure of pro-apoptotic peptide sequences in lov proteins modulates bcl-2 family interactions. *Chembiochem*, 17(8):698–701.
- Maul, G. G. and Deaven, L. (1977). Quantitative determination of nuclear pore complexes in cycling cells with differing dna content. *The Journal of cell biology*, 73(3):748–760.
- May, P. and May, E. (1999). Twenty years of p53 research: structural and functional aspects of the p53 protein. *Oncogene*, 18(53):7621.
- Meek, D. W. (2004). The p53 response to dna damage. *DNA repair*, 3(8-9):1049–1056.
- Melanson, B. D., Bose, R., Hamill, J. D., Marcellus, K. A., Pan, E. F., and McKay, B. C. (2011). The role of mrna decay in p53-induced gene expression. *Rna*.
- Mihara, M., Erster, S., Zaika, A., Petrenko, O., Chittenden, T., Pancoska, P., and Moll, U. M. (2003). p53 has a direct apoptogenic role at the mitochondria. *Molecular cell*, 11(3):577–590.
- Mills, E., Chen, X., Pham, E., Wong, S., and Truong, K. (2011). Engineering a photoactivated caspase-7 for rapid induction of apoptosis. *ACS synthetic biology*, 1(3):75–82.
- Möglich, A., Ayers, R. A., and Moffat, K. (2009a). Design and signaling mechanism of light-regulated histidine kinases. *Journal of molecular biology*, 385(5):1433–1444.
- Möglich, A., Ayers, R. A., and Moffat, K. (2009b). Structure and signaling mechanism of per-arnt-sim domains. *Structure*, 17(10):1282–1294.
- Möglich, A., Yang, X., Ayers, R. A., and Moffat, K. (2010). Structure and function of plant photoreceptors. *Annual review of plant biology*, 61.
- Mohr, D., Frey, S., Fischer, T., Güttler, T., and Görlich, D. (2009). Characterisation of the passive permeability barrier of nuclear pore complexes. *The EMBO journal*, 28(17):2541–2553.
- Momand, J., Zambetti, G. P., Olson, D. C., George, D., and Levine, A. J. (1992). The mdm-2 oncogene product forms a complex with the p53 protein and inhibits p53-mediated transactivation. *cell*, 69(7):1237–1245.
- Muhlinen, N., Horikawa, I., Alam, F., Isogaya, K., Lissa, D., Vojtesek, B., Lane, D. P., and Harris, C. C. (2018). p53 isoforms regulate premature aging in human cells. *Oncogene*, 37(18):2379.

- Müller, M. R. and Rao, A. (2010). Nfat, immunity and cancer: a transcription factor comes of age. *Nature Reviews Immunology*, 10(9):645.
- Muller, P. A. and Vousden, K. H. (2013). p53 mutations in cancer. *Nature cell biology*, 15(1):2.
- Murphy, L. O. and Blenis, J. (2006). Mapk signal specificity: the right place at the right time. *Trends in biochemical sciences*, 31(5):268–275.
- Murphy, L. O., MacKeigan, J. P., and Blenis, J. (2004). A network of immediate early gene products propagates subtle differences in mitogen-activated protein kinase signal amplitude and duration. *Molecular and cellular biology*, 24(1):144–153.
- Murphy, L. O., Smith, S., Chen, R.-H., Fingar, D. C., and Blenis, J. (2002). Molecular interpretation of erk signal duration by immediate early gene products. *Nature cell biology*, 4(8):556.
- Nagata, T., Shirakawa, K., Kobayashi, N., Shiheido, H., Tabata, N., Sakuma-Yonemura, Y., Horisawa, K., Katahira, M., Doi, N., and Yanagawa, H. (2014). Structural basis for inhibition of the mdm2: p53 interaction by an optimized mdm2-binding peptide selected with mrna display. *PLoS one*, 9(10):e109163.
- Nagel, G., Brauner, M., Liewald, J. F., Adeishvili, N., Bamberg, E., and Gottschalk, A. (2005). Light activation of channelrhodopsin-2 in excitable cells of caenorhabditis elegans triggers rapid behavioral responses. *Current Biology*, 15(24):2279–2284.
- Natan, E., Hirschberg, D., Morgner, N., Robinson, C. V., and Fersht, A. R. (2009). Ultraslow oligomerization equilibria of p53 and its implications. *Proceedings of the National Academy of Sciences*, 106(34):14327–14332.
- Negulescu, P. A., Shastri, N., and Cahalan, M. D. (1994). Intracellular calcium dependence of gene expression in single t lymphocytes. *Proceedings of the National Academy of Sciences*, 91(7):2873–2877.
- Nelson, D., Ihekweaba, A., Elliott, M., Johnson, J., Gibney, C., Foreman, B., Nelson, G., See, V., Horton, C., Spiller, D., et al. (2004). Oscillations in nf- κ b signaling control the dynamics of gene expression. *Science*, 306(5696):704–708.
- Nguyen, T., Scimeca, J., Filloux, C., Peraldi, P., Carpentier, J., and Van Obberghen, E. (1993). Co-regulation of the mitogen-activated protein kinase, extracellular signal-regulated kinase 1, and the 90-kda ribosomal s6 kinase in pc12 cells. distinct effects of the neurotrophic factor, nerve growth factor, and the mitogenic factor, epidermal growth factor. *Journal of Biological Chemistry*, 268(13):9803–9810.
- Ni, M., Tepperman, J. M., and Quail, P. H. (1999). Binding of phytochrome b to its nuclear signalling partner pif3 is reversibly induced by light. *Nature*, 400(6746):781.
- Nikolaev, A. Y., Li, M., Puskas, N., Qin, J., and Gu, W. (2003). Parc: a cytoplasmic anchor for p53. *Cell*, 112(1):29–40.
- Niopek, D., Benzinger, D., Roensch, J., Draebing, T., Wehler, P., Eils, R., and Di Ventura, B. (2014). Engineering light-inducible nuclear localization signals for precise spatiotemporal control of protein dynamics in living cells. *Nature communications*, 5:4404.
- Niopek, D., Wehler, P., Roensch, J., Eils, R., and Di Ventura, B. (2016). Optogenetic control of nuclear protein export. *Nature communications*, 7:10624.
- Ogryzko, V. V., Schiltz, R. L., Russanova, V., Howard, B. H., and Nakatani, Y. (1996). The transcriptional coactivators p300 and cbp are histone acetyltransferases. *Cell*, 87(5):953–959.
- O’Keefe, K., Li, H., and Zhang, Y. (2003). Nucleocytoplasmic shuttling of p53 is essential for mdm2-mediated cytoplasmic degradation but not ubiquitination. *Molecular and cellular biology*, 23(18):6396–6405.

- Olivier, M., Hollstein, M., and Hainaut, P. (2010). Tp53 mutations in human cancers: origins, consequences, and clinical use. *Cold Spring Harbor perspectives in biology*, 2(1):a001008.
- Paek, A. L., Liu, J. C., Loewer, A., Forrester, W. C., and Lahav, G. (2016). Cell-to-cell variation in p53 dynamics leads to fractional killing. *Cell*, 165(3):631–642.
- Pazgier, M., Liu, M., Zou, G., Yuan, W., Li, C., Li, C., Li, J., Monbo, J., Zella, D., Tarasov, S. G., et al. (2009). Structural basis for high-affinity peptide inhibition of p53 interactions with mdm2 and mdmx. *Proceedings of the National Academy of Sciences*, 106(12):4665–4670.
- Perry, M. E., Piette, J., Zawadzki, J. A., Harvey, D., and Levine, A. J. (1993). The mdm-2 gene is induced in response to uv light in a p53-dependent manner. *Proceedings of the National Academy of Sciences*, 90(24):11623–11627.
- Petenkaya, A., Bozkurt, B., Akilli-Ozturk, O., Kaya, H. S., Gur-Dedeoglu, B., and Yulug, I. G. (2006). Lack of association between the mdm2-snp309 polymorphism and breast cancer risk. *Anticancer research*, 26(6C):4975–4977.
- Pham, E., Mills, E., and Truong, K. (2011). A synthetic photoactivated protein to generate local or global ca2+ signals. *Chemistry & biology*, 18(7):880–890.
- Phillips, A., Teunisse, A., Lam, S., Lodder, K., Darley, M., Emaduddin, M., Wolf, A., Richter, J., de Lange, J., Verlaan-de Vries, M., et al. (2010). Hdmx-l is expressed from a functional p53-responsive promoter in the first intron of the hdmx gene and participates in an autoregulatory feedback loop to control p53 activity. *Journal of Biological Chemistry*, 285(38):29111–29127.
- Picelli, S., Björklund, Å. K., Faridani, O. R., Sagasser, S., Winberg, G., and Sandberg, R. (2013). Smart-seq2 for sensitive full-length transcriptome profiling in single cells. *Nature methods*, 10(11):1096.
- Planey, S., Kumar, R., and A Arnott, J. (2013). Post-translational modification of transcription factors: mechanisms and potential therapeutic interventions. *Current molecular pharmacology*, 6(3):173–182.
- Porter, J. R., Fisher, B. E., and Batchelor, E. (2016). p53 pulses diversify target gene expression dynamics in an mrna half-life-dependent manner and delineate co-regulated target gene subnetworks. *Cell systems*, 2(4):272–282.
- Pudasaini, A., El-Arab, K. K., and Zoltowski, B. D. (2015). Lov-based optogenetic devices: light-driven modules to impart photoregulated control of cellular signaling. *Frontiers in molecular biosciences*, 2:18.
- Pudasaini, A. and Zoltowski, B. D. (2013). Zeitlupe senses blue-light fluence to mediate circadian timing in arabidopsis thaliana. *Biochemistry*, 52(40):7150–7158.
- Purvis, J. E., Karhohs, K. W., Mock, C., Batchelor, E., Loewer, A., and Lahav, G. (2012). p53 dynamics control cell fate. *Science*, 336(6087):1440–1444.
- Purvis, J. E. and Lahav, G. (2013). Encoding and decoding cellular information through signaling dynamics. *Cell*, 152(5):945–956.
- Raffelberg, S., Mansurova, M., Gärtner, W., and Losi, A. (2011). Modulation of the photocycle of a lov domain photoreceptor by the hydrogen-bonding network. *Journal of the American Chemical Society*, 133(14):5346–5356. PMID: 21410163.
- Ren, R., Mayer, B. J., Cicchetti, P., and Baltimore, D. (1993). Identification of a ten-amino acid proline-rich sh3 binding site. *Science*, 259(5098):1157–1161.
- Renicke, C., Schuster, D., Usherenko, S., Essen, L.-O., and Taxis, C. (2013). A lov2 domain-based optogenetic tool to control protein degradation and cellular function. *Chemistry & biology*, 20(4):619–626.

- Rho, J. K., Choi, Y. J., Ryoo, B.-Y., Na, I. I., Yang, S. H., Kim, C. H., and Lee, J. C. (2007). p53 enhances gefitinib-induced growth inhibition and apoptosis by regulation of fas in non-small cell lung cancer. *Cancer research*, 67(3):1163–1169.
- Ringshausen, I., O'Shea, C. C., Finch, A. J., Swigart, L. B., and Evan, G. I. (2006). Mdm2 is critically and continuously required to suppress lethal p53 activity in vivo. *Cancer Cell*, 10(6):501–514.
- Rodriguez, M. S., Desterro, J. M., Lain, S., Lane, D. P., and Hay, R. T. (2000). Multiple c-terminal lysine residues target p53 for ubiquitin-proteasome-mediated degradation. *Molecular and cellular biology*, 20(22):8458–8467.
- Rogel, A., Popliker, M., Webb, C. G., and Oren, M. (1985). p53 cellular tumor antigen: analysis of mrna levels in normal adult tissues, embryos, and tumors. *Molecular and cellular biology*, 5(10):2851–2855.
- Roth, J., Dobbstein, M., Freedman, D. A., Shenk, T., and Levine, A. J. (1998). Nucleo-cytoplasmic shuttling of the hdm2 oncoprotein regulates the levels of the p53 protein via a pathway used by the human immunodeficiency virus rev protein. *EMBO J.*, 17(2):554–564.
- Saez-Rodriguez, J., Alexopoulos, L. G., Epperlein, J., Samaga, R., Lauffenburger, D. A., Klamt, S., and Sorger, P. K. (2009). Discrete logic modelling as a means to link protein signalling networks with functional analysis of mammalian signal transduction. *Molecular systems biology*, 5(1):331.
- Saito, S., Goodarzi, A. A., Higashimoto, Y., Noda, Y., Lees-Miller, S. P., Appella, E., and Anderson, C. W. (2002). Atm mediates phosphorylation at multiple p53 sites, including ser46, in response to ionizing radiation. *Journal of Biological Chemistry*, 277(15):12491–12494.
- Salomon, M., Christie, J. M., Knieb, E., Lempert, U., and Briggs, W. R. (2000). Photochemical and mutational analysis of the fmn-binding domains of the plant blue light receptor, phototropin. *Biochemistry*, 39(31):9401–9410.
- Salomon, M., Eisenreich, W., Dürr, H., Schleicher, E., Knieb, E., Massey, V., Rüdiger, W., Müller, F., Bacher, A., and Richter, G. (2001). An optomechanical transducer in the blue light receptor phototropin from *avena sativa*. *Proceedings of the National Academy of Sciences*, 98(22):12357–12361.
- Santos, S. D., Verveer, P. J., and Bastiaens, P. I. (2007). Growth factor-induced mapk network topology shapes erk response determining pc-12 cell fate. *Nature cell biology*, 9(3):324.
- Sasagawa, S., Ozaki, Y.-i., Fujita, K., and Kuroda, S. (2005). Prediction and validation of the distinct dynamics of transient and sustained erk activation. *Nature cell biology*, 7(4):365.
- Schmidt, D., Tillberg, P. W., Chen, F., and Boyden, E. S. (2014). A fully genetically encoded protein architecture for optical control of peptide ligand concentration. *Nature Communications*, 15(7):3019.
- Seoane, J., Le, H.-V., and Massagué, J. (2002). Myc suppression of the p21 cip1 cdk inhibitor influences the outcome of the p53 response to dna damage. *Nature*, 419(6908):729.
- Sharrock, R. A. and Quail, P. H. (1989). Novel phytochrome sequences in *arabidopsis thaliana*: structure, evolution, and differential expression of a plant regulatory photoreceptor family. *Genes & Development*, 3(11):1745–1757.
- Shibagaki, I., Tanaka, H., Shimada, Y., Wagata, T., Ikenaga, M., Imamura, M., and Ishizaki, K. (1995). p53 mutation, murine double minute 2 amplification, and human papillomavirus infection are frequently involved but not associated with each other in esophageal squamous cell carcinoma. *Clinical cancer research*, 1(7):769–773.
- Shiheido, H., Takashima, H., Doi, N., and Yanagawa, H. (2011). mrna display selection of an optimized mdm2-binding peptide that potently inhibits mdm2-p53 interaction. *PLoS One*, 6(3):e17898.

- Shvarts, A., Steegenga, W., Riteco, N., Laar, T. v., Dekker, P., Bazuine, M., Ham, R. v., Houven van Oordt, W., Hateboer, G., Eb, A., et al. (1996). Mdmx: a novel p53-binding protein with some functional properties of mdm2. *The EMBO journal*, 15(19):5349–5357.
- Smart, A. D., Pache, R. A., Thomsen, N. D., Kortemme, T., Davis, G. W., and Wells, J. A. (2017). Engineering a light-activated caspase-3 for precise ablation of neurons in vivo. *Proceedings of the National Academy of Sciences*, 114(39):E8174–E8183.
- Spiltoir, J. I., Strickland, D., Glotzer, M., and Tucker, C. L. (2015). Optical control of peroxisomal trafficking. *ACS synthetic biology*, 5(7):554–560.
- Spudich, J. L. and Bogomolni, R. A. (1984). Mechanism of colour discrimination by a bacterial sensory rhodopsin. *Nature*, 312(5994):509.
- Stewart-Ornstein, J. and Lahav, G. (2017). p53 dynamics in response to dna damage vary across cell lines and are shaped by efficiency of dna repair and activity of the kinase atm. *Sci. Signal.*, 10(476):eaah6671.
- Stockley, J. H., Evans, K., Matthey, M., Volbracht, K., Agathou, S., Mukanowa, J., Burrone, J., and Káradóttir, R. T. (2017). Surpassing light-induced cell damage in vitro with novel cell culture media. *Sci. Rep.*, 7(1):849.
- Stommel, J. M., Marchenko, N. D., Jimenez, G. S., Moll, U. M., Hope, T. J., and Wahl, G. M. (1999). A leucine-rich nuclear export signal in the p53 tetramerization domain: regulation of subcellular localization and p53 activity by nes masking. *The EMBO journal*, 18(6):1660–1672.
- Strickland, D., Lin, Y., Wagner, E., Hope, C. M., Zayner, J., Antoniou, C., Sosnick, T. R., Weiss, E. L., and Glotzer, M. (2012). Tulips: tunable, light-controlled interacting protein tags for cell biology. *Nature methods*, 9(4):379.
- Strickland, D., Moffat, K., and Sosnick, T. R. (2008). Light-activated dna binding in a designed allosteric protein. *Proceedings of the National Academy of Sciences*, 105(31):10709–10714.
- Strickland, D., Yao, X., Gawlak, G., Rosen, M. K., Gardner, K. H., and Sosnick, T. R. (2010). Rationally improving lov domain-based photoswitches. *Nature methods*, 7(8):623.
- Sun, W., Zhang, W., Zhang, C., Mao, M., Zhao, Y., Chen, X., and Yang, Y. (2017). Light-induced protein degradation in human-derived cells. *Biochemical and biophysical research communications*, 487(2):241–246.
- Sykes, S. M., Mellert, H. S., Holbert, M. A., Li, K., Marmorstein, R., Lane, W. S., and McMahon, S. B. (2006). Acetylation of the p53 dna-binding domain regulates apoptosis induction. *Molecular cell*, 24(6):841–851.
- Takahashi, R., Giannini, C., Sarkaria, J. N., Schroeder, M., Rogers, J., Mastroeni, D., and Scoble, H. (2013). p53 isoform profiling in glioblastoma and injured brain. *Oncogene*, 32(26):3165.
- Tang, Y., Luo, J., Zhang, W., and Gu, W. (2006). Tip60-dependent acetylation of p53 modulates the decision between cell-cycle arrest and apoptosis. *Molecular cell*, 24(6):827–839.
- Tang, Y., Zhao, W., Chen, Y., Zhao, Y., and Gu, W. (2008). Acetylation is indispensable for p53 activation. *Cell*, 133(4):612–626.
- Tao, W. and Levine, A. J. (1999). Nucleocytoplasmic shuttling of oncoprotein hdm2 is required for hdm2-mediated degradation of p53. *Proceedings of the National Academy of Sciences*, 96(6):3077–3080.
- Tay, S., Hughey, J. J., Lee, T. K., Lipniacki, T., Quake, S. R., and Covert, M. W. (2010). Single-cell nf- κ b dynamics reveal digital activation and analogue information processing. *Nature*, 466(7303):267.
- Taylor, B. L. and Zhulin, I. B. (1999). Pas domains: internal sensors of oxygen, redox potential, and light. *Microbiology and Molecular Biology Reviews*, 63(2):479–506.

- Teufel, D. P., Bycroft, M., and Fersht, A. R. (2009). Regulation by phosphorylation of the relative affinities of the n-terminal transactivation domains of p53 for p300 domains and mdm2. *Oncogene*, 28(20):2112.
- Tibbetts, R. S., Brumbaugh, K. M., Williams, J. M., Sarkaria, J. N., Cliby, W. A., Shieh, S.-Y., Taya, Y., Prives, C., and Abraham, R. T. (1999). A role for atr in the dna damage-induced phosphorylation of p53. *Genes & development*, 13(2):152–157.
- Toettcher, J. E., Voigt, C. A., Weiner, O. D., and Lim, W. A. (2011). The promise of optogenetics in cell biology: interrogating molecular circuits in space and time. *Nature methods*, 8(1):35.
- Toettcher, J. E., Weiner, O. D., and Lim, W. A. (2013). Using optogenetics to interrogate the dynamic control of signal transmission by the ras/erk module. *Cell*, 155(6):1422–1434.
- Tomida, T., Hirose, K., Takizawa, A., Shibasaki, F., and Iino, M. (2003). Nfat functions as a working memory of ca²⁺ signals in decoding ca²⁺ oscillation. *The EMBO journal*, 22(15):3825–3832.
- Traverse, S., Gomez, N., Paterson, H., Marshall, C., and Cohen, P. (1992). Sustained activation of the mitogen-activated protein (map) kinase cascade may be required for differentiation of pc12 cells. comparison of the effects of nerve growth factor and epidermal growth factor. *Biochemical Journal*, 288(2):351–355.
- Tudelska, K., Markiewicz, J., Kochańczyk, M., Czerkies, M., Prus, W., Korwek, Z., Abdi, A., Błoński, S., Kaźmierczak, B., and Lipniacki, T. (2017). Information processing in the nf- κ b pathway. *Scientific reports*, 7(1):15926.
- Van Bergeijk, P., Adrian, M., Hoogenraad, C. C., and Kapitein, L. C. (2015). Optogenetic control of organelle transport and positioning. *Nature*, 518(7537):111.
- van der Horst, M. A. and Hellingwerf, K. J. (2004). Photoreceptor proteins, “star actors of modern times”: a review of the functional dynamics in the structure of representative members of six different photoreceptor families. *Accounts of chemical research*, 37(1):13–20.
- Van der Watt, P. J., Maske, C. P., Hendricks, D. T., Parker, M. I., Denny, L., Govender, D., Birrer, M. J., and Leaner, V. D. (2009). The karyopherin proteins, crm1 and karyopherin β 1, are overexpressed in cervical cancer and are critical for cancer cell survival and proliferation. *International journal of cancer*, 124(8):1829–1840.
- Van der Watt, P. J., Zemanay, W., Govender, D., Hendricks, D. T., Parker, M., and Leaner, V. D. (2014). Elevated expression of the nuclear export protein, crm1 (exportin 1), associates with human oesophageal squamous cell carcinoma. *Oncology reports*, 32(2):730–738.
- Vassilev, L. T., Vu, B. T., Graves, B., Carvajal, D., Podlaski, F., Filipovic, Z., Kong, N., Kammlott, U., Lukacs, C., Klein, C., et al. (2004). In vivo activation of the p53 pathway by small-molecule antagonists of mdm2. *Science*, 303(5659):844–848.
- Vaziri, H., Dessain, S. K., Eaton, E. N., Imai, S.-I., Frye, R. A., Pandita, T. K., Guarente, L., and Weinberg, R. A. (2001). hsir2/sirt1 functions as an nad-dependent p53 deacetylase. *cell*, 107(2):149–159.
- Vilborg, A., Glahder, J. A., Wilhelm, M. T., Bersani, C., Corcoran, M., Mahmoudi, S., Rosenstierne, M., Grandér, D., Farnebo, M., Norrild, B., and Wiman, K. G. (2009). The p53 target Wig-1 regulates p53 mRNA stability through an AU-rich element. *Proc. Natl. Acad. Sci. U.S.A.*, 106(37):15756–15761.
- Vogelstein, B., Lane, D., and Levine, A. J. (2000). Surfing the p53 network. *Nature*, 408(6810):307.
- Wang, H., Vilela, M., Winkler, A., Tarnawski, M., Schlichting, I., Yumerefendi, H., Kuhlman, B., Liu, R., Danuser, G., and Hahn, K. M. (2016). Lovtrap: an optogenetic system for photoinduced protein dissociation. *Nature methods*, 13(9):755.

- Wang, S., Zhao, Y., Aguilar, A., Bernard, D., and Yang, C.-Y. (2017). Targeting the mdm2–p53 protein–protein interaction for new cancer therapy: progress and challenges. *Cold Spring Harbor perspectives in medicine*, page a026245.
- Watai, Y., Sase, I., Shiono, H., and Nakano, Y. (2001). Regulation of nuclear import by light-induced activation of caged nuclear localization signal in living cells. *FEBS letters*, 488(1-2):39–44.
- Waterman, M. J., Stavridi, E. S., Waterman, J. L., and Halazonetis, T. D. (1998). Atm-dependent activation of p53 involves dephosphorylation and association with 14-3-3 proteins. *Nature genetics*, 19(2):175.
- Wei, C.-L., Wu, Q., Vega, V. B., Chiu, K. P., Ng, P., Zhang, T., Shahab, A., Yong, H. C., Fu, Y., Weng, Z., et al. (2006). A global map of p53 transcription-factor binding sites in the human genome. *Cell*, 124(1):207–219.
- Weissleder, R. and Ntziachristos, V. (2003). Shedding light onto live molecular targets. *Nature medicine*, 9(1):123.
- Werner, S. L., Barken, D., and Hoffmann, A. (2005). Stimulus specificity of gene expression programs determined by temporal control of ikk activity. *Science*, 309(5742):1857–1861.
- Williams, G. T. and Farzaneh, F. (2012). Are snornas and snorna host genes new players in cancer? *Nature reviews cancer*, 12(2):84.
- Wilson, M. Z., Ravindran, P. T., Lim, W. A., and Toettcher, J. E. (2017). Tracing information flow from erk to target gene induction reveals mechanisms of dynamic and combinatorial control. *Molecular cell*, 67(5):757–769.
- Winkler, A., Barends, T. R., Udvarhelyi, A., Lenherr-Frey, D., Lomb, L., Menzel, A., and Schlichting, I. (2014). Structural details of light activation of the lov2-based photoswitch pa-rac1. *ACS chemical biology*, 10(2):502–509.
- Wong, S., Mosabbir, A. A., and Truong, K. (2015). An engineered split intein for photoactivated protein trans-splicing. *PLoS one*, 10(8):e0135965.
- Wu, D., Hu, Q., Yan, Z., Chen, W., Yan, C., Huang, X., Zhang, J., Yang, P., Deng, H., Wang, J., et al. (2012). Structural basis of ultraviolet-b perception by uvr8. *Nature*, 484(7393):214.
- Wu, X., Bayle, J. H., Olson, D., and Levine, A. J. (1993). The p53-mdm-2 autoregulatory feedback loop. *Genes & development*, 7(7a):1126–1132.
- Wu, Y. I., Frey, D., Lungu, O. I., Jaehrig, A., Schlichting, I., Kuhlman, B., and Hahn, K. M. (2009). A genetically encoded photoactivatable rac controls the motility of living cells. *Nature*, 461(7260):104.
- Yang, X., Jost, A. P.-T., Weiner, O. D., and Tang, C. (2013). A light-inducible organelle-targeting system for dynamically activating and inactivating signaling in budding yeast. *Molecular biology of the cell*, 24(15):2419–2430.
- Yao, F., Svensjö, T., Winkler, T., Lu, M., Eriksson, C., and Eriksson, E. (1998). Tetracycline repressor, tetr, rather than the tetr–mammalian cell transcription factor fusion derivatives, regulates inducible gene expression in mammalian cells. *Human gene therapy*, 9(13):1939–1950.
- Yao, X., Rosen, M. K., and Gardner, K. H. (2008). Estimation of the available free energy in a lov2-j α photoswitch. *Nature chemical biology*, 4(8):491.
- Yi, J. J., Wang, H., Vilela, M., Danuser, G., and Hahn, K. M. (2014). Manipulation of endogenous kinase activity in living cells using photoswitchable inhibitory peptides. *ACS synthetic biology*, 3(11):788–795.
- Yin, Y., Stephen, C. W., Luciani, M. G., and Fåhræus, R. (2002). p53 stability and activity is regulated by Mdm2-mediated induction of alternative p53 translation products. *Nat. Cell Biol.*, 4(6):462.

- Yissachar, N., Fischler, T. S., Cohen, A. A., Reich-Zeliger, S., Russ, D., Shifrut, E., Porat, Z., and Friedman, N. (2013). Dynamic response diversity of nfat isoforms in individual living cells. *Molecular cell*, 49(2):322–330.
- Yumerefendi, H., Dickinson, D. J., Wang, H., Zimmerman, S. P., Bear, J. E., Goldstein, B., Hahn, K., and Kuhlman, B. (2015). Control of protein activity and cell fate specification via light-mediated nuclear translocation. *PLoS One*, 10(6):e0128443.
- Yumerefendi, H., Lerner, A. M., Zimmerman, S. P., Hahn, K., Bear, J. E., Strahl, B. D., and Kuhlman, B. (2016). Light-induced nuclear export reveals rapid dynamics of epigenetic modifications. *Nature chemical biology*, 12(6):399.
- Zambrano, S., De Toma, I., Piffer, A., Bianchi, M. E., and Agresti, A. (2016). NF- κ B oscillations translate into functionally related patterns of gene expression. *Elife*, 5:e09100.
- Zayner, J. P., Antoniou, C., French, A. R., Hause Jr, R. J., and Sosnick, T. R. (2013). Investigating models of protein function and allostery with a widespread mutational analysis of a light-activated protein. *Biophysical journal*, 105(4):1027–1036.
- Zayner, J. P., Antoniou, C., and Sosnick, T. R. (2012). The amino-terminal helix modulates light-activated conformational changes in aslov2. *Journal of molecular biology*, 419(1-2):61–74.
- Zhao, R., Gish, K., Murphy, M., Yin, Y., Notterman, D., Hoffman, W. H., Tom, E., Mack, D. H., and Levine, A. J. (2000). Analysis of p53-regulated gene expression patterns using oligonucleotide arrays. *Genes & development*, 14(8):981–993.
- Zhu, Y., Tepperman, J. M., Fairchild, C. D., and Quail, P. H. (2000). Phytochrome b binds with greater apparent affinity than phytochrome a to the basic helix–loop–helix factor pif3 in a reaction requiring the pas domain of pif3. *Proceedings of the National Academy of Sciences*, 97(24):13419–13424.
- Ziegler, T. and Möglich, A. (2015). Photoreceptor engineering. *Frontiers in molecular biosciences*, 2:30.
- Zoltowski, B. D. and Gardner, K. H. (2010). Tripping the light fantastic: blue-light photoreceptors as examples of environmentally modulated protein–protein interactions. *Biochemistry*, 50(1):4–16.
- Zoltowski, B. D., Vaccaro, B., and Crane, B. R. (2009). Mechanism-based tuning of a LOV domain photoreceptor. *Nat. Chem. Biol.*, 5(11):827.
- Zydowicz-Machtel, P., Swiatkowska, A., Popenda, Ł., Gorska, A., and Ciesiołka, J. (2018). Variants of the 5′-terminal region of p53 mRNA influence the ribosomal scanning and translation efficiency. *Sci. Rep.*, 8(1):1533.

6 List of Figures

1.1	The intricacies of p53 regulation	2
1.2	Functional domains of p53 and key sites of post-translational modification	3
1.3	MDM2 is the main regulator of p53 protein levels	5
1.4	Signal as information - A theory of dynamic signal processing	8
1.5	Different stimuli trigger distinct temporal behaviours	9
1.6	Identity and intensity of upstream trigger are decoded in p53 dynamics and determine cellular outcome	13
1.7	Excitation spectra of different photoreceptor families	15
1.8	Blue light-induced exposure of the C-terminal J α -helix of AsLOV2	16
1.9	Overview of different optogenetic strategies employed using the AsLOV2	17
1.10	Peptide photocaging within the C-terminal J α helix of AsLOV2	19
1.11	LINuS and LEXY - small tags to gain photoactive, reversible control of protein import or export	21
3.1	Evaluation of effect of photocaged MIP peptide on p53 levels	30
3.2	Re-evaluating the light-depended effect of the photocaged MIP peptide on endogenous p53 levels	31
3.3	Characterisation of the MIP peptide in HCT116 cells	32
3.4	Photocaging the endogenous Mdm2-binding site of p53	34
3.5	Photocaging p53's endogenous transactivation domain	35
3.6	Characterisation of the PMI peptide in HCT116 cells	36
3.7	Using LINuS to control PMI localization by blue light	38
3.8	Using LEXY to control PMI translocation by light	39
3.9	Evaluation of recovery potential of PMI_LEXY	40
3.10	Characterisation of p53wt-LINuS in H1299 cells	44
3.11	Manipulation of p53's endogenous NES sequence	45
3.12	Mutation of p53's NLS sequence to improve translocation properties	46
3.13	Evaluation of impact on transcriptional activity of introduced p53 mutations	47
3.14	Introduction of acetylation mimicking mutants to recover transcriptional activity	48
3.15	Characterisation of p53 NLS mutants	49
3.16	Screening of p53 NLS mutant-LINuS variants to investigate their translocation efficiency	50
3.17	Assessment of effect of introducing NES's on translocation of p53 ^{R306A} -biLINuS02	51
3.18	Characterisation of p53 ^{wt} -LEXY	53
3.19	p53 ^{wt} -LEXY can be repeatedly translocated into the cytosol	54
3.20	Light-mediated expression of p21 by p53 ^{wt} -LEXY	55
3.21	High p53-LEXY expression levels impair translocation	56
3.22	Generation of a stable cell line expressing p53-LEXY	58
3.23	Characterisation of the monoclonal C29-36 cell line	60
3.24	p53-LEXY transcription correlates with blue light intensity and doxycycline concentration	62
3.25	Evaluation of translocation efficiency upon activation with reduced light energy	64
3.26	Induction of selective fluorescence and increased adherence of individual cells using single-cell laser tag.	66

3.27	Design of self-made LED chambers to track translocation during an experiment	67
3.28	Live cell monitoring visualizes impaired translocation of p53-LEXY	68
3.29	Cytosolic localisation of p53-LEXY after prolonged activation is independent of p53	70
3.30	Adjustment of the initial illumination period increased translocation efficiency	71
3.31	Expression of p53 target genes upon exposure with different illumination regimes	73
3.32	Evaluation of btg2 expression upon NCS treatment	75
3.33	Evaluation of puma expression upon NCS treatment	76
3.34	Evaluation of btg2 expression upon gefitinib treatment	77
3.35	Evaluation of puma expression upon gefitinib treatment	78
3.36	Evaluation of the contribution to un-reproducibility of the individual treatments	79
7.1	Translocation kinetics monitored of cells receiving no, constant or pulsatile light	115
7.2	p53 target gene expression upon neocarzinostatin treatment	116
7.3	p53 target gene expression upon gefitinib treatment	117
7.4	Gefitinib treatment induced puma expression	118

7 Appendix

7.1 List of Constructs used in this study

Number	Name	Backbone	Promoter	Source
PW001	reg4-MIP	pcDNA 3.1 (+)	CMV	Christian Scheeder
PW002	reg5-MIP	pcDNA 3.1 (+)	CMV	Christian Scheeder
PW003	reg5-3A	pcDNA 3.1 (+)	CMV	Christian Scheeder
PW004	NLS-trx-MIP	pcDNA 3.1 (+)	CMV	This work
PW005	NLS-trx-3A	pcDNA 3.1 (+)	CMV	This work
PW006	Reg5-enBI1	pcDNA 3.1 (+)	CMV	This work
PW007	Reg5-enBI2	pcDNA 3.1 (+)	CMV	This work
PW008	Reg5-enBI3	pcDNA 3.1 (+)	CMV	This work
PW009	Reg5-enBI4	pcDNA 3.1 (+)	CMV	This work
PW010	AsLOV2-538-TAD	pcDNA 3.1 (+)	CMV	This work
PW011	AsLOV2-539-TAD	pcDNA 3.1 (+)	CMV	This work
PW012	AsLOV2-540-TAD	pcDNA 3.1 (+)	CMV	This work
PW013	AsLOV2-541-TAD	pcDNA 3.1 (+)	CMV	This work
PW014	AsLOV2-542-TAD	pcDNA 3.1 (+)	CMV	This work
PW015	AsLOV2-543-TAD	pcDNA 3.1 (+)	CMV	This work
PW016	AsLOV2-544-TAD	pcDNA 3.1 (+)	CMV	This work
PW017	AsLOV2-545-TAD	pcDNA 3.1 (+)	CMV	This work
PW018	AsLOV2-546-TAD	pcDNA 3.1 (+)	CMV	This work
PW019	AsLOV2-547-TAD	pcDNA 3.1 (+)	CMV	This work
PW020	AsLOV2-539-PMI	pcDNA 3.1 (+)	CMV	This work
PW021	AsLOV2-540-PMI	pcDNA 3.1 (+)	CMV	This work
PW022	AsLOV2-541-PMI	pcDNA 3.1 (+)	CMV	This work
PW023	AsLOV2-542-PMI	pcDNA 3.1 (+)	CMV	This work
PW024	AsLOV2-543-PMI	pcDNA 3.1 (+)	CMV	This work
PW025	PMI-biLINuS02	pcDNA 3.1 (+)	CMV	This work
PW026	PMI-biLINuS09	pcDNA 3.1 (+)	CMV	This work
PW027	PMI-biLINuS11	pcDNA 3.1 (+)	CMV	This work
PW028	p53-NES-mCherry	pcDNA 3.1 (+)	CMV	This work
PW029	p53-NLS-mCherry	pcDNA 3.1 (+)	CMV	This work
PW030	p53-mCherry	pcDNA 3.1 (+)	CMV	This work
PW031	NLS-trx-PMI	pcDNA 3.1 (+)	CMV	This work
PW032	NES-trx-PMI	pcDNA 3.1 (+)	CMV	This work
PW033	PMI-1xGGS-mCherry	pcDNA 3.1 (+)	CMV	This work
PW034	PMI-2xGGS-mCherry	pcDNA 3.1 (+)	CMV	This work
PW035	PMI-1xGGS-Lexy	pcDNA 3.1 (+)	CMV	This work

PW036	PMI-1xCGS-Lexy	pcDNA 3.1 (+)	CMV	This work
PW037	p53 ^{wt} -PKit-biLINuS02	pcDNA 3.1 (+)	CMV	This work
PW038	p53 ^{wt} -PKit-biLINuS22	pcDNA 3.1 (+)	CMV	This work
PW039	p53 ^{wt} -biLINuS02	pcDNA 3.1 (+)	CMV	This work
PW040	p53 ^{wt} -biLINuS22	pcDNA 3.1 (+)	CMV	This work
PW041	p53 ^{wt} -Ikb α -biLINuS02	pcDNA 3.1 (+)	CMV	This work
PW042	p53 ^{wt} -Ikb α -biLINuS22	pcDNA 3.1 (+)	CMV	This work
PW043	p53 ^{L348L350A} -PKit-biLINuS02	pcDNA 3.1 (+)	CMV	This work
PW044	p53 ^{L348L350A} -PKit-biLINuS22	pcDNA 3.1 (+)	CMV	This work
PW045	p53 ^{K305AL348L350A} -PKit-biLINuS22	pcDNA 3.1 (+)	CMV	This work
PW046	p53 ^{K306AL348L350A} -PKit-biLINuS22	pcDNA 3.1 (+)	CMV	This work
PW047	p53 ^{K305AK306AL348L350A} -PKit-biLINuS22	pcDNA 3.1 (+)	CMV	This work
PW048	p53 ^{K319AL348L350A} -PKit-biLINuS22	pcDNA 3.1 (+)	CMV	This work
PW049	p53 ^{K320AL348L350A} -PKit-biLINuS22	pcDNA 3.1 (+)	CMV	This work
PW050	p53 ^{K321AL348L350A} -PKit-biLINuS22	pcDNA 3.1 (+)	CMV	This work
PW051	NLS-p53 ^{K320A} -mCherry	pcDNA 3.1 (+)	CMV	This work
PW052	NLS-p53 ^{L348A} -mCherry	pcDNA 3.1 (+)	CMV	This work
PW053	NLS-p53 ^{L350A} -mCherry	pcDNA 3.1 (+)	CMV	This work
PW054	NLS-p53 ^{K120RL348L350A} -mCherry	pcDNA 3.1 (+)	CMV	This work
PW055	NLS-p53 ^{K120QL348L350A} -mCherry	pcDNA 3.1 (+)	CMV	This work
PW056	NLS-p53 ^{K164RL348L350A} -mCherry	pcDNA 3.1 (+)	CMV	This work
PW057	NLS-p53 ^{K164QL348L350A} -mCherry	pcDNA 3.1 (+)	CMV	This work
PW058	NLS-p53 ^{K165RL348L350A} -mCherry	pcDNA 3.1 (+)	CMV	This work
PW059	NLS-p53 ^{K165QL348L350A} -mCherry	pcDNA 3.1 (+)	CMV	This work
PW060	NLS-p53 ^{K164RK165RL348L350A} -mCherry	pcDNA 3.1 (+)	CMV	This work
PW061	NLS-p53 ^{K164QK165QL348L350A} -mCherry	pcDNA 3.1 (+)	CMV	This work
PW062	NLS-p53 ^{K305A} -mCherry	pcDNA 3.1 (+)	CMV	This work
PW063	NLS-p53 ^{K306A} -mCherry	pcDNA 3.1 (+)	CMV	This work
PW064	NLS-p53 ^{K305AK306A} -mCherry	pcDNA 3.1 (+)	CMV	This work
PW065	NLS-p53 ^{K319A} -mCherry	pcDNA 3.1 (+)	CMV	This work
PW066	NLS-p53 ^{K321A} -mCherry	pcDNA 3.1 (+)	CMV	This work
PW067	p53 ^{K305A} -mCherry	pcDNA 3.1 (+)	CMV	This work
PW068	p53 ^{K306A} -mCherry	pcDNA 3.1 (+)	CMV	This work
PW069	p53 ^{K305AK306A} -mCherry	pcDNA 3.1 (+)	CMV	This work
PW070	p53 ^{K319A} -mCherry	pcDNA 3.1 (+)	CMV	This work
PW071	p53 ^{K321A} -mCherry	pcDNA 3.1 (+)	CMV	This work
PW072	p53 ^{K305A} -biLINuS02	pcDNA 3.1 (+)	CMV	This work
PW073	p53 ^{K305A} -biLINuS09	pcDNA 3.1 (+)	CMV	This work
PW074	p53 ^{K305A} -biLINuS22	pcDNA 3.1 (+)	CMV	This work
PW075	p53 ^{K306A} -biLINuS02	pcDNA 3.1 (+)	CMV	This work
PW076	p53 ^{K306A} -biLINuS09	pcDNA 3.1 (+)	CMV	This work
PW077	p53 ^{K306A} -biLINuS22	pcDNA 3.1 (+)	CMV	This work
PW078	p53 ^{K305AK306A} -biLINuS02	pcDNA 3.1 (+)	CMV	This work
PW079	p53 ^{K305AK306A} -biLINuS09	pcDNA 3.1 (+)	CMV	This work

PW080	p53 ^{K305AK306A} -biLINuS22	pcDNA 3.1 (+)	CMV	This work
PW081	p53 ^{K306A} -PKit-biLINuS02	pcDNA 3.1 (+)	CMV	This work
PW082	p53 ^{K306A} -synthNES11-biLINuS02	pcDNA 3.1 (+)	CMV	This work
PW083	p53 ^{K306A} -synthNES12-biLINuS02	pcDNA 3.1 (+)	CMV	This work
PW084	p53 ^{K306A} -synthNES21-biLINuS02	pcDNA 3.1 (+)	CMV	This work
PW085	p53 ^{wt} -cMyc-LEXY	pcDNA 3.1 (+)	CMV	This work
PW086	p53 ^{wt} -cMyc ^{P1A} -LEXY	pcDNA 3.1 (+)	CMV	This work
PW087	TetR-Krab	pcDNA 3.1 (+)	CMV	kind gift from Benjamin Kachel
PW088	CMV _{min} -p53-LEXY	pcDNA4.0 TO (+)	CMV	This work
PW089	mCherry-cMyc-LEXY	pcDNA 3.1 (+)	CMV	Dominik Niopek

7.2 List of qPCR Primer

Name	Sequence
qPCR-bax fw	agcaaaactgggtgctcaagg
qPCR-bax rv	ggaggaagtccaatgtccag
qPCR-beta-actin fw	caccatgtaccctggcatt
qPCR-beta-actin rv	aatgatcttgatcttcattgtgc
qPCR-btg2 fw	aggcactcacagagcactac
qPCR-btg2 rv	tgggggtccatcttggttg
qPCR-eGadd45 fw	tgctggtgacgaatccacatt
qPCR-eGadd45 rv	tgatccatgtagcgactttccc
qPCR-fas fw	cccggacccagaataccaag
qPCR-fas rv	tgtcacatttgggtgcaaggg
qPCR-p53 fw	cctgaggttggctctgactg
qPCR-p53 rv	gcccatgcaggaactgtta
qPCR-MDM2 fw	tcctgaaatttccttagctgact
qPCR-MDM2 rv	ccaacatctgttgcaatgtg
qPCR-p21 fw	cagaccagcatgacagatttc
qPCR-p21 rv	ggattagggcttctcttgg
qPCR-puma fw	ggagacaagaggagcagcag
qPCR-puma rv	ctgggtaagggcaggagtc
qPCR-PML fw	ccgcaagaccaacaacatct
qPCR-PML rv	gtagatgctggtcagcgtagg
qPCR-wip1 fw	gaagaaactggcggaatggc
qPCR-wip1 rv	ccaagaaccaccctgagtc
qPCR-Rpl0 fw	agggtcctggctttgtctgtgg
qPCR-Rpl0 rv	agctgcaggagcagcagtg
qPCR-XPC fw	gccatcactggctttgattt
qPCR-XPC rv	cagtcacgggatgggagtag

7.3 Supplemental Figures

7.3.1 Monitoring of translocation kinetics

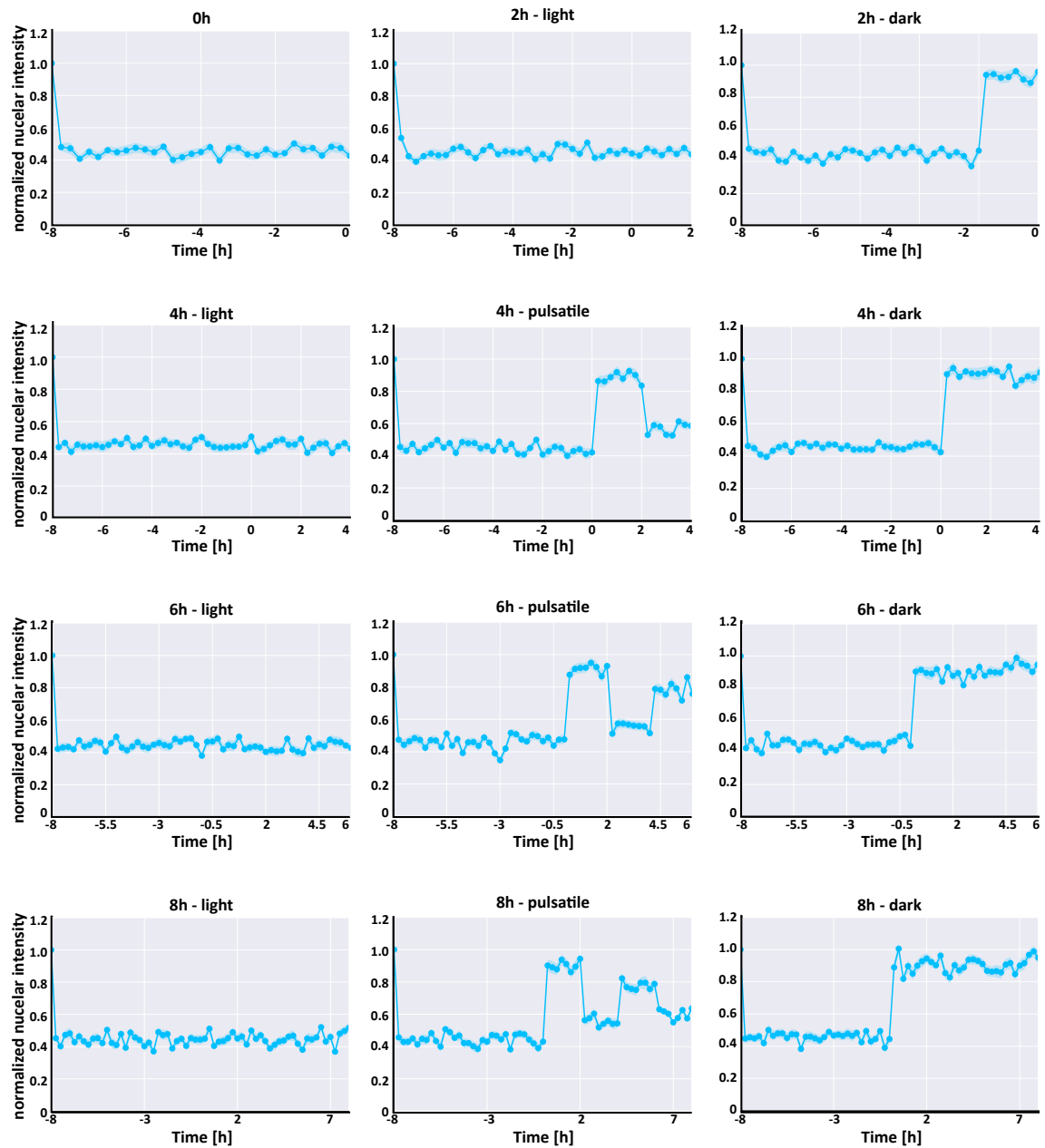


Figure 7.1: Translocation kinetics monitored of cells receiving no, constant or pulsatile light

Quantification of relative nuclear intensity of samples of experiment described in **Figure 3.31**. Nuclear intensity over time was normalized to initial nuclear intensity of the respective sample. Dots represent images taken (mean \pm SD, $n=20-30$).

7.3.2 p53 target gene expression upon neocarzinostatin treatment

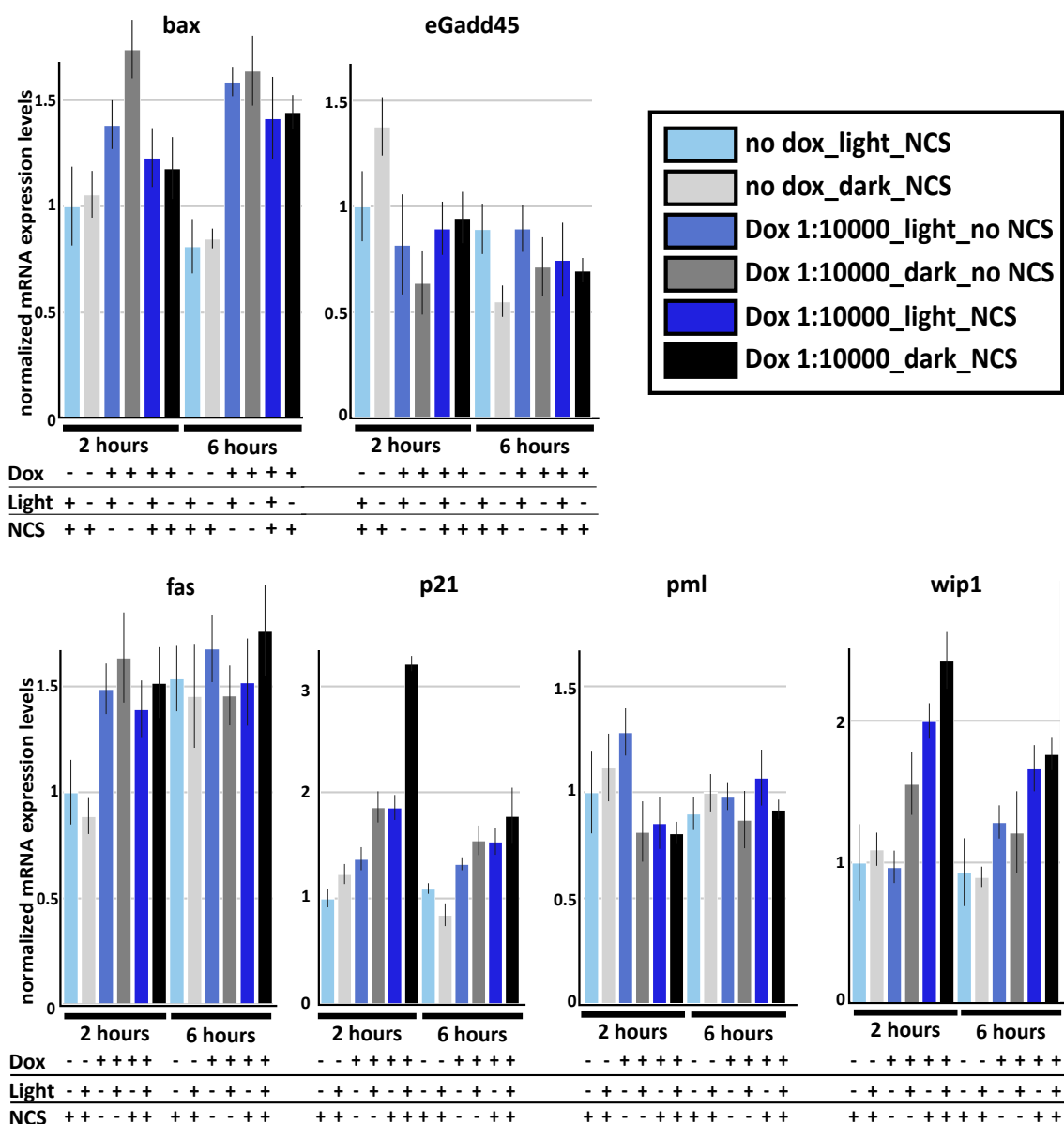


Figure 7.2: p53 target gene expression upon neocarzinostatin treatment

Normalized mRNA expression of indicated p53 target genes. Cells were induced with 100 ng/ml doxycycline for 8 hours, followed by 16 hour incubation in the dark. Then, cells were treated with 500 ng/ml NCS and blue light for 2 or 6 hours. Controls were not treated with NCS and blue light. Next, cells were lysed and RNA was extracted. Expression levels were first normalized to beta actin and Rpl0, then to the expression values of the non-induced, light exposed and neocarzinostatin treated sample at time point 2 h (mean \pm SD, technical replicates n=3)

7.3.3 p53 target gene expression upon gefitinib treatment

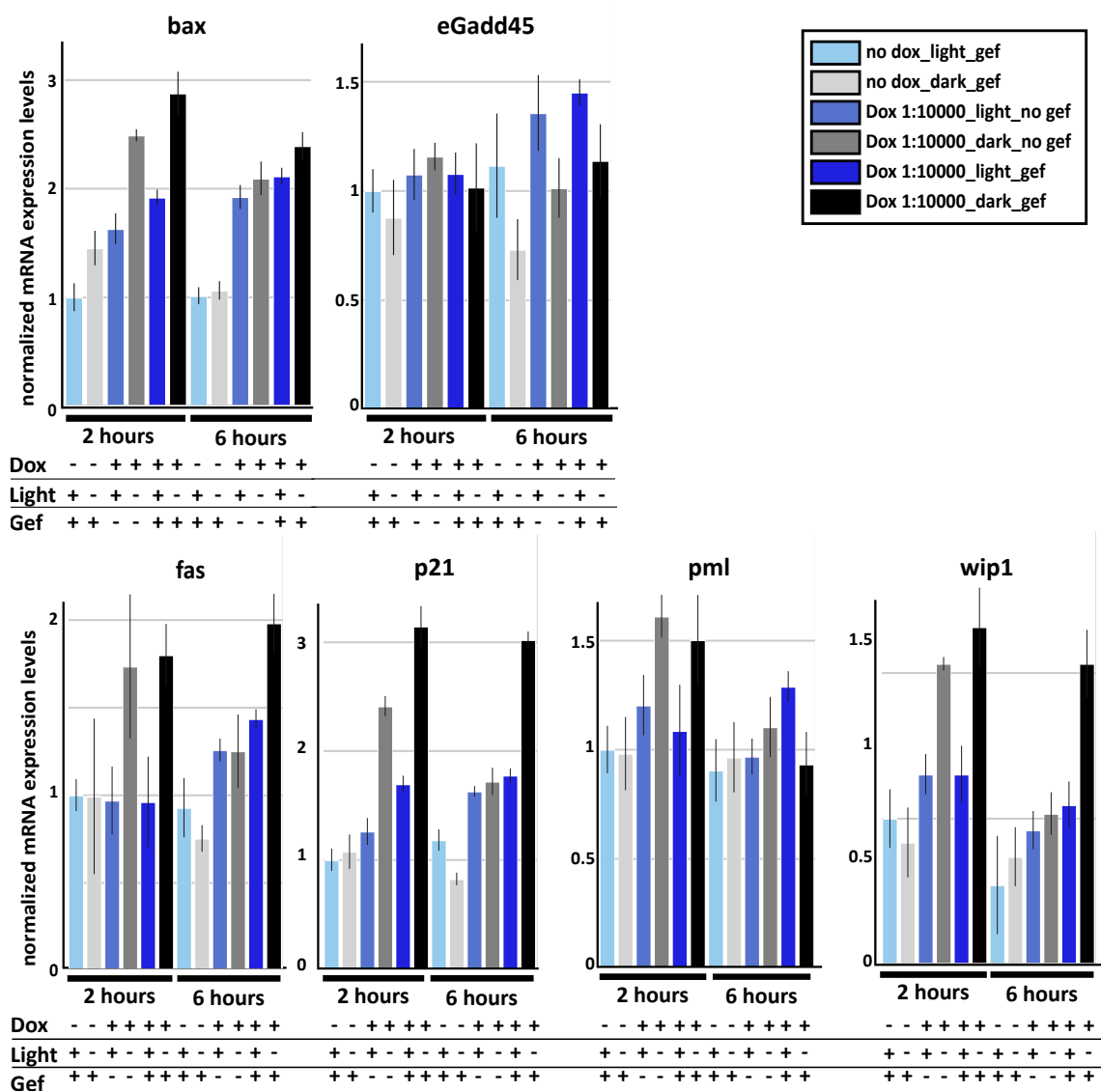


Figure 7.3: p53 target gene expression upon gefitinib treatment

Normalized mRNA expression of indicated p53 target genes. Cells were induced with 100 ng/ml doxycycline for 8 hours, followed by 16 hour incubation in the dark. Then, cells were treated with 1 μ M gefitinib and blue light for 2 or 6 hours. Controls were not treated with gefitinib and blue light. Next, cells were lysed and RNA was extracted. Expression levels were first normalized to beta actin and Rpl0, then to the expression values of the non-induced, light exposed and gefitinib treated sample at time point 2 h (mean \pm SD, technical replicates n=3)

7.3.4 Gefitinib treatment resulted in reproducible puma expression in HCT116 and MCF7-p53-Venus cells

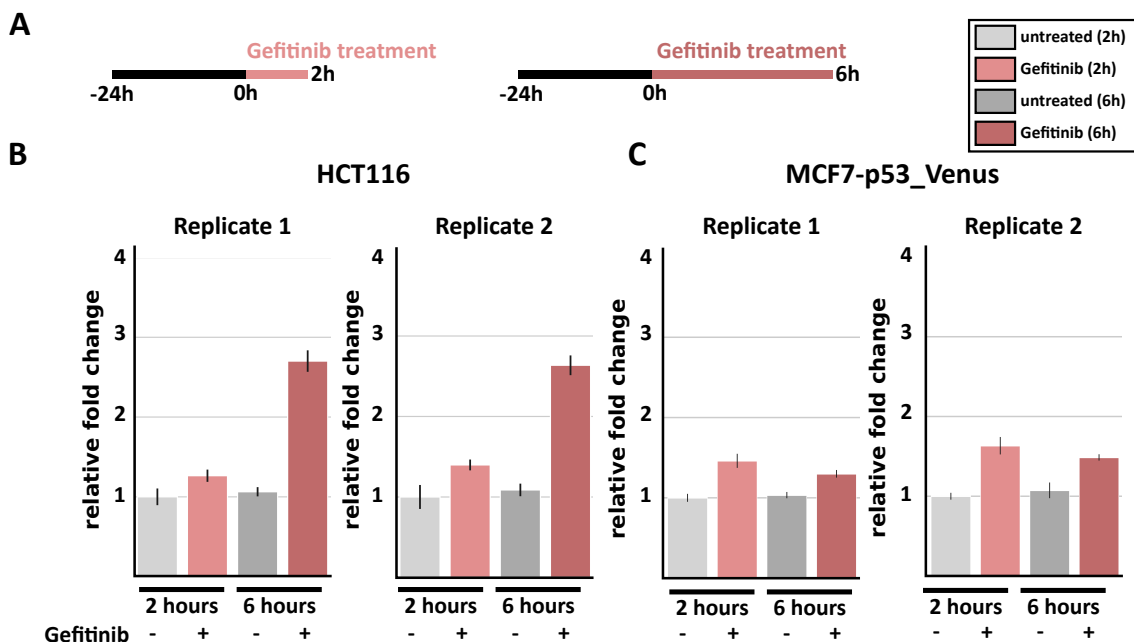


Figure 7.4: Gefitinib treatment induced puma expression

A | Schematic protocol of the experimental work flow. Cells were treated with 1 μ M gefitinib for 2h or 6h.

B | Normalized mRNA expression levels of puma in HCT116 cells treated according to protocol shown in **A**. Then, cells were lysed and RNA was extracted. Expression levels were first normalized to beta actin and Rpl0, then to the expression values of the non-treated sample at time point 2 h. (left) replicate 1 (mean \pm SD, n=3), (right) replicate 2 (mean \pm SD, n=3).

C | Normalized mRNA expression of puma in MCF7-p53-Venus cells treated according to protocol shown in **A**. Then, cells were lysed and RNA was extracted. Expression levels were first normalized to beta actin and Rpl0, then to the expression values of the non-treated sample at time point 2 h. (left) replicate 1 (mean \pm SD, n=3), (right) replicate 2 (mean \pm SD, n=3).

7.4 Abbreviations

ATM	ataxia-telangiectasia mutated protein
ATR	Ataxia telangiectasia and Rad3 related
Bak	Bcl-2 homologous antagonist killer
Bax	Bcl-2-associated X protein
Bcl2	B-cell lymphoma 2
Bcl-xL 2	B-cell lymphoma-extra large
BLUB	blue-light sensors utilizing flavin adenine dinucleotide
CLaP	cell labelling via photobleaching
CRM1	Chromosome region maintenance 1 or exportin 1
CMV	cytomegalovirus
DBD	DNA-binding domain
DSB	double strand brake
EGF	epidermal growth factor
Erk	extracellular signal-regulated kinase
HAT	histone acetyltransferases
IEG	immediate-early gene
iLID	improved light-induced dimer
LINuS	Light-inducible nuclear localization signals
LOV	Light oxygen voltage
MAPK	mitogen-activated protein kinase
Mcl1	induced myeloid leukemia cell differentiation protein
MDM2	murine double minute 2
MIP	MDM2 inhibitory peptide
NCS	neocarzinostatin
NES	nuclear export sequence
Nfat	nuclear factor of activated T cells
NGF	nerve growth factor
NLS	nuclear localization sequence
p14ARF	alternate reading frame protein product of the CDKN2A locus
p300/CBP	protein 300/CREB binding protein
pDI	peptide dual inhibitor
PAS	Period-ARNT-Singleminded
PCB	Phycocyanobilin
PCR	polymerase chain reaction
PhyB/PIF	Pythochon B/Pythochrome interacting factor
PRD	Proline rich domain
PTM	posttranslational modification
PYP	Photoactive yellow proteins
qPCR	quantitative polymerase chain reaction
Rap1	Ras-proximate-1
SD	Standard deviation
SNP	single nucleotide polymorphism
SOS	Son of Sevenless

SSB	single stand break
TAD	transactivation Domain
tetO	tet operator sequences
TetR	tet repressor proteins
TNF- α	tumour necrosis factor- α
TP53	tumor protein p53
TrpR	trp repressor
TULIPs	light-controlled interacting protein tags